UTS UNIVERSITY OF TECHNOLOGY SYDNEY

Development of Mixed Hardening Hyper-Viscoplastic Constitutive Models for Soils Incorporating Creep & Fabric Effects

by YE AUNG
BEng (1st Class Hons with University Medal, UTS)

Thesis submitted in fulfilment of the requirements for the degree of

DOCTOR OF PHILOSOPHY

under the supervision of
A/Prof. Hadi Khabbaz & A/Prof. Behzad Fatahi

University of Technology Sydney
Faculty of Engineering and Information Technology

December 2019

Certificate of Original Authorship

Graduate research students are required to make a declaration of original authorship when they submit the thesis for examination and in the final bound copies. Please note, the Research Training Program (RTP) statement is for all students. The Certificate of Original Authorship must be placed within the thesis, immediately after the thesis title page.

Required wording for the certificate of original authorship

CERTIFICATE OF ORIGINAL AUTHORSHIP

I, *Ye Aung*, declare that this thesis, is submitted in fulfilment of the requirements for the award of *Doctor of Philosophy*, in the *Faculty of Engineering and Information Technology* at the University of Technology Sydney.

This thesis is wholly my own work unless otherwise referenced or acknowledged. In addition, I certify that all information sources and literature used are indicated in the thesis.

This document has not been submitted for qualifications at any other academic institution.
**If applicable, the above statement must be replaced with the collaborative doctoral degree statement (see below).*

**If applicable, the Indigenous Cultural and Intellectual Property (ICIP) statement must be added (see below).*

This research is supported by the Australian Government Research Training Program.

Signature: Production Note:
Signature removed prior to publication.

Date: 06/12/2019

ABSTRACT

During the past several decades, the constitutive modelling for the prediction of time-dependent behaviour of soft soils has attracted an increasing attention within the geotechnical research society due to the scarcity of appropriate types of soil for construction as the regions around the globe have struggled to keep up with the meteoric rise in the infrastructure developments to cater for the substantial growth in population. Therefore, the consideration of time- and rate-dependent behaviour of geomaterials, particularly soft soils, such as creep, strain-rate dependent effects and stress relaxation behaviour, becomes a fundamental concern towards the long-term settlement deformation behaviour.

In this study, a mixed hardening hyper-viscoplastic constitutive model and its extended model are developed for describing the time-dependent stress-strain evolution of soil deformation, with the additional consideration of the arrangement of particles and the interparticle bonding, prominent in deformation of natural soils. The proposed model is intended to capture the loading-rate or strain-rate dependent behaviour of soils, accounting for the variations in the fundamental shapes of the yield loci along with the kinematic hardening and non-associated flow behaviour, with the extended model supplementing the proposed one with a β-line defining the inclination of the non-symmetrical elliptical yield locus in the p'-q plane, along with the auxiliary rotational hardening effects to the kinematic hardening behaviour. The proposed models are formulated within the context of hyperplasticity framework, mainly due to the fact that the hyperplastic constitutive models obey the fundamental laws of thermodynamics, and the resulting approach provides a well-established structure and reduces the need for 'ad hoc' assumptions. The distinctive departure from the existing viscoplasticity

models is the application of thermodynamics, based upon the use of internal variables, to postulate free-energy and dissipation potential functions, from which the elasticity law, the yield condition and corresponding flow behaviour, the isotropic and kinematic hardening laws, are derived based on a standardised systematic procedure. Firstly, the proposed model is presented, in which the free-energy function is decomposed into the elastic and the viscoplastic components, incorporating the dependence on both volumetric and deviatoric viscoplastic strains, and the viscoplastic dissipation potential function accounting for both the instantaneous energy dissipation and the additional energy dissipation due to delayed deformation. The additional viscoplastic component of the free-energy function results in the modified shift stress, to describe the kinematic hardening behaviour of the yield locus. Besides, a non-linear creep formulation is postulated to address the limitation of over-estimating long-term settlement, which is incorporated into the proposed model. Being introduced as a rational and logical extension towards the proposed model, the extended model enhances the free-energy and dissipation potential functions, in which not only the additional viscoplastic free-energy function depends on both volumetric and deviatoric viscoplastic strains, but also the fabric coupling parameter is incorporated into the free-energy and dissipation potential functions. Accordingly, the constitutive relations of the solid soil skeleton are expressed from the perspective of hyperplasticity framework in order to capture a wide variety of viscous behaviour of soils, with the emphasis on the strain-softening or hardening behaviour during the time-dependent delayed deformation in soils. The proposed model and the extended model only require minimal number of material parameters, which can readily be determined using standard laboratory testing equipment.

The performance and applicability of the proposed and extended models are investigated and validated using the triaxial and oedometer experimental results available in the existing literature. Comparisons between the numerical results and the laboratory measurements are

conducted to demonstrate the versatility and capability of the proposed model in reproducing the rate-dependent behaviour of natural soft soils subjected to a variety of loading conditions. Due to the advantages of strong theoretical foundation with rigorous, yet compact and consistent procedure, with a relatively small number of required model parameters, the proposed and extended models have been signified as ideal for the numerical implementations to predict the time-dependent behaviour of soft soils, including long-term settlement behaviour in geotechnical structures.

ACKNOWLEDGEMENTS

The road to the completion of my PhD journey has been mostly enjoyable and challenging, yet frustrating at times. At the jubilation end of this successful completion, I am delighted to look back over the journey and remember the support and encouragement that I have received from my family, friends, and colleagues throughout this lengthy, yet satisfying journey. I would like to take this opportunity to express my sincere gratitude towards everyone, who have helped this thesis come to fruition.

First and foremost, I would like to pay my deepest homage to my principal supervisor, Associate Professor Hadi Khabbaz, and my co-supervisor, Associate Professor Behzad Fatahi, for their continued support, and guidance on not only the research but also the other developments in my life. Under their patience and guidance, I have developed and accumulated many important skills, including technical and interpersonal, from their broad knowledge, ideas, advice and suggestions have inspired and motivated me in achieving the important objectives of my research as well as the major milestones in my life.

Secondly, my appreciation is likewise extended to Dr Lam Nguyen, along with my colleagues and other staff members in the UTS laboratory for their kind assistance and contribution at the commencement of my research project in finding the soil properties and the feasibility of conducting creep tests in the laboratory.

This research has been carried out in the School of Civil and Environmental Engineering Faculty within University of Technology, Sydney, with the support from the International Postgraduate Research Scholarship (IPRS) and the Australian Postgraduate Award (APA) by

the Australian Government for three and a half years. All the support from the Faculty and University throughout my study are also gratefully appreciated and acknowledged. Moreover, I would like to thank my friends and colleagues, particularly from my geotechnical group, not only for their help but also for keeping my study life more enjoyable and pleasant.

Last, but not least, I am hugely indebted to my family for their unconditional love, moral support and encouragement throughout this arduous journey. I am deeply grateful towards my parents in always showing the faith and allowing me to study and follow my lifelong pursuit and ambition to achieve this major milestone of my life. Additionally, for my loving, caring and supportive partner, I would like to express much appreciation for her love and mental support throughout my PhD journey.

LIST OF PUBLICATIONS

- Aung, Y., Khabbaz, H. & Fatahi, B. 2019, 'Mixed Hardening Hyper-viscoplasticity Model for Soils Incorporating Nonlinear Creep Rate – H-Creep Model', *International Journal of Plasticity,* vol. 120, pp. 88-114.
- Aung, Y., Khabbaz, H. & Fatahi, B. 2019, 'Extended Mixed Hardening Hyper-viscoplasticity Model for Soft Soils Incorporating Soil Fabric', International Journal of Plasticity (Submitted).
- Aung, Y., Khabbaz, H. & Fatahi, B. 2016, 'Review on Thermo-mechanical Approach in the Modelling of Geo-materials Incorporating Non-Associated Flow Rules', 3rd International Conference on Transportation Geotechnics, Procedia Engineering, vol. 143, pp. 331-338.
- Aung, Y., Khabbaz, H. & Fatahi, B. 2016, 'Review on Thermo-mechanical Approach in the Modelling of Geo-materials Incorporating Non-Associated Flow Rules', 3rd International Conference on Transportation Geotechnics (3rd ICTG), 4-7 September, Guimarães, Portugal.
- Aung, Y., Khabbaz, H. & Fatahi, B. 2020, 'A Generalised Hyper-viscoplasticity framework for Developing Rate-dependent Plasticity Models', 4th International Conference on Transportation Geotechnics (4th ICTG), 30 August – 2 September, Chicago, Illinois (Accepted).

Table of Contents

LIST OF FIGURES

LIST OF TABLES

Nomenclature & Abbreviations

Latin Notations

A, B	functions for stress-like quantities
$C_{\alpha e}$	secondary compression coefficient
C_β	material constant controlling the extent of coupling
C_r	swelling index
C_c	compressive index
D_β	relative contribution from the volumetric and deviatoric viscoplastic strains in determining the extent of coupling
$C_v(\eta)$	volumetric target value for β
$C_q(\eta)$	deviatoric target value for β
e_0	initial void ratio
e	void ratio
e_R	reference void ratio
Δe	change in void ratio
F	overstress function
G	elastic shear modulus
G_0	initial elastic shear modulus
g	elastic shear modulus gradient

J	cross-coupling elastic modulus
K	elastic bulk modulus
k	elastic bulk modulus gradient
M	slope of the critical state line
m	power value (material constant) representing the slope of the $\log \mu - \log e$ curve
n	power order (dimensionless material constant)
p	effective stress
$\dot{p}$	change in effective stress
p_R	reference mean stress
p_0	effective stress at initial state (or reference time)
p_c	pre-consolidation pressure
$\dot{p}_c$	change in pre-consolidation pressure
p_{c0}	initial pre-consolidation pressure
p_s	volumetric shift stress
p_D	volumetric dissipative stress
Q	viscoplastic potential function
q	deviatoric stress
$\dot{q}$	change in deviatoric stress
q_s	deviatoric shift stress
t_R	reference time (or absolute equivalent time)
V	specific volume
w_L	liquid limit
w_P	plastic limit
w	flow potential function
z	force potential function

Greek Notations

δ_{ij}	Kronecker's delta
α	material constant linking to the amount of deviatoric dissipation
β	cross-coupling between volumetric and deviatoric dissipation
ε_1	strain in axial direction
ε_3	strain in radial direction
ε_{ij}	total strain tensor
ε_v	total volumetric strain

ε_q	total shear strain
$\dot{\varepsilon}_v$	total volumetric strain increment
$\dot{\varepsilon}_q$	total shear (or deviatoric) strain increment
ε_{ij}^e	elastic strain tensor
ε_v^e	elastic volumetric strain
ε_q^e	elastic shear strain
$\dot{\varepsilon}_v^e$	elastic volumetric strain increment
$\dot{\varepsilon}_q^e$	elastic shear strain increment
ε_{ij}^p	plastic strain tensor
ε_{ij}^{vp}	viscoplastic strain tensor
ε_v^{vp}	viscoplastic volumetric strain
ε_q^{vp}	viscoplastic shear (or deviatoric) strain
$\dot{\varepsilon}_v^{vp}$	viscoplastic volumetric strain increment
$\dot{\varepsilon}_q^{vp}$	viscoplastic shear (or deviatoric) strain increment
γ	material constant linking to the amount of stored plastic work
κ^*	slope of swelling line in $\ln v - \ln p$ plot
λ^*	slope of normal consolidation line in $\ln v - \ln p$ plot
η	stress ratio
μ	creep coefficient
μ_0	initial creep coefficient
ϱ	Thermodynamics-based overstress function (in true stress space)
ϱ_D	Thermodynamics-based overstress function (in dissipative stress space)
σ_0	effective stress at a reference time
σ_1	effective stress in axial direction
σ_3	effective stress in radial direction
ν	Poisson's ratio
$\delta\Phi$	dissipation increment function
Ψ^g	Gibbs free-energy function
Ψ_e^g	Elastic Component of Gibbs free-energy function
Ψ_{vp}^g	Viscoplastic Component of Gibbs free-energy function
$\dot{\Psi}$	the differential of the free-energy function
ψ	viscosity function
$\bar{\chi}'_{ij}$	generalised stress tensor
χ'_{ij}	dissipative stress tensor

Common Acronyms

CRS	Constant Rate of Strain

CSL	Critical State Line
EVP	Elastic-viscoplastic
MCC	Modified Cam-clay
OCR	Over-consolidation Ratio
UTC	Undrained Triaxial Compression (UTC)
UTE	Undrained Triaxial Extension

CHAPTER 1

INTRODUCTION

1.1 Background

As a result of rapid advancement in social, and infrastructural development of the world, accompanying the massive growth in its population, there has been an alarming concern for the availability of suitable types of soil for construction in recent years. As a consequence, it has become increasingly likely that the relatively inappropriate construction areas, such as lakes, river and coastal regions, are to be considered as alternative options for future construction projects. The most prevalent type of soils found in these areas are mostly soft clays, which exhibit low permeability and shear strength, with high compressibility. One of the major challenges when dealing with soft soils in geotechnical engineering design and analyses, is the long-term deformation associated with soft soils. Inevitably, the constitutive modelling for the simulation of time-dependent behaviour of soft soils has captivated much attention in the geotechnical research society. The prediction of time-dependent behaviour of geomaterials, such as creep, stress-relaxation and strain-rate dependency, bears considerable importance, particularly in the ground settlements, which in turn, may result in significant deformation in the long-term.

Figure 1.1: Requirements for construction in inappropriate ground profiles (Soil Stabilisation System, viewed 22 November 2019, < https://allustabilization.wordpress.com/>)

The experimental investigation of time-dependent deformation in a wide variety of materials has been performed by numerous researchers, such as for frozen soils (Lai et al., 2000; Liu et al., 2018), rock-like materials (Wang et al., 2015; Nguyen et al., 2017; Cao et al., 2018; Zhao et al., 2018), asphalt concrete (Darabi et al., 2012a,b; Cheng et al., 2016), plasticine materials (Feng et al., 2017) and polymeric materials (Ghorbel, 2008). In addition, a multitude of geotechnical researchers have developed a plethora of constitutive soil models to consider the time- and rate-dependent behaviour of clays, varying from simple Elastic-Plastic to Elastic-Visco-Plastic (EVP) models (Kelln et al., 2008; Fatahi et al., 2013; Karim and Gnanendran, 2014; Azari et al., 2016; Le et al., 2015; Yin et al., 2015a,b). Yin (2006) has also discussed the fundamental facts related to elastic viscoplastic modelling of the time-dependent stress-strain behaviour of geomaterials and stated that the EVP models are more general than the traditional elastic-plastic constitutive models. Among the abundance in a variety of constitutive models for the time-dependent behaviour of soft soils, the EVP model proposed by Yin and Graham (1989) is considered as simple yet practical for the numerical analyses related to long-term settlement of soft soils. Afterwards, they have extended this model for triaxial and general stress states with the adoption of the elliptical flow surface from Modified Cam-clay model, and Mises failure criterion. However, the postulated linear logarithmic function results in the creep strain being infinite as time approaches to infinity. In order to rectify this shortcoming, Yin (1999) proposed a non-linear creep formulation with the introduction of creep coefficient and stress-dependent creep strain limit. Although the non-linear creep model can reproduce more accurate results in the simulation of long-term settlement of soft soils, the parameter determination related to the non-linear creep parameters exhibited several restrictions for its adoption in geotechnical applications. Notwithstanding this improvement, Yin et al. (2015a) and Zhu et al. (2016a) pointed out that the non-linear creep formulation postulated by Yin (1999) as being only applicable to one particular constant applied stress level, as the non-linear

creep coefficient did not continuously decrease with the void ratio when the applied stresses were continuously increasing and hence, a negative void ratio could only be avoided under a constant applied pressure. In order to address this shortfall, Yin et al. (2015a) have proposed an improved non-linear creep formulation with consecutively decreasing consolidation coefficient. Besides, Le and Fatahi (2016) have proposed a more rigorous numerical optimisation technique, i.e. Trust-Region Reflective Least Square (TRRLS) approach and applied the algorithm to obtain the EVP model parameters of the clay samples in the laboratory conditions.

Concomitantly, Zhou et al. (2005) and Leoni et al. (2008) have extended the isotropic creep models by Vermeer and Neher (1999) and Yin et al. (2002), in which the volumetric viscoplastic strain remains constant on the yield surface, regardless of the stress state. This has resulted in the unrealistic predictions of volumetric viscoplastic strains when the stress state approaches the critical state line; instead, the value should be nearly zero based on the laboratory measurements. In recent years, the modelling of combined anisotropic and viscoplastic effects for clays (Yin et al., 2010; Sivasithamparam et al., 2015; Jiang et al., 2017; Leal et al., 2017; Castro et al., 2018), along with the consideration of strain rate and temperature (Leroueil and Marques, 1996; Laloui et al., 2008) or strain rate and structure (Hinchberger et al., 2010; Yin and Karstunen, 2011; Zhang, 2018) have also been carried out.

Overall, it has been acknowledged that most of the existing viscoplastic constitutive models have been based on the elastic viscoplastic modelling (EVP) framework (Perzyna, 1963; 1966) or the non-stationary flow surface framework (Naghdi and Murch, 1963; Olszak and Perzyna, 1970). The most profound impediment in the overstress-based models stems from the arbitrariness of the postulated overstress function. Moreover, they do not satisfy with the consistency condition and it is also difficult to justify their compliance with the fundamental laws of thermodynamics.

Besides, although all these models have enlightened the understanding of time-dependent behaviour of soils, they still have their own deficiencies. The most profound limitations are the basic assumption of the flow surface being elliptical as defined in Modified Cam-clay (MCC) model, developed by Roscoe and Burland (1968), the flow rule being associated, and the elastic behaviour being strictly isotropic. Moreover, they often require a considerable number of assumptions without being related to the physical phenomena of real soils.

1.2 Problem Statement

It is important to acknowledge that the most important attribute of the constitutive models is their compliance with the physical phenomena. The fact that they must obey certain principles or axioms that govern the physical phenomena, such as conservation of mass, conservation of energy and the fundamental laws of thermodynamics, should be emphasised. Taking this into strong consideration, the aforementioned constitutive frameworks do not take into account of the fundamental laws of thermodynamics and they may eventually violate one or the other physical phenomena. According to Houlsby and Puzrin (2006), the constitutive models that do not comply with the laws of thermodynamics may not be used with any confidence to predict the material behaviour.

To circumvent the problem of having a substantial number of assumptions and using 'ad hoc' procedures, the major objective of this research is to develop a constitutive soil model based on the laws of thermodynamics, from which the constitutive behaviour of soils is derived in a systematic procedure. Accordingly, the extraction of plasticity theory with the major emphasis on the fundamental laws of thermodynamics was originated from the early works of Halphen and Nguyen (1974) and Ziegler (1983), in which the derivation of the entire

constitutive response for predicting stress-strain behaviour of plastic materials is based on two scalar thermodynamic potential functions. Considerably, this is a relatively new approach to the development of elastic-plastic constitutive models, which was termed 'hyperplasticity by Collins and Houlsby (1997) and Houlsby and Puzrin (2000, 2006) for the modelling of time-independent behaviour of soils. Collins and Houlsby (1997) discussed the application of thermomechanical principles to the modelling of geotechnical materials and emphasised on the mathematical technique, called Legendre transformation, in developing rate-independent hyperplasticity models.

During recent years, a few attempts have been made for the extension towards rate-dependent behaviour of soils (Vlahos et al., 2006; Likitlersuang and Houlsby, 2007; Puzrin and Rabaiotti, 2009; Zhang, 2017; Zhang and Buscarnera, 2017), frozen soils (Zhou et al., 2016), peat (Boumezerane et al., 2015), rubbers (Guo et al., 2018), polymeric materials (Gudimetla and Doghri, 2017) and steel behaviour (Benaarbia et al., 2018). Moreover, Abu Al-Rub and Darabi (2012) have proposed a thermodynamic-based framework for the constitutive modelling of temperature-, time- and rate-dependent behaviour of viscous materials and Zhu et al. (2016b) have presented a coupled EVP model based on thermodynamics to predict the cyclic deformation of metals. Furthermore, Darabi et al. (2012a; b) have adopted the former approach to simulate the behaviour of asphaltic materials over a wide range of time- and rate-dependent experiments. Recently, Darabi et al. (2018) have further discussed on a thermodynamic-based approach to systematically derive generalised non-associative rate-independent and rate-dependent plasticity theories. However, most of the existing thermodynamic-based models often require a substantial number of parameters and they still adopt the aforementioned limitations, such as the assumption of the flow rule being associated and the shape of the yield surface being adopted as symmetric elliptical one defined in the MCC model, without considering the possibilities of deformed shapes of the yield surface.

As suggested by the laboratory experiments presented in Dafalias and Taiebat (2013; 2014) and Zhou et al. (2017), the yield loci not only expand but also translate in the stress space and the shapes of the yield loci do vary depending on the types of soils. In order to address the experimental findings, Mroz (1998) introduced the kinematic hardening mechanism to the constitutive modelling of soils, along with the hardening function, in order to control the movement and the variation in size of the yield loci. Kinematic hardening during inelastic deformations is usually described by a so-called 'back' or 'shift' stress, which is considered as an internal variable, for which an adequate constitutive equation is formulated (Sansour et al., 2006). Recently, Zhou et al. (2018) have proposed a kinematic hardening EVP constitutive model, adopting Perzyna's overstress theory, to predict the stress- strain behaviour of saturated cohesive anisotropic soils. However, their EVP model still employs associated flow rule and requires a sizeable number of parameters based on a considerable number of assumptions. From the perspective of hyperplasticity, the kinematic hardening behaviour is considered in the form of 'shift' stress, referred to as 'stored plastic work', which is determined by the additional plastic free-energy function, i.e. not contributing to the plastic dissipation. It is to be emphasised here that some portion of the plastic work is stored in the form of continuum plastic strain (i.e. the residual strain when a continuum element is unloaded back to a particular predefined reference loading condition due to the inhomogeneous nature of the micro-level deformation). Consequently, some of the micro-level elastic energy is 'frozen', resulting in recoverable stored plastic work (Collins, 2005). This contradicts the conventional perfect plasticity theory, which often assumes that the 'plastic work' and 'plastic dissipation' are equal (i.e. all the plastic work is assumed to be dissipated). Most importantly, this kinematic hardening behaviour has not been widely considered in modelling the viscoplastic stress-strain behaviour of soils.

1.3 Research Objectives and Scope

This research is a rational effort in adopting the conservative thermodynamics-based hyperplasticity concept to propose a simple yet versatile constitutive soil model to simulate the non-linear creep behaviour, along with the incorporation of both isotropic and kinematic hardening effects. Due to the important fact that the hyperplasticity theory is mainly based on the fundamental laws of thermodynamics, it also avoids the need to introduce a considerable number of 'ad hoc' assumptions without being related to the physical phenomena of soils. One of the key benefits bears in the development of relatively rigorous, compact and consistent constitutive framework, as the resulting model cannot produce thermodynamically unreasonable outcomes. The proposed model is developed in a relatively succinct mathematical form, as the entire constitutive response is determined through the specification of two scalar thermodynamic potential functions, i.e. the free-energy and dissipation potential functions, using a systematic standardised procedure. These two fundamental potential functions are related through Legendre transformation, which results in the natural incorporation of non-associated flow, which is now widely regarded as a proper approximation for improved predictions in the behaviour of soils, being derived logically and naturally without postulating any further potential functions, which are usually introduced to arbitrate the associativity of the flow rule in conventional plasticity theory. In addition, the proposed model takes into account of kinematic hardening behaviour of soils in the form of 'shift' stress within the context of hyperplasticity. It is emphasised that not all the plastic work is dissipated; but some portion is stored when an element is unloaded back to a predefined reference stress level at the continuum level (Lai et al., 2014). As a result, the kinematic hardening behaviour is modelled by incorporating a 'back or shift stress', as part of the additional viscoplastic component of the free-energy function into the proposed model. The extended thermodynamic potential

functions are postulated, considering the variation in shapes of the yield loci, for the simulation of time- or rate-dependent stress-strain behaviour of soils.

Figure 1.2: Long-term settlement issues highlighting the importance of modelling rate-dependent behaviour of soils (What Exactly Causes Foundation Settlement?, viewed 23 November 2019, < https://www.therealsealllc.com/what-exactly-causes-foundation-settlement>)

Furthermore, the proposed model has been extended to incorporate the effects of the arrangement of particles and the interparticle bonding, i.e. termed as 'structure' by Mitchell (1993; 1956), which was also referred to as "fabric" by Muhunthan et al. (1996). Considering the importance of acknowledging the effects of the interparticle bonding of particles and their arrangement, particularly in natural soils, the current study furthers in a radical extension of the proposed model to incorporate the consideration of 'fabric' effects on the time-dependent stress-strain behaviour of natural soils. The extended model intends to capture the loading-rate or strain-rate dependent behaviour of soils, considering the variations in the fundamental shapes of critical surface with a β-line defining the inclination of the non-symmetrical elliptical

critical surface in the p'-q plane, along with rotational, kinematic hardening effects and non-associated behaviour, derived as a natural consequence of this approach.

The proposed model's predictions demonstrate the capability and versatility in reproducing the viscous behaviour of soft soils, including natural ones, under different loading conditions, which has been validated by using comparisons with the existing triaxial and oedometer laboratory measurements available in the literature.

1.4 Organisation of Thesis Structure

The composition of the thesis comprises of six key chapters, which can be described as follows:

Chapter 1 presents a brief introductory background on the constitutive modelling of stress-strain behaviour of soils, along with the problem statement, the major objectives and scope of the current study.

Chapter 2 describes a comprehensive literature review on the real soil behaviour and the importance of modelling time-dependent viscoplastic behaviour of geomaterials, particularly soils. Moreover, the challenges associated with the development of constitutive soil models and the distinctive characteristics of the existing advanced constitutive modelling frameworks are also presented to emphasise on the problem statement of the current study.

In Chapter 3, the underlying principles of the Hyperplasticity theory, signifying its essential components and requisite foundation towards the development of a new Hyper-viscoplasticity theory have been elaborated. Moreover, the fundamental laws of thermodynamics have been discussed. This has been accompanied by the practical summary

of rate-independent hyperplasticity approach, from which the rate-dependent hyperplasticity framework has been built upon using a constructive and consistent approach and thus, highlighting the rigidity, compactness and reliability acting as a strong foundation for the development of hyper-viscoplastic soil models in the current study.

Chapter 4 proposes a novel mixed hardening hyper-viscoplasticity model to simulate the time- or rate-dependent stress-strain behaviour of soils, along with the consideration in varying shapes of the yield loci by pursuing non-associated flow and accounting for kinematic hardening effects. The important characteristics of the proposed model, including the non-associated flow rule derived as a natural consequence, rather than imposed arbitrary application compared with the traditional viscoplasticity models, the postulated additional viscoplastic free-energy function and the dissipation potential function, along with the hypothesised non-linear creep formulation based on experimental findings, are provided and further elaborated in details. Moreover, the proposed model is extended to account for the effects of the combination of the arrangement of particles and the interparticle bonding, particularly crucial in modelling stress-strain behaviour of natural soils. The extended aspects of the free-energy and dissipation potential functions, from which the rotational, kinematic hardening law stems from the additional viscoplastic free-energy potential, are elaborated and discussed in details.

In Chapter 5, the summary and related procedures to determine the required model parameters have been extensively elaborated. The proposed H-Creep model requires 10 model parameters in total, whereas the extended model introduces only one additional parameter compared to its original counterpart, resulting in a relatively straightforward parameter determination procedure, which has been discussed. Accordingly, the proposed and extended models are applied to a wide range of laboratory experiments, including the normally consolidated, overconsolidated and K_0-consolidated undrained strain-controlled and stress-controlled triaxial compression and extension tests, undrained triaxial shearing tests with

stress-relaxation and constant rate of strain tests. Moreover, the comparisons between the numerical simulations and the laboratory measurements, are performed to investigate the validity and performance of the proposed and extended models in reproducing the viscous behaviour of soft soils, including natural ones, under a variety of loading conditions.

Chapter 6 summarises the significant findings of this research, together with the main concluding remarks and recommendations for further research. This is followed by the Appendix sections elaborating further details to supplement the important findings throughout this research.

CHAPTER 2

LITERATURE REVIEW

2.1 Introduction

For several decades, time-dependent behaviour of soils has been a debatable subject for many researchers in the area of geotechnical engineering. It has been widely acknowledged that Terzaghi's classical theory of one-dimensional consolidation, published in 1943, can provide a reasonable approximation of the settlement induced by the pore water pressure dissipation. Although the conventional or simplified methods can offer an appropriate estimation of the settlement of soils in relatively simple soil scenarios, they cannot be applied to predict the complicated real soil behaviour, such as the relationship between stress-strain-strain rate or the effects of temperature. This chapter presents a review on the importance of understanding the real soil behaviour, along with the most crucial time-dependent aspects observed in relation to the mechanical behaviour of soils. Moreover, the time-dependent behaviour of geomaterials, including creep, stress relaxation and strain-rate dependency are discussed. Furthermore, the significance of capturing such behaviour of geomaterials, particularly soils, and the challenges associated with the development of constitutive soil models are investigated. In addition, a number of the existing advanced constitutive soil models are examined and elaborated in details.

2.2 Real Soil Behaviour

In stark contrast to reality, the material behaviour is still often assumed to be linear elastic in most of the geotechnical analyses of engineering problems. However, real soils do not simply behave linear elastically and the understanding of real soil behaviour is extremely crucial to achieve a reasonable level of accuracy in predicting the associated stress-strain characteristics. The non-linearity is highly present in the real soil behaviour, i.e. both strength

and stiffness are dependent on the stress and strain level. Therefore, considerable knowledge and understanding is important to identify some important aspects of these complicated soil behaviour before delving into the development of constitutive models.

In general, the stress-strain characteristics of soils should fall into the following categories. For elastic material behaviour, the strain follows the stress immediately, and becomes zero after the removal of stress. For elastoplastic material behaviour, the strain also follows the stress immediately, but there is some permanent strain after stress release. For viscoelastic material behaviour, the strain shows time delayed response on a stress step, indicating the time-dependent behaviour. For viscoplastic material behaviour, the time-dependent behaviour is accompanied by permanent strain.

2.3 Time-dependent Behaviour of Soils

Another major aspect in modelling soil behaviour is that soils exhibit time-dependent behaviour as well as plastic deformation. It is commonly understood that time-dependent settlement in soils, for instance, saturated clay, results mainly due to two important factors: (i) volume changes due to viscous deformations, and (ii) volume changes due to pore-water dissipation. Consequently, soils are also called as viscous material. The viscous properties define the time dependence of the state of stress and strain, whilst plastic properties make these states depend on the loading path. This section describes the important constituents of the time-dependent settlement of soft soils, such as time effects, strain rate effects and stress dependency.

2.3.1 Creep

When soil is subjected to a constant load, it will deform over time and this phenomenon is called creep. As demonstrated in Figure 2.1, a creep test is performed at a low stress level following a strain path from point 1 to point 2. Consider, a soil is sheared to the stress-strain state at point 1, from which creep is commenced with the constant stress, as shown in Figure 2.1b. As depicted in Figure 2.1c, the strain state progress to point 2, as the strain is gradually increasing.

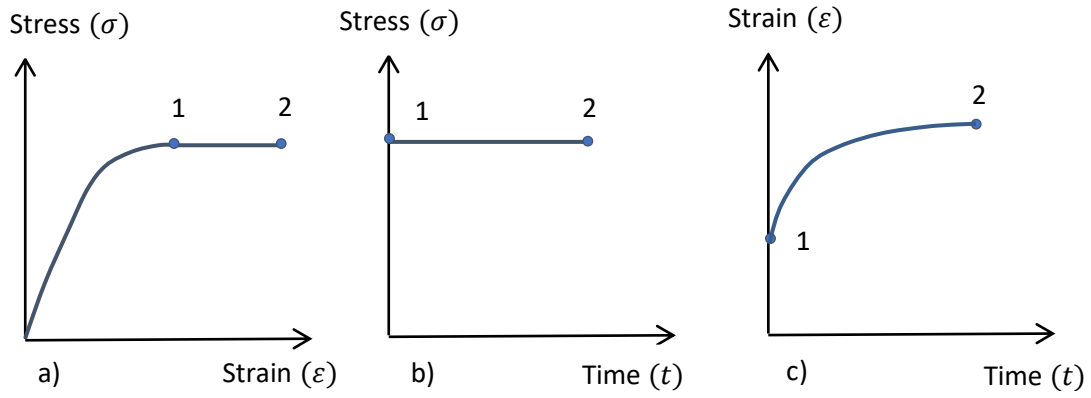

Figure 2.1: Creep test performed at a low stress level: (a) Stress-strain relationship; (b) stress history; (c) strain history (after Wood, 1990)

2.3.2 Stages of Creep Process

The creep response under a constant effective stress performed using triaxial apparatus can be classified into three main components: i) primary or transient creep; ii) secondary or stationary creep; iii) tertiary or acceleration creep. The primary stage of creep is referred to as the transient creep corresponding to the decreasing strain rate, while the secondary and tertiary creep stages are the stationary creep with constant creep strain rate and the acceleration creep with the increasing strain rate, respectively. The tertiary creep phase gradually and eventually

leads to the creep rupture or creep fracture of soils, as observed in the triaxial creep tests (Augustesen et al. 2004). The corresponding creep test results can be depicted in either a strain vs time graph or logarithm of strain rate vs logarithm of time graph, as shown in Figure 2.2.

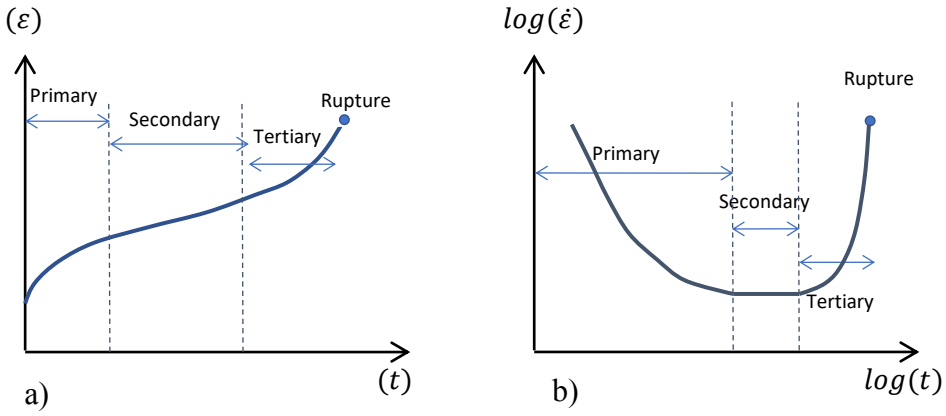

Figure 2.2: Creep stages for a creep test performed by a triaxial apparatus: (a) Strain versus time; (b) log strain rate versus log time (after Augustesen et al. 2004)

In drained creep tests, the effective stresses, i.e. the mean effective stress p' and the deviatoric stress q, are kept constant. In undrained creep tests, p' decreases due to increase in pore pressure, while the deviatoric stress q remains constant. Therefore, only the drained creep represents a pure creep process, as pointed out in Augustesen et al. (2004).

2.3.3 Strain Rate Effects

As pointed out in a number of researchers, such as Leroueil et al. (1985), Mesri and Feng (1986) and Jia et al. (2010), strain rate is another significant factor that influences the time-dependent compressibility of soft soils. In order to study the stress-strain-time relationship at different strain rates, Constant Rate of Strain (CRS) consolidation tests have been broadly employed, from which a unique relationship is found among stress-strain-strain rate, suggested by Leroueil et al. (1985). As emphasised in Feng (1991), a CRS test can provide more direct

and accurate relationship between stress-strain, as the stress-strain curve can be continuously monitored. In general, a larger strain rate results in a higher effective stress at a certain strain and hence, the stiffness of soil increases with the increasing strain rate (Augustesen et al. 2004). Moreover, the influence of the strain rate on the pre-consolidation pressure is also observed.

2.3.3.1 Constant Rate of Strain (CRS) Tests

In a constant rate of strain (CRS) test, the total strain rate is kept constant throughout the test, while the stress is then monitored to determine the stress-strain relationship. In general, it can be observed that the effective stress at a constant strain rate increases with the increase in the loading rate, as depicted in Figure 2.3. In other words, the stiffness of the soil increases with the rising strain rate (Augustesen et al. 2004).

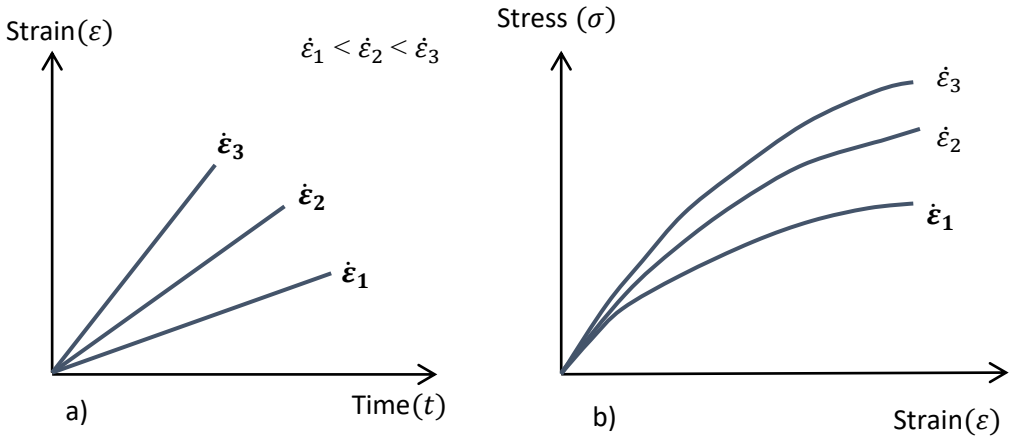

Figure 2.3: Constant rate of strain (CRS) tests: (a) Strain history, and (b) stress-strain response (after Augustesen et al. 2004)

Although CRS tests have some advantages compared to the standard oedometer tests, particularly in the relatively shorter test duration required for CRS tests, the major challenge in CRS tests is the difficulty in the selection of the imposed strain rate to obtain an appropriate stress-strain curve as an output. Hence, it is crucial to emphasise that a rational imposed strain

rate, based on the conventional primary consolidation data, is necessary in order to determine the information related to End of Primary (EOP) consolidation stress-strain relationship.

According to Leroueil et al. (1985), a unique relationship among stress – strain – strain rate is observed from a series of CRS tests, in one-dimensional and triaxial conditions, on Batisan clay (shown in Figure 2.4). Due to the fact that the stress-strain curve can be continuously monitored, the stress-strain relationship obtained from a CRS test is more direct and accurate (Feng, 1991). Figure 2.5 demonstrates the influence of strain rate on the stress-strain behaviour of overconsolidated Saint-Jean-Vianny clay, from the CRS tests conducted by Vaid et al. (1979). Furthermore, Figure 2.6 depicts the effects of various constant strain rates on peak strength and the size of the yield surface, as discussed in Augustesen et al. (2004).

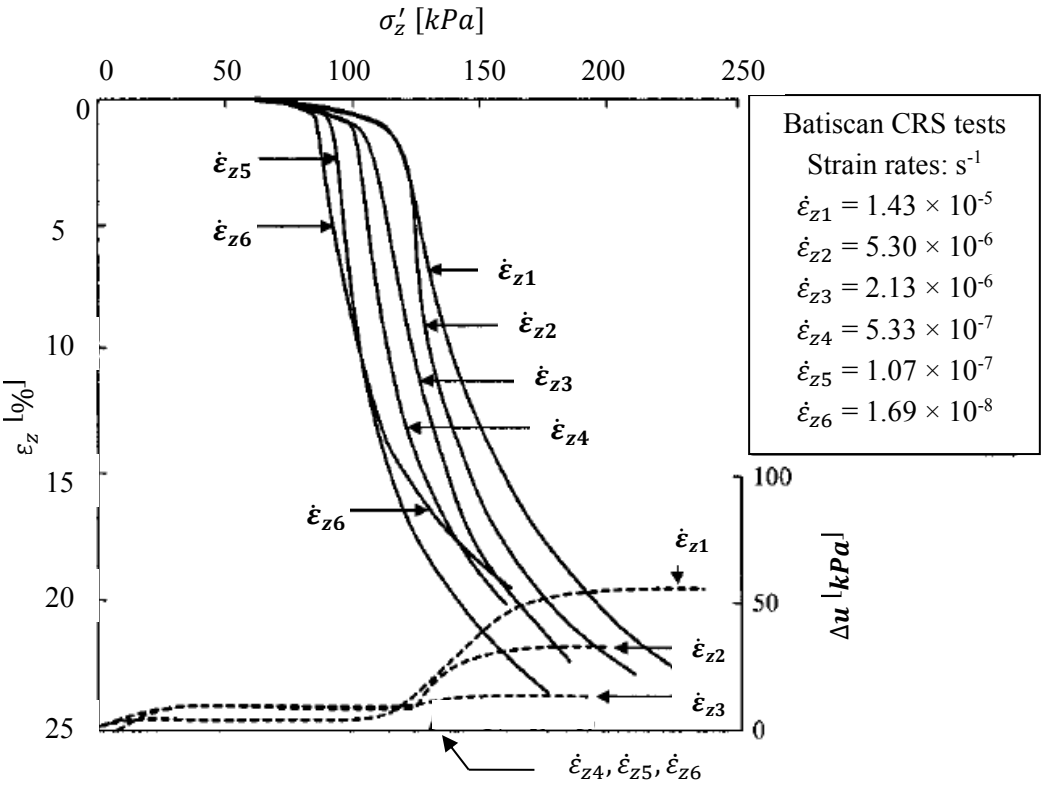

Figure 2.4: The results of the constant rate of strain tests on Batiscan clay (after Leroueil et al., 1985)

As shown in Figure 2.6, the corresponding yield surface related to the particular constant strain rate is denoted as 'static yield surface', which is one of the vital ingredients in the existing

constitutive EVP models developed based on Perzyna's overstress theory (discussed in details in the next section).

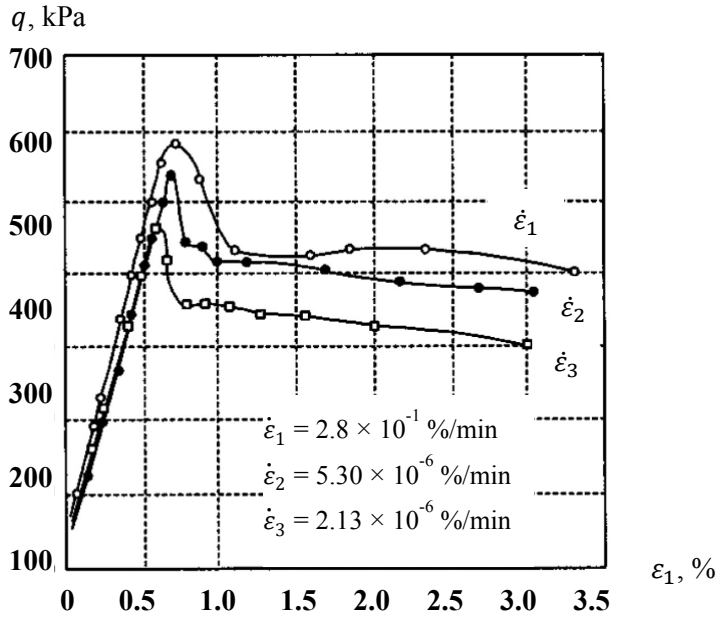

Figure 2.5: Stress-strain behaviour of Saint-Jean-Vianny Clay in undrained constant rate of strain tests (after Vaid et al., 1979)

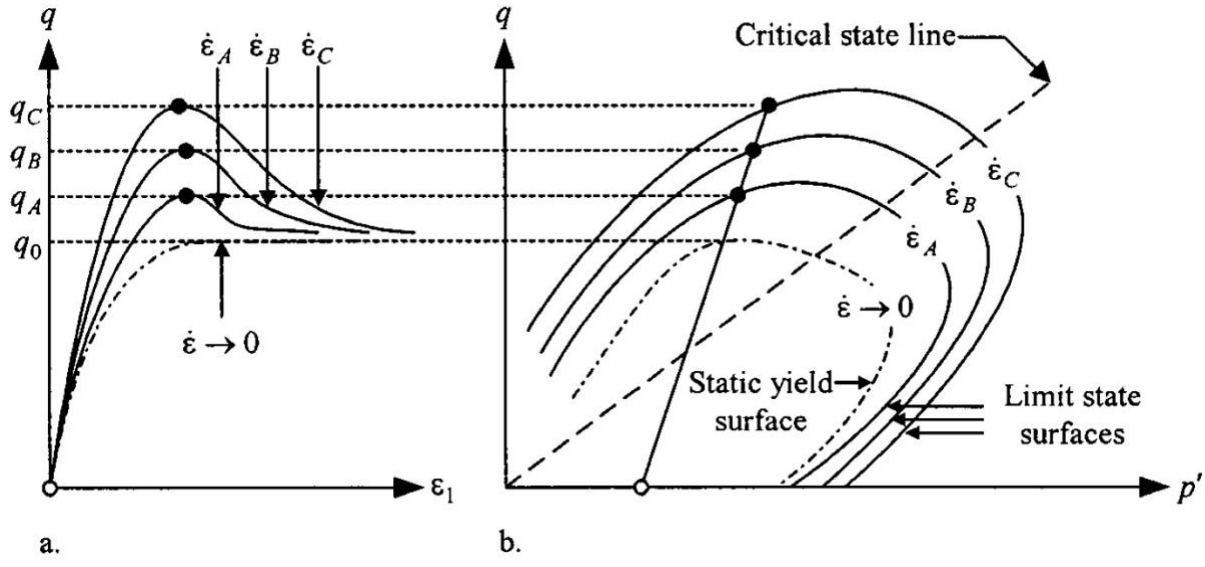

Figure 2.6: (a) Drained stress-strain curves for different constant rate of strain tests (q_A, q_B, q_c are peak strengths), (b) Strain rate effects on yield surface (after Augustesen et. al, 2004)

According to Leroueil (2006), the range of strain rates for different soils in in-situ state for corresponding strain rates from different laboratory measurements are shown in Figure 2.7. As demonstrated in Figure 2.7, the strain rates corresponding to the 24-hour incremental loading tests are relatively closer to the strain rates compared to the strain rates obtained from other tests.

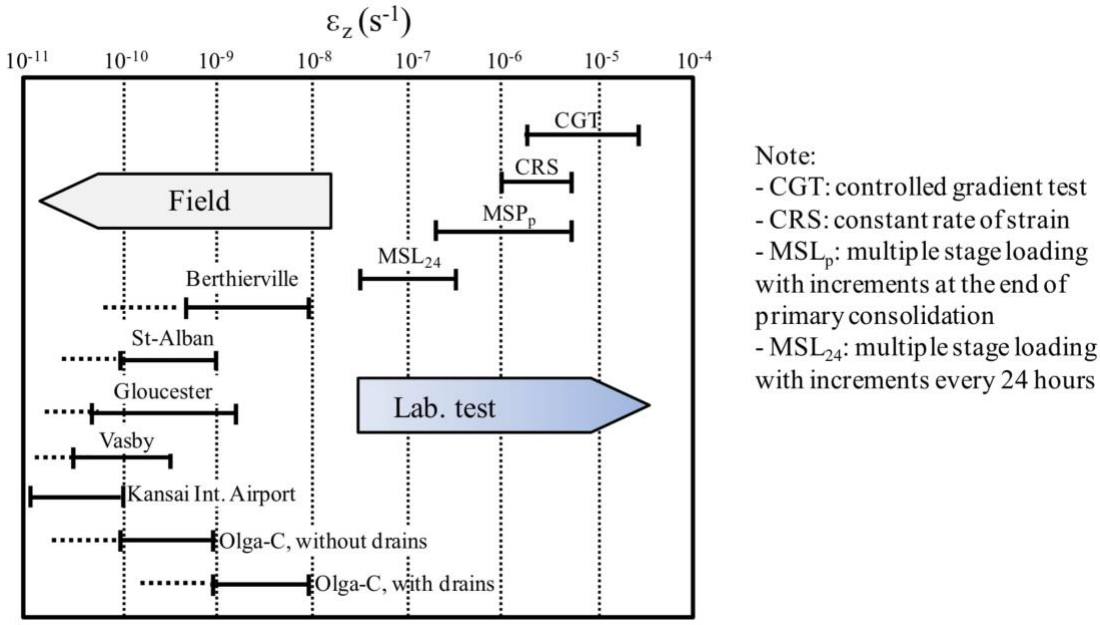

Figure 2.7: Ranges of strain rates in the in-situ state and laboratory tests (after Leroueil, 2006)

2.3.3.2 Change in Rate of Strain Tests

As in the CRS tests, a unique relationship is also obtained among the effective vertical stress, strain and strain rate in the specialised CRS tests, in which the strain rates are changed at various strain and maintained for a period of time. Based on the two tests conducted by Leroueil et al. (1985) on Batisan clay, the influence of the change in strain rate is continuous and the resulting curve stays on the same stress-strain graph during the step-changed strain rate tests, as shown in Figure 2.8.

2.3.4 Stress Effects

Depending on the applied stress level, three important types of time-depending compression curves are identified:

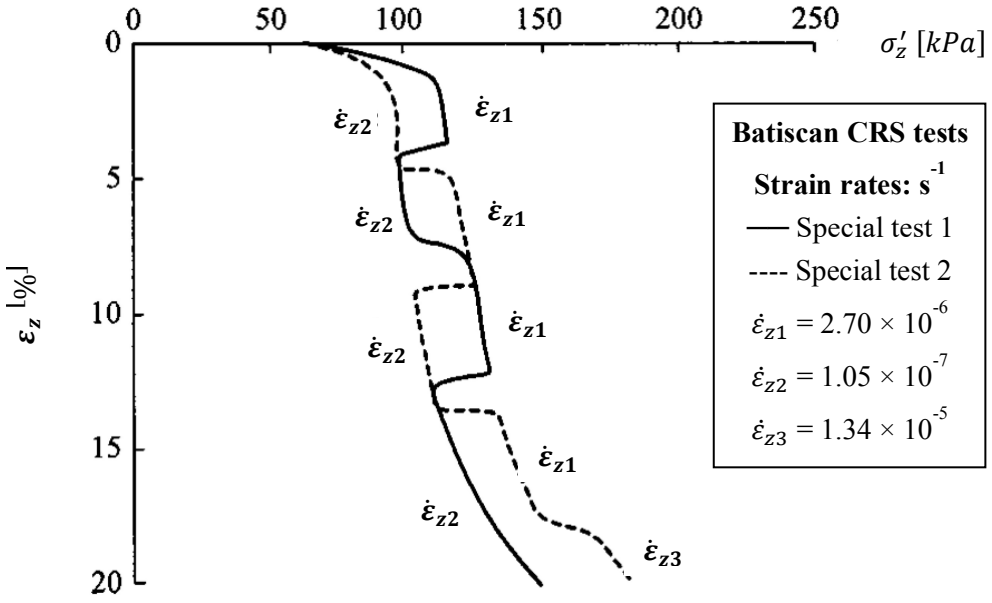

Figure 2.8: Special constant rate of strain oedometer tests on Batiscan clay (after Leroueil et al., 1985)

i) When the final effective stress is less than the pre-consolidation pressure, the compression is not significant and the slope of the compression curve progressively increases after EOP, as in the case of overconsolidated soils in Figure 2.9. The slope of the corresponding strain rate curve decreases linearly with time.

ii) When the final effective stress is approximately equal to the pre-consolidation pressure, the slope of the compression curve after the EOP is higher than the corresponding value observed in Type (i). When the effective stress increases from the overconsolidated range to the normally consolidated range, similar compression curve is observed.

iii) When the effective stress is within the normally consolidated range, as commonly observed in the behaviour of soft soils, the compression is excessive during the

excess pore water pressure dissipation, and the slope of the corresponding strain rate curve after EOP keeps decreasing with time.

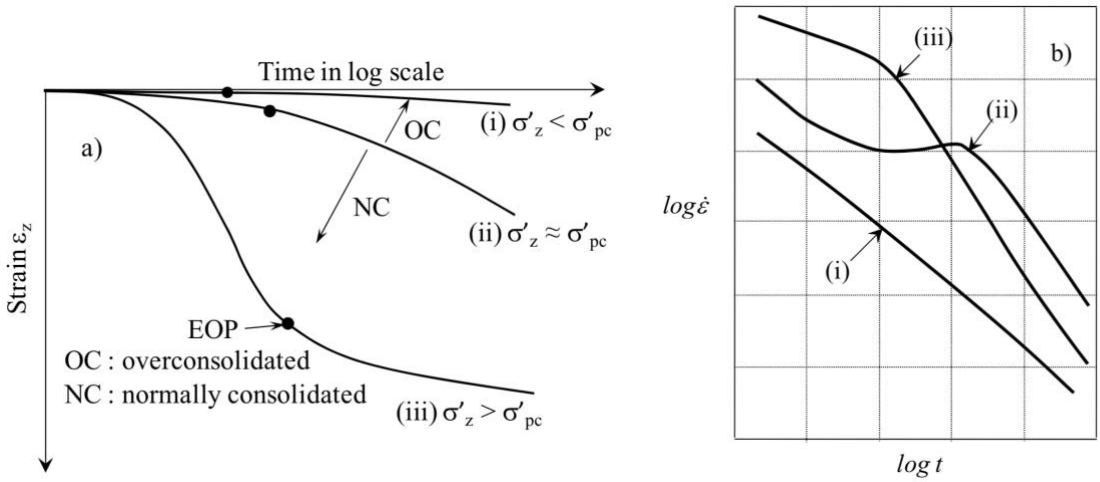

Figure 2.9: (a) Types of compression curves dependent on the stress level (after Leroueil et al., 1985); (b) the corresponding strain rate (after Augustesen et al., 2004)

2.3.5 Stress Relaxation

Stress relaxation is a process, in which the decrease in effective stress with time at a constant value of strain. As depicted in Figure 2.10, a stress relaxation test is conducted, in which the stress relaxation process is commenced at Point 1 by maintaining the identical total strain over a certain time period. As time progresses, the stress-strain rate moves towards Point 2. During this process, the gradual decrease in effective stress is observed, which is called stress relaxation.

Stress relaxation tests are usually conducted using triaxial apparatus in order to observe the variation in the deviatoric stress under constant strain level (Drumright and Nelson, 1985; Yin and Cheng, 2006). Based on the observations discussed in Silvestri et al. (1988), the deviatoric stress reached the stabilised stress relaxation level in less than 1 day from the stress relaxation tests performed on Louiseville clay. Based on the observation and the analysis of

several triaxial stress relaxation test data, the normalised deviatoric stress q/q_0, i.e. the ratio of the deviatoric stress q at time t and the deviatoric stress at the beginning of stress relaxation q_0, decreases linearly with the increase in logarithm of time after an initial time period, as shown in Figure 2.11 (Lacerda and Houston, 1973).

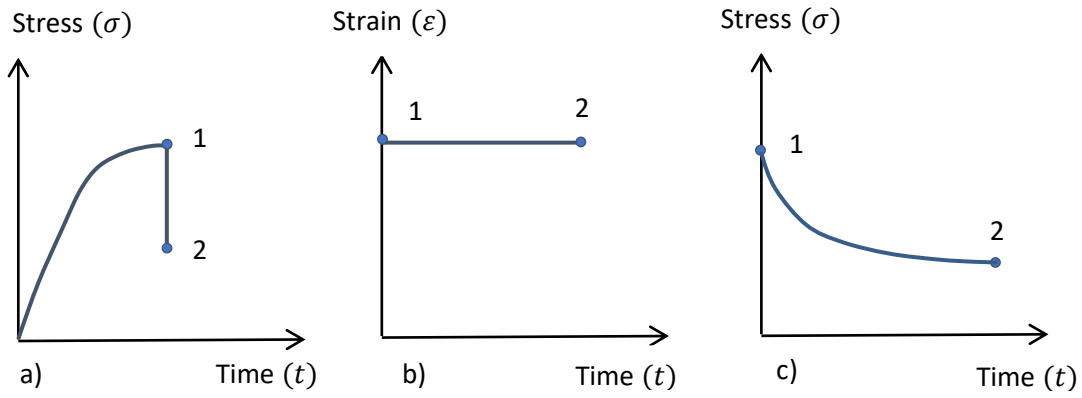

Figure 2.10: Stress relaxation test (A→B): (a) Stress-Strain relationship; (b) strain history; (c) stress history (after Wood, 1990)

Moreover, Yin and Cheng (2006) also observed that the corresponding strain rate at the beginning of the test had an impact on when the stress-relaxation commenced from the triaxial tests performed on Hong Kong marine clay. Hence, it can be concluded that the slower the initial strain rate, the longer it takes for the stress relaxation process to commence (Lacerda and Houston, 1973). Similar laboratory observations were also reported in Graham et al. (1983) and Fodil et al. (1997). It was suggested that the curve joining the stress relaxation states would represent a "static effective stress state", analogic to the term "static yield surface" in the Perzyna's overstress theory (Perzyna 1963; 1966). Furthermore, it was observed that the excess pore water pressure remained almost constant during the undrained stress relaxation tests, as stress relaxation tests were mostly conducted under undrained conditions (Lacerda and Houston, 1973; Sheahan et al. (1994)).

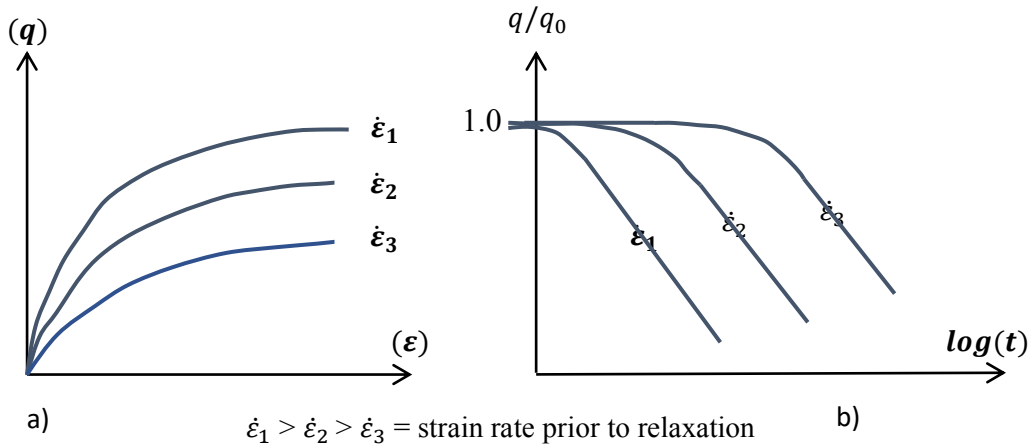

Figure 2.11: Stress relaxation: (a) Stress-strain diagram for three different relaxation tests; (b) stress decay versus log time for the stress relaxation tests (after Augustesen et al. 2004)

2.3.6 Consolidation and Creep – Hypotheses A and B

In the past several decades, a plethora of approaches have been developed for the simulation of time-dependent behaviour of soft soils. In the existing EVP models, some researchers have insisted that the total strain rate is decomposed into elastic strain rate, plastic strain rate and viscoplastic strain rate, whilst others have considered that the total strain rate is divided into elastic strain rate and viscoplastic strain rate. The former approach is so-called Hypothesis A, and the latter is denoted as Hypothesis B, respectively. Hypothesis A mainly assumes that creep only occurs after the end of primary consolidation, i.e. after complete dissipation of pore water pressure. Hypothesis A has been adopted in Ladd et al. (1977), Mesri and Godlewski (1977), and Mesri and Choi (1985). Hypothesis A has suggested that the value of void ratio at the end of primary consolidation (e_{EOP}) is unique regardless of the thickness of the soil sample, drainage conditions and loading duration. Although the time taken to reach the end of primary consolidation (t_{EOP}) is longer for the thick sample compared to that of the thin sample, the void ratios of both samples remain the same, as illustrated in Figure 2.12.

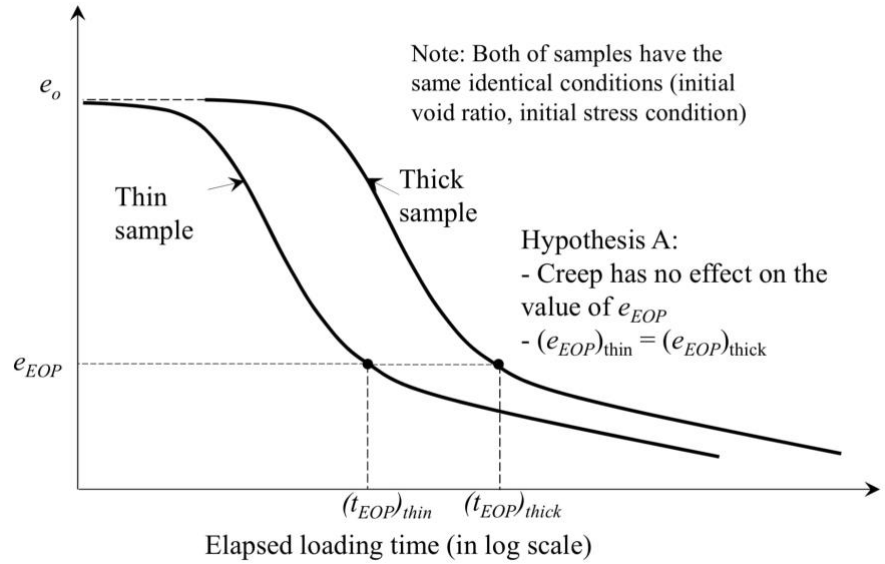

Figure 2.12: Void ratio versus time for thick and thin samples using Hypothesis A (after Le et al. 2015)

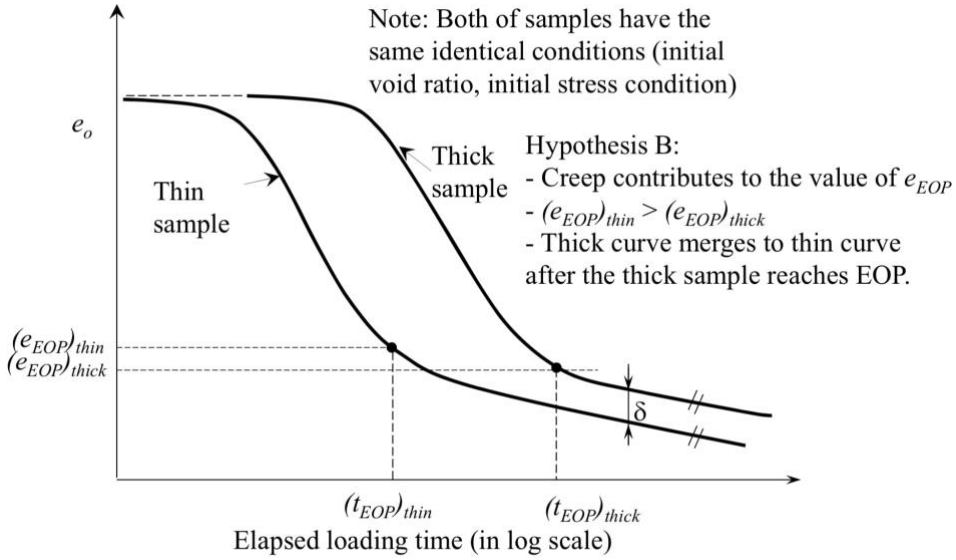

Figure 2.13: Void ratio versus time for thick and thin samples using Hypothesis B (after Le et al. 2015)

In Hypothesis B, it is assumed that secondary compression occurs during the whole consolidation process. Hypothesis B has been supported by Suklje (1957), Bjerrum (1967), Leroueil et al. (1985) and Yin (1999). In contrast to Hypothesis A, Hypothesis B insists that the longer it takes to reach the end of primary consolidation results in more compression under

a particular effective stress. Therefore, the void ratio at t_{EOP} (i.e. e_{EOP}) for a particular applied stress depends on the thickness of the soil sample, drainage conditions and loading duration. Consequently, the e_{EOP} of thin sample tends to be higher compared to that of the thick sample due to its shorter drainage path and t_{EOP}, as depicted in Figure 2.13.

According to Ladd et al. (1977), the compression curves for both thin and thick samples merge together with time. In contrast, Aboshi (1973) suggested that the compression curve after the end of primary consolidation continue to be parallel, based on the laboratory observations.

As a result, two suggestions potentially exist at the end of primary consolidation:

1) Both compression curves merge together with time
2) Both compression curves continue to be parallel with time

Figure 2.14 further illustrates the contradicting nature of Hypotheses A and B based on the compression curves at the end of primary consolidation. The adoption of Hypothesis A results in a unique e_{EOP}, thus leading to a unique value of pre-consolidation pressure (σ'_{pc}) for a particular soil. In contrast, the adoption of Hypothesis B results in the reduction of pre-consolidation pressure (σ'_{pc}) due to the accumulation of secondary compression with the increasing thickness of the sample; hence, causing the EOP stress-strain curve to shift downward, as portrayed in Figure 2.14.

Therefore, the major difference between Hypotheses A and B is the influence of the soil sample thickness on the induced secondary compression with time. As indicated in Figure 2.14, the thickness of the soil sample has a significant influence on the pre-consolidation pressure, drainage path and t_{EOP}, and hence, on the predictions of the total settlement. However, the real

soil behaviour lies somewhere between these two extreme hypotheses A and B, based on the experimental observations performed by Aboshi (1973).

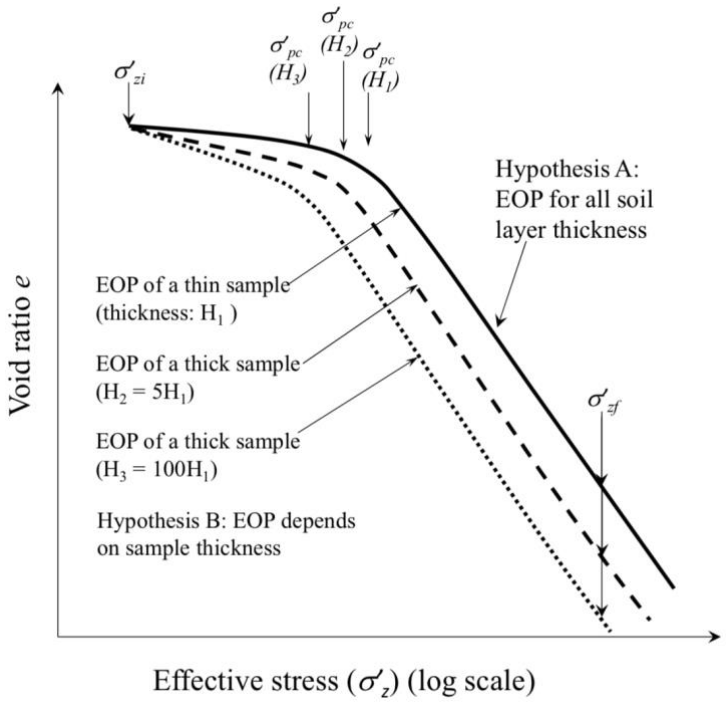

Figure 2.14: Void ratio versus effective stress at the end of primary consolidation (after Jamiolkowski et al., 1985)

2.4 Modelling Time-dependent Behaviour of Soils

As proved in Casagrande and Wilson (1951), Tavenas et al. (1978) and Graham, Crooks and Bell (1983), the observed stress-strain behaviour of clays and natural soils is time-dependent. Moreover, Bjerrum (1967) pointed out that the time dependency on the stress-strain behaviour of soils, especially highly plastic clays, is generally too significant to be ignored. Therefore, the constitutive modelling of time-dependent behaviour of soils has attracted much attention towards the geotechnical research community in the past decades. As a variety of mathematical models have been developed to capture the time-dependent effects in geological

materials, particularly soils, these can be categorised into three major approaches; (i) the empirical models, the rheological models, and general constitutive stress-strain-time/strain rate models, as shown in Figure 2.15 (Liingaard et al., 2004).

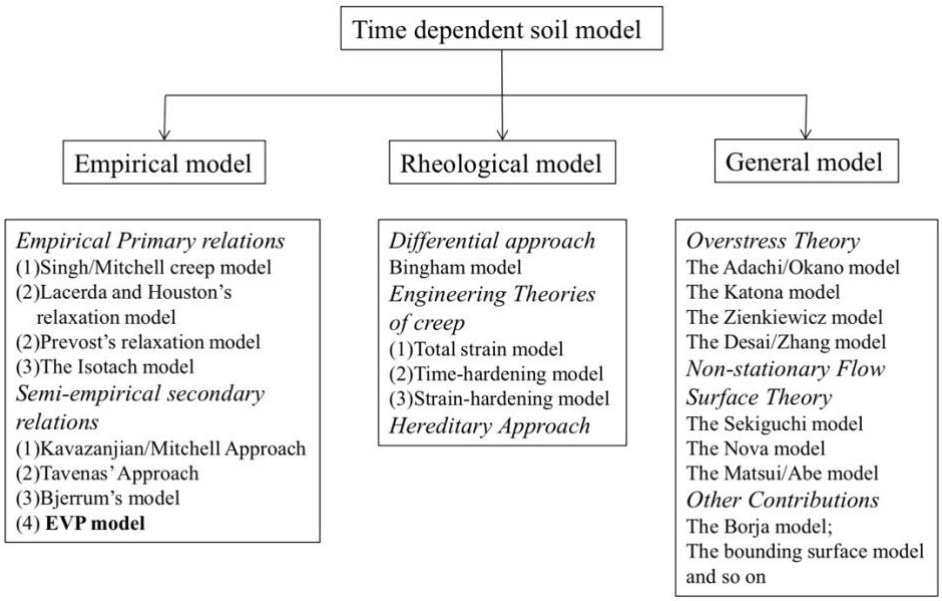

Figure 2.15: Classification of Time-dependent soil models (after Liingaard et al., 2004)

2.4.1 Empirical Soil Models

The empirical laws are directly obtained by fitting experimental data from creep, stress relaxation, and CRS tests in order to develop empirical relations to describe the time-dependent behaviour of soils. In general, these constitutive relationships are expressed in closed-form solutions or differential equations. The empirical relationships usually provide a reasonable approximation of the behaviour of soils and a good foundation for developing more sophisticated constitutive soil models. However, the arbitrary functions are strictly limited to a specific boundary and loading conditions, together with the time spans of a particular experiment, from which they are derived. Therefore, the empirical models are applicable to engineering problems, especially due to their simplicity, as long as the boundary conditions

comply with the ones in the laboratory experiments. According to Liingaard et al. (2004), the empirical models are classified as primary empirical relations and secondary semi-empirical relations.

2.4.1.1 Primary Empirical Models

The primary empirical relationships are generally derived from the fitting of observed laboratory data with simple mathematical functions, which can reproduce the actual behaviour of the test sample. However, they are often strictly limited to specific test phenomena. The empirical relations for creep are most commonly based on the semi-logarithmic law, which describes the secondary compression observed in oedometer tests against the logarithm of time.

One of the most common and simplest empirical models is based on the concept of constant coefficient of secondary compression $C_{\alpha e}$ or $C_{\alpha \varepsilon}$, defined in Mesri and Godlewski (1977) and Terzaghi and Karl (1996) as follows:

$$C_{\alpha e} = \frac{\Delta e}{\Delta \log t} \quad or \quad C_{\alpha \varepsilon} = \frac{C_{\alpha e}}{1 + e_i} \tag{2.1}$$

where, e_i is defined as initial void ratio and Δe is the change in void ratio. The parameters $C_{\alpha e}$ and $C_{\alpha \varepsilon}$ are the coefficients of secondary compression with respect to e and ε, respectively.

This empirical relationship in Equation (2.1) was modified by Ladd et al. (1977), to estimate the secondary settlement, as follows:

$$C_{\alpha \varepsilon} = \frac{C_\alpha}{1 + e_0} \quad \text{and} \quad S_s = C_{\alpha \varepsilon} H_0 \cdot \log \frac{t}{t_p} \tag{2.2}$$

On the other hand, Walker and Raymond (1968) defined the compression index from the laboratory tests on sensitive Leda clay, as follows:

$$C_{ce} = \frac{\Delta e}{\Delta \log(\sigma_z')} \quad or \quad C_{c\varepsilon} = \frac{C_{ce}}{1 + e_i} \tag{2.3}$$

where, σ_z' is the effective vertical stress and C_{ce} and $C_{c\varepsilon}$ are denoted as compression indices with respect to e and ε, respectively. Moreover, an average ratio for the value of C_α/C_c was reported to be approximately 0.025. As discussed in Mesri and Godlewski (1977), C_α not only depends on the applied effective vertical stress but also relates to the pre-consolidation pressure. Both the value of C_c and C_α increase with an increase in effective stress towards the pre-consolidation pressure, which then reach their corresponding peak values at or just beyond the pre-consolidation pressure, and afterwards, remain reasonably constant. The ratio of C_α/C_c remains approximately constant throughout the changes in effective stresses.

If the relationship in Equation (2.2) is applied to evaluate in terms of axial strains, Taylor (1942) have developed a well-known equation for secondary compression for a given soil, expressed as follows:

$$\varepsilon_z = C_{\alpha\varepsilon} \cdot \log \frac{t + t_0}{t_0} \tag{2.4}$$

where, ε_z is axial creep strain, t and t_0 are denoted as elapsed time and reference time, respectively. Besides, Yin (1999) presented the concept, in which the creep parameter varies with time. Consequently, the following modified logarithmic function from Equation (2.4) was introduced to describe the linear creep behaviour, as follows:

$$\varepsilon_z = \frac{\psi}{V} \cdot \ln \frac{t + t_0}{t_0} \tag{2.5}$$

The parameter V is the specific volume, defined as $V = 1 + e$, whereas ψ and ε_l are denoted as creep parameter and limiting creep strain, respectively. The relationship in. Equation (2.5) becomes non-linear logarithmic creep law when the ratio ψ/V depends on time, which is to be discussed in the next section.

Based on the primary empirical concept, various models have been proposed; for instance, the three-parameter viscosity model by Singh and Mitchell (1968), the stress-relaxation model for clay and sand by Lacerda and Houston (1973), the non-linear stress-relaxation model based on undrained triaxial tests by Prevost (1976), the viscous model based on strain rate approach by Leroueil et al. (1985) and the viscosity model proposed by Yin et al. (2011), which was subsequently extended to three-dimensional form, for the modelling of time-dependent behaviour of clayey soils.

One of the major benefits of primary empirical models is their ultimate simplicity. However, they are strictly restricted to the boundary conditions that are identical to the laboratory test conditions, from which the relationships are obtained, and are only applicable for one-dimensional conditions; for instance, logarithmic creep law proposed by Yin et al. (1999) causing creep to become infinite in infinite time and thus, resulting in the over-estimation of the long-term creep settlements due to its over-simplified assumption. Moreover, they can only describe certain particular aspects of the viscous behaviour of soil, rather than being able to express a wider variety of time-dependent characteristics of soil behaviour.

2.4.1.2 Secondary Semi-Empirical Models

Basically, the secondary semi-empirical models are the class of models obtained by merging one or more primary empirical models. These models are composed of closed-form solutions for the different time-dependent phenomena, as for instance, they are capable of capturing both creep and stress relaxation behaviour with one particular model. To some extent, these models can be employed as stress-strain-time or stress-strain-strain rate models to reproduce more than one characteristic of time-dependent behaviour of soils.

One of the first semi-empirical models was introduced by Kavazanjian and Mitchell (1977), based on the decomposition of volumetric and deviatoric strains into instantaneous and

delayed components to describe the multi-axial stress-strain-time behaviour of fine-grained soils. Similarly, based on the laboratory test results on lightly overconsolidated clay, Tavenas et al. (1978) decomposed time-dependent deformation into volumetric and deviatoric components, expressed as follows:

$$\dot{\varepsilon}_v = B \cdot f(\sigma'_{ij}) \cdot \left(\frac{t_0}{t}\right)^m \tag{2.6a}$$

$$\dot{\varepsilon}_q = A \cdot g(\sigma'_{ij}) \cdot \left(\frac{t_0}{t}\right)^m \tag{2.6b}$$

where, A and B are material parameters that reflect composition, structure and stress history of soil and m is the power law constant that controls the rate at which the strain rate decreases with time. The stress functions $f(\sigma'_{ij})$ and $g(\sigma'_{ij})$ are expressed in terms of the current effective stress state σ'_{ij} related to the yield surface. This approach has been further studied and improved upon by several researchers, including Feda (1992), Lade and Liu (1998) and Tatsuoka (2000).

Besides, Bjerrum (1967) insisted that the compressions should be classified as "instant" and "delayed" components; the former is the volume change due to the increase in the effective stress, and the latter deals with the deformation under a constant effective stress, as illustrated in Figure 2.16. The major assumption is that the change in void ratio comprises of three components: (i) the elastic change (e), (ii) the time-independent elastic-plastic reaction of the soil skeleton to effective stress changes (ep), and (iii) the time-dependent change at constant effective stress (c). Consequently, Bjerrum (1967) developed a system of lines to represent the relationship between compression, applied stress and time, as depicted in Figure 2.17, based on two baselines:

(i) A system of parallel timelines or curves defined in a logarithm of effective vertical stress versus void ratio, where each line represents the void ratio

equilibrium for different vertical stress values at a given time of sustained loading,

(ii) A unique relationship between effective vertical stress, void ratio and time.

The Bjerrum's time-line concept was formulated in terms of logarithmic functions by Garlanger (1972), expressed as follows:

$$e = e_0 - C_r \log\left(\frac{\sigma'_{z,pc}}{\sigma'_{z,0}}\right) - C_c \log\left(\frac{\sigma'_z}{\sigma'_{z,pc}}\right) - C_\alpha \log\left(\frac{t + t_0}{t_0}\right) \quad (2.7)$$

where, C_r is the slope on $e - \log \sigma'_z$ diagram of the compression line from $\sigma'_{z,0}$ to $\sigma'_{z,pc}$, C_c is the slope of the instant compression line, C_α is the slope of the $e - \log t$ curve, e and e_0 are the void ratio and the initial void ratio, respectively. Similarly, σ'_z and $\sigma'_{z,0}$ are the current effective vertical stress and the initial effective vertical in-situ stress, respectively, whereas, t_0 is the time corresponding to the instant compression line and t is the sustained loading time.

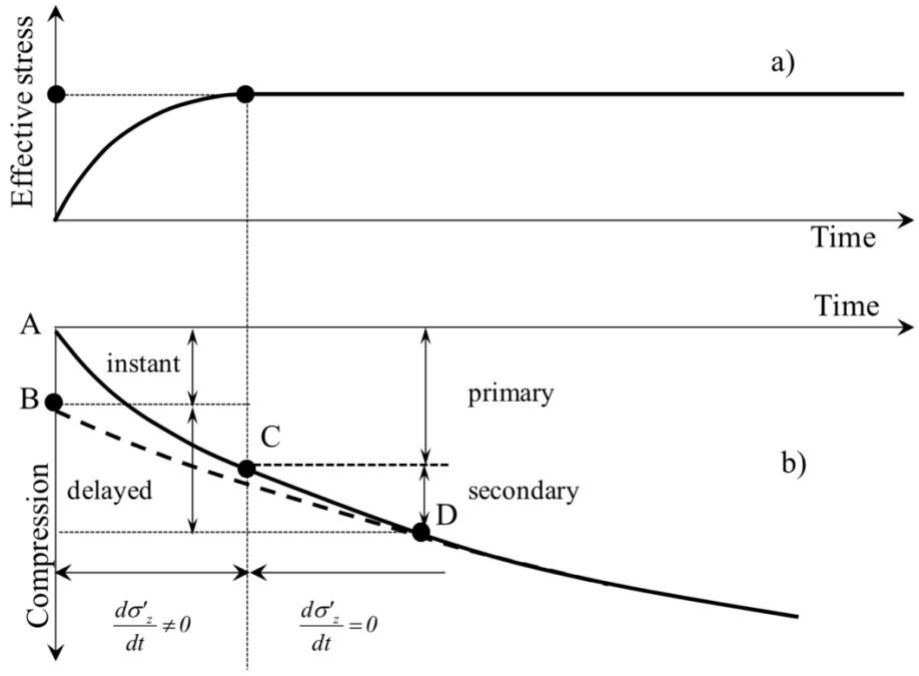

Figure 2.16: Definition of instant compression and delayed compression compared to primary and secondary compression (after Bjerrum, 1967): (a) the change in effective stress; and (b) compression versus time

However, the individual handling of time-dependent deformations from plastic deformation is irrational, as only combined aspects of plastic deformation may be measurable (Zienkiewicz and Cormea, 1974). Moreover, the Bjerrum's formulation is based on logarithmic laws, whose major drawbacks have previously been discussed, such as the over-estimation of long-term settlements.

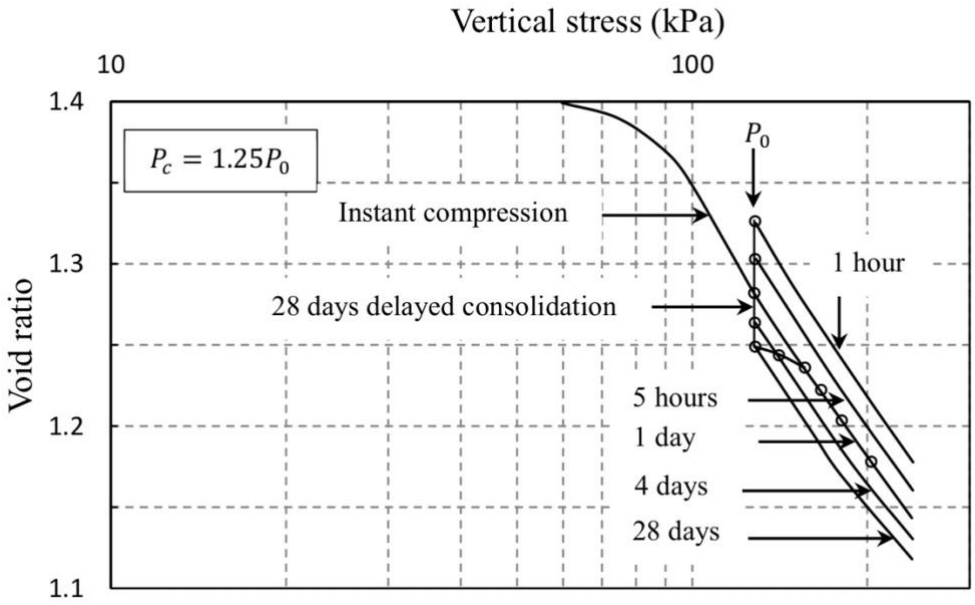

Figure 2.17: Bjerrum's Time-line system (after Bjerrum, 1967)

Later, Yin and Graham (1989, 1994) have proposed 'equivalent timeline' concept based on the 'timeline' idea introduced by Bjerrum (1967). According to Yin (1990), timelines are the lines with the same values of 'equivalent time' t_e, other than the loading duration t, which is different from the concept of Bjerrum (1967) and Garlanger (1972). Therefore, the resulting timeline system introduces an instant timeline, a reference timeline and a set of equivalent timelines with a unique creep strain rate defined by a unique value of t_e. Initially, the creep formulation was described by Equation (2.5), in which the loading duration t is replaced by 'equivalent time' t_e. Due to the fact that the linear creep compression continues to infinity with time, the linear creep formulation was improved by Yin (1999), in which ψ/V is not only time-

dependent but also stress-dependent. Additionally, the creep strain limit ε_l^{vp} was introduced in the non-linear creep function, expressed as follows:

$$\varepsilon_z^{vp} = \frac{{}^{\psi_0}/_{V}}{1 + \frac{{}^{\psi_0}/_{V}}{\varepsilon_l^{vp}} \cdot \ln\frac{t_e + t_0}{t_0}} \cdot \ln\frac{t_e + t_0}{t_0} \tag{2.8}$$

where, the linear constant ψ/V in Equation (2.5) is replaced by:

$$\frac{\psi}{V} = \frac{{}^{\psi_0}/_{V}}{1 + \frac{{}^{\psi_0}/_{V}}{\varepsilon_l^{vp}} \cdot \ln\frac{t_e + t_0}{t_0}} \tag{2.9}$$

where, ε_z^{vp} is the creep strain, ${}^{\psi_0}/_{V}$ is the creep coefficient, ε_l^{vp} is the creep strain limit and t_e and t_0 are the equivalent time and the reference time, respectively. Hence, the non-linear creep function in Equation (2.8) addresses the major drawback of the linear logarithmic creep formulation in Equation (2.5), as the resulting creep strain approaches its limit, with the time reaching infinity; thus, capturing the decreasing strain rate with time. Subsequently, Yin (1990) and Yin and Graham (1999) developed three-dimensional EVP models using the 'equivalent timeline' approach. Although these non-linear EVP models have many merits in describing the time-dependent behaviour of soft soil, the difficulties and uncertainties still exist in the parameter determination, with model parameters not being related to the physical phenomena of soils.

2.4.2 Rheological Models

The term 'rheological' models is often used in the description of linear visco-elastic behaviour of materials. Although the rheological models are typically developed for metals,

steel and fluids, they have been, to some extent, used in studying the time-dependent characteristics of geomaterials. Typical rheological models consist of arrangements, including springs, sliders and dashpots, to represent soil behaviour, i.e. elastic, viscous, or plastic behaviour; for instance, Gibson and Lo (1961)'s model based on the Maxwell model, the Barden (1965)'s model as an extended Kelvin-Voigt model, and the Rijot (1922)'s model as an extended Bingham model, as shown in Figure 2.18.

The first conceptual approach to estimate secondary compression was proposed by Gibson and Lo (1961), as a modification of Terzaghi (1923)'s consolidation theory, in which it was assumed that a linear spring with a Kelvin element, retarded by the viscosity of the dashpot. The former linear spring element was used to model the instantaneous compression that represents primary compressibility, while the latter dashpot element is related to the secondary compression.

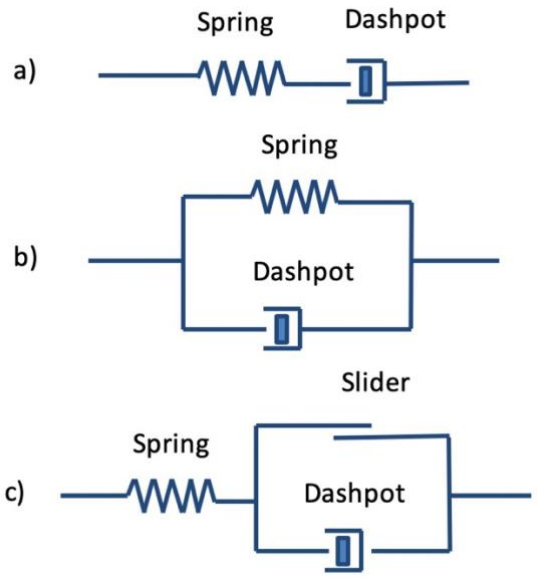

Figure 2.18: Rheological Models: a) Maxwell model; b) Kelvin-Voigt model; and c) Bingham model

In disagreement to the Terzaghi's consolidation theory, Barden (1965) highlighted the fact that creep is present during primary consolidation stage, and the loading conditions bear

an influence on the total settlement. Consequently, Barden (1965) proposed a system with a non-linear spring and dashpot (Figure 2.19a), in which the load increment was carried by the linear spring, the dashpot and the excess pore pressure. Afterwards, Barden (1965) simplified his model by assuming a linear spring, along with the adoption of Kelvin's element, as shown in Figure 2.19b. Although the resulting model depicts creep behaviour reasonably well, it should be noted that the yielding of the soil skeleton, as well as non-linear stress-strain behaviour of soils are not considered.

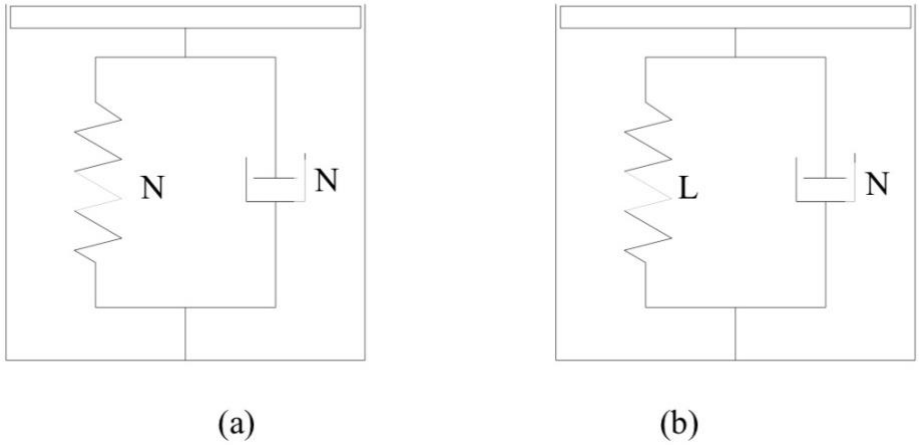

Figure 2.19: Rheological models proposed by Barden: (a) Barden's proposed non-linear model; and (b) Barden's simplified model (after Barden, 1965) (Note: N and L denote non-linear and linear, respectively)

The above rheological models were improved upon by Rajot (1992), by introducing a mechanism involving two springs, a dashpot and a slider to simulate the observed phenomena of timelines, including secondary compression and stress relaxation. The instantaneous compression, i.e. elasto-plastic, is represented by an elastic spring and a rigid plastic slider, in which the recoverable changes in volume are simulated by the deformation of the spring and the instantaneous irrecoverable changes in volume that occur when the effective vertical stress goes beyond the effective yield stress, are simulated by the deformation of the slider. On the other hand, the time-dependent non-recoverable changes in volume, i.e. creep, are simulated

by the extended Kelvin element. As a result, the instantaneous compression and the simultaneous plastic creep deformation are formulated by placing the spring and slider in series with the extended Kelvin element, as in Figure 2.20. In general, the schematic representation of the response of springs, dashpots and sliders, to represent soil behaviour, is provided in Figure 2.21 (Liingaard et al., 2004).

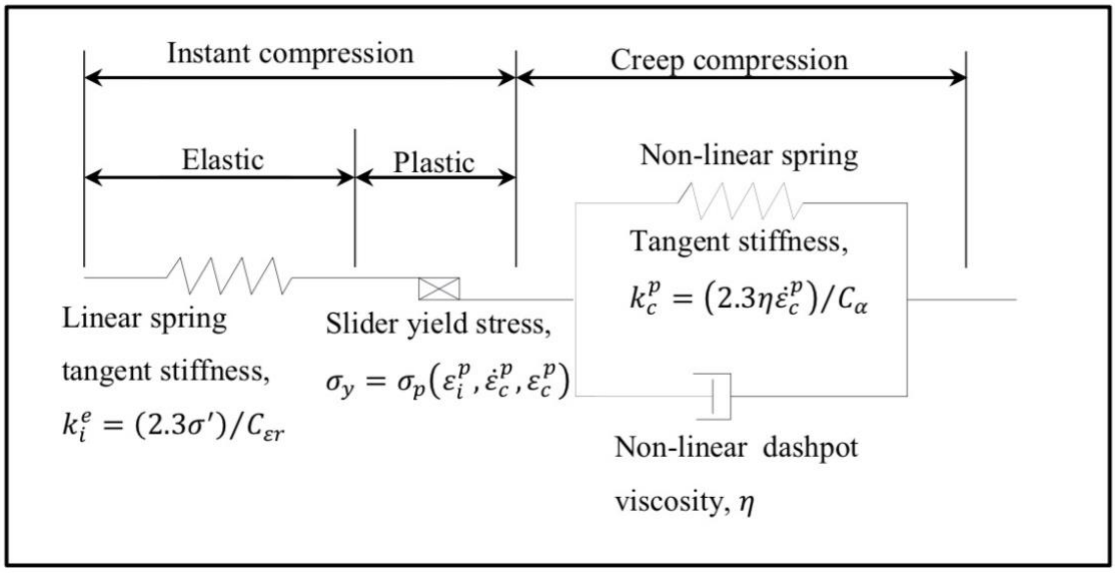

Figure 2.20: Rheological Model proposed by Rajot (1992) (after Perrone, 1998)

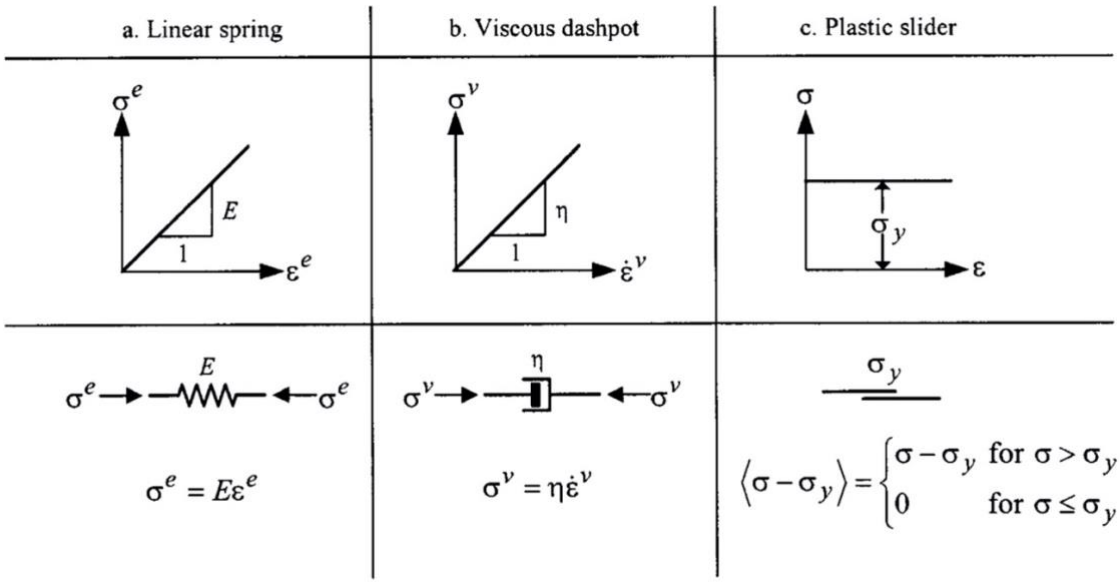

Figure 2.21: Schematic representation of typical rheological elements: a. Hookean linear spring; b. Viscous dashpot; and c. Plastic slider (after Liingaard et al., 2004)

Although these mathematical rheological models provide some intriguing insights and foundation for time-dependent effects, particularly creep and relaxation characteristics, they may not be sufficient to represent the quantitative behaviour of geomaterials, realistically. Since the spring, the dashpot and the slider are assumed to be linear, geomaterials, particularly soils, demonstrate highly non-linear elastic and plastic behaviour. Moreover, rheological models require too many parameters to describe the strain rate behaviour, along with the necessity of significant approximation on the governing equations in order to accommodate the time-dependent behaviour of soils. Furthermore, these models are not capable of capturing the effects of pre-consolidation pressure; thus, resulting in the requirement of unfamiliar model parameters that cannot be directly determined from standard laboratory testing procedures.

2.5 Constitutive Models for Soil Behaviour

A general constitutive soil model can be expressed in the following form:

$$d\varepsilon = F(d\sigma, dt) \tag{2.10}$$

where, $d\sigma$ and dt are denoted as changes in the effective stresses, i.e. not total stresses, as in the models for other materials, such as concrete and steel, and time, respectively. Since the development of most constitutive soil models have been based on the experimental results using axi-symmetric condition, e.g. triaxial and oedometer tests, the Cambridge parameters for stress and strain are used for the description of stress-strain behaviour. For simplicity, it follows that:

$$p' = \frac{(\sigma_1' + 2\sigma_3')}{3} \tag{2.11a}$$

$$q = (\sigma_1' - \sigma_3') \tag{2.11b}$$

$$\varepsilon_v = (\varepsilon_1 + 2\varepsilon_3) \tag{2.11c}$$

$$\varepsilon_q = \frac{2(\varepsilon_1 - \varepsilon_3)}{3} \tag{2.11d}$$

where, the subscripts 1 and 3 refer to axial and radial directions, respectively. The parameters p' and q are mean effective and deviatoric stress components, respectively; whereas ε_v and ε_q are volumetric and shear strains, respectively. In general, the bulk modulus K and the shear modulus G are expressed using these parameters as follows:

$$K = \frac{\dot{p}'}{\dot{\varepsilon}_v} \tag{2.12a}$$

$$3G = \frac{\dot{q}}{\dot{\varepsilon}_q} \tag{2.12b}$$

According to Graham and Houlsby (1983) a general constitutive equation for soil can be expressed as follows:

$$\begin{bmatrix} \dot{\varepsilon}_v \\ \dot{\varepsilon}_q \end{bmatrix} = \begin{bmatrix} 1/K & 1/J \\ 1/J & 1/3G \end{bmatrix} \begin{bmatrix} \dot{p}' \\ \dot{q} \end{bmatrix} \tag{2.13}$$

Where, J results in cross-coupling between volumetric and deviatoric components. The coupling modulus in Equation (2.13) is being considered as $J = \pm\infty$ when only isotropic consolidation conditions are considered. In such case, the bulk modulus and the shear modulus become elastic being defined based on Hooke's law and the constitutive elastic matrix can be extracted from Equation (2.13) as follows:

$$\begin{bmatrix} \dot{\varepsilon}_v \\ \dot{\varepsilon}_q \end{bmatrix} = \begin{bmatrix} 1/K & 0 \\ 0 & 1/3G \end{bmatrix} \begin{bmatrix} \dot{p}' \\ \dot{q} \end{bmatrix} \tag{2.14}$$

On the other hand, the elastic bulk and shear moduli can also be defined in terms of Young's modulus E and Poisson's ratio ν by the expressions $G = E/2 \cdot (1 + \nu)$ and $K = E/3 \cdot (1 - 2\nu)$, respectively.

2.5.1 Classical Constitutive Soil Models

In the 1960s, the early developments of constitutive soil models are often collectively referred to as Critical State Soil Mechanics (CSSM), initially introduced by Schofield and Wroth (1968), including three major concepts, i.e. the Critical State line (CSL), the State Boundary surface (SBS) and the normalisation with respect to pre-consolidation pressure, which became the foundation of Cam-Clay model developed by Roscoe, Schofield and Thurairajah (1963). However, the original Cam-clay model assumed that the energy dissipation was only due to plastic shear distortion, which was later found to be invalid for normally overconsolidated clay. As a result, Roscoe and Burland (1968) improved the original Cam-clay model to consider both plastic volumetric strain and plastic shear deformation in the dissipation of energy, and subsequently called as the modified Cam-clay (MCC) model (Figure 2.2(a)).

As illustrated in Figure 2.22, the yield locus of the MCC model is assumed to be in elliptical shape, which is expressed in the following form:

$$F = (p')^2 + \frac{q^2}{M^2} - p' \cdot p_c = 0 \tag{2.15}$$

Where, p_c is denoted as pre-consolidation pressure indicating the size of the yield surface dependent upon the stress history. The constitutive response for the plastic behaviour of soil can be derived by adopting SBS as a yield surface, together with the adoption of associated flow rule. It follows that:

$$\begin{bmatrix}\dot{\varepsilon}_v \\ \dot{\varepsilon}_q\end{bmatrix} = \begin{bmatrix}\dfrac{(\lambda-\kappa)(M^2(p')^2-q^2)}{pv(M^2(p')^2+q^2)}+\dfrac{\kappa}{pv} & \dfrac{2q(\lambda-\kappa)}{v(M^2(p')^2+q^2)} \\ \dfrac{2q(\lambda-\kappa)}{v(M^2(p')^2+q^2)} & \dfrac{4p'q^2(\lambda-\kappa)}{v(M^4(p')^4-q^4)}+\dfrac{1}{3G}\end{bmatrix}\begin{bmatrix}\dot{p}' \\ \dot{q}\end{bmatrix} \qquad (2.16)$$

Although the Cam-clay models provide a considerable benefit in modelling soil behaviour, they still have some drawbacks, most notably, the prediction of purely elastic behaviour inside the yield surface and the ignorance of the effects of immediate soil history. Consequently, it cannot provide reasonable accuracy in predicting the behaviour of heavily consolidated clay, particularly deviatoric strains, due to the former drawback. Moreover, it cannot describe anisotropic consolidation behaviour due to the symmetric nature of the shape of the yield surface about the p-axis.

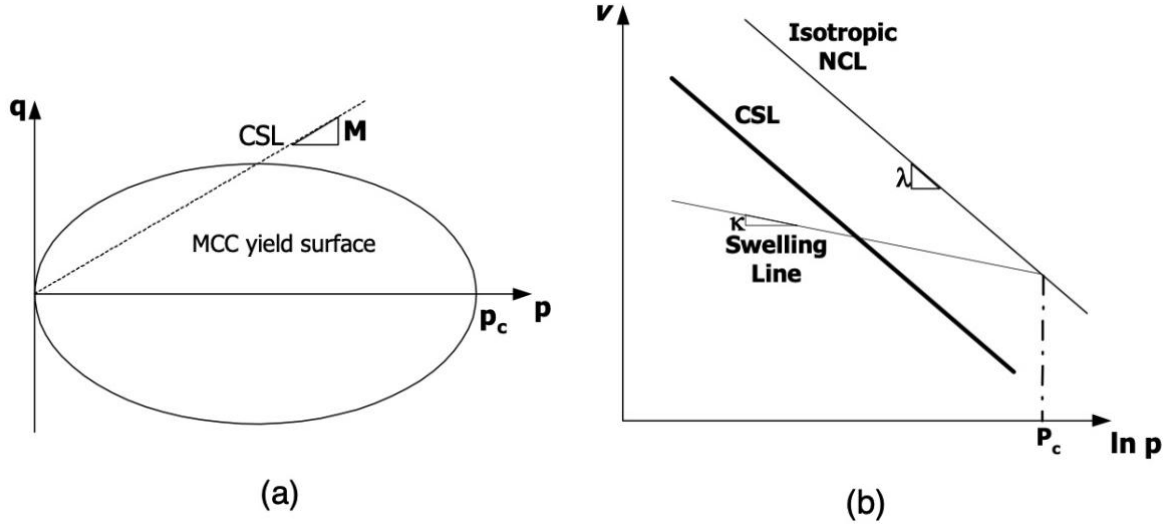

Figure 2.22: (a) Yield Locus of Modified Cam-clay model; (b) Critical State Soil Mechanics (Likitlersuang, 2006)

2.5.2 Advanced Constitutive Soil Models

For the past few decades, a large plethora of advanced constitutive soil models have been developed based on different approaches and concepts and often, a particular soil model exuded

its superiority and advantages over the others. However, the reality is that each model can be valid within its own realm, and that no universal constitutive model has yet been successful in predicting all materials under all possible conditions. As previously mentioned, it must be noted that all the constitutive models must obey certain principles, or axioms that govern the physical phenomena, such as conservation of mass, conservation of energy, and laws of thermodynamics.

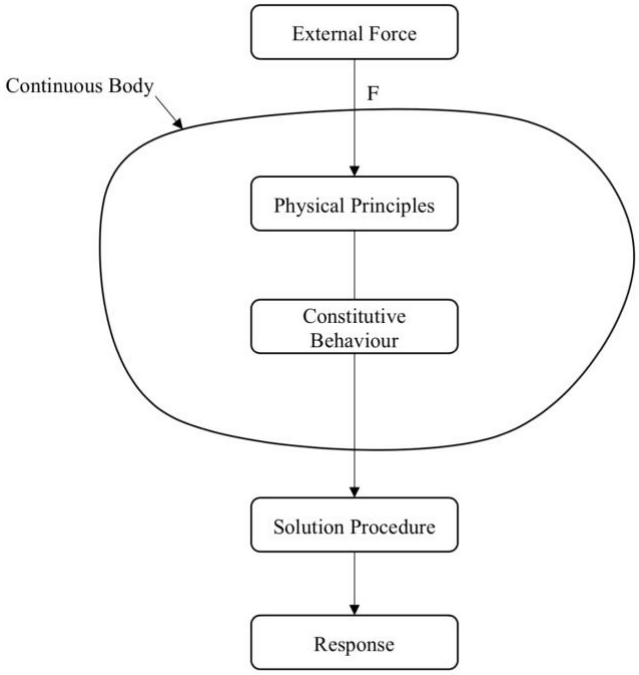

Figure 2.23: Place of constitutive laws and physical principles in continuum mechanics (after Desai and Siriwardane, 1984)

2.5.2.1 Multiple-Surface Constitutive Soil Models

To build upon the deficiencies associated with the CSSM, it was a necessary step to introduce plasticity within the State Boundary Surface (SBS) in order to be able to capture more realistic soil behaviour. Several approaches have been proposed and developed, in which there are two major concepts in introducing plastic strain inside the SBS. The first idea postulates a 'radial mapping rule', in which the current stress state inside the SBS is projected

onto a corresponding image point on an extra surface denoted as the bounding surface. The plastic constitutive response is derived from the hardening rule, which relates the stress inside the SBS and the image point on the bounding surface. The second one introduces multiple yield surfaces to describe a smooth transformation from elastic to plastic behaviour, along with the effects of recent loading history.

2.5.2.1.1 Bounding Surface Plasticity Model

The original bounding surface plasticity model was developed by Dafalias and Herrmann (1982), in which a 'radial mapping rule' was postulated to map the stress state inside the SBS to a correlating image point on the bounding surface. The SBS is defined as the MCC yield surface and the image stress point on the bounding surface is defined using a 'radial mapping rule' to project from the current stress state.

As illustrated in Figure 2.24, every stress point on the SBS is projected onto the image point on a bounding surface based on the mapping rule. The major assumption is that the soil behaviour is elastic, when the incremental stress vector is directed inside the bounding surface. If the incremental stress vector is directed outward from the loading surface, the behaviour becomes elasto-plastic. The schematic representation of the principles associated with bounding surface concept is illustrated in Figure 2.24.

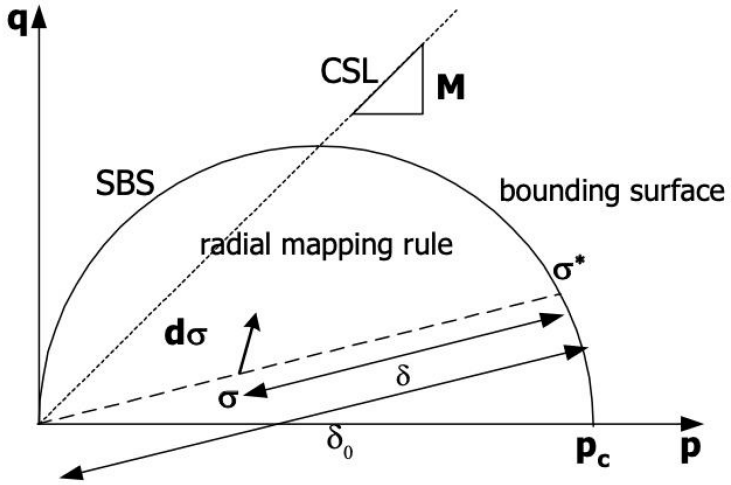

Figure 2.24: Schematic representation of the Principles of Bounding Surface Plasticity (after Dafalias and Herrmann, 1982)

Consequently, the plastic constitutive response is determined based on the postulated hardening rule using the relationship between the current stress and the image points, which is expressed in the following form:

$$H = H_p + H_0 \cdot \frac{\delta}{\delta_0 - c}\left[1 + \left|\frac{M}{\eta}\right|^n\right] \tag{2.17}$$

Where, H_p is defined as plastic stiffness at the image point, δ and δ_0 are the distance from the current stress point to the SBS and the radial distance measured between the SBS and the origin point passing through the current stress point, respectively. The remaining H_0 and n are the non-linear hardening parameters. The model can be retraced back to the MCC model when $\delta = 0$, i.e. the value of H becomes equal to H_p.

Although the models can predict smooth transitions in stiffness and are quite realistic for monotonic loading, they cannot describe unloading-reloading or a sudden change in the stress path. Several attempts have been made to improve on this aspect, most notably by introducing elastic hysteretic formulation in the MIT-E3 model developed by Hueckel and Nova (1979); 'recent stress history' in Atkinson, Richardson and Stallebrass (1990) and 'immediate past

history' in Houlsby (1999). The difference between 'recent stress history' and 'immediate past history' is that the former one takes into account of either an abrupt change in the stress path direction or the time taken at a constant stress state before an imposed variation in stress, whilst the latter considers only the change in the direction of the stress path. More recently, Russell and Khalili (2004) and Khalili et al. (2005) have introduced the bounding surface plasticity model based on the critical state soil mechanics framework, consisting of a unique three-part shaped critical state line to capture pseudo-elastic deformation, particle re-arrangement and crushing of particles, to successfully reproduce the stress-strain behaviour of many soil types under monotonic and cyclic loading conditions.

Besides, there have been attempts to incorporate the consideration of viscous effects into the bounding surface approach by adopting Dafalias and Herrmann mapping rule (Dafalias and Herrmann, 1982, 1986) and either the constant C_α concept (Borja and Kavazanjian, 1985; Kutter and Sathialingam, 1992) or the non-linear C_α concept (Islam, 2014). Moreover, Islam and Gnanendran (2017) have developed an elastic-viscoplastic constitutive soil model based on a bounding surface theory, along with the adoption of a critical-state soil mechanics framework. Although the bounding surface models are quite computationally efficient, they often have some shortcomings, including the need for a considerable number of arbitrary functions, (e.g. the mapping rule and the hardening function), that cannot be related to the physical aspects of the materials.

2.5.2.1.2 Kinematic Yield Surfaces Plasticity Model

In order to improve upon the deficiencies related to bounding surface plasticity, the concept of kinematic hardening surfaces was proposed to describe a more realistic response of overconsolidated soil. In this concept, a kinematic hardening surface, which encapsulates the elastic nucleus, is located within the SBS. The plastic strains will occur when the stress state

reaches the surface, in which the plastic strain increment is determined by means of plastic flow rule. Based on a kinematic hardening rule, the surface is then dragged until it comes into contact with the SBS. The simplest version of the kinematic yield surfaces model involves only two distinctive yield surfaces, illustrated in Figure 2.25. This double-surface kinematic hardening model is used to describe three important types of constitutive soil behaviour:

i) Fully elastic behaviour for stress states within the inner yield surface, i.e. the elastic surface

ii) Elastic-Plastic transition zone, for stress states on the elastic surface but inside the outer yield surface

iii) Fully plastic behaviour for stress states when the elastic surface comes into contact with the outer yield surface, i.e. the normally consolidated state.

The original two-surface kinematic hardening plasticity model was developed by Mroz (1967) and Iwan (1967), takes into account of isotropic and kinematic hardening effects. This was followed by the extension of two-surface model to include multiple kinematic hardening yield surfaces by Prevost (1978). Subsequently, Mroz and Norris (1982) have developed the multiple "nested" yield surfaces model, which is the best-known example to highlight the capability of multiple yield surfaces concept. The important assumption in the multiple "nested" yield surfaces model is that the yield surfaces are only allowed to touch each other tangentially, but not permitted to overlap each other. On the other hand, a number of researchers have attempted to develop elastic-viscoplastic constitutive models based on two or more yield surfaces, including Miao et al. (2008) and most recently, Aldo (2015).

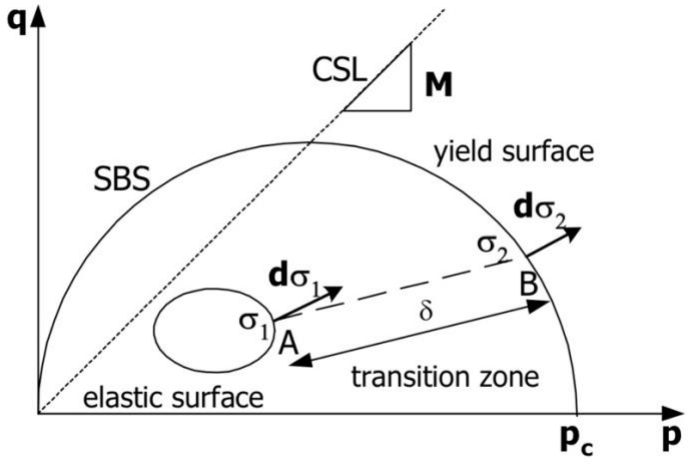

Figure 2.25: Schematic representation of the Principles of Kinematic Yield Surface Plasticity (after Mroz, 1967 and Iwan, 1967)

Although the multiple yield surfaces model can competently describe the effects of immediate loading effects of soil behaviour, they often require a substantial number of material parameters, leading to a sizeable extent of computational analysis.

2.5.2.2 Elastic Viscoplastic (EVP) Soil Models

Although the advanced non-linear elasto-plastic models have achieved success in predicting the behaviour of geotechnical materials to a considerable extent, these elasto-plastic models are not sufficient to describe the full extensive behaviour, such as the long-term excess pore pressure dissipation and undrained deformation, as they do not consider the time-dependent and the subsequent rate effects on the behaviour of geotechnical materials, particularly soils. Therefore, the advanced time-independent elasto-plastic models based on MCC model, have become incapable of describing the stress-strain behaviour of such soils to a more reasonable extent. Consequently, it has become widely accepted that a constitutive soil model should combine three important aspects, i.e. elasticity, plasticity and viscosity, to provide an accurate description of the stress-strain behaviour of soils.

Most of the existing EVP models have so far been based on the overstress EVP framework developed by Perzyna (1963, 1966) and the non-stationary flow surface theory proposed by Olszak and Perzyna (1966, 1970). The key assumption in the overstress approach is the negligence of viscous effects in the elastic region; in other words, viscous strains are not allowed to occur within the static yield surface. As a consequence, the total strain rate $\dot{\varepsilon}_{ij}$ is additively decomposed into the elastic strain rate $\dot{\varepsilon}_{ij}^{e}$ and viscoplastic strain rate $\dot{\varepsilon}_{ij}^{vp}$, i.e.

$$\dot{\varepsilon}_{ij} = \dot{\varepsilon}_{ij}^{e} + \dot{\varepsilon}_{ij}^{vp} \tag{2.18}$$

where, $\dot{\varepsilon}_{ij} = (i, j)$ component of the total strain-rate tensor.

The elastic strain rate $\dot{\varepsilon}_{ij}^{e}$ is assumed to follow the generalised Hooke's law and the viscoplastic strain rate $\dot{\varepsilon}_{ij}^{vp}$ is determined based on the flow rule, which is postulated as follows:

$$\dot{\varepsilon}_{ij}^{vp} = \gamma \langle \emptyset(F) \rangle \frac{\partial Q}{\partial \sigma_{ij}} \tag{2.19}$$

where, γ is a positive viscosity coefficient of the soil skeleton. The $\emptyset(F)$ is defined as a scalar function, denoted as viscoplastic flow function postulated based on experimental data. The function Q is called viscoplastic potential function, which is hypothesised based on either associated or non-associated flow behaviour, corresponding to the direction of $\dot{\varepsilon}_{ij}^{vp}$ with respect to the flow surface, as illustrated in Figure 2.26. The function F is a static yield function, which may be provided as follows:

$$F = \frac{f - K_s}{K_s} \tag{2.20}$$

where, f is the so-called dynamic loading function and K_s is a work or strain hardening parameter. The dynamic loading function f may be expressed in the following general form:

$$f = f\left(\sigma'_{ij}, \varepsilon^{vp}_{ij}, K_s\right) \tag{2.21}$$

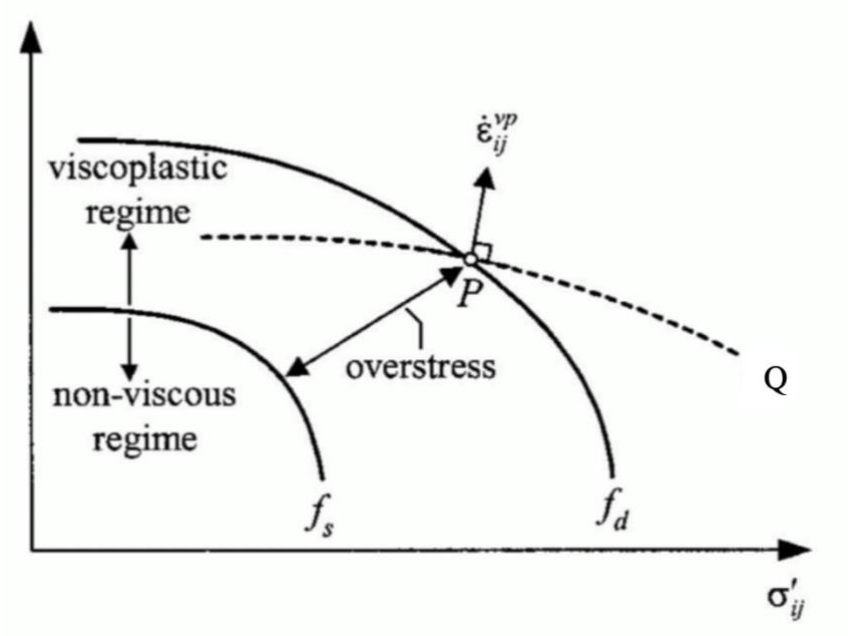

Figure 2.26: Schematic representation of the Overstress-type EVP Models (after Perzyna, 1963)

The overstress approach, which is also regarded as a generalisation of the model proposed by Hohenemser and Prager (1932), differs from the classical plasticity theory in that the consistency condition is not necessarily satisfied, which is of primary importance in the derivation of stress-strain response in the general plasticity theory. In general, there are two major forms of overstress function, i.e. the power overstress function and the exponential overstress function.

$$\emptyset(F) = \left(\frac{F}{F_0}\right)^N \tag{2.22a}$$

$$\emptyset(F) = \exp\left(\frac{F}{F_0}\right)^N - 1 \tag{2.22b}$$

where, N is an empirical constant and F_0 is used as a normalised constant to obtain a dimensionless flow function. Following the key assumption in the overstress-type models, i.e.

viscous effects are ignored in the elastic domain, the viscoplastic flow function is defined as follows:

$$\langle \emptyset(F) \rangle = \emptyset(F) \quad \text{for} \quad F > 0$$
$$\langle \emptyset(F) \rangle = 0 \quad \text{for} \quad F \leq 0 \tag{2.23}$$

A large number of EVP models have been developed to validate the overstress theory for various types of soils, including Adachi and Okano (1970) and Adachi and Oka (1982) to describe the time-dependent behaviour of fully saturated normally consolidated clay, Oka et al. (1988) for time-dependent behaviour of overconsolidated clay and Desai and Zhang (1987) to simulate the time-dependent behaviour of sand and rock salt. Moreover, Dafalias (1982, 1986) and Kaliakin and Dafalias (1990) have attempted to extend the overstress EVP models with the incorporation of Bounding Surface theory to predict the time-dependent behaviour of cohesive soils. A few of the other notable developments based on overstress approach includes Matsui and Abe (1988), Graham et al. (1983) and Yin et al. (2002).

However, the fundamental hypothesis of the conventional overstress models, i.e. the viscoplastic strains do not occur when the stress state is within the static yield surface, is observed to be in conflict with the experimental interpretation, which indicates that the viscoplastic strains always occur and thus, the static yield surface neve exists. Although the overstress-based EVP models can capture the effects of strain rate on the soil strength and pre-consolidation pressure of soils, the major difficulty lies in the arbitrary postulation of the overstress function, without the need to satisfy the consistency condition. Therefore, the overstress models often require a considerable number of assumptions and parameters without being related to the physical phenomena of soils.

On the other hand, the Non-Stationary Flow Surface (NSFS) theory is founded on the basic concept of inviscid theory of elasto-plasticity. The key difference between the NSFS

theory and the conventional plasticity theory lies in the definition of the yield condition. In the latter approach, the yield surface is time-independent when the plastic strains are held constant; in other words, the yield surface in the conventional plasticity theory is denoted as "stationary". In contrast, the former NSFS concept implies that the yield condition is time-dependent, and the yield surface becomes "non-stationary", which may be expressed as follows:

$$f = f\left(\sigma'_{ij}, \varepsilon_{ij}^{vp}, \beta_s\right) = 0 \tag{2.24}$$

where, ε_{ij}^{vp} and β_s are viscoplastic strains and a time-dependent function, respectively. It can be implied from Equation 2.24 that the yield surface varies with time even when the plastic strains are held constant. The difference in the definition of yield surface employed in classical elasto-plastic models and the NSFS theory is represented in Figure 2.27 for an elasto-viscoplastic material, in which the yield surface corresponding to any given viscoplastic strain under a particular loading condition is reached at points A, A_1, or A_2 with respect to time-dependent function β.

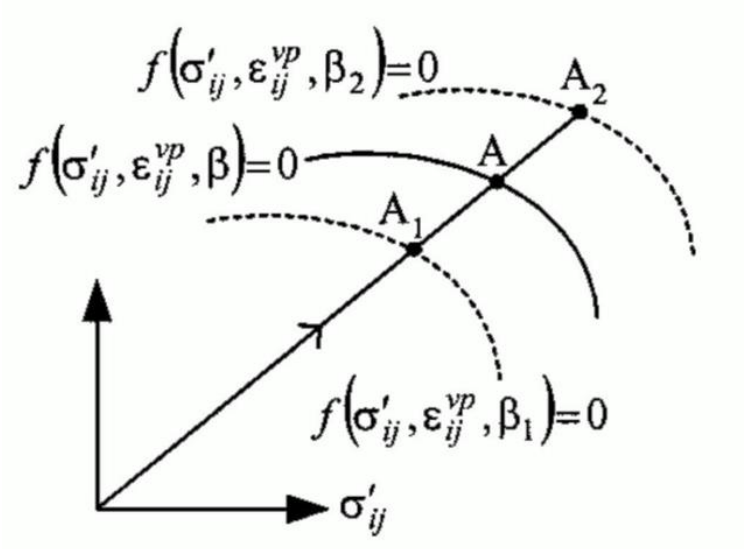

Figure 2.27: Schematic representation of the NSFS-type EVP Models (after Olszak and Perzyna, 1966)

Similar to the overstress-type EVP model, the NSFS theory follows the identical decomposition of the total strain rate $\dot{\varepsilon}_{ij}$ into the elastic strain rate $\dot{\varepsilon}_{ij}^{e}$ and viscoplastic strain rate $\dot{\varepsilon}_{ij}^{vp}$, as in Equation 2.18. Similarly, the elastic strain rate is calculated by using generalised Hooke's law and the viscoplastic strain rate is defined based on the flow rule expressed as follows:

$$\dot{\varepsilon}_{ij}^{vp} = \langle \Lambda \rangle \frac{\partial Q}{\partial \sigma_{ij}} \tag{2.25}$$

where, Λ is a non-negative multiplier and Q is so-called viscoplastic potential function. In contrast to the overstress theory, the multiplier Λ in NSFS theory is determined using the consistency condition, which is similar to the plastic multiplier defined in the traditional elasto-plastic models.

The NSFS theory was first proposed by Naghdi and Murch (1963), and later extended by Olszak and Perzyna (1966) and Olszak (1970). The NSFS-based EVP models, developed by Sekiguchi (1984), Matsui and Abe (1985, 1986, 1988) and Matsui et al. (1989), can be used to describe the time-dependent behaviour of normally consolidated clay under undrained conditions. Most recently, Qiao et al. (2016) and Kavvadas and Kalos (2019) have developed EVP models based on NSFS theory to capture the creep behaviour of geomaterials. Although NSFS theory can achieve better accuracy compared to overstress one, the NSFS-based EVP models are not capable of describing the stress relaxation process or the initiation of creep from a stress state inside the yield surface (Liingaard et al., 2004).

Based on the 'equivalent timeline' approach, Borja and Kavazanjian (1985), Hsieh et al. (1990) and Borja et al. (1990) have proposed the double-surface EVP models for reproducing time-dependent stress-strain behaviour of soils. More recently, Kelln et al. (2008b) developed an analytical elastic-viscoplastic model by presenting triaxial results in different loading

conditions. However, the detailed approaches used in all of these models differ, mainly due to the various methods of deriving the scaling function that controls the magnitude of viscoplastic strain rates and determining the model parameters. Although all these models achieve reasonable accuracy in predicting the time-dependent behaviour of soils, they still have their own limitations and require a considerable number of assumptions and parameters without being related to the physical phenomena of real soils.

2.5.2.3 Hypoplasticity Models

Unlike the traditional plasticity models, the direction of the plastic strain rate depends on the stress rate in the hypoplasticity theory, which was first introduced by Wu and Kolymbas (1990). The major characteristic of this approach is that the yield surface is defined as a kind of material memory. There is no yield function, no elastic domain and all the past stress history is concentrated in the current stress. This is in stark contrast to the conventional plasticity, in which the yield function and material state parameters define the yield surface, which contains the elastic domain. Afterwards, Wu et al. (1993) followed up with several concepts for the visco-hypoplastic constitutive models by combining the concept of hypoplasticity with viscoplastic overstress theory by Perzyna (1963, 1966). This formulation introduces a characteristic viscoplastic strain rate $\dot{\varepsilon}_{ij}^{vp}$ that depends on the stress and other structural tensors, considering past deformation history, but not on their rates. In general, a viscous flow rule is expressed in the following form:

$$\dot{\varepsilon}_{ij}^{vp} = \gamma \cdot \emptyset(F) \cdot f_v = 0 \qquad (2.26)$$

where, γ is denoted here as the fluidity parameter and a yield function is introduced inside the viscous nucleus function as $\emptyset(F) = (f_d/f_s)^n$, with f_d and f_s defined as the dynamic yield surface and static yield surface, respectively. The parameter f_v represents the direction of the

viscous flow, i.e. $f_v = \dot{\varepsilon}_{ij}^{vp} / \left\| \dot{\varepsilon}_{ij}^{vp} \right\|$. In other words, the direction of the plastic flow corresponds to a strain rate in the limited state when the stress is constant. Although Wu et al. (1993) outlined a number of visco-hypoplasticity, no specific constitutive formations have been proposed. This basic visco-hypoplasticity concept was improved by Niemunis (2003a, b) and Niemunis et al. (2009) with the adoption of Olszak and Perzyna (1966)'s overstress theory, along with the laboratory measurements using oedometer tests conducted by Niemunis and Krieg (1996). Gudehus (2004) and Mašín (2005) have also proposed modified viscous hypoplastic model by replacing the Cam-clay component with the genuine hypoplasticity. More recently, the Niemunis' visco-hypoplastic concept has been adopted to perform numerical implementations on creeping slope (Van Den Ham et al., 2009), structured soils (Fuentes et al., 2010) and footing (Qiu and Grabe, 2011). Although these existing models have proved that the concept of visco-hypoplasticity is an appealing and interesting approach for the development of constitutive soil models, the resulting models are rather complicated and essentially, there is no physical meaning in deriving the formulations and justification in complying with the fundamental laws of physics.

2.5.2.4 Hyperplasticity Model

Although many variants of the plasticity theory have been developed for improved simulations of real soil behaviour, as detailed above, the resulting constitutive models are yet flexible enough to disobey the fundamental laws of thermodynamics. It is important that the constitutive models that do not comply with the fundamental laws of physics should not be used with any confidence, as emphasised in Houlsby and Puzrin (2006). Therefore, the constitutive models must be founded on the rudimentary physical phenomena and the subsequent developments must also ensure that the fundamental principles or axioms that govern the physical phenomena are taken into consideration. Based on this strong foundation,

Halphen and Nguyen (1974) and Ziegler (1983) have developed the concept of extracting plasticity theory with the major emphasis on the fundamental laws of thermodynamics, in which the entire constitutive response for modelling deformable solid is encapsulated within two scalar thermodynamic potential functions, namely free-energy and dissipation potential functions. This is in stark contrast to some conventional plasticity models, in which thermodynamic principles are not taken into consideration, such as the original Cam-clay model. In the hyperplasticity approach, the two scalar potential functions are postulated based on the first and second laws of thermodynamics, securing the fact that the derived incremental stress-strain responses always automatically obey them. This relatively new approach to the modelling of elasto-plastic constitutive models was termed 'hyperplasticity' by Collins and Houlsby (1997) and Houlsby and Puzrin (2000, 2006). The first potential function, i.e. the free-energy potential function, may be expressed in four possible forms, as provided in Table 2.1.

Table 2.1: Four possible forms of the free-energy potential function

Internal Energy	Helmholtz free-energy	Enthalpy	Gibbs free-energy
$U = U(\varepsilon_{ij}, \varepsilon_{ij}^{p}, S)$	$f = f(\varepsilon_{ij}, \varepsilon_{ij}^{p}, \theta)$	$h = h(\sigma_{ij}, \varepsilon_{ij}^{p}, S)$	$g = g(\sigma_{ij}, \varepsilon_{ij}^{p}, \theta)$

where, S is the specific entropy and θ is denoted as temperature constant. The different forms of energy function are related by Legendre transformation. The second potential function, i.e. the dissipation potential function, basically allows for the Second Laws of Thermodynamics to be satisfied within the hyperplasticity framework. It is assumed that the dissipation potential function is a homogeneous first order function of the thermodynamic state and the rate of change of state of the material, which can also be expressed in four possible ways, depending on which the form of specified free-energy potential function:

$$\delta\Phi = \delta\Phi(\sigma_{ij} \text{ or } \varepsilon_{ij}, \alpha_{ij}, s \text{ or } \theta, \dot{\alpha}_{ij}) \geq 0 \qquad (2.27)$$

where, α_{ij} and $\dot{\alpha}_{ij}$ are the internal variable and its corresponding rate of change, respectively. It is to be emphasised that the dissipation potential function must always be positive to comply with the second laws of thermodynamics. In order to impose the first law of thermodynamics, the generalised and dissipative stress tensors are defined as follows:

$$\bar{\chi}_{ij} = -\frac{\partial u}{\partial \alpha_{ij}} = -\frac{\partial f}{\partial \alpha_{ij}} = -\frac{\partial h}{\partial \alpha_{ij}} = -\frac{\partial g}{\partial \alpha_{ij}} \tag{2.28a}$$

$$\chi_{ij} = \frac{\partial(\delta \Phi)}{\partial(\dot{\alpha}_{ij})} \tag{2.28b}$$

In this approach, the yield function Y^D is derived as a degenerate special case of the Legendre transformation of the dissipation function, which can be expressed in general form as follows:

$$\delta\Phi(\sigma_{ij}, \alpha_{ij}, \dot{\alpha}_{ij}) + \lambda \cdot Y^D(\sigma_{ij}, \alpha_{ij}, \chi_{ij}) = \chi_{ij}\dot{\alpha}_{ij} \tag{2.29}$$

Consequently, the flow rule arises from the properties of Legendre transformation as follows:

$$\dot{\alpha}_{ij} = \lambda \cdot \frac{\partial(Y^D)}{\partial \chi_{ij}} \tag{2.30}$$

where, λ is a non-negative multiplier resulting from the Legendre transformation based on homogeneous first order function. Since the current study adopts the core of the hyperplasticity framework, the major details related to the hyperplasticity framework is further elaborated in details in Chapter 3.

One of the most profound benefits from this approach is that the identification of the two thermodynamic potentials (i.e. the free-energy and dissipation potential functions) is sufficient to predict the entire constitutive behaviour of elastic-plastic materials, entailing the elasticity law, the yield condition and its associated flow rule. Moreover, the distinctive characteristic of

the resulting constitutive models is their compliance with the physical phenomena, including the conservation of mass and energy and the fundamental laws of thermodynamics. Moreover, the resulting hyperplastic constitutive models are developed within a compact, rigorous and consistent framework for the determination of entire incremental stress-strain response. In recent years, Houlsby and Puzrin (2000, 2006) have made an extensive contribution to the development of generalised hyperplasticity framework for modelling constitutive stress-strain behaviour of soils. Moreover, this approach is then generalised to incorporate multiple yield surfaces and then to the case of infinite number of yield surfaces, where the latter is denoted as 'continuous hyperplasticity' framework (Puzrin and Houlsby, 2001a, 2001b). The resulting models within this latter approach are capable of simulating smooth transitions from elastic to plastic behaviour, where truly elastic region vanishes altogether. Furthermore, this approach has subsequently extended to introduce the use of internal functions, within which the stress-reversal history is memorised, to represent infinite number of internal variables; thus, resulting in a couple of scalar thermodynamic functionals, instead of functions.

On the other hand, Houlsby and Puzrin (2001) have extended the generalised hyperplasticity framework to capture the rate-dependent behaviour of soils. To incorporate the modelling of rate-dependent behaviour, the description of the free-energy potential function remains the same, whereas the dissipation potential function is replaced by two potential functions, i.e. the force potential and the flow potential functions. With the use of Legendre-Fenchel transformation, the force potential and flow potential functions are related and the summation of these two potential functions is equal to the dissipation potential function. The rudimentary elements related to the extension towards rate-dependent hyperplasticity approach is further elaborated in Chapter 3.

2.5.3 Comparisons of Advanced Constitutive Soil Models

Taking the aforementioned discussions into consideration, it is observed that a large number of advanced constitutive soil models have been proposed, developed and extended based on various concepts and laboratory findings. Each of the existing models possesses its own advantages and shortcomings and up until now, no universal constitutive model has yet been developed that is applicable for all the geological materials subjected to a wide range of loading conditions.

For the case of multiple-surface constitutive soil models, the bounding surface models are more computationally efficient compared to the multiple-surface models. However, the former ones often require a considerable number of somewhat arbitrary functions, postulated without being related to the physical phenomena of materials. On the other hand, although the latter ones are usually considered as the most promising approach, they still require to hypothesise inherently complicated functions, consisting of a large number of model parameters that are often difficult to obtain from traditional laboratory measurements. Moreover, the multiple-surface models are computationally inconvenient for the implementation of numerical analyses.

The hypoplasticity models, basically, are not based on definite physical meanings and therefore, usually require a considerable amount of assumptions for the derivations of formulations that are difficult to justify for the compliance with the fundamental laws of physics. Although they reproduce reasonable simulations, the relationships are often the ones fitted by polynomial functions with curve-fitting parameters, which are not suitable to physically quantify and hence, inappropriate for very complicated boundary value problems. This could also result in misconceptions and misunderstandings of the behaviour of geomaterials, particularly soils.

The existing EVP models, somehow, enlighten the understanding of time-dependent behaviour of soils but they still have their own limitations and drawbacks, particularly with the emphasis on the necessity of a considerable number of assumptions, such as constant viscoplastic strain rate on the flow surface and the negligence of 'fabric' effects observed in the behaviour of natural soils, without being in tandem with the physical phenomena of real soils' behaviour.

2.6 Summary and Findings

As previously emphasised in the earlier sections, the constitutive models must be developed without violating certain principles or axioms that govern the physical phenomena of materials; for instance, the fundamental laws of thermodynamics. In order to circumvent the problem of having a substantial number of assumptions and using 'ad hoc' procedures, while complying with the fundamental laws of physics, the current study adopts the hyperplasticity framework to describe the time-dependent behaviour of soils. This framework offers a rigorous, compact and consistent derivation procedure, making considerable use of potential functions and internal variables related to the physical phenomena of materials, for predicting the entire stress-strain response of soils subjected to a specified sequence of stress or strain increment over time. As a consequence, the resulting models developed within a single framework allows for efficient, yet convenient comparisons for further improvements. Most importantly, the need for additional 'ad hoc' assumptions and somewhat arbitrary formulations, can also be minimised to a certain extent, while providing the confidence and reliability for the implementation of numerical analyses as the framework is founded upon the fundamental laws of thermodynamics. Accordingly, the fundamental elements of the basic hyperplasticity theory, with the emphasis on its essential components and requisite foundation towards the

development of a new hyper-viscoplasticity theory to overcome the aforementioned drawbacks of the conventional approach, is reviewed in Chapter 3.

CHAPTER 3

RATE-INDEPENDENT AND RATE-DEPENDENT HYPERPLASTICITY THEORY

3.1 Introduction

In a conventional plasticity theory, the major specification of the incremental stress-strain response requires (i) the elasticity law, (ii) the yield condition, (iii) the flow rule or plastic potential, and (iv) the hardening/softening rule to take into account of the expansion and translation of yield surface for improved predictions on real soil behaviour. As previously highlighted, many existing variants of plasticity theory are flexible enough to violate the fundamental laws of thermodynamics. In contrast, the extraction of plasticity approach based on the laws of thermodynamics has also been emerged, within which the entire constitutive behaviour of a deformable solid is fully encapsulated in two potential functions, i.e. free-energy and dissipation potential functions. The general consideration of thermodynamics for the modelling of elastic-plastic materials is discussed in Halphen and Nguyen (1974), Ziegler (1983), Lubliner (1990) and Maugin (1992). This relatively new approach in developing constitutive models based on thermodynamics, was denoted as 'hyperplasticity' by Collins and Houlsby (1997) and Houlsby and Puzrin (2000) for modeling time-independent behaviour of soils.

3.2 Basics of Hyperplasticity Theory

The hyperplastic approach commences with the thermodynamic hypotheses and then develops plasticity theories from them. In classical thermodynamics, there are the "Zeroth", "First", "Second" and "Third" laws. In this hyperplasticity framework, it is emphasised particularly on the "First" and "Second" laws. Basically, they establish the existence of two important properties of a body in thermodynamic equilibrium: the internal free-energy and the entropy.

3.2.1 Laws of Thermodynamics

3.2.1.1 The First Law

In general, the first law can be stated in the following form: there is a property of the system in thermodynamic equilibrium, called internal energy U, such that:

$$\dot{U} = \dot{W} - \dot{Q} \tag{3.1}$$

where, $\dot{U}$ is the change in the internal energy, $\dot{W}$ is the work done on the system, and $\dot{Q}$ is referred to as the amount of heat dissipated from the system. For any process within a closed system, the change in the internal energy ($\dot{U}$) is due to a combination of the amount of work done towards the system and the amount of heat dissipated from the system. Besides, Equation (3.1) also represents the important energy conservation phenomenon.

3.2.1.2 The Second Law

The second law of thermodynamics is considerably more subtle than the first law and can be expressed in a number of equivalent ways. In general, it imposes certain restrictions to the processes that can occur. For instance, one of the basic consequences is that work can be dissipated in the form of heat, but that heat cannot be converted back into work without some external influences. Within the context of hyperplasticity, it is emphasised that the second law simply requires the dissipation of energy. It can best be expressed by making the hypothesis that there is a further material property, called entropy (S), which is defined as follows:

$$\dot{S} = \frac{\dot{Q}}{\theta} \tag{3.2}$$

where, $\dot{S}$ is the change in entropy, $\dot{Q}$ is referred to as the flow of heat into or out of the system from somewhere else, and θ is the absolute temperature. Since the amount of heat

dissipated from the element must always be non-negative, the following function is denoted as the dissipation potential function ($\delta\Phi$), provided that the rate of entropy production within the element is the irreversible part ($\dot{S}^i$), which satisfies the following inequality:

$$\delta\Phi \equiv \dot{Q} = \theta\dot{S}^i \geq 0 \tag{3.3}$$

As discussed in Chapter 2, the free-energy function can be expressed using either one of the four alternative expressions, which are the internal energy (u), Helmholtz free-energy (f), Gibbs free-energy (g) or enthalpy (h). For instance, the internal energy function $U(\varepsilon_{ij}, \varepsilon_{ij}^p, S)$ is related to the Helmholtz free-energy function $\Psi^f(\varepsilon_{ij}, \varepsilon_{ij}^p, \theta)$ by Legendre transformation, which is expressed as follows:

$$U(\varepsilon_{ij}, \varepsilon_{ij}^p, S) - \Psi^f(\varepsilon_{ij}, \varepsilon_{ij}^p, \theta) = \theta.S \tag{3.4}$$

Along with the property from Legendre transformation that:

$$S = -\frac{\partial\Psi^f}{\partial\theta} \tag{3.5}$$

Regarding Equations (3.3) and (3.4), it is much more convenient to control the temperature while conducting experiments rather than controlling the entropy. Therefore, on the other hand as the replacement of the entropy (S) with temperature (θ), for simplicity, using Legendre transformation.

Replacing the internal energy function (U) with Helmholtz free-energy function (Ψ^f) in Equation (3.1) results as follows:

$$\dot{\Psi}^f = \dot{W} - \delta\Phi \tag{3.6}$$

Using $\dot{W} = \sigma_{ij}\dot{\varepsilon}_{ij}$ for the change in work-done, and substituting the relationship from Equation (3.3) into Equation (3.6),

$$\sigma'_{ij}\dot{\varepsilon}_{ij} = \dot{\Psi}^f + \delta\Phi \tag{3.7}$$

Therefore, the power of deformation is equal to the sum of the rate of change of free-energy and the dissipation in an isothermal deformation.

3.3 Rate-independent Hyperplasticity Framework

Referring to Equation (3.7), the basic formulation for an isothermal deformation of materials is expressed as follows:

$$\dot{W} = \dot{\Psi} + \delta\Phi, \qquad where\ \delta\Phi \geq 0 \tag{3.8}$$

where, $\dot{W}$ is the effective incremental work done on a continuum element, $\dot{\Psi}$ is the differential of the free-energy defined per unit volume and $\delta\Phi$ is the dissipation increment function defined per unit volume. Since there are four alternative forms available for the free-energy function, namely the internal energy (Ψ^u), Helmholtz free-energy (Ψ^f), Gibbs free-energy (Ψ^g), or the enthalpy (Ψ^h), the general expression Ψ is used for representation. In order to comply with the second law of thermodynamics, $\delta\Phi$ in Equation (3.8) must be non-negative. As previously discussed, the free-energy function is defined in terms of total elastic strain tensor and plastic strain tensor, $\varepsilon_{ij}\ and\ \varepsilon_{ij}^p$, respectively. On the other hand, the dissipation function is assumed to depend additionally on plastic strain rate tensor, i.e., $\delta\Phi\left(\varepsilon_{ij}, \varepsilon_{ij}^p, \dot{\varepsilon}_{ij}^p\right)$. Consequently, the free-energy, in general, is allowed to depend on both elastic and plastic strains. This requires additional assumption, in which the material must be 'decoupled' in the sense that the instantaneous elastic moduli do not depend on the plastic strains. The special case comes from the above assumption that the free-energy is defined as

an additive composition of two separate functions, comprising of only elastic strains in one and only plastic strains in the other one. The validity of these assumptions is discussed in Collins and Houlsby (1997) and Collins and Kelly (2002). From this 'decoupled' assumption, it follows that:

$$\Psi = \Psi^e\left(\varepsilon_{ij}^e\right) + \Psi^p\left(\varepsilon_{ij}^p\right) \tag{3.9}$$

where Ψ^e and Ψ^p are the elastic and plastic components of the free-energy function, respectively; whereas, ε_{ij}^e and ε_{ij}^p are the elastic and plastic strain tensors, respectively. The expression in Equation (3.9) is also termed as the 'principle of separation of energy' by Ulm and Coussy (2003). In general, the free-energy should only depend on elastic strain, as it represents the elastic energy stored in an individual grain. In conventional plasticity theory, it is often assumed that the energy associated with plastic strain is irrecoverable. However, the contact stresses acting on an individual grain are not the same during the loading and unloading phases due to the highly inhomogeneous nature of the stress distributions found on the micro scale (Collins, 2005). As a result, when unloading situation occurs, i.e. the reduction in the applied pressure resulting in the negative work increment, the minor portion of elastically compressed grains are allowed to expand and give up their stored elastic energy. Afterwards, these particles return to their compressed state upon reloading. The changes in energy related to this reversible elastic deformation are given by the elasticity component of the continuum, free-energy increment $\dot{\Psi}^e$. However, a certain extent of the elastically compressed particles are still 'trapped' within the compacted volume and these particles have the capacity to expand and release their stored elastic energy only when the simultaneous rearrangement occurs in some of the surrounding particles. Necessarily, this rearrangement entails frictional dissipation, which in turn, results in the induced dilatational plastic strains.

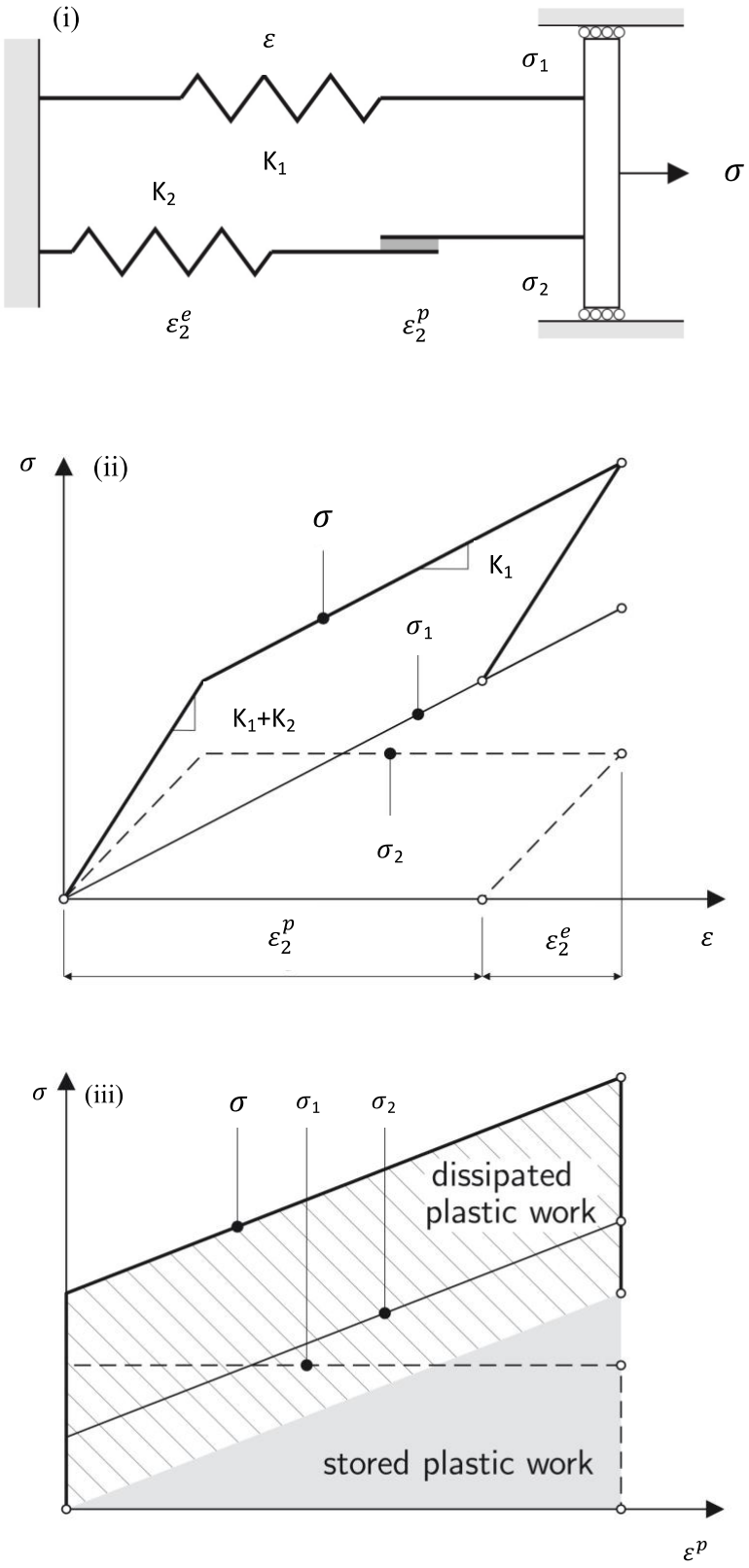

Figure 3.1: (i) One-dimensional rheological model representing stored and dissipated plastic work; (ii) total stress-strain response; (iii) total stress-plastic strain response (after Collins, 2005)

The presence of stored plastic work can also be considered as the remaining plastic strain when the 'system' returns to its original stress level. The concepts of stored and dissipated plastic work is represented using the one-dimensional rheological model in Figure 3.1 (i), consisting of a spring that is placed in parallel with a second spring in series with a slider. The system is subjected to an increasing total stress, which is followed by unloading until $\sigma = 0$, as shown in Figure 3.1 (ii); where, the components of stored and dissipated plastic work are depicted in Figure 3.1 (iii).

Consider the situation in which there were no 'trapped' energy, all the energy contained within the compressed grain particles should be recovered without resulting in any grain re-arrangement. According to Thornton and Liu (2000), such re-arrangement strains are observed during decompression in discrete element simulations. Moreover, the existence of 'stored' or 'frozen' elastic energy has also been explained in the context of general elastic-plastic materials by Mroz (1973), Maugin (1992). Furthermore, Palmer (1967) and Houlsby (1981) have scrutinised the energy decomposition of the original Cambridge models within this context of stored plastic work, and more recently, Jefferies (1997) have corroborated the possibility of some portion of plastic work being stored.

Hence, it is possible to recover the micro-elastic energy associated with these trapped particles only if reversed, i.e. dilatational volumetric plastic strains also occur. However, such deformations are not allowed to happen within the current yield surface. Correspondingly, the magnitude of the plastic strains resulting from the rearrangements taken place within the compression phase governs the portion of the trapped micro-elastic energy. Thus, the plastic strains are used to determine the magnitude of this locked-in elastic energy at the continuum level. Therefore, this frozen energy is termed as the stored plastic work by Collins (2005), and its increment, which is not restricted in sign, is denoted by $\dot{\Psi}^p$, as indicated above. As a result,

the function Ψ^p is not dependent upon the elastic strains, but only on the plastic strains. Substituting Equation (3.9) into Equation (3.8) yields:

$$\dot{W} = \dot{\Psi}^e\left(\dot{\varepsilon}_{ij}^e\right) + \dot{\Psi}^p\left(\dot{\varepsilon}_{ij}^p\right) + \delta\Phi \tag{3.10}$$

Similarly, the total work increment can also be written as the sum of elastic and plastic components:

$$\dot{W} = \dot{W}^e + \dot{W}^p \tag{3.11}$$

It follows from Equations (3.10) and (3.11) that:

$$\dot{W}^e = \sigma_{ij}^{'}\dot{\varepsilon}_{ij}^e = \frac{\partial \Psi^e\left(\varepsilon_{ij}^e\right)}{\partial \varepsilon_{ij}^e}\dot{\varepsilon}_{ij}^e \;\; and \;\; \sigma_{ij}^{'} = \frac{\partial \Psi^e\left(\varepsilon_{ij}^e\right)}{\partial \varepsilon_{ij}^e} \tag{3.12}$$

where, σ_{ij}' is the effective stress tensor. The basic elasticity component of the constitutive law is then deduced in Equation (3.12). On the other hand, it follows from Equations (3.10) and (3.11) that:

$$\dot{W}^p = \sigma_{ij}^{'}\dot{\varepsilon}_{ij}^p = \dot{\Psi}^p\left(\dot{\varepsilon}_{ij}^p\right) + \delta\Phi\left(\dot{\varepsilon}_{ij}^p\right) = \frac{\partial \Psi^p\left(\varepsilon_{ij}^p\right)}{\partial \varepsilon_{ij}^p}\dot{\varepsilon}_{ij}^p + \frac{\partial(\delta\Phi)}{\partial \dot{\varepsilon}_{ij}^p}\dot{\varepsilon}_{ij}^p \tag{3.13a}$$

$$\dot{W}^p = \frac{\partial \Psi^p\left(\varepsilon_{ij}^p\right)}{\partial \varepsilon_{ij}^p}\dot{\varepsilon}_{ij}^p + \frac{\partial(\delta\Phi)}{\partial \dot{\varepsilon}_{ij}^p}\dot{\varepsilon}_{ij}^p \tag{3.13a}$$

Since $\delta\Phi$ is a homogeneous first order function of plastic strain rates $\dot{\varepsilon}_{ij}^p$, Euler's theorem for homogeneous functions is used to obtain the last term in equation Equation (3.13a). Comparing with Equation (3.13a), this relationship is only satisfied if:

$$\rho_{ij} = \frac{\partial \Psi^p\left(\varepsilon_{ij}^p\right)}{\partial \varepsilon_{ij}^p} \;\; and \;\; \chi_{ij}' = \frac{\partial(\delta\Phi)}{\partial \dot{\varepsilon}_{ij}^p} \tag{3.14}$$

where, $\rho_{ij}\ and\ \chi_{ij}$ are termed 'shift' stress and 'dissipative' stress, respectively. This derivation in Equation (3.14) is supported by Collins and Hilder (2002) and YangPing et al. (2013). However, Equation (3.14) cannot be deduced formally as in the previous case of deducing elasticity law in Equation (3.12). In order to achieve this, the status of a constitutive postulate termed as 'Ziegler's orthogonality postulate' needs to be satisfied (Collins and Houlsby, 1997; Houlsby and Puzrin, 2000). Referring to Equations (3.13a), (3.13a) and (3.14), it is deduced that the effective stress is the sum of the 'shift' stress and 'dissipative' stress, expressed as follows:

$$\sigma'_{ij} = \rho'_{ij} + \chi'_{ij} \tag{3.15}$$

Therefore, the re-written form of Equation (3.13a) is provided as follows:

$$\dot{W}^p = \sigma'_{ij}\dot{\varepsilon}^p_{ij} = \Psi^p + \delta\Phi = \rho'_{ij}\dot{\varepsilon}^p_{ij} + \chi'_{ij}\dot{\varepsilon}^p_{ij} \tag{3.16}$$

As similar to the derivation in Equation (3.12), the relationships, i.e. $\dot{W}^p = \sigma'_{ij}\dot{\varepsilon}^p_{ij}$, $\Psi^p = \rho'_{ij}\dot{\varepsilon}^p_{ij}\ and\ \delta\Phi = \chi'_{ij}\dot{\varepsilon}^p_{ij}$, are deduced from Equation (3.16). Therefore, it is apparent that the product of the true stress with the plastic strain increment results in the plastic work, whereas the multiplication of dissipative stress with the plastic strain increment results in the plastic dissipation. In contrast to the conventional soil mechanics, where the plastic work and the plastic dissipation are normally assumed to be equal, these are only equal if the shift stress ρ'_{ij} is zero; in other words, the free-energy is assumed to depend only on the elastic strains within the context of hyperplasticity. Hence, this viewpoint is a cornerstone of modern soil mechanics. The importance of the shift stress in the modelling of the unloading situations is discussed in Collins and Hilder (2002). Moreover, Collins and Kelly (2002) recognised the importance of this 'stored plastic work' as they discussed the concept in terms of both the thermo-mechanical and the micromechanical viewpoints.

The summary of how the hyperplastic approach is based on the First and Second law of thermodynamics is provided in Table 3.1 and Table 3.2 using triaxial notations. In addition, the basic formulations for rate-independent hyperplasticity framework is also presented in Table 3.3.

Table 3.1: Summary of Derivations for Rate-independent Hyperplasticity Framework

	Formulations	
First Law of Thermodynamics	$\dot{\Psi} = \dot{W} - \dot{Q}$	
Second Law of Thermodynamics (Definition of Entropy)	$\dot{S} = \frac{\dot{Q}}{\theta}$	
Work or Energy Equation	$\dot{W} = \dot{\sigma}'_{ij}\varepsilon_{ij}$ *or* $\dot{W} = \sigma'_{ij}\dot{\varepsilon}_{ij}$	
1. Equation – Power of Deformation	$\dot{\Psi}^g = \dot{\sigma}'_{ij}\varepsilon_{ij} - \delta\Phi^g$	$\dot{\Psi}^f = \sigma'_{ij}\dot{\varepsilon}_{ij} - \delta\Phi^f$
Where, $\dot{Q} \equiv \delta\Phi$, where the amount of heat being dissipated is assumed to be equal to the dissipation increment function.		
Free-energy Function	$\Psi^g = \Psi^g\left(\sigma'_{ij}, \varepsilon^p_{ij}\right)$	$\Psi^f = \Psi^f\left(\varepsilon_{ij}, \varepsilon^p_{ij}\right)$
2. Differentiation – Free-energy function	$\dot{\Psi}^g = \frac{\partial\Psi^g}{\partial\sigma_{ij}}\dot{\sigma}'_{ij} + \frac{\partial\Psi^g}{\partial\varepsilon^p_{ij}}\dot{\varepsilon}^p_{ij}$	$\dot{\Psi}^f = \frac{\partial\Psi^f}{\partial\varepsilon_{ij}}\dot{\varepsilon}_{ij} + \frac{\partial\Psi^f}{\partial\varepsilon^p_{ij}}\dot{\varepsilon}^p_{ij}$
Equating like terms from 1 and 2	$\varepsilon_{ij} = \frac{\partial\Psi^g}{\partial\sigma'_{ij}}$	$\sigma'_{ij} = \frac{\partial\Psi^f}{\partial\varepsilon_{ij}}$
	$\delta\Phi^g = \chi'_{ij}\dot{\varepsilon}^p_{ij} = -\frac{\partial\Psi^g}{\partial\varepsilon^p_{ij}}\dot{\varepsilon}^p_{ij}$	$\delta\Phi^f = \chi'_{ij}\dot{\varepsilon}^p_{ij} = -\frac{\partial\Psi^f}{\partial\varepsilon^p_{ij}}\dot{\varepsilon}^p_{ij}$

Table 3.2: Summary of Derivations for Rate-independent Hyperplasticity Framework (Using Triaxial Notation)

	Formulations	
Equation – Power of Deformation	$\dot{W} = \sigma'_{ij}\dot{\varepsilon}_{ij} = \dot{\Psi}^e(\varepsilon^e_{ij}) + \dot{\Psi}^p(\varepsilon^p_{ij}) + \delta\Phi(\dot{\varepsilon}^p_{ij})$	
Total Work Increment Equation	$\dot{W} = \dot{W}^e + \dot{W}^p$	
Elastic Work Increment Function	$\dot{W}^e = \dot{\Psi}^e(\varepsilon^e_{ij})$	
Elastic Component	$\dot{W}^e = \sigma'_{ij}\dot{\varepsilon}^e_{ij} = \dot{\Psi}^e(\varepsilon^e_{ij}) = \frac{\partial\Psi^e(\varepsilon^e_{ij})}{\partial\varepsilon^e_{ij}}\dot{\varepsilon}^e_{ij};$ $\sigma'_{ij} = \frac{\partial\Psi^e(\varepsilon^e_{ij})}{\partial\varepsilon^e_{ij}}$	
	$p' = \frac{\partial\Psi^e}{\partial\varepsilon_v}$	$q = \frac{\partial\Psi^e}{\partial\varepsilon_q}$
Plastic Work Increment Function	$\dot{W}^p = \dot{\Psi}^p(\varepsilon^p_{ij}) + \delta\Phi(\dot{\varepsilon}^p_{ij})$	
Plastic Components	$\dot{W}^p = \sigma'_{ij}\dot{\varepsilon}^p_{ij} = \frac{\partial\Psi^p(\varepsilon^p_{ij})}{\partial\varepsilon^p_{ij}}\dot{\varepsilon}^p_{ij} + \frac{\partial(\delta\Phi)}{\partial(\dot{\varepsilon}^p_{ij})}\dot{\varepsilon}^p_{ij}$	
Shift Stress	$p'_s = \frac{\partial\Psi^p(\varepsilon^p_v)}{\partial\varepsilon^p_v}$	$q_S = \frac{\partial\Psi^p(\varepsilon^p_q)}{\partial\varepsilon^p_q}$
Dissipative Stress	$p'_D = \frac{\partial(\delta\Phi)}{\partial(\dot{\varepsilon}^p_v)}$	$q_D = \frac{\partial(\delta\Phi)}{\partial(\dot{\varepsilon}^p_q)}$
Total Stress Components	$p' = p'_s + p'_D$	$q = q_S + q_D$

Table 3.3: Basic Formulations for Rate-independent Hyperplasticity Framework

	Gibbs Free-Energy (g)	**Helmholtz Free-Energy (f)**
Free-energy Function	$\Psi^g = \Psi^g\left(\sigma'_{ij}, \varepsilon^p_{ij}\right)$	$\Psi^f = \Psi^f\left(\varepsilon_{ij}, \varepsilon^p_{ij}\right)$
Stress or Strain	$\varepsilon_{ij} = -\frac{\partial \Psi^g}{\partial \sigma'_{ij}}$	$\sigma'_{ij} = \frac{\partial \Psi^f}{\partial \varepsilon_{ij}}$
Generalised Stress	$\bar{\chi}'_{ij} = -\frac{\partial \Psi^g}{\partial \varepsilon^p_{ij}}$	$\bar{\chi}'_{ij} = -\frac{\partial \Psi^f}{\partial \varepsilon^p_{ij}}$
Dissipation Function	$\delta\Phi^g = \delta\Phi^g\left(\sigma'_{ij}, \varepsilon^p_{ij}, \dot{\varepsilon}^p_{ij}\right) \geq 0$	$\delta\Phi^f = \delta\Phi^f\left(\varepsilon_{ij}, \varepsilon^p_{ij}, \dot{\varepsilon}^p_{ij}\right) \geq 0$
Dissipative Stress	$\chi'_{ij} = \frac{\partial(\delta\Phi^g)}{\partial\left(\dot{\varepsilon}^p_{ij}\right)}$	$\chi'_{ij} = \frac{\partial\left(\delta\Phi^f\right)}{\partial\left(\dot{\varepsilon}^p_{ij}\right)}$
Legendre Transformation	$\delta\Phi^g\left(\sigma'_{ij}, \varepsilon^p_{ij}, \dot{\varepsilon}^p_{ij}\right)$ $+ \lambda \cdot (Y^D)^g\left(\sigma'_{ij}, \varepsilon^p_{ij}, \chi'_{ij}\right) = \chi'_{ij}\dot{\varepsilon}^p_{ij}$	$\delta\Phi^f\left(\varepsilon_{ij}, \varepsilon^p_{ij}, \dot{\varepsilon}^p_{ij}\right) + \lambda$ $\cdot (Y^D)^f\left(\varepsilon_{ij}, \varepsilon^p_{ij}, \chi'_{ij}\right) = \chi'_{ij}\dot{\varepsilon}^p_{ij}$
Yield Function in Dissipative Stress Space	$(Y^D)^g = (Y^D)^g\left(\sigma'_{ij}, \varepsilon^p_{ij}, \chi'_{ij}\right) = 0$	$(Y^D)^f = (Y^D)^f\left(\varepsilon_{ij}, \varepsilon^p_{ij}, \chi'_{ij}\right) = 0$
Flow Rule in Dissipative Stress Space	$\dot{\varepsilon}^p_{ij} = \lambda\frac{\partial[(Y^D)^g]}{\partial \chi'_{ij}}$	$\dot{\varepsilon}^p_{ij} = \lambda\frac{\partial\left[(Y^D)^f\right]}{\partial \chi'_{ij}}$
Yield Function in True Stress Space	$Y^g = Y^g\left(\sigma'_{ij}, \varepsilon^p_{ij}\right) = 0$	$Y^f = Y^f\left(\varepsilon_{ij}, \varepsilon^p_{ij}, \sigma'_{ij}\right) = 0$
Flow Rule in True Stress Space	$\dot{\varepsilon}^p_{ij} = \lambda\frac{\partial Y^g}{\partial \sigma'_{ij}}$	$\dot{\varepsilon}^p_{ij} = \lambda\frac{\partial Y^f}{\partial \sigma'_{ij}}$
Consistency Condition	$\dot{Y} = \frac{\partial Y}{\partial \sigma'_{ij}}\dot{\sigma}'_{ij} + \frac{\partial Y}{\partial \varepsilon^p_{ij}}\dot{\varepsilon}^p_{ij}$	
	If $Y < 0$, stress state fully within the elastic domain. $\lambda = 0$ (No plastic deformation)	
	If $Y = 0$, plastic deformation occurs. $\lambda > 0;\ \lambda = -\frac{\left[\frac{\partial Y^D}{\partial \chi'_{ij}}\dot{\chi}'_{ij}\right]}{\left[\frac{\partial Y^D}{\partial \varepsilon^p_{ij}}\right]\left[\frac{\partial Y}{\partial \sigma'_{ij}}\right]}$	

The flow rule in the dissipative stress space is extracted as part of the property of Legendre transformation performed using the dissipation potential function. The non-negative multiplier λ, results from the degenerate special case of Legendre transformation due to the assumption of dissipation potential being a homogeneous first order function. If plastic deformation occurs, i.e. the stress state is on the yield surface ($Y = 0$), the non-negative plastic multiplier, i.e. λ, is determined based on the consistency condition of the corresponding yield criterion to ensure that the stress states do not go beyond the yield limit.

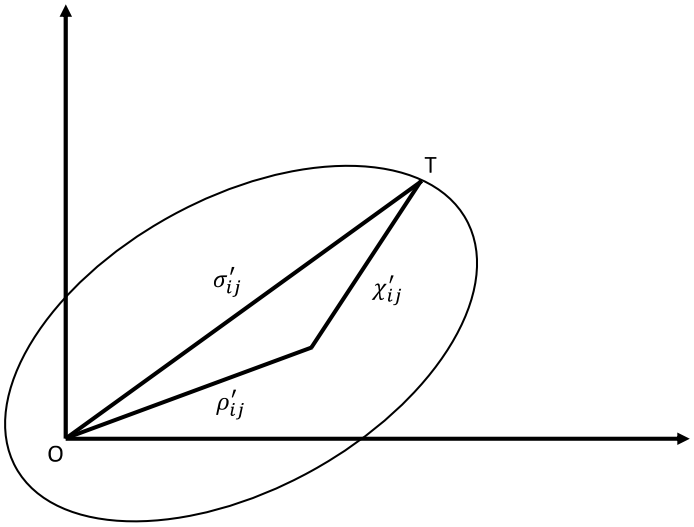

Figure 3.2: Schematic representation of the decomposition of the true stress into shift stress and dissipative stress components

As previously mentioned, this formulation adopts the Ziegler's orthogonality principle, which in the form of $\bar{\chi}'_{ij} = \chi'_{ij}$, in order to transform the yield function and the flow rule from the dissipative stress space to true stress space. Ziegler's orthogonality condition is effectively considered as a much stronger statement than the laws of thermodynamics (Collins and Houlsby, 1997; Houlsby and Puzrin, 2000). Besides, it can loosely be stated as a principle of maximal dissipation in some cases, due to the assumption that the amount of heat dissipated, i.e. $\dot{Q}$ used in the first law of thermodynamics, is equal to the dissipation increment function. Ziegler (1983) also stated that the difference between the generalised stress $\bar{\chi}'_{ij}$ and dissipative

stress χ'_{ij} is zero and if it is accepted that the knowledge of the dissipation function $\delta\Phi$ is sufficient to determine the corresponding dissipative stress χ'_{ij}, then the relationship, i.e. $\chi'_{ij} = \partial(\delta\Phi^g)/\partial(\dot{\varepsilon}^p_{ij})$ is the only feasible solution, as the normal to the level surfaces is the only vector field uniquely determined by a scalar valued dissipation function $\delta\Phi$. Moreover, Ziegler (1981) provided some clarities for the criticisms on the status of this postulate on a number of grounds. Since the debate on the justification of 'Ziegler's orthogonality condition' is not visited in this study, it is simply emphasised that this condition enables a compact formulation of constitutive behaviour that is consistent with the laws of thermodynamics.

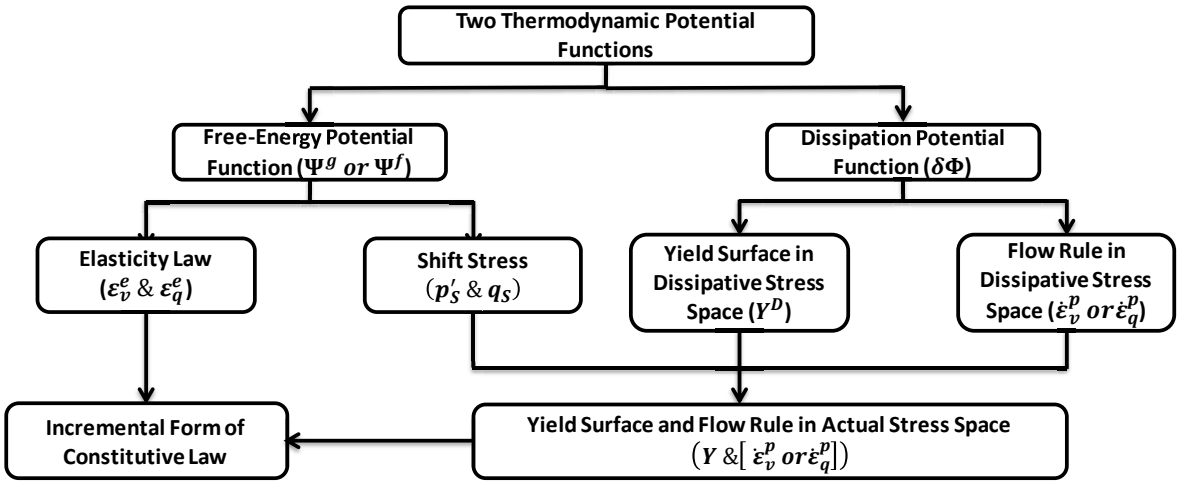

Figure 3.3: Flow Chart illustrating the steps in constructing the Incremental Form of the Elastic/Plastic Constitutive Law for the Development of Rate-independent Hyperplasticity Models

Therefore, the entire constitutive stress-strain response for soils is fully determined by using two thermodynamic potential functions, i.e. free-energy function and dissipation function, based on hyperplasticity theory. Hence, the flow chart for representing the step-by-step development of the rate-dependent hyperplasticity approach is deduced as in Figure 3.3. It is important to note here that thermal effects are not considered in this rate-independent scenario.

3.4 Rate-dependent Hyperplasticity Framework

Considering the benefits, rigidity and transparency of the hyperplasticity framework, it is rational to study the extension of rate-independent hyperplasticity concepts towards the incorporation of time-dependent effects for exploring the feasibility to build a strong foundation for the development of mixed hardening hyper-viscoplasticity model. In reality, almost all the materials in nature exhibit the rate-dependent behaviour and thus, soil is not an exception. As a result, these materials, while primarily classified as rate-independent, do demonstrate minor dependence on time and/or rate effects. Therefore, the consideration of modelling rate-dependent behaviour becomes a major necessity, particularly for the constitutive modelling of soil behaviour. Typically, it is observed from most frictional geomaterials that the yield stress may increase marginally with the strain rate, along with creep under sustained loading and stress relaxation at fixed strain.

Although many existing constitutive soil models have attempted to reproduce the aforementioned types of rate-dependent effects, these are often modelled semi-empirically by applying various plasticity theories to predict the rate dependence of strength, creep and stress relaxation. However, all these rate-dependent phenomena should be encompassed within a single approach with rigidity, compactness and consistency, which also allows for competing models to cast within the same framework for convenient comparisons. The extension of rate-independent hyperplasticity concept towards the rate-dependent one begins by overcoming the assumption that the dissipation increment function is a homogeneous first order function in plastic strain increments.

Consequently, the dissipation potential function, which is still homogeneous but of certain order “n” instead of one, is considered in this rate-dependent case. However, the general form of the dissipation potential function remains identical to the one provided in Table 3.3.

Considering the developments in Equations (3.13a), (3.13a) and (3.14), the following expression is obtained using the Euler's theorem for homogeneous functions of certain order "n":

$$n \cdot \delta\Phi = \frac{\partial(\delta\Phi)}{\partial\left(\dot{\varepsilon}_{ij}^{p}\right)}\dot{\varepsilon}_{ij}^{p} \tag{3.17}$$

It is emphasised in Equation (3.17) that $n = 1$ for homogeneous first order dissipation functions for the rate-independent case. Re-arranging Equation (3.17):

$$\delta\Phi = \frac{1}{n} \cdot \frac{\partial(\delta\Phi)}{\partial\left(\dot{\varepsilon}_{ij}^{p}\right)}\dot{\varepsilon}_{ij}^{p} \tag{3.18}$$

Here, a scalar factor v is introduced in Equation (3.18), which is re-written as follows:

$$\delta\Phi = v \cdot \frac{\partial(\delta\Phi)}{\partial\left(\dot{\varepsilon}_{ij}^{p}\right)}\dot{\varepsilon}_{ij}^{p} \tag{3.19}$$

As similar to Equation (3.17), it is emphasised in Equation (3.19) that $v = 1$ for the rate-independent case. For any dissipation function $\delta\Phi$, which is a homogeneous function of degree n in plastic strain rate $\dot{\varepsilon}_{ij}^{p}$, the factor v is simply equal to $1/n$. Then, the dissipative stress χ_{ij} in rate-independent case, i.e. from Table 3.3, is required to be modified as follows:

$$\chi_{ij}' = v \cdot \frac{\partial(\delta\Phi)}{\partial\left(\dot{\varepsilon}_{ij}^{p}\right)} \tag{3.20}$$

As a result, if the Orthogonality principle, i.e. $\bar{\chi}_{ij} = \bar{\chi}_{ij}'$, is applied, the expressions from the rate-independent case are modified as follows:

$$-\frac{\partial\Psi^{g}}{\partial\varepsilon_{ij}^{p}} = v \cdot \frac{\partial(\delta\Phi)}{\partial\left(\dot{\varepsilon}_{ij}^{p}\right)} \tag{3.21}$$

The introduction of a scalar factor v in Equations (3.20) and (3.21) specifies that the dissipation function $\delta\Phi$ is referred to as pseudo-potential function for the dissipative stress χ_{ij}'.

The following assumption is adopted, in which it is adequate to consider that the function "z" is only dependent upon the rate of change of the internal variable (e.g. plastic strain increments), as in the case of dissipation function; thus, resulting in the expression of the dissipation potential function $\delta\Phi$ as follows:

$$\delta\Phi = \frac{\partial z}{\partial\left(\dot{\varepsilon}_{ij}^{p}\right)}\,\dot{\varepsilon}_{ij}^{p} \tag{3.22}$$

If $\delta\Phi$ is homogeneous first order in $\dot{\varepsilon}_{ij}^{p}$, i.e. $n = 1$, then it is emphasised that $z \equiv \delta\Phi$, by comparing Equation (3.17) to Equation (3.22). The advantages of the above assumption are explored later in the section.

Since $\delta\Phi$ is homogeneous but not first order in $\dot{\varepsilon}_{ij}^{p}$ for the rate-dependent case, the following generalised definition for the dissipative stress, rather than Equation (3.20), is expressed as follows:

$$\chi'_{ij} = \frac{\partial z}{\partial\left(\dot{\varepsilon}_{ij}^{p}\right)} \tag{3.23}$$

As similar to the rate-independent case, Ziegler's orthogonality principle, i.e. $\bar{\chi}'_{ij} = \chi'_{ij}$, is still adopted for the rate-dependent case. However, the principal advantage is that the function z, unlike the dissipation potential function $\delta\Phi$, serves as a potential for the dissipative stress χ'_{ij}. Hence, the function z could properly be defined as the dissipative generalised stress potential using Equation (3.23). However, the function z is referred to as the force potential function for simplicity and brevity, as also suggested by Houlsby and Puzrin (2002). Consequently, a simple Legendre-Fenchel transformation, like Legendre transformation, is applied to the force potential function z to introduce a new potential function "w", which is as follows:

$$z\left(\sigma_{ij}^{'}, \varepsilon_{ij}^{p}, \dot{\varepsilon}_{ij}^{p}\right) + w\left(\sigma_{ij}^{'}, \varepsilon_{ij}^{p}, \chi_{ij}^{\prime}\right) = \chi_{ij}^{\prime}\dot{\varepsilon}_{ij}^{p} \tag{3.24}$$

Accordingly, the following property from Legendre-Fenchel transformation is deduced from Equation (3.24), such that:

$$\dot{\varepsilon}_{ij}^{p} = \frac{\partial w}{\partial \chi_{ij}^{\prime}} \tag{3.25}$$

The corresponding fact is deduced from Equations (3.24) and (3.25) that the function $w\left(\sigma_{ij}^{'}, \varepsilon_{ij}^{p}, \chi_{ij}^{\prime}\right)$ has a clear analogy with the yield function $Y^{D}\left(\sigma_{ij}^{\prime}, \varepsilon_{ij}^{p}, \chi_{ij}^{\prime}\right)$ in dissipative stress space obtained from $\delta\Phi$ in the previous rate-independent case, compared with Table 3.3. Since the force potential function z is not homogeneous first order in $\dot{\varepsilon}_{ij}^{p}$, the Legendre-Fenchel transformation, no longer, results in a degenerate special case. Therefore, in contrast to the condition, i.e. $Y^{D}\left(\sigma_{ij}^{\prime}, \varepsilon_{ij}^{p}, \chi_{ij}^{\prime}\right) = 0$, in the rate-independent case, $w\left(\sigma_{ij}^{\prime}, \varepsilon_{ij}^{p}, \chi_{ij}^{\prime}\right) = 0$ from Equation (3.24) does not apply in this case of rate-dependency. Similar to the force potential function z, the function w could properly be defined as the plastic strain rate potential function, but for simplicity and brevity, function w is referred to as the flow potential function, as also suggested by Houlsby and Puzrin (2002). Re-arranging Equation (3.24) results in the following expression:

$$\delta\Phi = z\left(\sigma_{ij}^{\prime}, \varepsilon_{ij}^{p}, \dot{\varepsilon}_{ij}^{p}\right) + w\left(\sigma_{ij}^{\prime}, \varepsilon_{ij}^{p}, \chi_{ij}^{\prime}\right) \tag{3.26}$$

It is determined from Equation (3.26) that the sum of the force and flow potential functions is equal to the dissipation potential function $\delta\Phi$. As previously mentioned that $v = {}^{1}/_{n}$, if $\delta\Phi$ is a homogeneous function of order n in the plastic strain rates, it is deduced from Equations (3.18), (3.19) and (3.22) as follows:

$$z = \frac{\delta\Phi}{n}, so\ that\ \delta\Phi = \mathrm{n} \cdot \mathrm{z} = \left(\frac{\partial z}{\partial\left(\dot{\varepsilon}_{ij}^{p}\right)}\right)\dot{\varepsilon}_{ij}^{p} \tag{3.27}$$

Hence, the factor $v = {}^{1}/_{n}$ is simply a constant when $\delta\Phi$ is a homogeneous function of $\dot{\varepsilon}_{ij}^{p}$. Taking into consideration of Equation (3.27), consider if the dissipation function can be represented in the following form:

$$\delta\Phi = \sum_{i=1}^{N} (\delta\Phi)_i \tag{3.28}$$

where, $(\delta\Phi)_i$ itself is homogeneous and of order n_i in the plastic strain increments in each of the N functions. Accordingly, the force potential function is defined from Equations (3.27) and (3.28) as follows:

$$z = \sum_{i=1}^{N} \frac{(\delta\Phi)_i}{n_i} \tag{3.29}$$

According to Valanis (1966), all smooth functions can be approximated by a finite polynomial series. Similar types of functions in the form of Equation (3.28) are denoted as pseudo-homogeneous functions, and in such case, the dissipation potential function acts as a pseudo-potential function.

As discussed above, the entire rate-dependent hyperplastic constitutive framework is encapsulated within two thermodynamic potential functions, i.e. the free-energy and dissipation potentials. Hence, the following Table 3.4 summarises the rate-dependent hyperplastic approach based on Gibbs free-energy function, Ψ^{g}, and Helmholtz free-energy function, Ψ^{f}. Moreover, the flow chart representing the step-by-step development of rate-dependent hyperplasticity framework is depicted in Figure 3.4.

Table 3.4: Basic Formulations for Rate-dependent Hyperplasticity Framework

Rate-dependent Formulation	**Gibbs Free-Energy (g)**	**Helmholtz Free-Energy (f)**
Free-energy Function	$\Psi^g = \Psi^g\left(\sigma'_{ij}, \varepsilon^p_{ij}\right)$	$\Psi^f = \Psi^f\left(\varepsilon_{ij}, \varepsilon^p_{ij}\right)$
Stress or Strain	$\varepsilon_{ij} = -\dfrac{\partial \Psi^g}{\partial \sigma'_{ij}}$	$\sigma'_{ij} = \dfrac{\partial \Psi^f}{\partial \varepsilon_{ij}}$
Generalised Stress	$\bar{\chi}'_{ij} = -\dfrac{\partial \Psi^g}{\partial \varepsilon^p_{ij}}$	$\bar{\chi}'_{ij} = -\dfrac{\partial \Psi^f}{\partial \varepsilon^p_{ij}}$
Force Potential Function (z)	$z^g = z^g\left(\sigma'_{ij}, \varepsilon^p_{ij}, \dot{\varepsilon}^p_{ij}\right)$	$z^f = z^f\left(\varepsilon_{ij}, \varepsilon^p_{ij}, \dot{\varepsilon}^p_{ij}\right)$
Dissipative Stress	$\chi'_{ij} = \dfrac{\partial (z^g)}{\partial \left(\dot{\varepsilon}^p_{ij}\right)}$	$\chi'_{ij} = \dfrac{\partial \left(z^f\right)}{\partial \left(\dot{\varepsilon}^p_{ij}\right)}$
Flow Potential Function (w)	$(w^D)^g = (w^D)^g\left(\sigma'_{ij}, \varepsilon^p_{ij}, \chi_{ij}\right)$	$(w^D)^f = (w^D)^f\left(\varepsilon_{ij}, \varepsilon^p_{ij}, \chi_{ij}\right)$
Flow Rule in Dissipative Stress Space	$\dot{\varepsilon}^p_{ij} = \dfrac{\partial [(w^D)^g]}{\partial \chi'_{ij}}$	$\dot{\varepsilon}^p_{ij} = \dfrac{\partial \left[(w^D)^f\right]}{\partial \chi'_{ij}}$

In this case of rate-dependency, the flow rule is extracted from the property of Legendre-Fenchel transformation using Equation (3.24). Unlike a degenerate special case in the rate-independent case, the flow rule does not contain the non-negative multiplier (λ) due to the fact that the force potential function (z) is homogeneous but not first order in $\dot{\varepsilon}^p_{ij}$. However, the rate-dependent formulation still conform to the Ziegler's orthogonality principle, which is in the form $\bar{\chi}'_{ij} = \chi'_{ij}$, in order to transform the yield function and the flow rule from the dissipative stress space to true stress space.

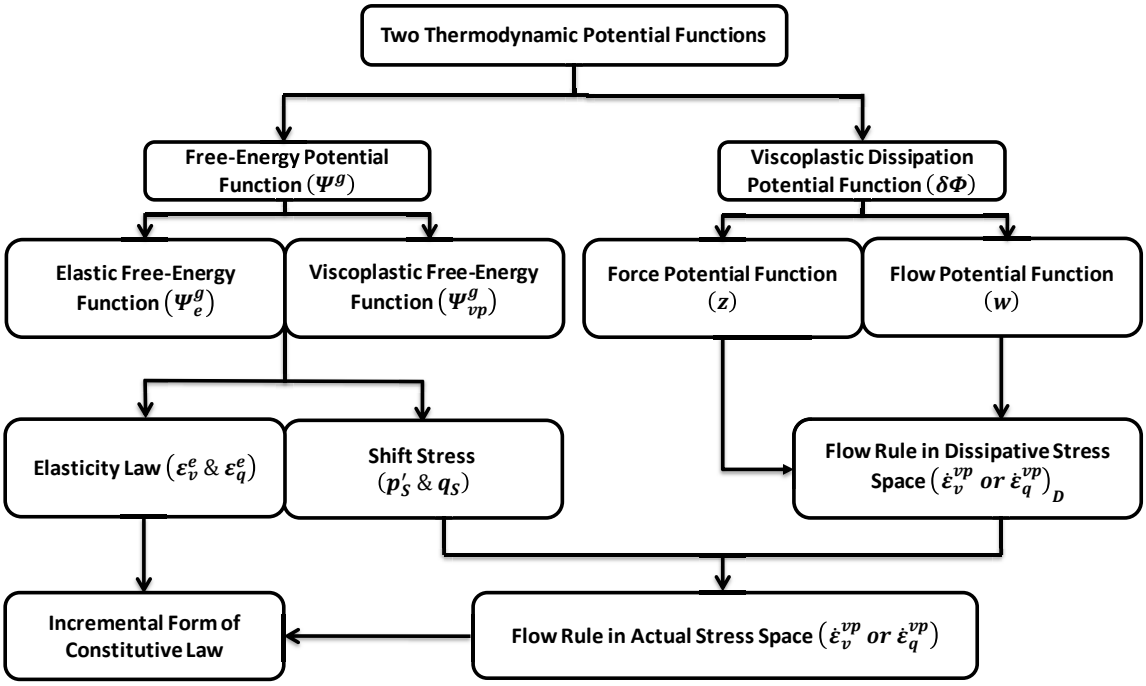

Figure 3.4: Flow Chart illustrating the steps in constructing the Incremental Form of the Elastic/Plastic Constitutive Law for the Development of Rate-dependent Hyperplasticity Models

3.5 Comparisons between Rate-independent and Rate-dependent Hyperplastic Formulation

Therefore, the comparisons between rate-independent and rate-dependent formulations based on hyperplasticity framework, highlighting the similarities and differences, are summarised in Table 3.5 and presented in the flow chart provided in Figure 3.5.

Table 3.5: Comparisons between Rate-independent and Rate-dependent Formulations for the Development of Hyperplasticity Models

Definition	**Rate-independent Formulation**	**Rate-dependent Formulation**
First Potential Function	The same definition for free-energy functions (Ψ)	
Second Potential Function	Dissipation function $(\delta\Phi)$ or Yield Function (Y)	Force Potential Function (z) and Flow Potential Function (w)
Generalised Stress	$\bar{\chi}'_{ij} = -\frac{\partial \Psi}{\partial \varepsilon^p_{ij}}$	$\bar{\chi}'_{ij} = -\frac{\partial \Psi}{\partial \varepsilon^p_{ij}}$
Dissipative Stress	$\chi'_{ij} = \frac{\partial(\delta\Phi)}{\partial\left(\dot{\varepsilon}^p_{ij}\right)}$	$\chi'_{ij} = \frac{\partial(z)}{\partial\left(\dot{\varepsilon}^p_{ij}\right)}$
Legendre and Legendre-Fenchel Transformations	$\delta\Phi\left(\sigma_{ij}, \varepsilon^p_{ij}, \dot{\varepsilon}^p_{ij}\right) + \lambda Y^D\left(\sigma_{ij}, \varepsilon^p_{ij}, \chi'_{ij}\right) = \chi'_{ij}\dot{\varepsilon}^p_{ij}$	$z\left(\sigma_{ij}, \varepsilon^p_{ij}, \dot{\varepsilon}^p_{ij}\right) + w^D\left(\sigma_{ij}, \varepsilon^p_{ij}, \chi'_{ij}\right) = \chi'_{ij}\dot{\varepsilon}^p_{ij}$
Flow Rule in Dissipative Stress Space	$\dot{\varepsilon}^p_{ij} = \lambda \frac{\partial Y^D}{\partial \chi'_{ij}}$	$\dot{\varepsilon}^p_{ij} = \frac{\partial w^D}{\partial \chi'_{ij}}$
Flow Rule in True Stress Space	$\dot{\varepsilon}^p_{ij} = \lambda \frac{\partial Y}{\partial \sigma_{ij}}$	$\dot{\varepsilon}^p_{ij} = \frac{\partial w}{\partial \sigma_{ij}}$

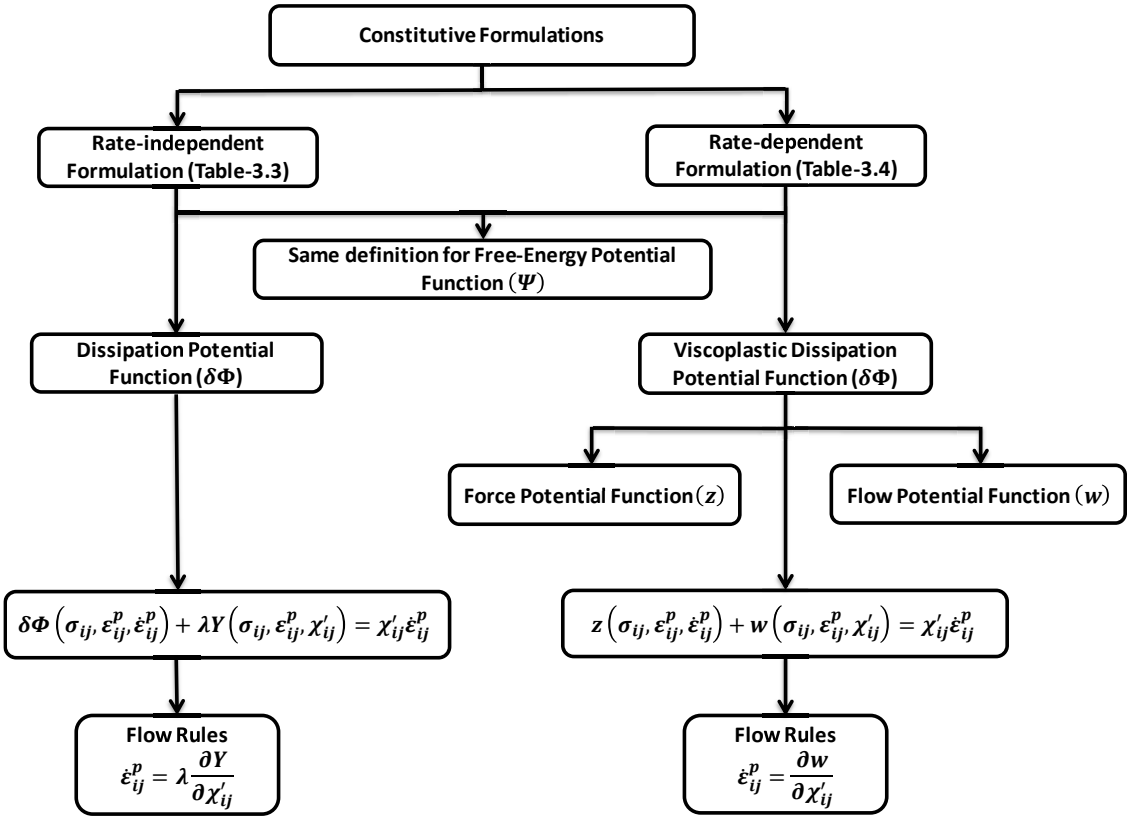

Figure 3.5: Flow Chart highlighting the Similarities and Differences between Rate-independent and Rate-dependent Formulations for the Development of Hyperplasticity Models

Considering the rigidity, and compactness of the hyperplasticity framework, along with its provision of confidence and reliability for building a strong foundation for the development of constitutive models, it is rational and logical that the development of a constitutive soil model is based on the rate-dependent hyperplasticity approach. Consequently, the following Chapter 4 discusses the development of a simple and versatile constitutive soil model based on hyperplasticity theory to simulate the non-linear creep behaviour, along with the prediction of both isotropic and kinematic hardening behaviour of soils. As distinctively different from most of the existing viscoplasticity models, the model avoids the need to introduce a considerable number of assumptions without being related to the physical phenomena of soils as it is based on the fundamental laws of thermodynamics.

CHAPTER 4

DEVELOPMENT OF MIXED HARDENING HYPER-VISCOPLASTICITY MODELS FOR SOFT SOILS - H-CREEP MODEL & EXTENDED MODEL

4.1 Introduction

In the early stages of the current study, the time-dependent behaviour of soils has been investigated comprehensively within the field of soil mechanics. Considerably, the sophisticated behaviour of soils, along with the associated complexities, including the highly non-linear time- and rate-dependent behaviour soil matrix and complicated interaction of fluid flow and deformation responses result in the necessity for further understanding of various observed time- and rate-dependent phenomena of soils, such as creep, stress relaxation and rate-dependency of strength characteristics. Therefore, there has been a burgeoning interest in studying the time-dependent behaviour of geomaterials to develop constitutive models has become the major subject of interest for researchers in the field of modern geomechanics. As previously discussed, several approaches have been developed to capture the time-dependent behaviour of soils, including empirical models, rheological models, and the elasto-viscoplastic constitutive models. Although a plethora of research work has been carried out to reproduce the time-dependent behaviour realistically, most of the existing constitutive models have had to compensate with a considerable number of assumptions and/or a large number of parameters and a lot of questions still remain to be answered due to the problematic nature of predicting the time-dependent deformation characteristics of real soils. As a consequence, the existing constitutive viscoplasticity models are yet flexible enough to disobey the fundamental laws of thermodynamics. Moreover, they often require a considerable number of assumptions without being related to the physical phenomena of real soils.

To circumvent the drawbacks of having a substantial number of assumptions, this chapter introduces a unique mixed hardening hyper-viscoplasticity model (H-Creep Model), based on the fundamental laws of thermodynamics, for the derivation of the time-dependent constitutive behaviour of soils, with the intention to capture the variation in the shapes of the yield loci by

pursuing non-associated flow rules and accounting for kinematic hardening effects. The most distinctive characteristic of the proposed model is their compliance with the physical phenomena, such as the conservation of mass and energy and the fundamental laws of thermodynamics. One of the most profound benefits from this approach, is that the identification of two thermodynamic potentials (i.e. the free-energy and the dissipation functions) is sufficient to predict the entire constitutive behaviour of elastic-plastic materials, entailing the yield condition and flow rule, along with the isotropic and kinematic hardening laws, as well as the elasticity law.

The next section of this chapter, i.e. Section 4.2, summaries the major characteristics of the proposed mixed hardening hyper-viscoplasticity model for soils incorporating non-linear creep rate, accompanied with the aforementioned attributes, based on the principles of hyperplasticity discussed in Chapter 3. Section 4.3 introduces the non-linear creep formulation, which is incorporated as part of the time-dependent viscosity scaling function embedded in the dissipation potential function. The following Section 4.4 outlines the rational extension towards the proposed mixed hardening hyper-viscoplasticity model for soils by incorporating soil fabric to emphasise on the importance of modelling strain-softening effects during time-dependent delayed deformation, particularly in natural soils. This is followed by a brief discussion on the major principle and one of the key characteristics of the proposed model in Section 4.5. This chapter concludes with the findings and observations on both the proposed and extended components of the mixed hardening hyper-viscoplasticity model in Section 4.6.

In this chapter, the majority of the formulations are expressed using principal stresses. The principal stresses are ordered, in which σ_1 is the most tensile, whereas σ_3 is the most compressive, i.e. $\sigma_1 \leq \sigma_2 \leq \sigma_3$. In tandem with the geotechnical sign convention, compressive

stresses are denoted as positive, whilst tensile stresses are negative. All the stresses throughout this chapter are considered as effective stresses with prime notation.

4.2 Formulation - Proposed Mixed Hardening Hyper-viscoplasticity Model for Soils

4.2.1 Theoretical Background

The extraction of plasticity theory with the major emphasis on the fundamental laws of thermodynamics stems from the early works of Halphen and Nguyen (1974) and Ziegler (1983), in which the derivation of the entire constitutive response for modelling plastic materials was based on two scalar thermodynamic potential functions. Collins and Houlsby (1997) and Houlsby and Puzrin (2000) have termed this relatively new approach as 'hyperplasticity' for developing constitutive models for time-independent behaviour of soils. Basically, the hyperplastic approach begins with the thermodynamic hypotheses, from which plasticity theories are developed for the modelling of constitutive models for soil behaviour. The entire constitutive response for stress-strain behaviour of soils is specified with two thermodynamic scalar potential functions, i.e. free-energy and dissipation potential functions.

Firstly, a free-energy potential function is defined as one of its four alternative free-energy forms, namely the internal energy (u), Helmholtz free-energy (f), Gibbs free-energy (g), or the enthalpy (h). These four alternative forms of free-energy function are not independent, but instead, they are related by Legendre transformations, as discussed in the previous Chapter 3.

Secondly, a dissipation potential function is postulated, in which it is a function of the thermodynamic state and the rate of change of material state. Consequently, it is sufficient to consider that the dissipation function depends only on the rate of change of the internal variable (e.g. plastic strain increments), but not on the total strain rate, as this indicates that purely elastic deformation would contribute to the dissipation. The influence of changes in temperature is neglected for simplicity. For rate-independent case, the dissipation potential function is assumed to a homogeneous first order function of plastic strain increments. Although the general form of the dissipation function remains unchanged, the dissipation potential function is still homogeneous but not first order in the plastic strain increments for the case of rate-dependency, as also emphasised in the previous Chapter 3. Hence, this serves as the strong foundation for the development of the proposed H-Creep model for modelling time-dependent behaviour of soils.

On the other hand, the non-associated flow rule is derived as a necessary consequence of the dependence of the dissipation potential function on the actual stress components (Aung et al., 2016) (See – Appendix A for detailed demonstrations). Compared with the conventional plasticity theory, in which it is common to express the plastic strain increments in terms of a plastic potential function to instigate the non-associated flow rule, there is no need to introduce arbitrary plastic flow potential function in this context of hyperplasticity. Although there was a constructive proof related to the existence of the plastic potential function (e.g. Hunter, 1976) for an isotropic incompressible material, where the plastic strain rates depend on the second and third stress invariants. However, such a potential cannot be expected to exist when the incompressibility condition ($\dot{\varepsilon}_{11} + \dot{\varepsilon}_{22} + \dot{\varepsilon}_{33} = 0$), i.e. the summation of strain rates along Cartesian co-ordinate, is relaxed. Therefore, plastic potential not always exist (Vardoulakis and Sulem, 1955; Collins and Hilder, 2002). In most of the existing conventional plasticity models, the yield surfaces and flow rules are postulated, and these surfaces are normally joined together

in an arbitrary condition at a certain transitional stress ratio. In contrast, the derivation of non-associated flow rule as a natural consequence from the stress-dependent dissipation function from the hyperplastic perspective is considered as more general, in which this transition is more seamless and continuous.

Besides, the observations from laboratory experiments have indicated that the yield loci not only expand but also translate in the stress space and the shapes of the yield loci do vary depending on the types of soils (Dafalias and Taiebat, 2013, 2014; Zhou et al., 2016). In order to take into consideration of the expansion and translation of the yield loci, one of the major developments in the constitutive modelling of soils is the introduction of kinematic hardening mechanism by Mroz (1967). In general, the kinematic hardening formulation not only controls the movement of the yield loci but also describes the variation of the plastic modulus. Accordingly, kinematic hardening during inelastic deformations is usually described by a so-called 'back' or 'shift' stress, which is considered as an internal variable, for which an adequate constitutive equation is formulated (Sansour et al., 2006). Within the context of hyperplasticity, the plastic work done by shift stress is referred to as 'stored plastic work', and hence, this work function determines the translational, kinematic hardening behaviour, and the dissipative stress determines the isotropic hardening or softening, i.e. the expansion or contraction of the yield surface (Collins, 2005). However, there has been insufficient recognition in that the shift stress and the dissipative stress share an important role, in tandem, for the formulation of mixed hardening constitutive soil models of geomaterials with different strengths in tension and compression (Collins and Kelly, 2002; Lai et al., 2016).

Therefore, a thorough knowledge of the mechanical processes governing the creation and release of stored plastic work is crucial in understanding the physical meaning behind the translation laws governing the motion of such surfaces. Consequently, 'kinematic hardening'

models are frequently developed to model the 'memory' of the soil, which leads to the fact that the stored plastic work plays the prominent role in such models. Hence, the hardening terms are introduced to the free-energy function to take into account of kinematic hardening effects, whereas the hardening terms are introduced into the dissipation potential function to consider for isotropic hardening effects, as inspired by the discussions in Likitlersuang (2003).

This section continues with the theoretical development of the proposed mixed hardening hyper-viscoplasticity (H-Creep) model for describing the time-dependent deformation of soils, to capture the variation in the shapes of the yield loci with the consideration of isotropic and kinematic hardening effects by pursuing the non-associated flow behaviour. To start with, the proposed model is developed based on the classical additive decomposition of the infinitesimal strain tensor, as it is a priori accepted that the total strain rate $\dot{\varepsilon}_{ij}$ is additively composed of the elastic strain rate $\dot{\varepsilon}_{ij}^{e}$ and viscoplastic strain rate $\dot{\varepsilon}_{ij}^{vp}$, which is expressed as follows:

$$\dot{\varepsilon}_{ij} = \dot{\varepsilon}_{ij}^{e} + \dot{\varepsilon}_{ij}^{vp} \tag{4.1}$$

where, $\dot{\varepsilon}_{ij} = (i, j)$ component of the total strain-rate tensor. The proposed model adopts the definition of the Cambridge parameters for stress and strain, as triaxial notation, to describe the stress-strain behaviour, which is provided as follows:

$$p' = \frac{(\sigma_1' + 2\sigma_3')}{3} \tag{4.2a}$$

$$q = (\sigma_1' - \sigma_3') \tag{4.2b}$$

$$\varepsilon_v = (\varepsilon_1 + 2\varepsilon_3) \tag{4.2c}$$

$$\varepsilon_q = \frac{2(\varepsilon_1 - \varepsilon_3)}{3} \tag{4.2d}$$

where, the subscripts 1 and 3 refer to axial and radial directions, respectively. The parameters p' and q are mean effective stress and deviatoric stress, respectively; whereas ε_v and ε_q are volumetric and deviatoric strains, respectively.

Since the free-energy function can be expressed in four alternative forms, as discussed above, each of the different forms of free-energy are most convenient for particular types of problems. For instance, the Helmholtz or Gibbs free-energy functions are most appropriate for isothermal conditions because they employ temperature as a state variable. In contrast, the internal energy or enthalpy forms are most suitable for isentropic (constant entropy) problems. As the thermal effects are not being considered, the proposed model pursues the form of Gibbs free-energy function (g), compared to that of Helmholtz free-energy function (f), due to its relative convenience in expressing formulations in terms of stress components.

In general, the free-energy is allowed to depend on both the elastic and inelastic strains. This contradicts with the common assumption in the conventional plasticity theory that the energy associated with plastic strains is irrecoverable, resulting in the assertion that the free-energy should depend only on the elastic strains, as it represents the elastic energy stored in an individual grain. As elaborated in Chapter 2, a certain portion of the micro-level elastic energy is 'trapped' or 'frozen' and thus, resulting in some of the inelastic deformation being stored due to the highly heterogeneous nature of the stress and inhomogeneous nature of the deformations at the micro level. Hence, the possibility of 'trapped' energy situation is much higher when the particles or sub-particles (platelets) are irregular in shapes and also when the cohesion between the particles/platelets is induced by the electrostatic forces. Consequently, it is very likely that a greater proportion of 'trapped' energy is expected in clays than in sands, which justifies the consideration of inelastic free-energy function in the proposed model. This magnitude of 'trapped elastic energy' or 'stored plastic work' at the continuum level is

determined by the inelastic strains. This, in conjunction with the 'decoupled' assumption that the instantaneous elastic moduli do not depend on the plastic strains, the proposed model embraces the additive decomposition of the free-energy function into the elastic component of the free-energy function $\left(\Psi_e^g\right)$ and the viscoplastic component of the free-energy function $\left(\Psi_{vp}^g\right)$, inspired by Collins and Houlsby (1997) and Zhou et al. (2016), which is expressed as follows:

$$\Psi^g = \Psi_e^g + \Psi_{vp}^g \tag{4.3}$$

The additional inelastic term takes into consideration of the frozen energy increment, which is unrestricted in sign, either positive or negative, as the energy described by this term can be both stored and released. The existence of additional energy terms, arising from internal variable formulation, is also in agreement with the early energy theory for clays, developed by Palmer (1967).

4.2.2 Elastic Free-Energy Function

In soil mechanics, a logarithmic elastic stress-strain relationship is applicable to describe the consolidation behaviour (Butterfield, 1979). Based on the semi-logarithmic elasticity in volumetric behaviour, and the linear elasticity in the deviatoric behaviour (e.g. Coombs, 2017), the elastic component of the free-energy function $\left(\Psi_e^g\right)$ is defined as follows:

$$\Psi_e^g = -\frac{\kappa^*}{V} p_0' \left[\mathrm{ilog}\left(p'/p_0'\right)\right] - \frac{q^2}{6G} \tag{4.4}$$

where, ilog function is defined as $\mathrm{ilog}(x) = xlog(x) - x$, so that $\frac{d}{dx}\mathrm{ilog}(x) = \log(x)$, p_0' and G are denoted as the reference pressure and the elastic shear modulus, respectively, and κ^* is the slope of the elastic swelling lines in the v - $\ln p$ plane.

Taking the partial derivative of Equation (4.4) with respect to corresponding applied pressure and total strains, the elastic stress-strain relationships can be determined as follows:

$$\varepsilon_v^e = -\frac{\partial \Psi_e^g}{\partial p'} = \frac{\kappa^*}{V} \cdot \log\left(p'/p_0'\right) \tag{4.5a}$$

$$\varepsilon_q^e = -\frac{\partial \Psi_e^g}{\partial q} = \frac{q}{3G} \tag{4.5b}$$

where, the parameters ε_v^e and ε_q^e are the elastic volumetric and elastic shear strains, respectively. In the $(p' - q)$ plane, the incremental elastic stress-strain relationship is determined using a compliance matrix (Sun and Shen, 2017; Sun et al., 2018), which is as follows:

$$\begin{bmatrix} \dot{\varepsilon}_v^e \\ \dot{\varepsilon}_q^e \end{bmatrix} = \begin{bmatrix} 1/K & 1/J \\ 1/J & 1/3G \end{bmatrix} \begin{bmatrix} \dot{p}' \\ \dot{q} \end{bmatrix} \text{ or } \begin{bmatrix} \dot{p}' \\ \dot{q} \end{bmatrix} = \begin{bmatrix} K & J \\ J & 3G \end{bmatrix} \begin{bmatrix} \dot{\varepsilon}_v^e \\ \dot{\varepsilon}_q^e \end{bmatrix} \tag{4.6}$$

The elastic bulk modulus (K) is then deduced from Equations (4.5a) and (4.6) and it is presumed that the shear modulus (G) is related to the elastic bulk modulus (K) by assuming a constant value of Poisson's ratio (v), rather than assuming a constant value of G. This is due to the fact that the variable bulk modulus, when used in conjunction with the constant Poisson's ratio, leads to pressure-dependent shear modulus. Besides, experimental evidence also suggests that the shear modulus does vary with the mean pressure (Yang et al., 2010; Zhou and Ng, 2015; Lai et al., 2016). Houlsby (1985) clearly pointed out that the adoption of a constant shear modulus could also lead to non-conservative behaviour. As in the case of the existing elastic-viscoplastic models for clays (Wroth and Houlsby, 1985; Zhou and Ng, 2015; Lai et al., 2016), the proposed model has been formulated within infinitesimal deformation hypothesis by adopting variable shear modulus.

On the other hand, the incremental elastic stress-strain relationship is also obtained by double-differentiation of the Gibbs free-energy function defined in Equation (4.4) can be written as following:

$$\begin{bmatrix} \dot{p}' \\ \dot{q} \end{bmatrix} = \begin{bmatrix} K & J \\ J & 3G \end{bmatrix} \begin{bmatrix} \dot{\varepsilon}_v^e \\ \dot{\varepsilon}_q^e \end{bmatrix} = \begin{bmatrix} -\dfrac{\partial^2 \Psi_e^g}{\partial p^2} & -\dfrac{\partial^2 \Psi_e^g}{\partial p \partial q} \\ -\dfrac{\partial^2 \Psi_e^g}{\partial p \partial q} & -\dfrac{\partial^2 \Psi_e^g}{\partial q^2} \end{bmatrix}^{-1} \begin{bmatrix} \dot{\varepsilon}_v^e \\ \dot{\varepsilon}_q^e \end{bmatrix} \tag{4.7}$$

Besides, the elastic bulk and shear moduli are deduced as follows:

$$K = \frac{Vp'}{\kappa^*} \tag{4.8a}$$

$$G = \frac{3(1-2v)K}{2(1+v)} \tag{4.8b}$$

The coupling modulus in Equation (4.6) is being considered as $J = \pm\infty$ when only the isotropic consolidation conditions are considered. Although most natural clays will exhibit anisotropy of elastic behaviour (Einav and Puzrin, 2004; Castro and Sivasithamparam, 2017), incorporation of elastic anisotropy could result in a considerable extent of complexity of any model where anisotropy is not fixed.

Since plastic deformations are likely to impose huge influence on many problems of practical interest, with elastic strains often being relatively insignificant, it is reasonable to assume the elastic behaviour to be isotropic in this model.

4.2.3 Viscoplastic Free-Energy Function – Kinematic Hardening Law

On the other hand, the additional inelastic (or viscoplastic) component of the free-energy function, which stems from the amount of stored plastic work, is defined as follows:

$$\Psi_{vp}^{g} = \gamma \cdot (\lambda^* - \kappa^*) p_0' \exp\left(\varepsilon_v^{vp} \Big/ (\lambda^* - \kappa^*)\right) \tag{4.9}$$

where, the new parameter γ is referred to as a material constant linking to the amount of stored plastic work. The parameters λ^* and κ^* are used to retain their usual relationship to the slopes of the virgin compression and swelling lines in a $v - \ln p'$ plot, respectively. A similar form of plastic free-energy function was proposed by Collins and Hilder (2002), but it was limited to rate-independent axisymmetric case. Hence, the inclusion of viscoplastic strains in the free-energy function or in other words, the addition of the inelastic component of the free-energy function makes it discernible from most of the conventional plasticity theories, in which the energy associated with plastic strains is often assumed to be non-recoverable. This is the key feature of the hyperplasticity approach to the modelling of elastic/plastic materials, in which it is explicitly acknowledged that not all the plastic work is dissipated, but some portion is stored.

Within the context of hyperplasticity, this additional viscoplastic free-energy function results in the shift stress to describe the kinematic hardening behaviour, accommodating the effect of stress history on stiffness of soils. In this study, it is assumed that this part of the free-energy potential function depends only on the volumetric part of the viscoplastic strain, similar to the model proposed by Samat (2016).

Taking the derivative of Equation (4.9) with respect to ε_v^{vp}, results in the volumetric component of the shift stress (i.e. p_S):

$$p_S' = \frac{\partial \Psi_p^g}{\partial \varepsilon_v^{vp}} = \gamma \cdot p_0' \exp\left(\varepsilon_v^{vp} \Big/ (\lambda^* - \kappa^*)\right) = \frac{1}{2}\gamma p_c' \tag{4.10}$$

where, the pre-consolidation pressure p_c' is defined as:

$$p_c' = 2p_0' \exp\left(\varepsilon_v^{vp} \Big/ (\lambda^* - \kappa^*)\right) \tag{4.11}$$

Since the inelastic free-energy function in Equation (4.9) is assumed to depend only on the viscoplastic volumetric strain, the deviatoric component of the shift stress (i.e. q_S) is zero in this paper. Due to the fact that the shift stress only has an isotropic component, the viscoplastic component of the free-energy function can also be expressed by using the volumetric shift stress components determined in Equation (4.10), which is as follows:

$$\Psi_{vp}^{g} = p_S' \, \dot{\varepsilon}_v^{vp} + q_S \, \dot{\varepsilon}_q^{vp} = \frac{1}{2}\gamma p_c' \, \dot{\varepsilon}_v^{vp} = \frac{1}{2}\gamma\left(p_c' \, \dot{\varepsilon}_v^{vp}\right) \tag{4.12}$$

It can be stated from Equation (4.12) that a fraction $\gamma/2$ is stored and the other portion (i.e. $1 - \gamma/2$) is dissipated, from all the plastic work done. The resulting shift stress defines the moving 'centre' of the critical surface, which is defined in Section 4.2.5, as the stored plastic work plays the role of a scalar memory parameter. According to Collins and Kelly (2002), the stored plastic work could be considered as the trapped elastic reversible energy related to the elastic deformations of the grains occurring in the relatively weak sub-networks and the resulting shift stress is integral to describe the isotropic compression and expansion of a material. Although the presence of shift stress in the modified Cam-clay model was acknowledged by Houlsby (1981) and Collins and Houlsby (1997), it is demonstrated as a natural component within the proposed model and hence, the resulting shift stress indicates that it is possible to induce 'plastic decompression' at zero effective stress in the proposed model. Considering the effects of isotropic compression and expansion, the determination of pre-consolidation pressure is not possible from Equation (4.11), as a total form of the inelastic strain is, typically, not available. Therefore, the evolution law must be formed to determine the extent of coupling, which can then be integrated to obtain a usable incremental response between the inelastic strains and the internal variables used in the hardening laws.

Assuming that the pre-consolidation pressure evolves as an independent variable and applying the chain rule to the relationship in Equation (4.11), the incremental evolution of the pre-consolidation pressure is determined as follows:

$$\dot{p}_c' = \frac{\partial p_c'}{\partial \varepsilon_v^{vp}} \dot{\varepsilon}_v^{vp} = \frac{p_c'}{(\lambda^* - \kappa^*)} \left(\dot{\varepsilon}_v^{vp}\right) \tag{4.13}$$

Although the pre-consolidation pressure is a function of the current specific volume, which depends on both the elastic and the plastic volumetric strains in classical critical state theory, this has led to unnecessary theoretical complications. Moreover, Butterfield (1979) has proved that the dependence of pre-consolidation pressure only on the volumetric components is pertinent to the laboratory observations as well as the traditional models. Therefore, it is reasonable to assume that the pre-consolidation pressure depends only on the plastic component of the volumetric strain (as in MCC), which was also pointed out by Nguyen et al. (2014) and Lai et al. (2016).

4.2.4 Proposed Viscoplastic Dissipation Function

In this time-dependent model, the viscoplasticity component is modelled by proposing the incremental dissipation in the form of the square root of a quadratic function of the viscoplastic strain increments, together with the incorporation of rate-dependent effects. Overall, the dissipation potential function is postulated in the form, provided in Equation (3.28), which is homogeneous but of order "n" in the plastic strain increments. Following the investigation of the isotropic two-parameter family of models, there are certain benefits in adopting dissipation functions, similar to those presented in Lai et al. (2014) and Coombs (2017). Consequently, the dissipation function used to define the rate-dependent viscoplastic

constitutive behaviour is proposed based on the existing triaxial compression data, which is expressed as follows:

$$\delta\Phi = \sqrt{A^2\left(\dot{\varepsilon}_v^{vp}\right)^2 + B^2\left(\dot{\varepsilon}_q^{vp}\right)^2} + \Lambda\left[\sqrt{A^2\left(\dot{\varepsilon}_v^{vp}\right)^2 + B^2\left(\dot{\varepsilon}_q^{vp}\right)^2}\right]^n \geq 0 \qquad (4.14)$$

where, the first square-root term on the right-hand side of the equation is referred to as the instantaneous dissipation and the second term takes into account of the additional dissipation due to delayed deformations. As distinctively different from the similar dissipation functions proposed by Lai et al. (2014) and Coombs (2017), the dissipation potential function defined in Equation (4.14) is no longer a homogenous first order function. The inequality in Equation (4.14) must be strictly positive when viscoplastic deformations are occurring to comply with the first and second laws of thermodynamics, valid for isothermal deformations (Ziegler, 1983). The volumetric and deviatoric components of the viscoplastic strain (i.e. $\dot{\varepsilon}_v^{vp}$ and $\dot{\varepsilon}_q^{vp}$) are used as the internal variables. The time-dependent effects are incorporated by assuming non-zero value for the parameter Λ, which is referred to as a time-dependent viscosity scaling function. Since the second term in Equation (4.14) represents the delayed plastic deformations, it is logical that both terms share the similar mathematical structure, with a particular case being considered as a power law function of n, which is a material constant.

Inspired by the discussions provided in Collins & Kelly (2002) and Coombs (2017), the functions A and B have the dimensions of stress, and it is assumed that A and B are linear functions of the three defining effective stress variables (i.e. p', q and p_c'). The stress-like quantities, A and B, are given by

$$A = (1-\gamma)p' + (1/2)\gamma p_c' \text{ and } B = (1-\alpha)Mp' + (1/2)\alpha\gamma M p_c' \qquad (4.15)$$

where, M is the slope of the Critical State Line (CSL). The parameter M can be related to the effective friction angle via $M = 6\sin\phi'/(3-\sin\phi')$. The new parameters γ and α are

material constants linked to the amount of stored plastic work and the deviatoric dissipation, respectively. It is important to note that it is still possible to make use of p' and q defined in Equations (2.11a) and (2.11b) as long as the triaxial states of stress are assumed to exclude principle stress rotation (i.e. $\sigma_2 = \sigma_3$). Moreover, the introduction of p' or q as parts of the functions A and B still complies with the thermodynamic rule, which does not require to specify work conjugate variables together as independent state variables (see Collins and Hilder (2002) for more discussion on this aspect).

On the other hand, the viscosity scaling function (Λ) incorporates viscosity parameter (ψ'), which takes a particular form in this model similar to Leoni et al. (2008), provided as follows:

$$\psi' = V \cdot t_R / \mu \tag{4.16}$$

where, the parameter V is the specific volume, defined as $V = 1 + e$, in which e is referred to as void ratio. The reference time t_R depends on the duration of incremental loading used in the conventional triaxial compression test, from which the initial reference pre-consolidation pressure is obtained. The parameter μ is referred to as creep parameter, defined as $\mu \approx C_{\alpha e}/\ln 10$, where $C_{\alpha e}$ represents secondary compression coefficient and it is generally assumed as constant in the traditional elasto-viscoplastic (EVP) models (e.g. Yin and Graham, 1999; Vermeer and Neher, 2000; Yin et al., 2011b).

If time-dependent effects are to be neglected, along with the condition when $\gamma = 1$ and $\alpha = 1$, the dissipation function in Equation (4.14) returns to the one used to derive the isotropic yield surface for the MCC model. Moreover, it can be deduced from Equation (4.12) that half the value of the total plastic work done is actually stored in the MCC model when using $\gamma = 1$ and $\alpha = 1$ within the context of hyperplasticity. As pointed out in Chapter 3, due to the

presence of the stress-like quantities (i.e. functions A and B) in the dissipation function presented in Equation (4.14), the hardening terms (e.g. p_c') are included in the dissipation function, capturing the isotropic hardening behaviour of soils (Collins and Hilder, 2002; Lai et al., 2016). Since the stress-strain behaviour of soils demonstrates both isotropic and kinematic hardening responses, it is rational for the proposed model to merge these two hardening approaches to predict the time-dependent behaviour of a wider class of soils. Moreover, the existence of stress components in the dissipation function can eventually result in the non-associated flow rule (Aung, et al., 2016), which is also demonstrated in the Appendix A.

4.2.5 Force and Flow Potential Functions

In this case of rate-dependency, the dissipation potential function in Equation (4.14) is separated into the force potential function and flow potential function, based on the principles outlined in Equation (3.26) and the definitions summarised in Table 3.4. Following the procedure discussed in Equations (3.27) - (3.29), the force potential function (z) is derived from Equation (4.14) as follows:

$$z = \sqrt{A^2\left(\dot{\varepsilon}_v^{vp}\right)^2 + B^2\left(\dot{\varepsilon}_q^{vp}\right)^2} + \frac{\Lambda}{n}\left[\sqrt{A^2\left(\dot{\varepsilon}_v^{vp}\right)^2 + B^2\left(\dot{\varepsilon}_q^{vp}\right)^2}\right]^n \tag{4.17}$$

Based on the procedure outlined in Equations (3.24) and (3.26), the flow potential function (w) is obtained using the Legendre-Fenchel transformation. Combining Equations (4.14) and (4.17), it follows that:

$$w = \delta\Phi - \mathrm{z} = \left[\frac{n-1}{n}\right]\Lambda\left[\sqrt{A^2\left(\dot{\varepsilon}_v^{vp}\right)^2 + B^2\left(\dot{\varepsilon}_q^{vp}\right)^2}\right]^n \tag{4.18}$$

The volumetric and deviatoric components of the dissipative stresses (i.e. p'_D and q_D) can then be derived from the force potential function determined in Equation (4.17) as follows:

$$p'_D = \frac{\partial z}{\partial \dot{\varepsilon}_v^{vp}} = \left[\frac{A^2\left(\dot{\varepsilon}_v^{vp}\right)}{\Pi}\right] + \left[\Lambda \cdot [\Pi]^{n-1} \cdot \frac{A^2\left(\dot{\varepsilon}_v^{vp}\right)}{\Pi}\right] \tag{4.19}$$

$$q_D = \frac{\partial z}{\partial \dot{\varepsilon}_q^{vp}} = \left[\frac{B^2 \cdot \left(\dot{\varepsilon}_q^{vp}\right)}{\Pi}\right] + \left[\Lambda \cdot [\Pi]^{n-1} \cdot \frac{B^2 \cdot \left(\dot{\varepsilon}_q^{vp}\right)}{\Pi}\right] \tag{4.20}$$

where, $\Pi = \sqrt{A^2\left(\dot{\varepsilon}_v^{vp}\right)^2 + B^2\left(\dot{\varepsilon}_q^{vp}\right)^2}$. Re-arranging Equations (4.19) and (4.20), and substituting the corresponding components of viscoplastic strain increments into the flow potential function in Equation (4.18) results in the flow potential function, being re-written as follows:

$$w = \left[\frac{n-1}{n}\right]\left[\frac{1}{(\Lambda)^{1/(n-1)}}\right][\langle \varrho_D \rangle]^{\frac{n}{n-1}} \tag{4.21}$$

where, $\langle \quad \rangle$ = Macaulay brackets; $\langle x \rangle = 0, x < 0$; and $\langle x \rangle = x, x \geq 0$ and ϱ_D is denoted as dissipative critical surface function, which is derived as follows:

$$\varrho_D = \sqrt{\frac{(p'_D)^2}{A^2} + \frac{(q_D)^2}{B^2}} - 1 \tag{4.22}$$

It is to be emphasised that the function ϱ_D in Equation (4.22) resembles the plastic criterion, which is derived when the time-dependent viscosity scaling function (Λ) is zero in Equation (4.14), i.e. when the dissipation potential function in Equation (4.14) becomes homogeneous first order in the plastic strain increments for the rate-independent case. In the proposed model, the function ϱ_D defines a surface, which is to be denoted as critical surface. The parameters γ and α, as part of the stress functions A and B, have considerable implications

on the shape of the critical surface (as demonstrated in Figure 4.1) and the degree of non-association of the viscoplastic flow rules, described in the following section.

Although most of the existing EVP models have employed the commonly adopted assumption of the yield surface being a symmetric elliptical about the mean effective stress axis, a few notable shortcomings have been observed, as pointed out in Leoni et al. (2008). As also signalled by Graham et al. (1983b), the behaviour of most plastic clays is more appropriately described by skewed ellipses that vary in orientation during loading. Moreover, one of the significant drawbacks, which the proposed model has intended to address, is the provision of poor predictions related to the undrained stress path and the loading response in one-dimensional normal compression.

In the proposed model, the emphasis also lies on the fact that the critical surface changes in time due to creep behaviour when considering rate-dependent effects. Considering Equations (4.21) and (4.22), it is to be accentuated that the critical surface presented in Equation (4.22) does not separate viscous from viscous-free behaviour and that the plastic strain is always occurring due to soil viscosity and this critical surface represents a nominal viscoplastic strain rate.

As depicted in Figure 4.1, when viscous scaling function is set to zero, the critical surface becomes narrower deviatorically with the reducing values of γ, whilst the critical surface becomes more tear-drop shaped with the declining values of α. When $\gamma = 0$, the radius of the critical surface disappears, whereas the critical surface lies entirely beneath the CSL when $\alpha = 0$. The value of γ has an influence on the intersection of the CSL and the critical surface, whereas the value of α has no effect on the location of that intersection.

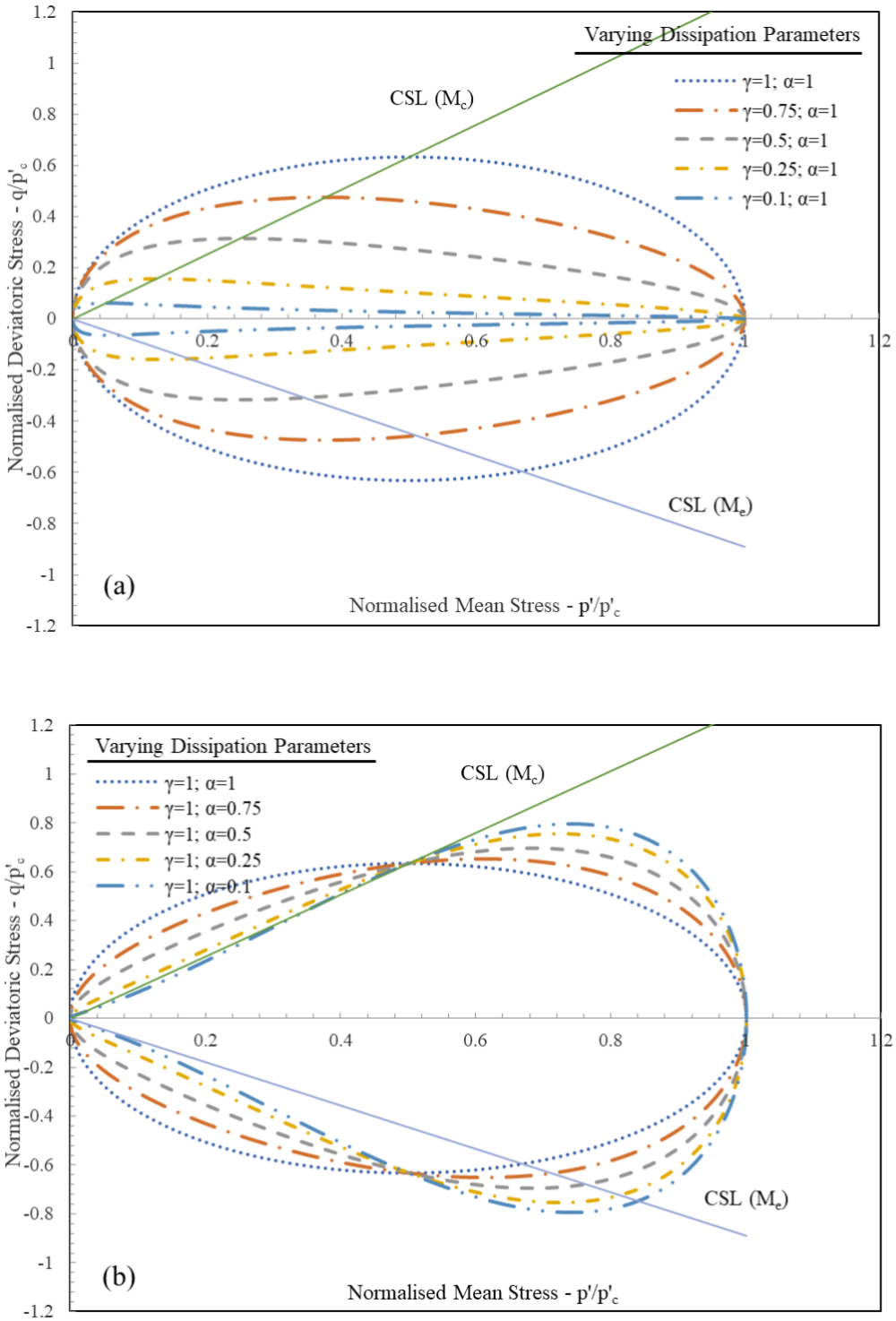

Figure 4.1: Changes in the Shapes of Critical Surface in $p' - q$ space, corresponding to the values of (a) γ and (b) α varying over the range 1.0 to 0.1

Here, the viscoplastic flow rules in the dissipative stress space are then determined by differentiating the flow potential function in Equation (4.21) with respect to the corresponding

dissipative stress, as outlined in Equation (3.24) following the property of Legendre-Fenchel transformation. This yields:

$$\dot{\varepsilon}_v^{vp} = \frac{\partial w}{\partial p'_D} = \left[\frac{1}{(\Lambda)^{\frac{1}{n-1}}}\right][\langle \varrho_D \rangle]^{\frac{1}{n-1}}\left[\frac{\partial \varrho_D}{\partial p'_D}\right] \tag{4.23}$$

$$\dot{\varepsilon}_q^{vp} = \frac{\partial w}{\partial q_D} = \left[\frac{1}{(\Lambda)^{\frac{1}{n-1}}}\right][\langle \varrho_D \rangle]^{\frac{1}{n-1}}\left[\frac{\partial \varrho_D}{\partial q_D}\right] \tag{4.24}$$

The above expressions for the viscoplastic strain rates in Equations (4.23) and (4.24) have clear analogy with the following general forms used in the viscoplastic framework proposed by Perzyna (1963, 1966):

$$\dot{\varepsilon}_{ij}^{vp} = \mu \cdot \langle F \rangle \frac{\partial Q}{\partial \sigma_{ij}} = S \cdot \frac{\partial Q}{\partial \sigma_{ij}} \tag{4.25}$$

where, the scaling function $S = \mu \cdot \langle F \rangle$ and Q is a viscoplastic potential function, termed as a plasticity potential function. The parameter μ is referred to the viscosity parameter and F represents the overstress function employed in the Perzyna's EVP modelling framework. Such form of viscoplasticity framework has been used in a variety of approaches for the modelling of time-dependent behaviour of soils (Adachi and Oka 1982; Borja and Kavazanjian 1985; Yin and Graham, 1999).

In analogous to the overstress function F, the function ϱ_D in Equation (4.22) can also be interpreted as a thermodynamics-based overstress function. The condition, $(\varrho_D = 0)$, represents the rate-independent yield threshold and increasing values of ϱ_D result in higher corresponding yield values; with the subscript "D" being used to denote the dissipative stress space, (i.e. $p'_D - q_D$ space). Furthermore, when $n = 2$, the flow potential function in Equation (4.21) leads to an overstress-based viscous model with a linear viscous nucleus function as reported by Perzyna (1966). Such linear hyperplastic viscous form (i.e. $n = 2$) has also been

employed by Likitlersuang and Houlsby (2007), but their model is limited to the isotropic hardening, along with the arbitrary adoption of elliptical critical surface defined in the MCC model for viscous-free materials.

The incremental stress-strain response is then obtained by adopting Equations (4.23) and (4.24) for the incremental updating of $\dot{\varepsilon}_v^{vp}$ and $\dot{\varepsilon}_q^{vp}$, together with Equation (4.10) by applying the Orthogonality principle. However, these viscoplastic strain rates are in dissipative stress space, (i.e. $p'_D - q_D$ space), and not in true stress space, (i.e. $p' - q$ space). In order to transform them into true stress space, the orthogonality principle is pursued, in which the effective stress is the sum of the shift stress and the dissipative stress, as outlined in Equation (3.15). Consequently, the corresponding shift stress components obtained in Equation (4.10) is substituted into the critical surface function in dissipative stress space, reported in Equation (4.22):

$$\varrho = \sqrt{\frac{\left(p' - \frac{1}{2}\gamma p'_c\right)^2}{A^2} + \frac{(q)^2}{B^2}} - 1 \tag{4.26}$$

Similarly, the corresponding shift stress components determined in Equation (4.10) is again substituted into the dissipative viscoplastic strain rates derived in Equations (4.23) and (4.24):

$$\dot{\varepsilon}_v^{vp} = \frac{\partial w}{\partial p'} = \left[\frac{1}{(\Lambda)^{\frac{1}{n-1}}}\right][\langle\varrho\rangle]^{\frac{1}{n-1}}\left[\frac{\partial \varrho}{\partial p'}\right] \tag{4.27}$$

$$\dot{\varepsilon}_q^{vp} = \frac{\partial w}{\partial q} = \left[\frac{1}{(\Lambda)^{\frac{1}{n-1}}}\right][\langle\varrho\rangle]^{\frac{1}{n-1}}\left[\frac{\partial \varrho}{\partial q}\right] \tag{4.28}$$

The representative graphs for the transformation of the critical surface from the dissipative stress space to true stress space are provided in Figure 4.2.

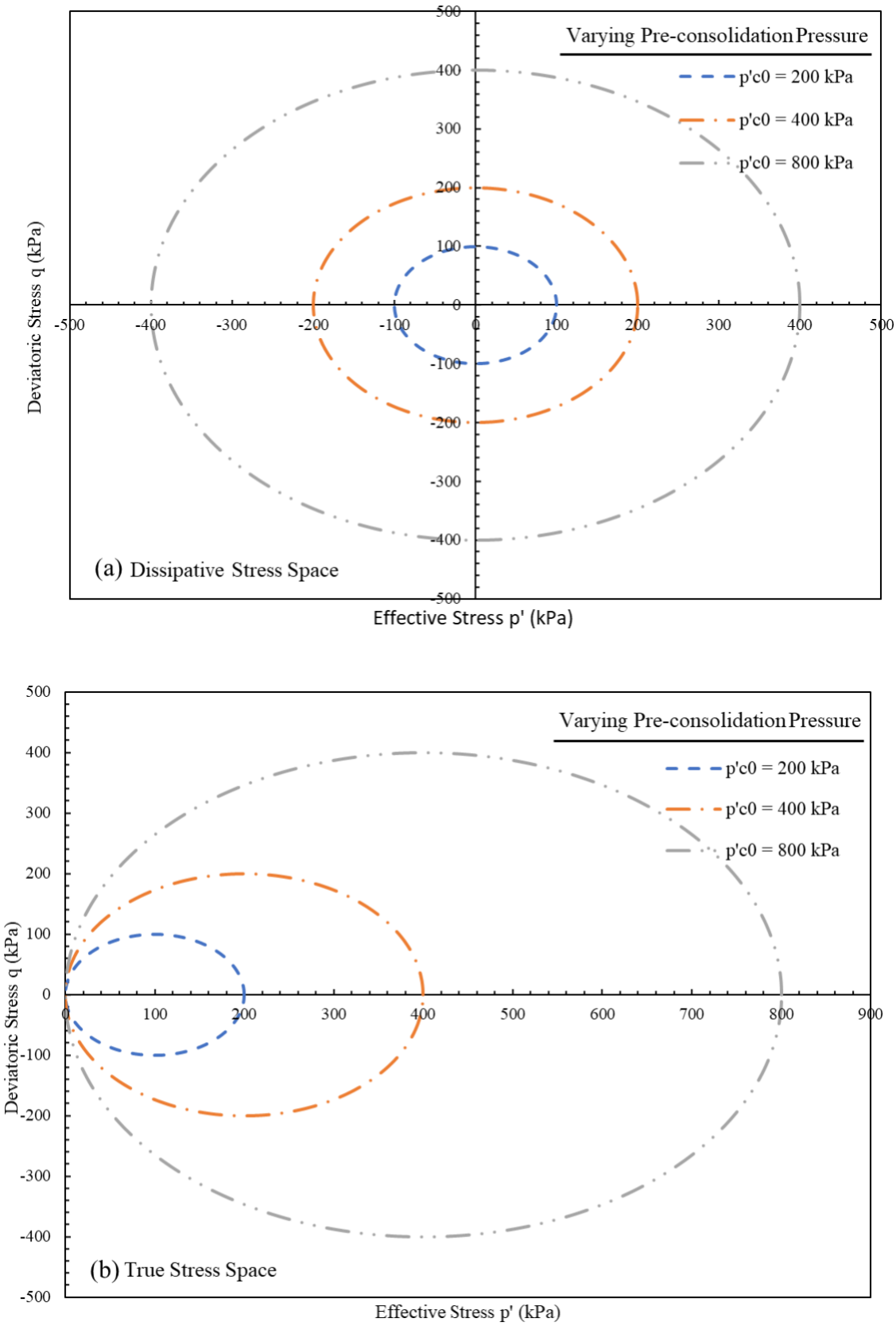

Figure 4.2: Transformation of critical surface from (a) dissipative stress space to (b) true stress space

At this stage, the proposed model formulates creep by incorporating the concept of a constant rate of viscoplastic multiplier, inspired by Grimstad et al. (2010), into the viscosity scaling function (Λ) as follows:

$$\Lambda = \psi' \cdot \left[\frac{p'_{eq}}{p'_c}\right]^{(\kappa^* - \lambda^*)/\mu} \cdot \frac{[(M)^2]}{[(M)^2 - (\eta)^2]} \tag{4.29}$$

where, the parameter p'_{eq} is referred to as the equivalent mean effective stress corresponding to an equivalent condition, in which the current stress lies on the normal consolidation surface, i.e. the soil state is normally consolidated. Accordingly, the intersection of the vertical tangent from the inner critical surface that represents the current effective stress state with the horizontal axis is termed as the equivalent effective mean stress, i.e. p'_{eq}. For instance, the normal consolidation surface can be defined as $p'_c = p'_{eq}$ when the current stress state reaches the normally consolidated state, from which the equivalent effective stress p'_{eq} is determined from the critical surface expression in Equation (4.26). The final term in Equation (4.29) is added to imply that the stress state is related to the critical state, which is reached when $M = \eta$, thus resulting in zero viscoplastic volumetric strain rate. Moreover, this term ensures that the resulting creep strain corresponds to the measured volumetric creep strain rate under one-dimensional loading conditions. Besides, the term p'_{eq}/p'_c represents the dependence of the volumetric creep strain on the current stress state in relation to the critical surface.

4.2.6 Non-Associated Viscoplastic Flow Rule

One of the promising characteristics of the proposed model is the derivation of non-associated viscoplastic flow rule as a natural outcome due to the presence of the effective stress components in functions A and B in the dissipation function provided in Equation (4.14) and

the force potential function derived in Equation (4.17). By solving and re-arranging the proposed energy equation using the dissipation function reported in Equation (4.14), the flow rule for the proposed model is derived (See Appendix B for detailed derivation) as follows:

$$\frac{\dot{\varepsilon}_q^{vp}}{\dot{\varepsilon}_v^{vp}} = \frac{2\eta}{(M[1-\alpha+\alpha\gamma])^2 - \eta^2} \tag{4.30}$$

where, the viscoplastic flow rules in Equations (4.27) and (4.28) become non-associated in the actual stress space, unless $\gamma = \alpha = 1$. Although most of the existing EVP models have adopted an associated flow rule based on the MCC model, in which the plastic potential surface is assumed to be identical to the yield surface, it has now been widely acknowledged that non-associated flow rule does offer better predictions for pressure-sensitive materials, such as soils, as the vectors of the strain parameter are not normal to the yield locus (Bousshine et al., 2002; Nguyen et al., 2017; Sun et al., 2018).

4.3 Non-Linear Creep Formulation

The experimental evidence from the long-term creep tests has demonstrated that the slope of the creep strain (or void ratio) to log(time), commonly denoted as creep coefficient, is not constant (Leroueil et al., 1985). However, creep coefficient decreases over time with the decreasing void ratio. Although Yin (1999) defined a non-linear creep function with time to overcome the limitation of infinite strains resulting in the negative void ratio during creep, it is only applicable to one particular constant applied stress level. The non-linear creep coefficient does not continuously decrease with the void ratio when applied stresses are continually increasing and hence, a negative void ratio can be avoided only under a constant applied stress level, which is also pointed out by Yin et al. (2015). However, in real situations, applied stresses

do vary from time to time not only within construction period but also along the service life of the structure. Taking this into consideration, this paper proposes the following non-linear creep function, assuming the creep parameter as a sole function of void ratio:

$$\mu = \mu_0 \cdot [1 - \varepsilon_v - \zeta_e]^m \tag{4.31}$$

where, μ is referred to as creep coefficient and the subscript "0" is used to denote the corresponding initial/reference value. The power value m is a material constant representing the slope of the $\log \mu - \log e$ curve, which can be measured in a straight-forward way. The parameter ζ_e represents the ratio of residual void ratio to initial void ratio to acknowledge the existing experimental evidence of the minimum void ratio not being exactly equal to zero (i.e. $\zeta_e = e_{\mathcal{R}}/e_0$).

According to Mitchell (1956), the void ratio can reach a minimum value regardless of the pressure or initial orientation for a particular soil. It is to be emphasised that the relatively minute gaps would still exist between the soil particles due to their irregular shapes (Le et al., 2012). This means the minimum void ratio may not be zero and also infinite deformation of the soil structure would not be possible. Referring to Equation (4.31), the creep coefficient μ approaches zero when the void ratio approaches $e_{\mathcal{R}}$, thus ensuring the void ratio would never be unrealistically negative. Moreover, μ continuously decreases with the continually decreasing void ratio, due to varying applied pressures during loading. Furthermore, μ also decreases over time at a particular stress level, as the void ratio decreases during creep deformation. In the proposed model in this study, the creep coefficient (μ) is no longer a constant but treated as a function of void ratio determined from Equation (4.31), in order to incorporate non-linear creep formulation as part of the time-dependent viscosity scaling function (Λ) in Equation (4.29). On the other hand, μ can be treated as a constant by assuming $m = 0$ to consider linear viscosity cases for the sake of simplicity.

In order to take into account of the non-linear creep behaviour, the creep coefficient (μ) determined from Equation (4.31) is substituted into the specified viscosity function (ψ') defined in the earlier Section 4.2.4, as part of the time-dependent viscosity scaling function (Λ), discussed in Equation (4.29). As a result, the modified viscosity function (ψ') is then substituted into the expressions for the viscoplastic strain rates presented in Equations (4.27) and (4.28).

4.4 Extended Mixed Hardening Hyper-viscoplasticity Model for Soft Soils Incorporating Soil Fabric

4.4.1 Theoretical Background

This section presents the logical and rational extension towards the proposed mixed hardening hyper-viscoplasticity (H-Creep) model in an attempt to address a few of the observed limitations, by particularly highlighting the necessity to emphasise on the importance of modelling strain-softening effects during the time-dependent delayed deformation, particularly in natural soils. The extended free-energy and dissipation potential functions, in which not only the additional viscoplastic component of the free-energy function incorporates the dependence on both volumetric and deviatoric viscoplastic strains, but also the fabric coupling parameter is introduced into the free-energy and dissipation potential functions, are discussed. The extended model intends to capture the loading-rate or strain-rate dependent behaviour of soils, considering the variations in the fundamental shapes of critical surface with a β-line defining the inclination of the non-symmetrical elliptical critical surface in the p'-q plane, along with

rotational, kinematic hardening effects and non-associated behaviour, derived as a natural consequence of this approach.

As the mechanical characteristics of natural soft clays, is considered as very complicated and the associated stress-strain behaviour being unpredictable owing to the composition of the material, the irregularity of the clay platelets, one-dimensional consolidation and deposition process, the sedimentary and stress history and so on. The deposition procedure of natural clays results in K_0-consolidation without lateral deformation. The soil properties and the associated behaviour, such as strength, stiffness and hydraulic conductivity in a K_0-consolidation condition normally differs for the vertical and horizontal directions, but essentially, identical in the horizontal plane. Consequently, the effects of structure in natural soft soils differ from reconstituted soils, being attributable to the arrangement of particles and the interparticle bonding, termed as "structure" by Mitchell (1993, 1956), which was also referred to as "fabric" by Muhunthan et al. (1996). Such an arrangement of particles and the particle contacts of most natural clays are initially anisotropic due to the platy shape of the clay particles, deposition process and the subsequent consolidation history of the deposit (Karstunen and Koskinen, 2008). The negligence regarding the effects of structure in natural clay behaviour may lead to inaccurate predictions of the stress-strain response under different loading conditions (Zdravkovic et al., 2002; Zhou et al., 2005; Rezania et al., 2016). From the practical perspective, the existing models have considered the initial orientation of soil fabric to be of cross-anisotropic nature, which is a realistic assumption due to the deposition of natural soils only in a one-dimensional vertical direction. Due to the initial orientation of soil fabric in the soil structure, it has been shown that the yield surfaces obtained from laboratory tests on undisturbed samples of natural clays are inclined in the stress space (Dafalias, 1986; Wheeler et al., 2003). Consequently, the plasticity models with skewed yield surfaces have been developed to recognize the laboratory observations and to address the shortcoming that the

elliptic yield surfaces result in a poor approximation to the stress-strain response of clays, particularly on the dry side of the CSL, where substantial over-prediction of the peak deviatoric stress is observed (Crouch and Wolf, 1995; Karstunen et al., 2005). Moreover, there has been a recent interest in incorporating material 'fabric' as one of the extensions towards the MCC model, with so-called structured Cam-clay models (Horpibulsuk et al., 2010; Suebsuk et al., 2010). These models introduce a destructuration index to model the changes in the internal fabric under deformation, resulting in the additional complications related to the calibration of model parameters. Moreover, it is very difficult to associate the destructuration index to the re-arrangement of the fabric through empirical relationships, without being related to the actual physical phenomena of structured soils (Karstunen et al., 2005). Besides, the modelling of material 'fabric' has been incorporated into the bounding surface plasticity model, originally proposed by Dafalias (1975) and developed by Dafalias and Herrmann (1982), through the use of a projection centre and an image point on the outer bounding surface (Gajo and Muir, 2001; Dafalias et al., 2006; Yao et al., 2009). However, the resulting bounding surface models enforce the consistency condition on the bounding surface and a simple proximity rule is employed to determine the plastic strain increment and hence, the consistency condition, explicitly on the inner loading surface, is not satisfied. Thus, overall, the elasto-plastic constitutive models involving an inclined yield surface that is either fixed (e.g. Sekiguchi & Ohta, 1977; Zhou et al., 2005) or varying inclination by adopting a rotational hardening law (e.g. Castro and Sivasithamparam, 2017; Leal et al., 2017; Zhang, 2018) have been developed to simulate the evolution of anisotropy during plastic straining. However, most of the latter-type of models have commonly assumed that the variations in the inclination of the yield curve are controlled by either plastic volumetric strains only (e.g. Dafalias, 1986; Whittle and Kavvadas, 1994; Lai et al., 2016) or plastic deviatoric strains only (e.g. Nova, 1985; Banerjee et al., 1988). This has

led to unrealistic prediction of certain stress paths and thus, contradicting the findings from laboratory observations, as pointed out in Wheeler (2003) and Zhang (2018).

In recent years, anisotropic EVP models have been developed by Zhou et al. (2005) and Leoni et al. (2008) as an extension of the isotropic creep models by Vermeer and Neher (1999) and Yin et al. (2002), in which the volumetric viscoplastic strain remains unchanged on the yield surface, which is independent of the stress state. This has resulted in the unrealistic value of volumetric viscoplastic strains, as the stress state approaches the critical state line; instead, the value should be nearly zero based on the laboratory observations. Moreover, the modelling of combined anisotropic and viscoplastic effects for clays (Yin et al., 2010; Sivasithamparam et al., 2015; Jiang et al., 2017; Leal et al., 2017; Castro et al., 2018), along with the consideration of strain rate and temperature (Leroueil and Marques, 1996; Laloui et al., 2008) or strain rate and structure (Hinchberger et al., 2010; Yin and Karstunen, 2011; Zhang, 2018) have also been carried out in the past decades. Moreover, the bounding surface concept has been adopted to combine 'fabric' effects and time-dependent deformation to predict the viscoplastic stress-strain response of soft clays (e.g. Al-Shamrani and Sture, 1998; Yue, 2001; Jiang et al., 2017). However, most of the existing EVP models have not been constructed based on a strong thermodynamic foundation, but rather from an empirical or semi-empirical approach.

Taking into consideration of the fact that comprehensive incorporation of the effects of structure require large number of parameters, which makes it highly impractical, the extended model places the emphasis on the reduced number of parameters while maintaining the reasonable capability of the model, as also prioritised in Leoni et al. (2008) and Sivasithamparam et al. (2015). Considering the importance of acknowledging the effects of structure in natural soils, this logical extension of the mixed hardening hyper-viscoplasticity

(H-Creep) model introduces the 'fabric' coupling parameter into both the modified viscoplastic free-energy potential function and dissipation potential function. Moreover, the viscoplastic component of the free-energy function, now depends on both volumetric and deviatoric viscoplastic strains to model the rotational kinematic hardening behaviour of soils. This viscoplastic free-energy potential function results in the shift stress, with the addition of rotational effects related to the kinematic hardening behaviour, which is crucial in accommodating the effect of stress history of stiffness of soils. The rotational kinematic law, based on Sivasithamparam and Castro (2016) and Zhang (2018), is incorporated in order to maintain a unique asymptotic critical state surface for stress paths that involve unloading, whilst making sure that the critical state surface concept is satisfied.

Correspondingly, this section extends the proposed H-Creep model by (a) incorporating fabric coupling effects to account for the combination of the arrangement of particles and the interparticle bonding, i.e. by allowing the critical surface to shear off the hydrostatic axis; (b) introducing the 'fabric' coupling parameter is introduced into the free-energy and dissipation potential functions; and (c) including the additional dependence on the deviatoric viscoplastic strains in the viscoplastic free-energy potential function to address for fundamental inconsistency of the existing constitutive plasticity models, in which the pre-consolidation pressure only depends on the volumetric strain component.

In tandem with the geotechnical sign convention used in the previous sections, compressive stresses are positive, while tensile stresses are negative. All the stresses are to be considered as effective stresses, i.e. total stress minus the pore pressure, with the use of prime notation. The definition of the Cambridge parameters for stress and strain, as triaxial notation, is adopted to describe the stress-strain behaviour.

4.4.2 Theoretical Formulation and Elasticity Law

In the extended model, the triaxial notation as specified in Equations (4.2a) - (4.2d) are adopted for the general quantities of stress and strain. Moreover, the extended model in this chapter adopts the same elastic free-energy function, together with the identical isotropic elastic relationship, as described in Section 4.2.2. Although most natural clays exhibit elastic anistropic behaviour (Castro and Sivasithamparam, 2017; Gu et al., 2017), the consideration of elastic anisotropy could potentially result in the additional 21 independent elastic parameters, which makes it rather impractical for implementation. Moreover, the incorporation of fully generalised elastic anisotropy could add enormous complexity to any constitutive mode, where anisotropy is not fixed. Since the viscoplastic deformations are most likely to impose huge influence on many problems of practical interest, it is rational to still assume the isotropic elastic relationship due to the fact that elastic strains are often considered as relatively insignificant.

4.4.3 Extended Viscoplastic Free-Energy Function

The extended model modifies the viscoplastic free-energy potential function in Section 4.2.3 by including the additional dependence on the deviatoric viscoplastic strains, together with the volumetric component. The importance rationale behind this inclusion is the intention to correct the fundamental inconsistency of plasticity theories and keep the hyperplasticity theory internally consistent due to the increasing appreciation that it is necessary to consider shear as well as volumetric strains in the hardening law (Nova, 1977; Krenk, 1996; Hashiguchi and Chen, 1998). Consequently, the modified viscoplastic free-energy function with its dependence on both volumetric and deviatoric viscoplastic strains, in combination with the introduction of ‘fabric’ parameter, is expressed as follows:

$$\Psi_{vp}^{g} = \gamma \cdot (\lambda^* - \kappa^*) \cdot p_0' \exp\left(\left(\varepsilon_v^{vp} + F\left(\varepsilon_q^{vp}\right)\right)\Big/_{(\lambda^* - \kappa^*)}\right) \tag{4.32}$$

where, the function $F\left(\varepsilon_q^{vp}\right)$ is defined as $F\left(\varepsilon_q^{vp}\right) = \beta \cdot \varepsilon_q^{vp}$, in which β is referred to the 'fabric' parameter, whilst the other parameters retain the same properties as described in Equation (4.9). In order to avoid additional complexity of the proposed model, the evolution of 'fabric' arrangements is assumed to be controlled by the value of a single scalar 'fabric' parameter β, partly inspired by the similar assumption pursued in Wheeler et al. (2003), Castro and Sivasithamparam (2017) and Zhou et al. (2018). This extended viscoplastic free-energy function in Equation (4.32) results in the modified shift stress, which now adds rotational effects to the kinematic hardening behaviour, which is crucial in describing the effect of stress history of stiffness of soils. A similar form of plastic free-energy function was proposed by Collins and Hilder (2002), it was limited to rate-independent axisymmetric case.

Taking the derivative of Equation (4.32) with respect to volumetric viscoplastic strain (ε_v^{vp}), results in the volumetric component of the shift stress, (i.e. p_S):

$$p_S' = \frac{\partial \Psi_p^g}{\partial \varepsilon_v^{vp}} = \gamma \cdot p_0' \, exp\left(\left(\varepsilon_v^{vp} + F\left(\varepsilon_q^{vp}\right)\right)\Big/_{(\lambda^* - \kappa^*)}\right) = \frac{1}{2}\gamma p_c' \tag{4.33}$$

where, pre-consolidation pressure p_c' is now defined as:

$$p_c' = 2p_0' exp\left(\left(\varepsilon_v^{vp} + F\left(\varepsilon_q^{vp}\right)\right)\Big/_{(\lambda^* - \kappa^*)}\right) \tag{4.34}$$

In this extended form, the deviatoric component of the shift stress, (i.e. q_S), is no longer zero as soon as the deviatoric strain components are included in Equation (4.32). Thus,

deviatoric shift stress q_S, is determined by taking the derivative of Equation (4.32) with respect to deviatoric viscoplastic strain (ε_q^{vp}):

$$q_S = \frac{\partial \Psi_p^g}{\partial \varepsilon_q^{vp}} = \gamma \cdot p_0' \, exp\left(\left(\varepsilon_v^{vp} + F\left(\varepsilon_q^{vp}\right)\right)\Big/_{(\lambda^* - \kappa^*)}\right)\left(\frac{\partial F\left(\varepsilon_q^{vp}\right)}{\partial \varepsilon_q^{vp}}\right) = p_S'\left(\frac{\partial F\left(\varepsilon_q^{vp}\right)}{\partial \varepsilon_q^{vp}}\right) \tag{4.35}$$

Referring to Equation (4.35), the derivative of $F\left(\varepsilon_q^{vp}\right)$ with respect to its argument is determined as the 'fabric' parameter (i.e. β), which is discussed further in the next section, with regards to the modified dissipation potential function. As similar to Equation (4.12), the volumetric and deviatoric shift stress components determined in Equations (4.33) and (4.35) are used to represent the viscoplastic free-energy function in Equation (4.32), which is re-written as follows:

$$\Psi_{vp}^g = p_S' \, \dot{\varepsilon}_v^{vp} + q_S \, \dot{\varepsilon}_q^{vp} = \frac{1}{2}\gamma p_c' \, \dot{\varepsilon}_v^{vp} + \beta \cdot \frac{1}{2}\gamma p_c' \, \dot{\varepsilon}_q^{vp} = \frac{1}{2}\gamma\left\{p_c'\left(\dot{\varepsilon}_v^{vp} + \beta \cdot \dot{\varepsilon}_q^{vp}\right)\right\} \tag{4.36}$$

Thus, of all the work done related to viscoplastic strains, a fraction $\gamma/2$ is stored and the other portion, $(1 - \gamma/2)$ is dissipated when Equation (4.36) is viewed from the hyperplastic perspective. The discussion related to hardening and stored or frozen plastic energy is provided at length in Ulm and Coussy (2003).

Applying the chain rule to Equation (4.34), the incremental evolution law for the pre-consolidation pressure, being considered as an independent variable, is derived as follows:

$$\dot{p}_c' = \frac{\partial p_c'}{\partial \varepsilon_v^{vp}} \dot{\varepsilon}_v^{vp} + \frac{\partial p_c'}{\partial \varepsilon_q^{vp}} \dot{\varepsilon}_q^{vp} = \frac{p_c'}{(\lambda^* - \kappa^*)} \left(\dot{\varepsilon}_v^{vp} + \beta \dot{\varepsilon}_q^{vp} \right) \tag{4.37}$$

The inclusion of a deviatoric component in the modified shift stress leads to the dependence of the evolution of the pre-consolidation pressure on viscoplastic shear strain rate. However, most of the existing constitutive models consider hardening laws that depend only on volumetric plastic strains, ignoring the coupling between volumetric and deviatoric plastic strains (Yin and Graham, 1999; Yin et al., 2015; Islam and Gnanendran, 2017). As previously emphasised, it is now widely acknowledged that it is necessary to include both deviatoric as well as volumetric strain components in the hardening law to properly model the stress-strain behaviour of soils, including granular materials (Nova, 1977; Collins & Hilder, 2002; Krabbenhoft, 2009).

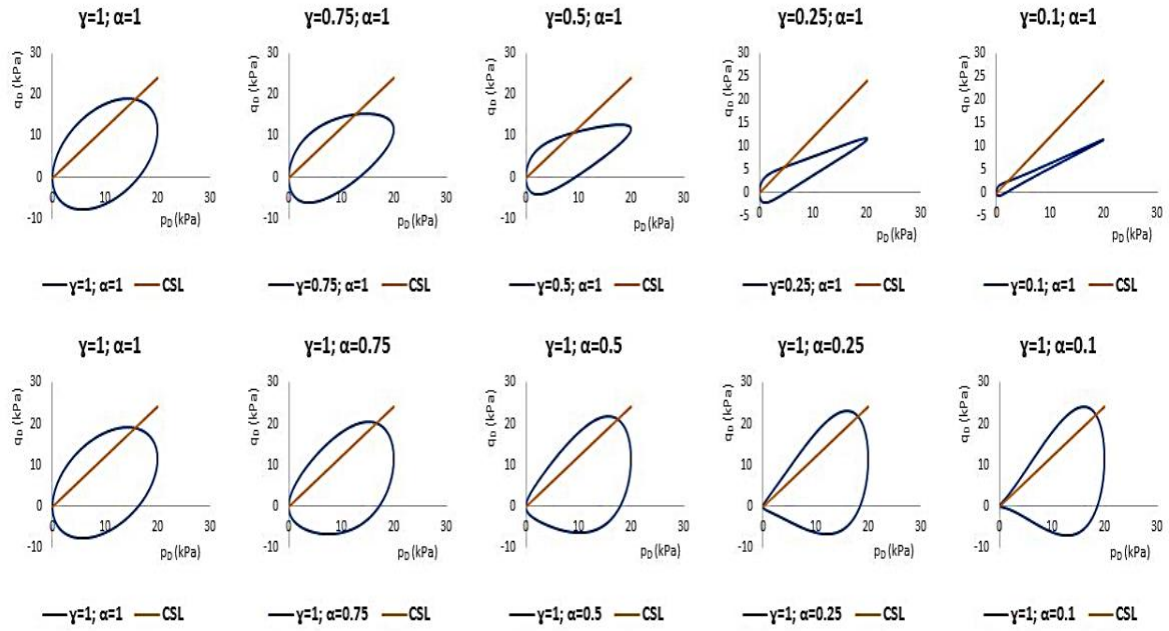

Figure 4.3: Changes in the Shapes of Critical Surface in $p_D - q_D$ space, corresponding to the values of γ and α varying over the range 1.0 to 0.1 (Using $\beta = tan\,30°$)

Hence, the inclusion of β results in the rotational effects being introduced to the kinematic hardening law of the model (as shown in Figures 4.3 and 4.4), due to the assumption

of keeping the origin on the yield loci in true stress space. This fact regarding rotational hardening was also highlighted by Coombs (2017) and Castro et al. (2018) as an integral feature of constitutive soil models but these models have been limited to the rate-independent scenarios, in comparison to the modelling of rate-dependent effects by the proposed model. Besides, the modelling related to rotational hardening with regards to the necessity of complying with the Critical State concept is presented and discussed in Section 4.4.7. Although the shift stress defining the moving 'centre' of the yield surface is most familiar in the existing kinematic hardening models, it is demonstrated that the shift stress is also required to describe the isotropic compression and expansion behaviour of rate-dependent materials.

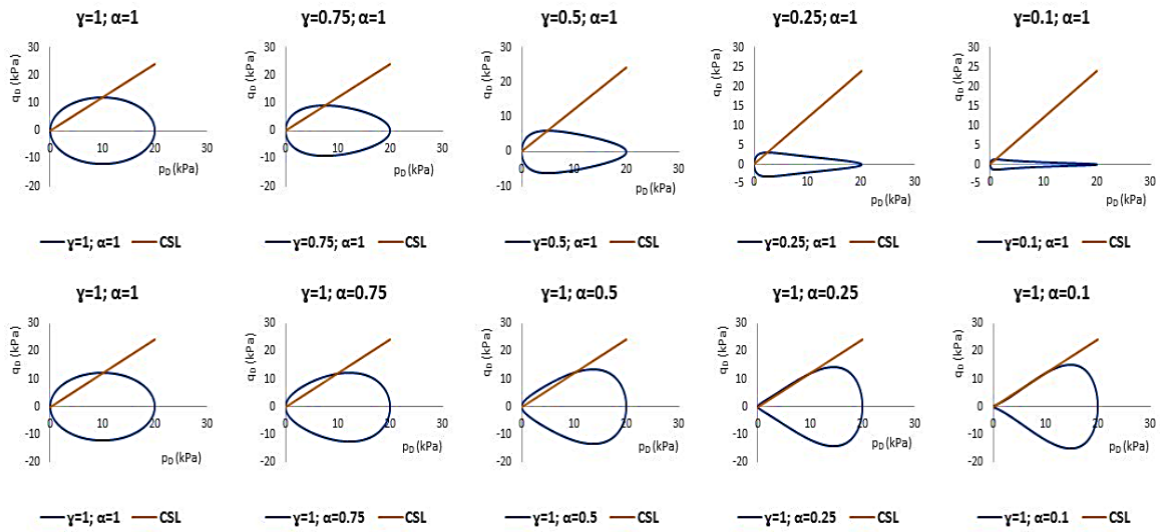

Figure 4.4: Changes in the Shapes of Critical Surface in $p_D - q_D$ space, corresponding to the values of γ and α varying over the range 1.0 to 0.1 (Using $\beta = 0$)

4.4.4 Extended Viscoplastic Dissipation Potential Function

In the extended model, the viscoplastic dissipation potential function incorporates the 'fabric' parameter β to take into consideration of the arrangement of particles and the interparticle bonding, especially observed in natural soils. Based on the existing triaxial

compression data, the extended viscoplastic dissipation increment function is postulated as follows:

$$\delta\Phi = \sqrt{A^2\left(\dot{\varepsilon}_v^{vp} + \beta\dot{\varepsilon}_q^{vp}\right)^2 + B^2\left(\dot{\varepsilon}_q^{vp}\right)^2} + \Lambda^*\left[\sqrt{A^2\left(\dot{\varepsilon}_v^{vp} + \beta\dot{\varepsilon}_q^{vp}\right)^2 + B^2\left(\dot{\varepsilon}_q^{vp}\right)^2}\right]^n \geq 0 \tag{4.38}$$

where, β takes into account of fabric coupling effects, whilst A and B are the same stress-like functions, given by Equation (4.15). The expression in Equation (4.38) must still be non-negative for all the viscoplastic deformations, under isothermal conditions, to comply with the first and second laws of thermodynamics (Einav and Collins, 2008; Lai et al., 2014). The inclusion of term β, which measures the slope of the inclination of the critical surface in the p'-q plane, accounts for the association between the volumetric and deviatoric dissipation components. This seems physically feasible due to the fact that some form of coupling should exist between the dissipation resulting from volumetric and shear straining, as the shearing of particles results in the volumetric change in the material due to the sliding and re-arranging of grains causing dilation or compaction. This 'fabric' parameter β is further elaborated, along with the determination of its initial value is discussed in the following section, in which β is defined based on the non-associated flow naturally derived from this approach, along with one-dimensional straining assumption. Similar forms of dissipation function were proposed by Muhunthan et al. (1996), Collins and Hilder (2002) and Coombs (2017), as an extension towards the isotropic family of critical state models but these models have been limited to elasto-plastic modelling of stress-strain behaviour of soils. Moreover, the fact that the extended dissipation potential function in Equation (4.38) is no longer a homogeneous first order function is to be emphasised, which is distinctively different from the ones used in the existing soil models (e.g. Lai et al., 2014 and Coombs, 2017).

Here, the first term on the right-hand side of Equation (4.38) describes the instantaneous dissipation, while the second term details the additional dissipation associated with delayed deformations. Hence, the investigation and consideration of the H-Creep model have suggested that it is still logical to retain the similar mathematical structure given in Equation (4.15). Although cross-coupling exists in the initial state of the soil sample, it is still possible to make use of the definition of p' and q from Equations (4.2a) and (4.2b), as long as the triaxial stress states are assumed to be without principle stress rotation (i.e. $\sigma_2' = \sigma_3'$) and the coupling being controlled by a single scalar fabric parameter (Zhang, 2018; Zhou et al., 2018). Moreover, the inclusion of p' or q in functions A and B still abides with the thermodynamic rule, which requires not to identify work conjugate variables together as independent state variables, as supported by Lai et al. (2016) and Darabi et al. (2018).

In the extended model, the dissipation potential function in Equation (4.38) returns back to the one in Equation (4.15) when fabric' effects are ignored, i.e. $\beta = 0$, while retaining the characteristics and the capabilities of the presented H-Creep model. Moreover, this goes a step further when the consideration of rate-dependent effects is neglected, i.e. $\Lambda^* = 0$, together when $\gamma = 1$ and $\alpha = 1$, the dissipation potential function in Equation (4.38) can be retracted all the way back to the one used in the MCC model for the derivation of the symmetrical yield surface, which has been widely adopted in most of the existing EVP models.

4.4.5 Extended Force and Flow Potential Functions

Following the principles and procedure outline in Equations (3.26) - (3.29), the force potential function (z) is derived from Equation (4.38) as follows:

$$z = \sqrt{A^2\left(\dot{\varepsilon}_v^{vp} + \beta\dot{\varepsilon}_q^{vp}\right)^2 + B^2\left(\dot{\varepsilon}_q^{vp}\right)^2} + \frac{\Lambda^*}{n}\left[\sqrt{A^2\left(\dot{\varepsilon}_v^{vp} + \beta\dot{\varepsilon}_q^{vp}\right)^2 + B^2\left(\dot{\varepsilon}_q^{vp}\right)^2}\right]^n \tag{4.39}$$

The volumetric and shear dissipative stresses (i.e. p'_D and q_D) are derived from Equation (4.39) using the standard procedure outlined in Table 3.4, as follows:

$$p'_D = \frac{\partial z}{\partial \dot{\varepsilon}_v^{vp}} = \left[\frac{A^2\left(\dot{\varepsilon}_v^{vp} + \beta\dot{\varepsilon}_q^{vp}\right)}{\Pi^*}\right] + \left[\Lambda^* \cdot [\Pi^*]^{n-1} \cdot \frac{A^2\left(\dot{\varepsilon}_v^{vp} + \beta\dot{\varepsilon}_q^{vp}\right)}{\Pi^*}\right] \tag{4.40}$$

$$q_D = \frac{\partial z}{\partial \dot{\varepsilon}_q^{vp}} = \left[\frac{A^2 \cdot \beta\left(\dot{\varepsilon}_v^{vp} + \beta\dot{\varepsilon}_q^{vp}\right) + B^2 \cdot \left(\dot{\varepsilon}_q^{vp}\right)}{\Pi^*}\right] + \left[\Lambda^* \cdot [\Pi^*]^{n-1} \cdot \frac{A^2 \cdot \beta\left(\dot{\varepsilon}_v^{vp} + \beta\dot{\varepsilon}_q^{vp}\right) + B^2 \cdot \left(\dot{\varepsilon}_q^{vp}\right)}{\Pi^*}\right] \tag{4.41}$$

where, $\Pi^* = \sqrt{A^2\left(\dot{\varepsilon}_v^{vp} + \beta\dot{\varepsilon}_q^{vp}\right)^2 + B^2\left(\dot{\varepsilon}_q^{vp}\right)^2}$. On the other hand, the flow potential function (w) is derived using Legendre-Fenchel transformation based on the procedure outlined in Equations (3.24) and (3.26). Thus, it follows from Equations (4.38) and (4.39) that:

$$w = \delta\Phi - \mathrm{z} = \left[\frac{n-1}{n}\right] \cdot \Lambda^* \left[\sqrt{A^2\left(\dot{\varepsilon}_v^{vp} + \beta\dot{\varepsilon}_q^{vp}\right)^2 + B^2\left(\dot{\varepsilon}_q^{vp}\right)^2}\right]^n \tag{4.42}$$

The above expression for the flow potential function is re-written using the corresponding viscoplastic strain components obtained from re-arranging Equations (4.40) and (4.41) in terms of dissipative stresses, which is as follows:

$$w = \left[\frac{n-1}{n}\right]\left[\frac{1}{\left(\Lambda^*\right)^{1/(n-1)}}\right][\langle \varrho_D^* \rangle]^{\frac{n}{n-1}} \tag{4.43}$$

Although the general structure of the flow potential function remains the same, as in Equation (4.21), the difference lies in the inclusion of the 'fabric' parameter β in the extended

critical surface function, which is automatically derived from the dissipation potential function in Equation (4.38) when the viscosity scaling function (Λ^*) is zero.

$$\varrho_D^* = \sqrt{\frac{(p'_D)^2}{A^2} + \frac{(q_D - \beta \cdot p'_D)^2}{B^2}} - 1 \tag{4.44}$$

The asterisk is used to denote the difference in the critical surface function from Equation (4.22). Accordingly, the presence of parameter β results in the critical surface being sheared off the hydrostatic axis, in which β is accountable for this traceless measure of deviatoric straining. In combination with the assumption that the origin of the critical surface must still lie on the locus in true stress space, the inclusion of parameter β adds rotational effects to the kinematic hardening behaviour of the critical surface. Hence, it is demonstrated that the dissipation parameters, γ and α, in combination with β, have a significant bearing on the shape of the critical surface (as demonstrated in Figures 4.3 and 4.4), and the degree of non-association of the viscoplastic flow rules, derived in the next section.

When $\beta = 0$, the isotropic dissipative critical surface presented in Section 4.2.5, with the ellipsoid's major axis being coincident with the volumetric axis (i.e. p'_D-axis), is recovered (as shown in Figure 4.4). Moreover, when $\beta = 0$ is combined with $\alpha = 1$ and $\gamma = 1$, the traditional MCC yield surface with an associated flow rule is retrieved (see Figure 4.4). Moreover, we can observe from Figure 4.4 that the slope of the critical surface at CSL depends only on α, and is independent of γ value, which influences only on the deviatoric aspect of the critical surface. Furthermore, the increasing β value reduces the deviatoric radius of the critical envelope, while retaining the deviatoric shape, whereas, the value of γ reduces with increasing anisotropy, whilst α increases with increasing anisotropy to maintain the critical state. Most importantly, the evolution of fabric parameter to achieve a unique asymptotic critical state

surface enables the two non-physical material constants, α and γ, to be associated with an experimentally quantifiable constant, i.e. p_c', which is further discussed in Section 4.4.7.

Following the standard procedure, the flow potential function in Equation (4.43) is then differentiated with respect to the corresponding dissipative stress components to derive the viscoplastic flow rules in the dissipative stress space, which results as follows:

$$\dot{\varepsilon}_v^{vp} = \frac{\partial w}{\partial p_D'} = \left[\frac{1}{(\Lambda^*)^{\frac{1}{n-1}}}\right][\langle \varrho_D^* \rangle]^{\frac{1}{n-1}} \left[\frac{{p_D'}/_{A^2} + (q_D - \beta \cdot p_D') \cdot (-\beta)/_{B^2}}{\varrho_D^* + 1}\right] \tag{4.45}$$

$$\dot{\varepsilon}_q^{vp} = \frac{\partial w}{\partial q_D} = \left[\frac{1}{(\Lambda^*)^{\frac{1}{n-1}}}\right][\langle \varrho_D^* \rangle]^{\frac{1}{n-1}} \left[\frac{(q_D - \beta \cdot p_D')/_{B^2}}{\varrho_D^* + 1}\right] \tag{4.46}$$

Having clear analogy with the general forms used in the Perzyna (1963, 1966)'s viscoplasticity framework, as provided in Equation (4.25), the function ϱ_D^* can also be elucidated as a hyper-viscoplastic overstress function (e.g. Rezania et al., 2016; Zhou et al., 2018). Besides, the flow potential function results in a linear overstress-based viscous nucleus function, as initially reported by Perzyna (1966) and further adopted in Zhou et al. (2016), Castro et al. (2018). Unlike classic Perzyna-type overstress models, it is to be emphasised from Equations (4.43) and (4.44) that the critical surface is regarded as a nominal viscoplastic strain rate; thus, not separating viscous from viscous-free behaviour and allowing viscoplastic strain to occur within the critical surface in the proposed model. This is crucial in the determination of the rate-dependent parameters, which can be extracted directly from the laboratory measurements without the need to calibrate the values using test simulations.

Adopting the Ziegler's Orthogonality postulate, as in the standard procedure outlined in Equation (3.15), the dissipative viscoplastic flow rules derived in Equations (4.45) and (4.46)

are transformed into true stress space by substituting the corresponding shift stress components from Equations (4.33) and (4.35) into Equations (4.45) and (4.46):

$$\dot{\varepsilon}_v^{vp} = \frac{\partial w}{\partial p'} = \left[\frac{1}{(\Lambda^*)^{\frac{1}{n-1}}}\right][\langle \varrho^* \rangle]^{\frac{1}{n-1}}\left[\frac{\left(p' - \frac{1}{2}\gamma p_c'\right)/_{A^2} + (q - \beta \cdot p') \cdot (-\beta)/_{B^2}}{\varrho^* + 1}\right] \tag{4.47}$$

$$\dot{\varepsilon}_q^{vp} = \frac{\partial w}{\partial q} = \left[\frac{1}{(\Lambda^*)^{\frac{1}{n-1}}}\right][\langle \varrho^* \rangle]^{\frac{1}{n-1}}\left[\frac{(q - \beta \cdot p')/_{B^2}}{\varrho^* + 1}\right] \tag{4.48}$$

where, the dissipative critical surface function in Equation (4.44) is also transformed into true stress space using a similar procedure, which results as follows:

$$\varrho^* = \sqrt{\frac{\left(p' - \frac{1}{2}\gamma p_c'\right)^2}{A^2} + \frac{(q - \beta p')^2}{B^2}} - 1 \tag{4.49}$$

Similar to the H-Creep model, the extended model considers rate-dependent effects by adopting constant rate of viscoplastic multiplier approach, partly influenced by Sivasithamparam et al. (2015). Accordingly, the creep parameter ψ' is incorporated into the viscosity scaling function (Λ^*), which is defined as follows:

$$\Lambda^* = \psi' \cdot \left[\frac{p_{eq}'}{p_c'}\right]^{(\kappa^* - \lambda^*)/\mu} \cdot \frac{[(M)^2 - (\beta)^2]}{[(M)^2 - (\eta)^2]} \tag{4.50}$$

The asterisk is used to denote the difference from the viscosity scaling function defined in Equation (4.29). The difference lies in the inclusion of the parameter β in the final term in Equation (4.50) to make sure that the critical state concept is adhered to, whilst the resulting viscoplastic strain corresponds to the measured volumetric viscoplastic strain rate under one-

dimensional K_0-consolidation condition, where η is denoted as the associated stress-ratio (i.e. $\eta = \eta_{K0}$) and the related coupling term, i.e. $\beta = \beta_{K0}$, defined later in Section 5.2.

4.4.6 Extended Non-Associated Viscoplastic Flow Rule

As previously highlighted, the non-associated viscoplastic flow behaviour is derived as a necessary consequence from the extended dissipation potential function in Equation (4.38) due to the presence of the effective stress components as part of functions A and B (see Appendix A for more details). Hence, the viscoplastic flow rule for the extended model is derived from solving and re-arranging of the energy equation using the extended dissipation potential function in Equation (4.38), which is as follows (Refer to Appendix C for detailed derivation):

$$\frac{\dot{\varepsilon}_v^{vp}}{\dot{\varepsilon}_q^{vp}} = \frac{\beta^2 + (M[1-\alpha+\alpha\gamma])^2 - \eta^2}{2(\eta-\beta)} \tag{4.51}$$

where, the non-associated viscoplastic flow rule in Equation (4.51) becomes associated when $\gamma = \alpha = 1$. Moreover, the viscoplastic flow expression derived in the H-Creep model, i.e. Equation (4.30), is recoverable when $\beta = 0$. This, in turn, is particularly important in retaining the hierarchical nature of the extended viscoplastic dissipation function postulated in Equation (4.38). As previously been emphasised, there has been an increasing appreciation that non-associated flow rule does offer marked improvements in simulating the behaviour of geomaterials, being recently supported by Nguyen et al. (2017) and Sun et al. (2018).

4.4.7 Compliance with Critical State Concept

Considering the critical surface and the non-associated flow behaviour derived in Sections 4.4.5 and 4.4.6, it is necessary that the coupling term approaches zero when the stress state reaches the critical state, (i.e. $\beta \to 0$ at CS) so that the original critical state surface is retained, while also making sure that the stress ratio at the final critical state is independent of the stress path taken to reach that state. Inspired by the developments in Sivasithamparam and Castro (2016) and Zhang (2018), the proposed model employs a limit, representing the development of erasure of 'fabric' with viscoplastic strains, which is expressed as follows:

$$\dot{\beta} = C_\beta \left[\left(\frac{3}{4}\eta - \beta \right) \langle \dot{\varepsilon}_v^{vp} \rangle + D_\beta \left(\frac{1}{3}\eta - \beta \right) \left| \dot{\varepsilon}_q^{vp} \right| \right] \tag{4.52}$$

where, the soil constant, D_β, controls the relative contribution from the volumetric and deviatoric viscoplastic strains in determining the overall target value for β. The other soil constant, C_β, controls the absolute rate at which β approaches its target value. The use of Macaulay brackets $\langle \quad \rangle$, i.e. $\langle x \rangle = 0, x < 0$; and $\langle x \rangle = x, x \geq 0$, results in the evolution of β being insensitive to negative (dilative) viscoplastic strains. Moreover, this implies that it is only the isochoric component of the rate that influences the value of β when subjected to dilative plastic straining. When $D_\beta = 0$, the development of β becomes solely dependent on the compressive viscoplastic strains and the value of β will asymptotically approach the target value of $3\eta/4$. However, setting $D_\beta = 0$ would imply that the unique critical state condition could not be attained, as the value of β being dependent on the accumulated volumetric viscoplastic strains along the stress path to the critical state surface. On the other hand, the evolution of β will be largely controlled by the deviatoric viscoplastic strains when $D_\beta \to 0$. Accordingly, the volumetric component of viscoplastic strain diminishes and the evolution of β is influenced by the deviatoric viscoplastic strains when the stress state approaches the

critical state conditions. In this limiting case, where $\dot{\varepsilon}_v^{vp} = 0$, the evolution law for β is expressed as follows:

$$\{\dot{\beta}\}_{\dot{\varepsilon}_v^{vp}=0} = C_\beta \cdot D_\beta \left[\frac{1}{3}\eta - \beta\right] |\dot{\varepsilon}_q^{vp}| \tag{4.53}$$

Consequently, the value of β is given by $\eta/3$ at the CS (where, η is equal to M at the CS). This seems physically plausible, provided that the CS corresponds to a condition, where the degree of coupling is being continuously disappeared and reappeared. This unique CS value for β results in the prediction of a unique CSL in the $v - \ln p$ plane, which is one of the most imminent features lacking in many of the existing soil constitutive models (e.g. in Dafalias, 1986; Whittle and Kavvadas, 1994). Therefore, the unique β value at the CS is solely dependent on stress conditions at the CS and should be independent of both the initial degree of coupling and the stress path taken to the CS.

One of the key novelties that differentiates the proposed model from a host of existing EVP models is embedded in the procedure to determine the reasonable approximations for the initial value of β, together with the additional parameters C_β and D_β, using the non-associated flow expression systematically derived in Equation (4.51). Correspondingly, the close estimate values for the parameters C_β and D_β are calculated in conjunction with an initial rotatory state of the critical surface, in contrast to the common adoption of associated flow rule for the estimation of these parameters in most of the existing EVP models (e.g. Wheeler et al., 2013; Rezania et al., 2016). Although, ideally, a diversity of specialised testing methods and a multitude of numerical simulations are required in order to calibrate the parameters C_β and D_β, the current study employs a simple empirical relation in tandem with the non-associated flow condition for the determination of the parameters, β, C_β and D_β, which is presented and elaborated in Section 5.2.

Besides, it is also feasible to determine the appropriate value for M to maintain the unique asymptotic stress ratio at the CS (η_{CS}) (for provided values of α and γ), provided the fact that η_{CS} can be experimentally determined at the critical state conditions, by defining the degree of coupling $\eta/3$ at the critical state using Equation (4.53). This argument for a unique CS value for β, regardless of their stress history, has been strengthened by recent two-dimensional discrete element analysis on granular materials carried out by Fu and Dafalias (2010, 2011).

4.5 Principle of Hyper-viscoplasticity Model

The key principle embedded in the proposed models are further illustrated in Figure 4.6, in which point 'A' represents the initial stress state, being assumed to correspond to the normally consolidated state, and point ‘B’ represents the stress state corresponding to the expansion of the critical surface in the stress space due to the presence of volumetric viscoplastic strains during loading along the stress path of a creep test. As the stress state 'B' approaches the CSL at 'C', the size of the critical surface remains the same, as the increments of the volumetric viscoplastic strains becoming zero. Since the critical state is reached, the soil is subjected to a constant amount of overstress, which leads to an increase in deviatoric viscoplastic strains at constant strain-rate.

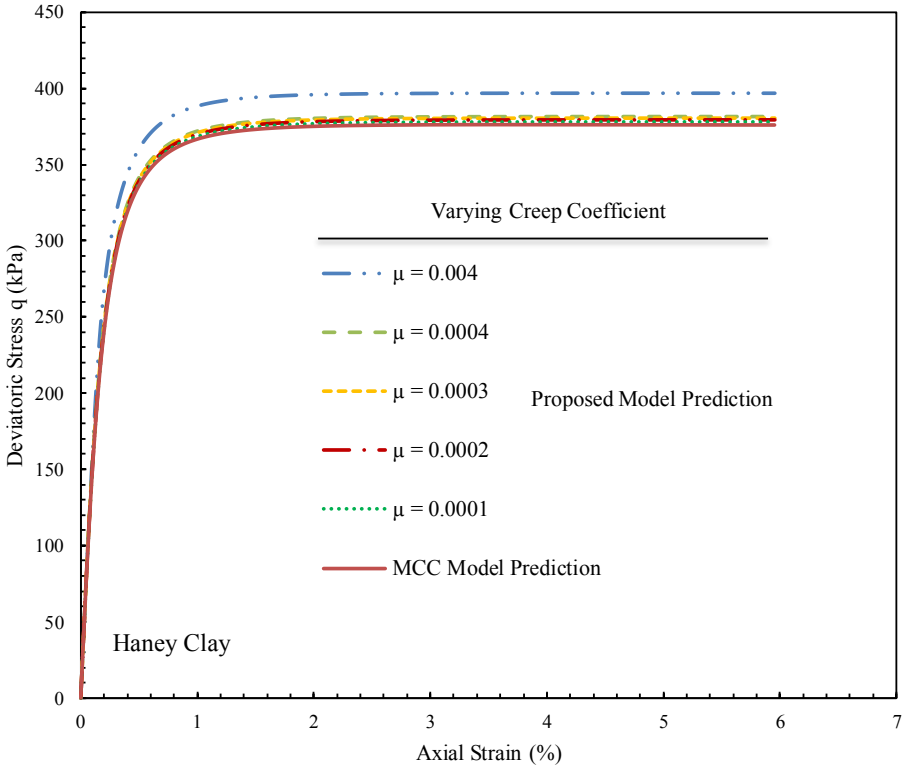

Figure 4.5: The effects of varying creep coefficient on the stress-strain behaviour using undrained triaxial test results on Haney clay

One of the major characteristics of the proposed model is that it is hierarchical, which means that a viscoplastic version of the Modified Cam-clay model can be retraced back from the proposed model, by setting the coupling factor (β) to zero and the value of parameters, α and γ, to one. In combination with a sufficiently small creep parameter, the proposed model converges to the universally acclaimed elastoplastic model (i.e. Modified Cam-clay model), as shown in Figure 4.5.

Unless the parameters α and γ are equal to one, the non-associated flow rule is naturally derived as a necessary consequence from the postulated stress-dependent dissipation increment function (see Appendix B), which enhances the versatility and usefulness of the proposed model in predicting the behaviour of a wider class of soils.

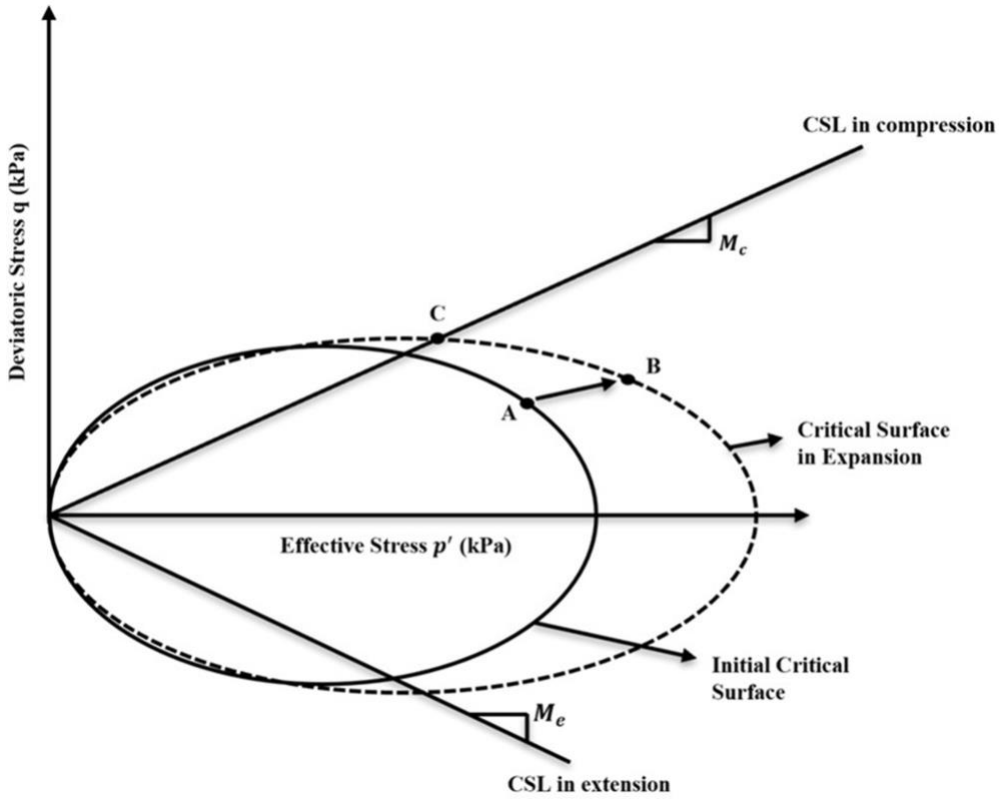

Figure 4.6: Schematic representation of the behaviour of the Hyper-viscoplasticity model in $p' - q$ space

4.6 Findings and Observations

The proposed model attempts to solve the problems encountered in the existing creep models developed by Yin et al. (2002) and Islam and Gnanendran (2017), in which the volumetric viscoplastic strain rate is determined from the secondary compression coefficient $C_{\alpha e}$ defined in $e - \ln t$ space, while the deviatoric viscoplastic strain rate is obtained from the volumetric strain-rate by means of associated flow rule. Moreover, the volumetric viscoplastic strain rate is assumed to be independent of the stress ratio (η), resulting in an unrealistically large volumetric strain rate when the stress ratio approaches the CSL (Yin et al., 2010). This is

in stark contrast to the experimental investigations, in which the volumetric strain rate is nearly zero when the stress state approaches CSL. Consequently, these models cannot predict the stress-strain response when the stress path overpasses the CSL in a step-changed undrained triaxial test, resulting in strain-softening behaviour for isotropically consolidated samples due to unreasonably large volumetric contraction, as pointed out by Yin et al. (2010).

In the proposed model, the volumetric viscoplastic strain rate is not constant, but instead, the viscosity scaling function is assumed to be constant and applied for both volumetric and deviatoric components of the time-dependent behaviour of soils. The volumetric and deviatoric viscoplastic strain rates are derived separately from the flow potential function, as discussed in Equations (4.23) and (4.24) from the original H-Creep model and Equations (4.45) and (4.46) from the extended model, which has clear analogy with the elliptical yield surface adopted by Zhou et al. (2018). Non-associated flow rules can also be derived as a natural consequence from the postulated stress-dependent dissipation function provided in Equations (4.14) and (4.38) (i.e. functions A and B consists of pressure components), which is discussed further in Appendix A. Most importantly, the volumetric viscoplastic strain rate is dependent on the stress ratio (η) and it approaches zero as the stress state approaches the CSL.

Besides, the extended study has also been carried out to consider for the fabric coupling effects, emphasising on the importance of strain-hardening or softening behaviour during the rate-dependent delayed deformation in natural soils. The viscoplastic free-energy function and the dissipation increment function are further extended with the introduction of fabric parameter, whilst the former also incorporates the dependence on both volumetric and deviatoric viscoplastic strains to address the fundamental inconsistency of existing EVP models. The viscoplastic free-energy component results in the modified shift stress, with the rotational effects being implied on the kinematic hardening law in a simplified standard

procedure. Not only the free-energy function but also the dissipation function are based on the fundamental laws of thermodynamics, whilst no separate arbitrary plastic potential function is required to instigate non-associated flow rule, as non-associated flow behaviour is derived as a natural consequence from the stress-dependent dissipation potential function, as previously been emphasised.

Hence, the following summaries are deduced from this chapter:

(i) the entire constitutive viscoplastic stress-strain response is encapsulated within two thermodynamic potential functions, namely the free-energy and the dissipation potential functions based on the fundamental laws of thermodynamics to describe non-linear behaviour of time-delayed deformations of soils;

(ii) the derivations of critical surface and non-associated flow rule from the postulated viscoplastic dissipation potential function in the proposed model are closely connected, while being demonstrated as necessary outcomes;

(iii) non-associated flow is naturally derived from the stress-dependent dissipation potential function, rather than having to establish an arbitrary plastic potential function for instigating the associativity of the flow rule;

(iv) the variations in the shape of the critical (or yield) loci, which can be retraced back to the shape of the yield surface employed in the MCC model, are taken into account;

(v) a novel non-linear creep formulation, which acknowledges the experimental evidence for the creep strain limit, is postulated and incorporated into the proposed model as part of the time-dependent viscosity scaling function in the dissipation potential function;

(vi) the extended model goes a step further in consideration of the variations in the fundamental shapes of critical surface, accounting for a β-line defining the inclination of the non-symmetrical elliptical critical surface in the p'-q plane, along with the non-

linear creep formulation considering the residual void ratio not being exactly equal to zero observed in the experiments, as discussed above;

(vii) the extended model also demonstrates the intimate association between the extended viscoplastic free-energy and dissipation potential functions, from which the critical surface, along with the rotational hardening and non-associated flow behaviour are derived as necessary outcomes;

CHAPTER 5

VALIDATIONS AND APPLICATIONS OF PROPOSED HYPER-VISCOPLASTICITY MODELS

5.1 Introduction

In this chapter, the performance and capabilities of the proposed mixed hardening Hyper-viscoplasticity model and its extended model are evaluated by comparing the numerical outcomes generated by the proposed models with the experimental data available from the existing literature. Firstly, the summary of the model parameters required for the proposed and extended H-Creep models, along with the explanations on how these parameters are determined in a relatively straightforward means are elaborated in Section 5.2. The application of the proposed H-Creep model for the prediction of time- and rate-dependent stress-strain behaviour of various types of soils, including Osaka clay (reported by Adachi et al., 1995), Hong Kong marine deposit (HKMD) clay (reported by Yin and Zhu, 1999 and Yin et al., 2002), Haney clay (reported by Vaid and Campanella, 1977), and Kaolin and Bentonite mixture (reported by Herrmann et al., 1981), has been investigated in:

- Section 5.3 for stress-controlled and strain-controlled undrained or drained compression and extension tests;
- Section 5.4 for undrained triaxial shearing tests using various strain rates;
- Section 5.5 for undrained triaxial shearing tests with stress-relaxation and constant rate of strain.

Moreover, comparisons are made between the predictions of the proposed model in this current study and the predictions produced by the recent EVP model developed by Islam (2014) and the refined EVP model developed by Yin and Zhu (1999).

In addition, the application of the extended model for the prediction of the rate-dependent stress-strain behaviour of K_0-consolidated soft soils, including soft Wenzhou Marine clay (reported by Yin et al., 2015), Shanghai soft clay (documented by Huang et al.,

2011) and Hong Kong marine deposit (HKMD) clay (outlined by Zhou et al., 2005), has been examined and scrutinised in:

- Section 5.6 for strain-controlled undrained triaxial compression and extension tests;
- Section 5.7 for undrained triaxial shearing tests using step-changed strain rates.

For the purpose of evaluating the performance of the proposed and extended models using triaxial tests, the numerical implementations have considered the triaxial soil specimen as an element of soil and hence, a single representative stress point was adopted. In the current study, the numerical simulations, employing Runge Kutta Fehlberg method, as applied in Wang (2017), for time-integration, were implemented using MATLAB software, inspired by executions in Gong et al. (2009). Using the proposed and extended models, a few of the prepared MATLAB codes are provided in Appendix E for further details. Although the laboratory measurements presented in this study might have involved finite strain values, the finite strain effects were not considered in both the proposed and extended models, as the proposed formulations have adopted infinitesimal-strain hypothesis, as in Wroth and Houlsby (1985), Zhou and Ng (2015) and Lai et al. (2016), developing in terms of effective stresses, and thus, relating to the fundamental stress-strain behaviour of the soil skeleton, as in Yin et al. (2002) and Yin (2006). The conclusion of this chapter in Section 5.8 summarises the findings and observations on the investigation and assessment of the performance and applicability of the proposed and extended models in predicting the time- and rate- dependent stress-strain behaviour of various types of soils under different loading and drainage conditions.

5.2 Summary and Determination of Model Parameters

This section presents the summary of the model parameters required for the proposed H-Creep, which, basically, is divided into three major categories:

1. The first set of parameters are termed as Modified Cam-clay parameters, including initial void ratio (e_0), slope of the swelling line (κ^*), slope of the compression line (λ^*), Poisson's ratio (ν), the initial reference pre-consolidation pressure (or the size of the initial reference surface) (p_{c0}) and the stress ratio at the Critical State in compression (M).

2. The second set is pertinent to time-dependent parameters, including the creep parameter (μ_0) and the material constant (m) representing the slope of the $\log \mu - \log e$ curve required for the non-linear creep function.

3. The third set includes the dissipation parameters γ and α.

Besides, the extended model introduces one additional category, while the other three sets remain identical as described above. The additional group of parameters is pertinent to the consideration of the arrangement of particles and the bonding between the particles,

4. The fourth set includes the initial fabric parameter (β_0), the soil constants (C_β) and (D_β).

The calibration procedure for the parameters of the first set is relatively straightforward, and no additional test is required, compared to the procedure used in the Modified Cam-clay (MCC) model (Roscoe and Burland, 1968). Accordingly, the slope of the Critical State Line (M) is obtained from drained or undrained triaxial compression tests.

The time-dependent parameters (i.e. the creep coefficients, μ and μ_0) as well as the values for the void ratio, e and e_0, is determined from either triaxial compression tests or conventional 1-day oedometer tests. The power value m is a curve-fitting parameter, which is determined from the $\log\ \mu - \log e$ curve, in a straightforward way.

The additional dissipation parameters γ and α are the material constants, which are determined from undrained triaxial and one-dimensional consolidation test data. The parameter γ is determined from Undrained Triaxial Compression (UTC) or Extension (UTE) data at a specific over-consolidation ratio (OCR). This depends on the distance between the CSL and the consolidation line, as this distance provides the ratio of the size of the yield surface to the pressure at the Critical State (Collins and Hilder, 2002). The value for γ is selected in the way that the position of the CSL relative to the size of the yield surface is close to that of the MCC model, (e.g. $(p'/p'_c)_{CS} = 0.5$). The parameter α can be considered as constant fixed at a particular value corresponding to the shape of the yield surface, in order to reduce the over-prediction of the peak deviatoric stress at high OCRs generated by the MCC model. The most appropriate values for γ and α result in the best fitted stress-strain curves, particularly in the post-yielding stages of the deformation. As previously discussed, the non-associated flow rule is naturally derived from the postulated stress-dependent dissipation function, unless γ and α values are equal to one.

The initial fabric parameter (β_0), and the related soil constants (C_β) and (D_β) included in the fourth set are pertinent to the evolution law related to the fabric parameter (β), provided in Equation (4.52). The parameters, C_β and D_β, are mainly associated with the initial size and degree of rotation of the critical surface accounting for the previous stress and strain history of the soil deformation. The in-situ rotary state of the critical surface is observed when the previous history of the soil is limited to one-dimensional straining to a normally consolidated

or lightly overconsolidated condition. However, the changes in the in-situ inclination of the critical surface are expected during the unloading stage, as the stress path during unloading process may have reached the critical surface in the triaxial extension region, for the case of heavily overconsolidated state. Hence, the initial inclination of the critical surface corresponds to the situation resulting from K_0-consolidation to a normally consolidated state, in which the initial rotary state of the critical surface is not influenced by any elastic unloading to a lightly overconsolidated state. Therefore, the initial β value is approximated from K_0-consolidated state, i.e. $\varepsilon_3 = 0$, from which the following expression is derived using Equations (4.2c) and (4.2d):

$$\frac{\varepsilon_v}{\varepsilon_q} = \frac{(\varepsilon_1 + 2\varepsilon_3)}{\frac{2(\varepsilon_1 - \varepsilon_3)}{3}} = \frac{\varepsilon_1}{\frac{2\varepsilon_1}{3}} = \frac{3}{2} \tag{4.54}$$

Assuming that the elastic strains are much smaller than the viscoplastic strains, the Equation (4.54) can be approximated by $\dot{\varepsilon}_v^{vp} / \dot{\varepsilon}_q^{vp} = 3/2$. In most of the existing EVP models, (see – for example, Zhou et al., 2005; Rezania et al., 2016), the initial value of β (i.e. β_0) corresponding to the one-dimensional consolidation is generally determined using the commonly adopted assumption based on the associated flow rule from the traditional MCC model, which is widely accepted as a reasonable approximation for natural clays when combined with an initial rotatory state of the critical surface. In stark contrast, the proposed model employs the non-associated flow expression derived in Equation (4.51), with an intention to maintain the internal consistency of the proposed constitutive framework. Accordingly, the initial rotatory value β_0 is derived, adopting the definition of the parametric angle (ω) based on the non-associated flow rule (See - Appendix D for more details) in combination with Equation (4.54), which yields:

$$\beta_0 = \beta_{K0} = \frac{B}{A}\cot\omega - \frac{3}{2} \tag{5.55}$$

where, ω is denoted as a parametric angle, determined at an initial K_0-consolidation stress ratio (i.e. η_{K0}), as shown in Figure 4.7. The stress ratio η_{K0} is calculated using $\eta_{K0} = 3M_c/(6 - M_c)$, derived from the estimated value of K_0 from Jaky's simplified formula (i.e. $K_0 \approx 1 - \sin\phi'$), as M is related to the friction angle ϕ'. The equilibrium value of β for any provided value of η can be found by setting $\dot{\beta} = 0$ in Equation (4.53) and combining with the adoption of non-associated flow rule derived in Equation (4.51) using the parametric angle (ω) defined based on the non-associated flow rule, as discussed in Appendix D, which sets the proposed model apart from the existing EVP models.

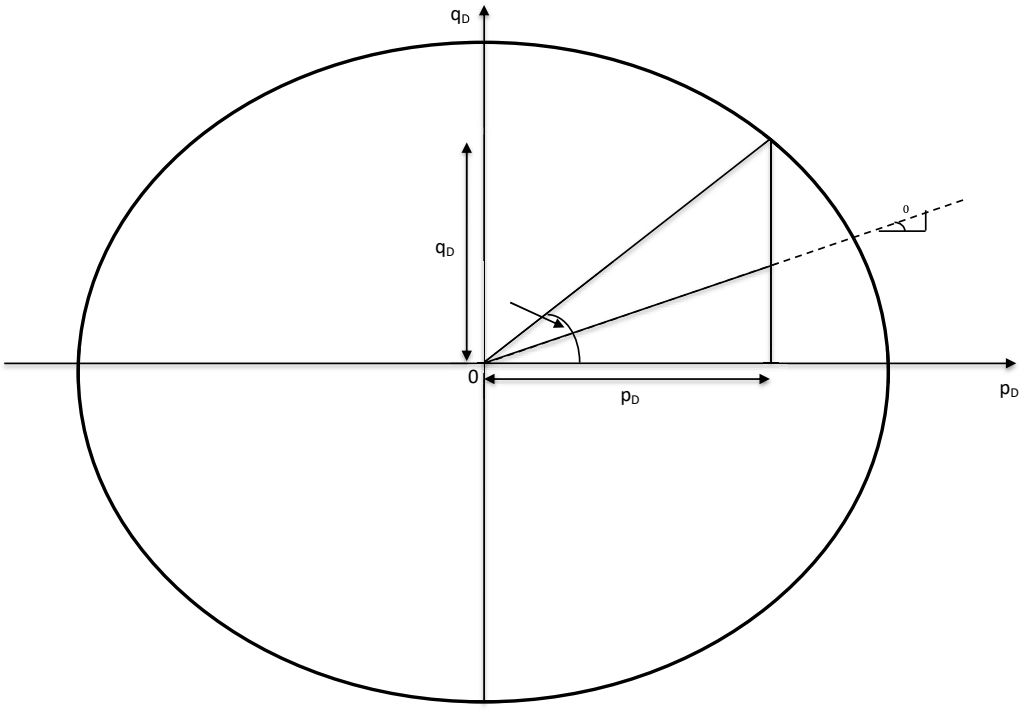

Figure 4.7: Definition of the parametric angle ω

Besides, a specific value of D_β results in a value of β corresponding to β_0 from Equation (5.55) for loading at the normally consolidated K_0 stress ratio (i.e. η_{K0}). It follows from the combination of Equations (4.52) and (5.55) that:

$$D_\beta = \frac{3(3\eta_{K0} - 4\beta_0)}{4(\eta_{K0} - 3\beta_0)}\left[\frac{B\cot\omega - \beta_0 \cdot A}{A}\right] \tag{4.56}$$

Although the procedure seems to be circuitous, the analysis has demonstrated that it is sensitive, in particular, to the value assumed for volumetric target value (i.e. $3\eta/4$). This represents a significant advantage over the existing EVP models in that a specific value for D_β can be selected using the aforementioned procedure, which results in improved accuracy in aligning with the normally consolidated value of K_0.

In comparison with the indirect method to determine D_β, it is difficult to suggest a possible route to estimate the value of C_β for a given soil, as also pointed out in Yin and Karstunen (2011) and Zhang (2018), unless model simulations with different values of D_β can be performed. Therefore, the appropriate value for C_β is estimated from the curve fitting based on simulations, particularly when the 'fabric' effects rein in either isotropic compression or triaxial extension tests. In the absence of a suitable experimental data, the range for C_β value lies between $10/\lambda^*$ to $15/\lambda^*$ for a particular soil, suggested by Zenter et al. (2002b). Alternatively, if there are no significant changes in the extent of coupling is expected, C_β could be set to zero by explicitly, assuming that an initial rotary state of the critical surface is fixed.

Although, ideally, specialised testing and numerous numerical simulations are required to calibrate the model parameters controlling the degree of rotation of the critical surface, close approximations for the initial inclination of the critical surface, i.e. β_0, and the material constant D_β, are estimated using a simple empirical relation based on the normally consolidated value of K_0, which in turn, can be estimated from friction angle ϕ', as previously discussed. Therefore, the proposed model has a great potential for geotechnical applications, as it does not require advanced soil testing compared to the existing models that require additional parameters in order to predict such a level of sophisticated behaviour of soils.

5.3 Application of the Proposed H-Creep Model to Stress-controlled and Strain-controlled Compression and Extension Tests

In this section, the application of the proposed H-Creep model in predicting the rate-dependent behaviour of HKMD clay, Osaka clay and Kaolin and Bentonite mixture subjected to stress-controlled and strain-controlled compression and extension tests is investigated. The required model parameters employed in the current section for the numerical implementations were calibrated based on the procedure detailed in Section 5.2, which are summarised in the following table.

Table 5.1: Values of Model Parameters for HKMD Clay, Osaka Clay and Kaolin and Bentonite Clay Mixture

Model Properties	Soil Types		
	HKMD Clay	Osaka Clay	Kaolin and Bentonite Clay Mixture
λ^*	0.1987	0.355	0.1507
κ^*	0.0451	0.047	0.0194
μ	0.0063	0.0142	0.006
M_c	1.265	1.278	1.2479
M_e	0.89	-	-
e_0	1.506266	2.41	0.6207
υ	0.3	0.3	0.3
α	1	1	1
γ	0.85 – 0.95	0.95 - 1	0.83-0.85
m	1.0881	1	1

5.3.1 Stress-controlled Undrained Compression Tests on HKMD Clay

Firstly, the calibrated model is used to predict the stress-strain behaviour of consolidated undrained compression test sheared at a constant deviatoric stress rate on HKMD clay, which was performed by Yin and Zhu (1999). The consolidation pressure of 400kPa was used to isotropically and normally consolidate the soil specimens, which was then followed by shearing at a constant deviatoric stress rate of 30kPa/h.

5.3.1.1 Model Performance

Figures 5.1a and 5.1b depict the measured and predicted results for the relationship between deviatoric stress versus axial strain and the effective stress paths, respectively, from the stress-controlled undrained compression tests on HKMD clay. Although it is apparent from Figure 5.1a that the proposed model results in slight over-prediction of the non-linear response at small strain levels, the predictions start to closely match the laboratory observations when the axial strain levels reach 4% onwards. The over-predictions could be rectified if hysteretic responses are to be modelled, based on discussions provided in Whittle and Kavvadas (1994) and Jiang et al. (2012), however, at the undesirable necessity of additional model parameters. Despite some minor discrepancies, the predictions, in general, are in good agreement with the measurements.

Moreover, Figures 5.1a and 5.1b demonstrate the comparisons between the predictions of the proposed H-Creep model and the enhanced EVP model proposed by Yin and Zhu (1999). Compared to the predictions reported by Yin and Zhu (1999), the proposed model in this study provides improved predictions for the deviatoric stresses and the effective stress paths, particularly while matching the laboratory trend of the latter in approaching the Critical State Line (CSL).

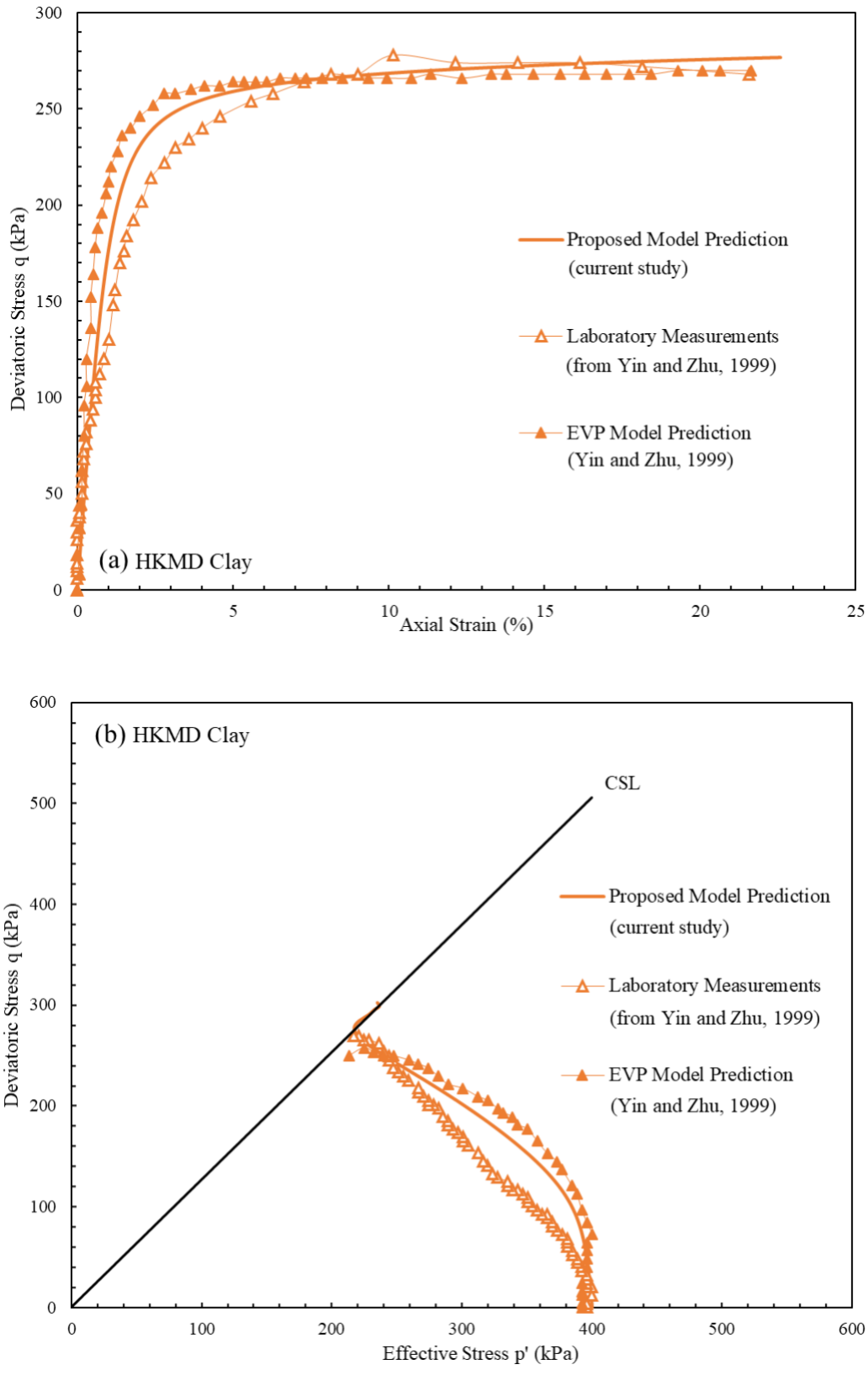

Figure 5.1: Comparison between the measured and predicted results for consolidated undrained shear test at a constant deviatoric stress rate on HKMD clay: (a) deviatoric stress (q) versus axial strain (ε_a); and (b) effective stress paths

5.3.2 Strain-controlled Drained Compression Tests on HKMD Clay

Here, the calibrated hyper-viscoplasticity model is applied to predict the stress-strain behaviour of consolidated drained compression tests with controlled strain rates on HKMD clay, which was conducted by Yin and Zhu (1999). The two consolidated drained compression tests were performed, in which the test specimens were isotropically and normally consolidated using the normal consolidation pressures of 300 kPa and 400 kPa, while subjected to similar axial strain rate of 0.0065%/min under test conditions.

5.3.2.1 Model Performance

The predictions generated by the numerical simulations for the relationships between deviatoric stress versus axial strain and volumetric strain versus axial strain are illustrated in Figures 5.2a and 5.2b, respectively. Overall, the predicted results are in good agreement with the laboratory measurements for the former relationship, whilst some discrepancies are observed with slight over-prediction for the latter one, with the predicted volumetric strains being larger than the measured data, particularly for the test corresponding to the consolidation pressure of 300 kPa. However, it is evident that the predicted trend for the volumetric strains followed exactly the same path as the experimental observations. It can be observed from Figure 5.2b that the predicted volumetric strain for both tests with different consolidation pressures were almost identical, whereas the volumetric strain test data for both effective pressures were very close for the axial strain up to 6% and began to slightly differ when the axial strains exceeded 6%. Therefore, referring to Figure 5.2b, the changes in the effective pressures have insignificant effect on the volumetric strains, which is also evident from the predictions reported by Yin and Zhu (1999). As it is concluded from Figure 5.2c, the proposed H-Creep model effectively captures the effective stress paths for both compression tests.

In order to further testify the applicability and usefulness of the proposed H-Creep model, the comparisons are made between the model's predictions and the enhanced EVP model proposed by Yin and Zhu (1999). Despite the relative simplicity of the proposed model with standardised procedure, improved predictions for the deviatoric stresses as well as the volumetric strains are observed when compared to predictions reported by Yin and Zhu (1999)'s enhanced EVP models.

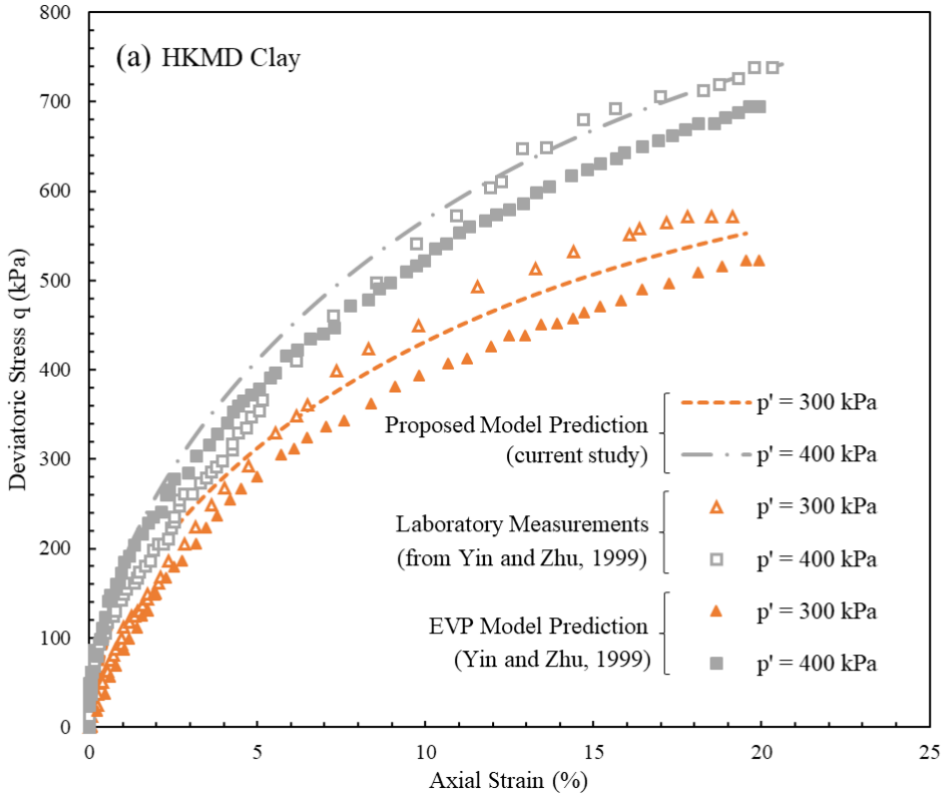

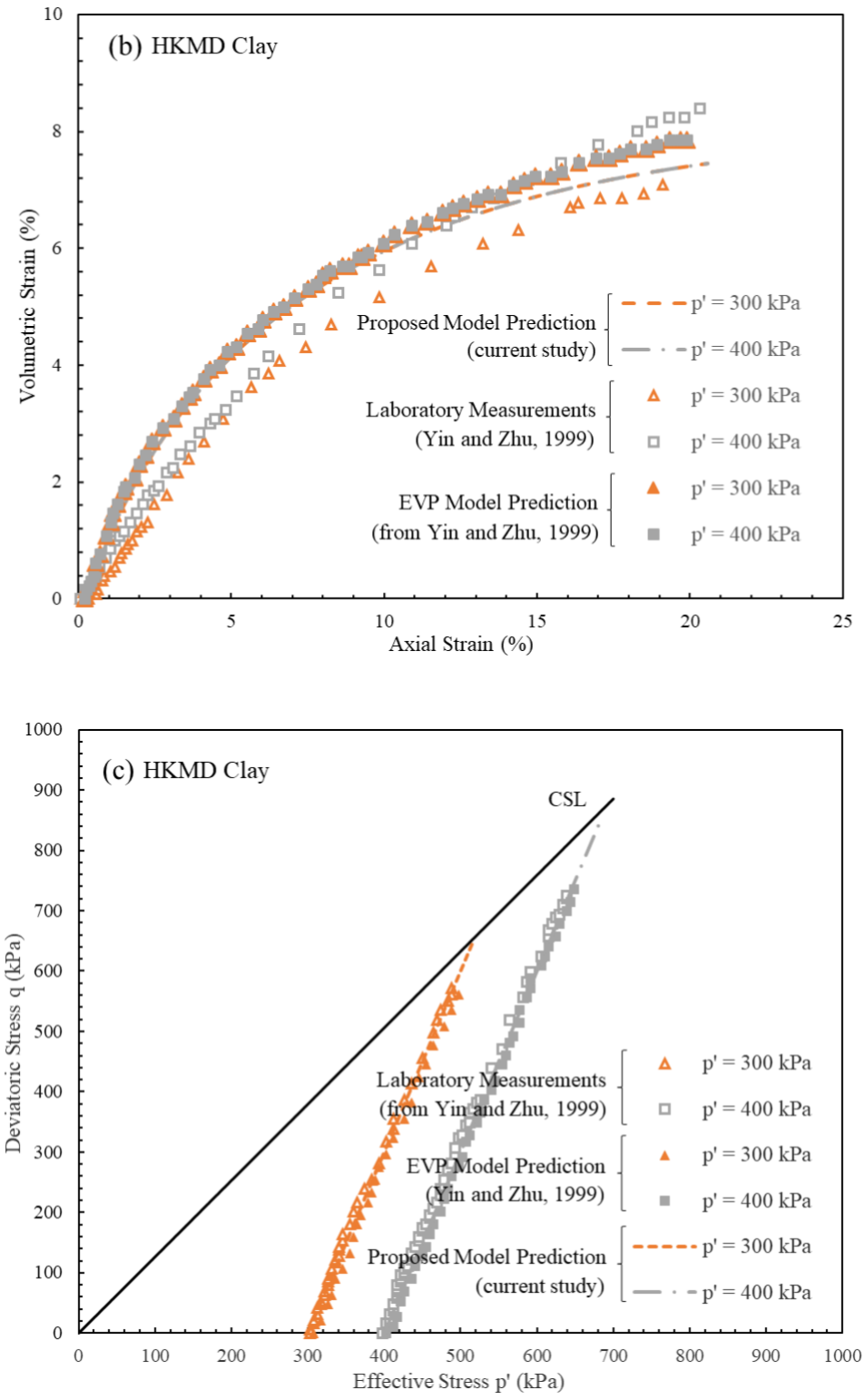

Figure 5.2: Comparison between the measured and predicted results for two consolidated drained shear tests on HKMD clay: (a) deviatoric stress (q) versus axial strain (ε_a); (b) volume strain (ε_v) versus axial strain (ε_a) and (c) effective stress paths

5.3.3 Strain-controlled Undrained Compression Tests on Osaka Clay

The proposed H-Creep model is used to predict the proposed model with the strain-controlled undrained triaxial compression test data on natural clays, in particular, the Osaka clay, using two confining pressures, reported by Adachi et al. (1995). The simulations using the calibrated model for the laboratory data from strain-controlled (0.01%/minute) undrained triaxial compression tests are depicted in Figures 5.3a and 5.3b.

5.3.3.1 Model Performance

The performance of the proposed model is evaluated by comparing the predictions of the proposed model with the experimental data. As shown in Figure 5.3a, the proposed model results in minor over-prediction of 5-7% for the deviatoric stresses at small strain levels below 4%, while the predictions start to match up with the laboratory measurements for strain levels greater than 4%. The consideration of hysteretic effects could resolve this particular issue, as previously discussed. On the other hand, the predicted effective stress paths are also compared with the laboratory data in the accompanying Figure 5.3b, in which it is identifiable that the proposed model provides improved predictions for the effective stress paths, as they gradually follow a 'narrow region' after attaining the peak deviatoric stress, which is also reflected in the experimental observations. Moreover, Figures 5.3a and 5.3b display comparisons between the predictions by the proposed model and the EVP model developed by Islam (2014) for the undrained triaxial compression test performed on Osaka clay. Following the simplified procedure with strong theoretical foundation, it is evident from Figure 5.3a that the proposed model in this study provides better predictions for the deviatoric stresses particularly for large axial strains (i.e. exceeding 4%). Furthermore, the proposed model reproduces better simulations compared to the predictions generated by a relatively contemporary EVP model.

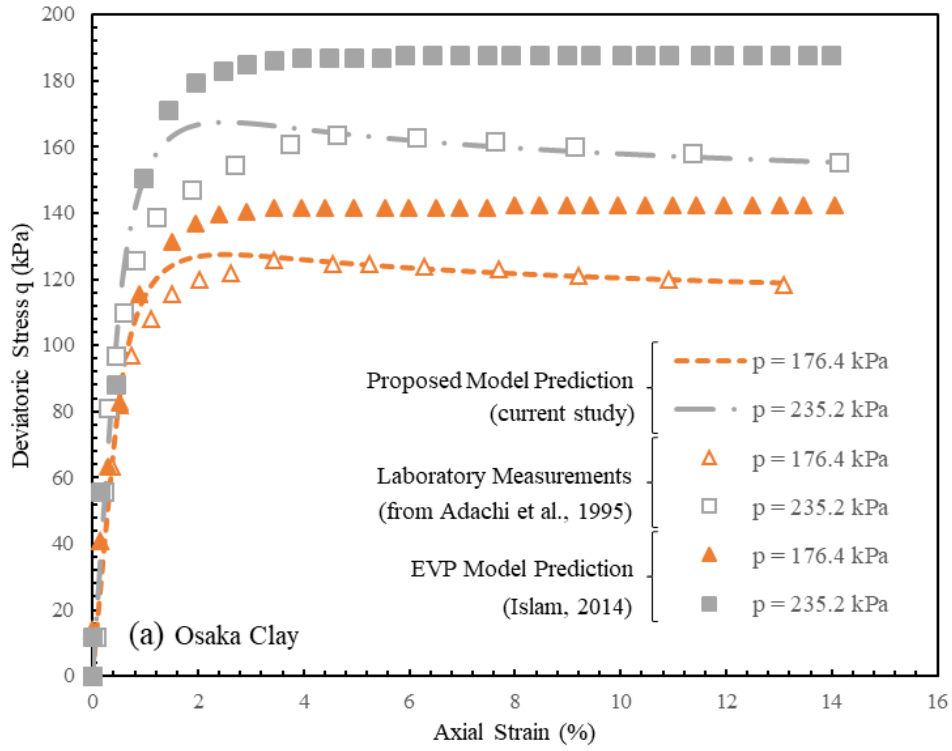

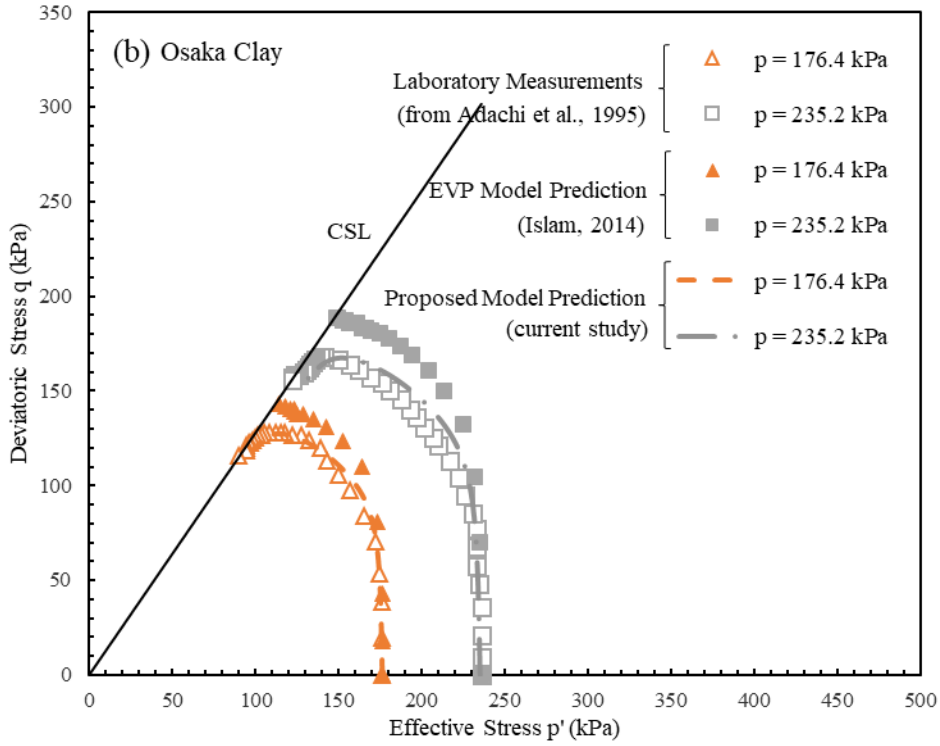

Figure 5.3: Comparison between the measured and predicted results for undrained triaxial tests on Osaka clay (Data from Adachi et al., 1995): (a) deviatoric stress (q) versus axial strain (ε_a); and (b) effective stress paths

In addition, the proposed model reinforces the 'narrow region' phenomena emphasised in Adachi et al. (1995) by demonstrating that critical state concepts are applicable to natural soft clays even at large strain levels, as highlighted in Figure 5.3b.

5.3.4 Strain-controlled Consolidated Undrained Triaxial Compression Tests using various OCRs on Kaolin and Bentonite mixture

The application of the proposed H-Creep model is further investigated to predict four strain-controlled consolidated-undrained triaxial compression tests with various OCRs on a mixture of kaolin and bentonite carried out by Herrmann et al. (1981). The pre-consolidation pressure of 392 kPa was applied on the test specimens with OCRs of 1, 1.3 and 2 and the axial strain rate applied during shearing was 0.6%/hr.

5.3.4.1 Model Performance

Figures 5.4a and 5.4b depict the comparisons between the proposed model's predictions and the laboratory results after Kutter and Sathialingam, 1992; Dafalias and Herrmann, 1986) for the CIU tests on the mixture of kaolin and bentonite. It is apparent from Figure 5.4a that the proposed model competently captures the rate-dependent stress-strain response to a reasonable level before reaching the peak deviatoric stress and after 4% axial strain level. As in the previous tests, slight discrepancies are observed for 1% to 4% axial strain levels. In Figure 5.4b, the comparisons of the experimental and predicted stress paths are depicted, where it is apparent that the model marginally over-predicted the stress paths for OCR = 1 and 1.3 but the predictions were markedly close to measurements for OCR = 2 and overall, in good and satisfactory agreement.

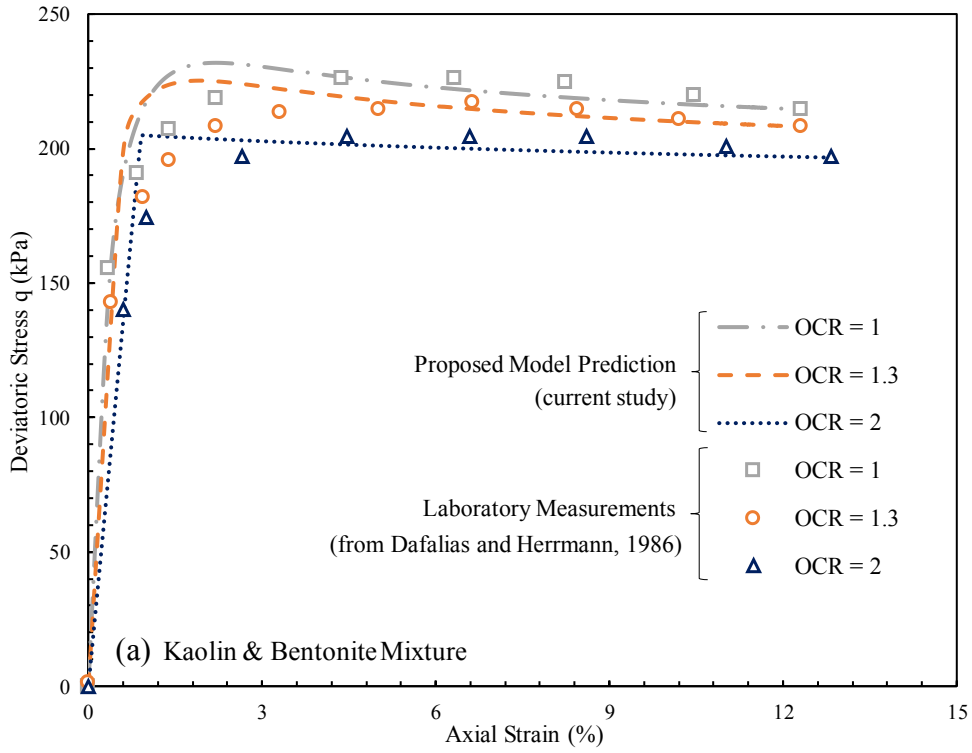
Deviatoric Stress q (kPa)
Axial Strain (%)
Proposed Model Prediction
(current study)
OCR = 1
OCR = 1.3
OCR = 2
Laboratory Measurements
(from Dafalias and Herrmann, 1986)
OCR = 1
OCR = 1.3
OCR = 2
(a) Kaolin & Bentonite Mixture

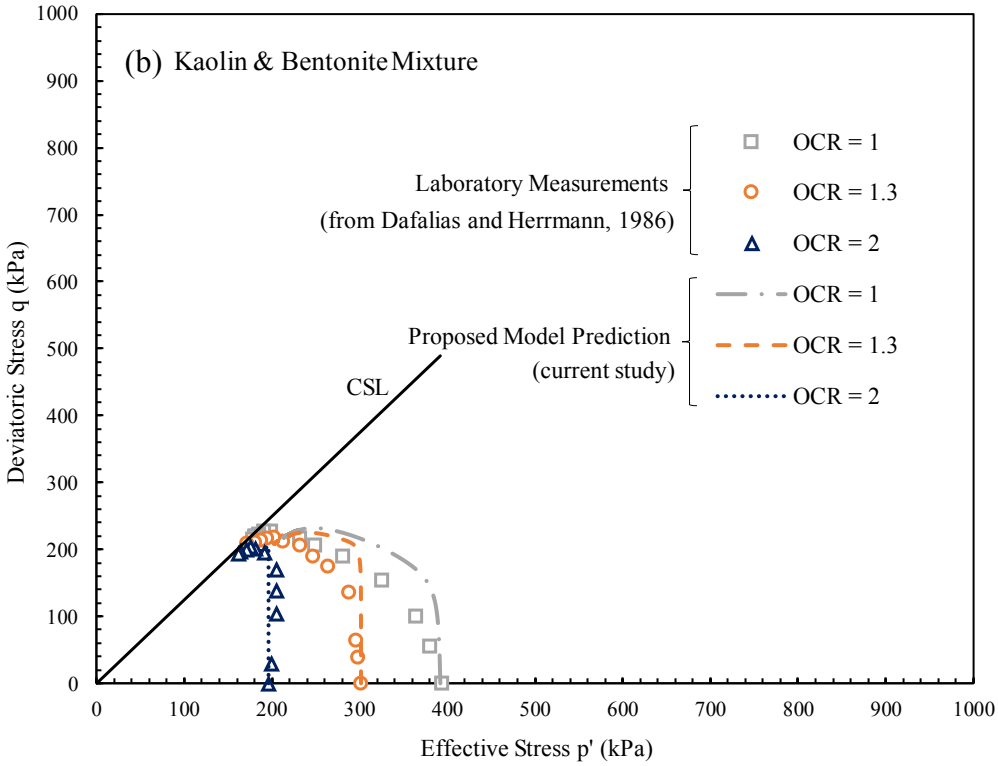
(b) Kaolin & Bentonite Mixture
Laboratory Measurements
(from Dafalias and Herrmann, 1986)
OCR = 1
OCR = 1.3
OCR = 2
Proposed Model Prediction
(current study)
OCR = 1
OCR = 1.3
OCR = 2
CSL
Deviatoric Stress q (kPa)
Effective Stress p' (kPa)

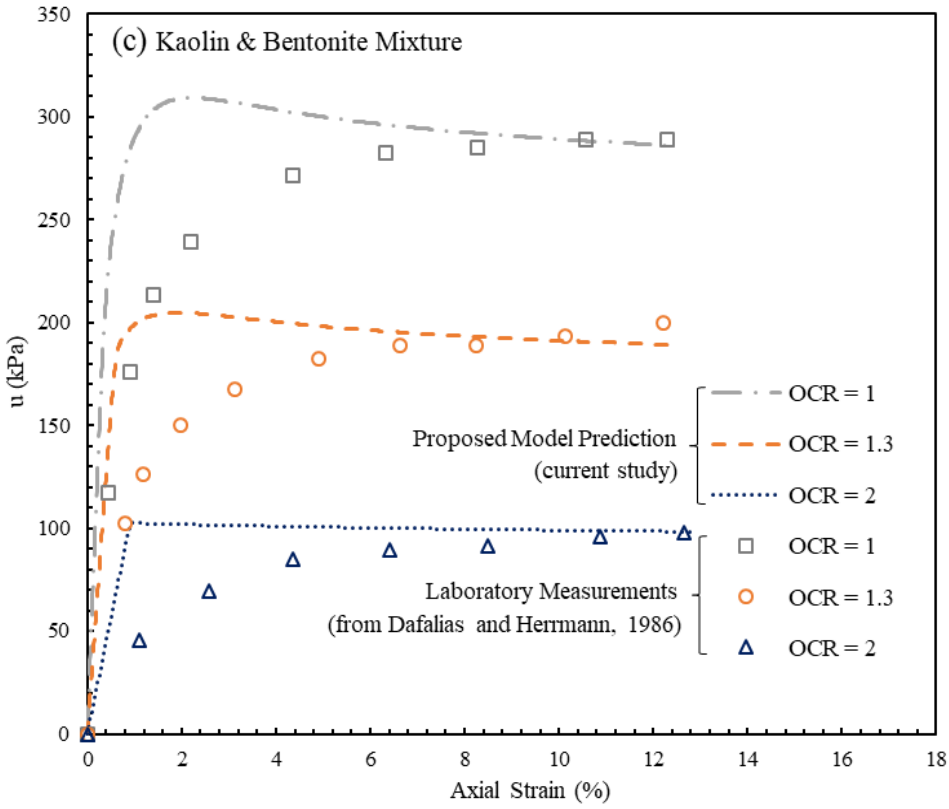

Figure 5.4: Comparisons between the measured and predicted consolidated undrained triaxial test results on a mixture of kaolin and bentonite: (a) deviatoric stress (q) versus axial strain (ε_a); (b) effective stress paths; and (c) axial strain (ε_a) versus pore-water pressure (u)

In addition, the proposed model is applied to predict the induced pore-water pressure response under various axial strain values, which is illustrated in Figure 5.4c. Since the current study does not consider the effect of the generation of a shear band within the specimen and inherent suction at failure, along with the fabric effects and the transitional yielding when the normally consolidated stress state is approached, for the sake of simplicity, some discrepancies are apparent between the proposed model's predictions and the laboratory results for different OCR values.

5.4 Application of the Proposed H-Creep Model to Undrained Triaxial Shearing Tests Using Various Strain Rates

The adopted model parameters related to Haney clay and HKMD clay for examining the performance and applicability of the proposed model in this section, were derived following the procedure described in the previous Section 5.2, while the ones related to HKMD clay are referred from Table 5.1. Both sets of parameters are summarised in Table 5.2.

Table 5.2: Values of Model Parameters for Haney Clay and HKMD Clay

Model Properties	Soil Types	
	Haney Clay	HKMD Clay
λ^*	0.1055	0.1987
κ^*	0.01635	0.0451
μ	0.004	0.0063
M_c	1.2872	1.265
M_e	-	0.89
e_0	0.896	1.506266
υ	0.15	0.3
α	1	1
γ	0.7 - 0.75	0.85 – 0.95
m	1	1.0881

5.4.1 Undrained Triaxial Shearing Tests Using Various Strain Rates on Haney Clay

The capability of the proposed model is further investigated against the laboratory data recorded by Vaid and Campanella (1977) on the undrained triaxial shearing tests using multi strain rates on Haney clay. In these tests, the soil specimens were consolidated using the effective confining pressure of 525 kPa for 36 hours and allow to stand for 12 hours under undrained conditions before the commencement of the shearing stage. The undrained triaxial compression tests were performed under constant rates of axial strain and constant confining pressure by applying prescribed displacement for three specific durations, i.e. a total of 12% axial strain over 8.865 days (0.00094%/min), 0.0556 days (0.15%/min) and 0.00758 days (1.10%/min).

5.4.1.1 Model Performance

Figure 5.5 demonstrates the applicability of the proposed model to reproduce the rate-dependent behaviour of Haney clay, capturing the deviatoric stress versus axial strain responses reasonably well. Moreover, the improved predictions are to be observed for the test samples with lower axial strain rates among the three testing conditions. Overall, the model predictions are in good agreement with the experimental data for the subsequent axial strain levels for all the reported aforementioned axial strain rates.

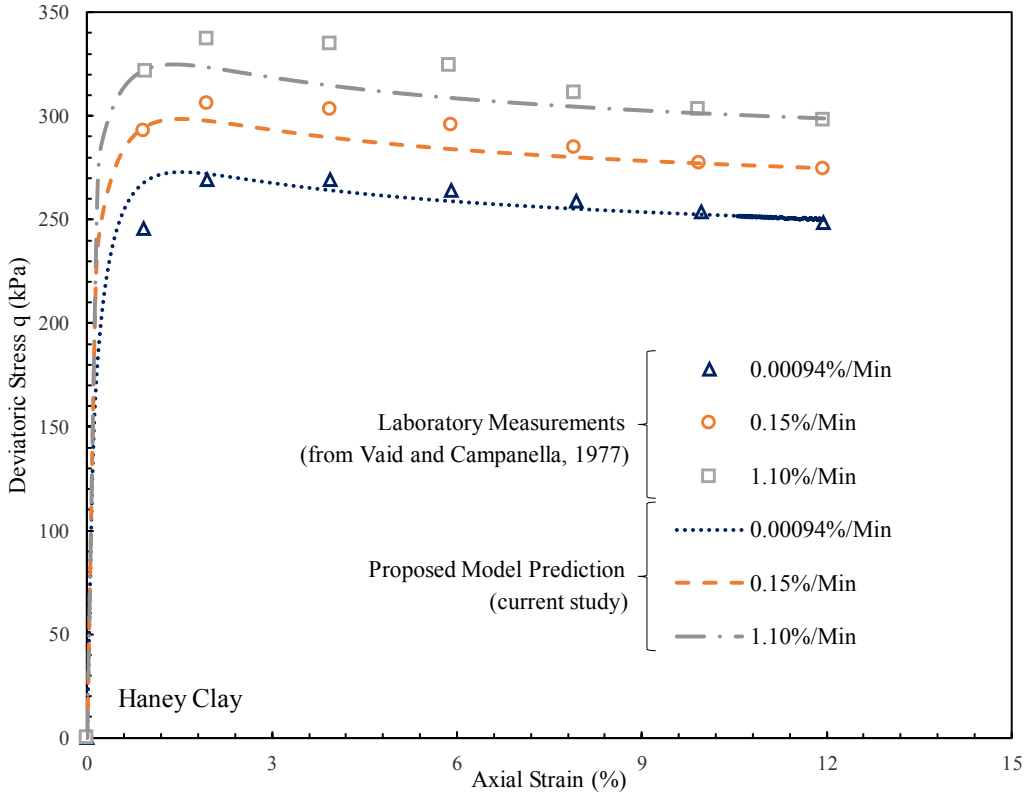

Figure 5.5: Comparison between the measured and predicted results for the relationship between deviatoric stress (q) and axial strain (ε_a) using undrained triaxial test results on Haney clay

5.4.2 Undrained Triaxial Shearing Tests at Various Strain Rates on HKMD Clay

The application of the proposed model is also assessed in simulating the behaviour of strain-rate effects of soils using six consolidated-undrained triaxial tests on the HKMD conducted by Yin et al. (2002). The effective consolidation pressure of 400 kPa (i.e. p_c = 400 kPa) and a back pressure of 200 kPa were used to isotropically consolidate the test specimens for 36 hours and 48 hours in compression and extension tests, respectively. In Figures 5.6a and 5.6b, the proposed model is used to predict the behaviour of the consolidated specimens being sheared at different axial strain rates of $\pm$0.15, $\pm$1.5 and $\pm$15%/hr under compression and extension.

5.4.2.1 Model Performance

Here, the relationships between the normalised deviatoric stress (q/p_c) and the axial strain (ε_a) and the effective stress paths, are recorded from the numerical simulations and illustrated in Figures 5.6a and 5.6b, respectively. The proposed model predictions have reached the acceptable level for compression tests, with only the under-predictions being observed within 2% to 5% of the axial strain level. However, discrepancies can be observed for the deviatoric stresses in extension when the axial strain levels progress from 3% due to the fact that the proposed model has not taken into account of destructuration effects, which might be responsible for the extension tests (Karstunen et al., 2005). Although disparities are apparent from the prediction of effective stress paths from Figure 5.6b, the general trend in stress-strain behaviour between the proposed model predictions and the laboratory measurements are in good accord to a justifiable extent.

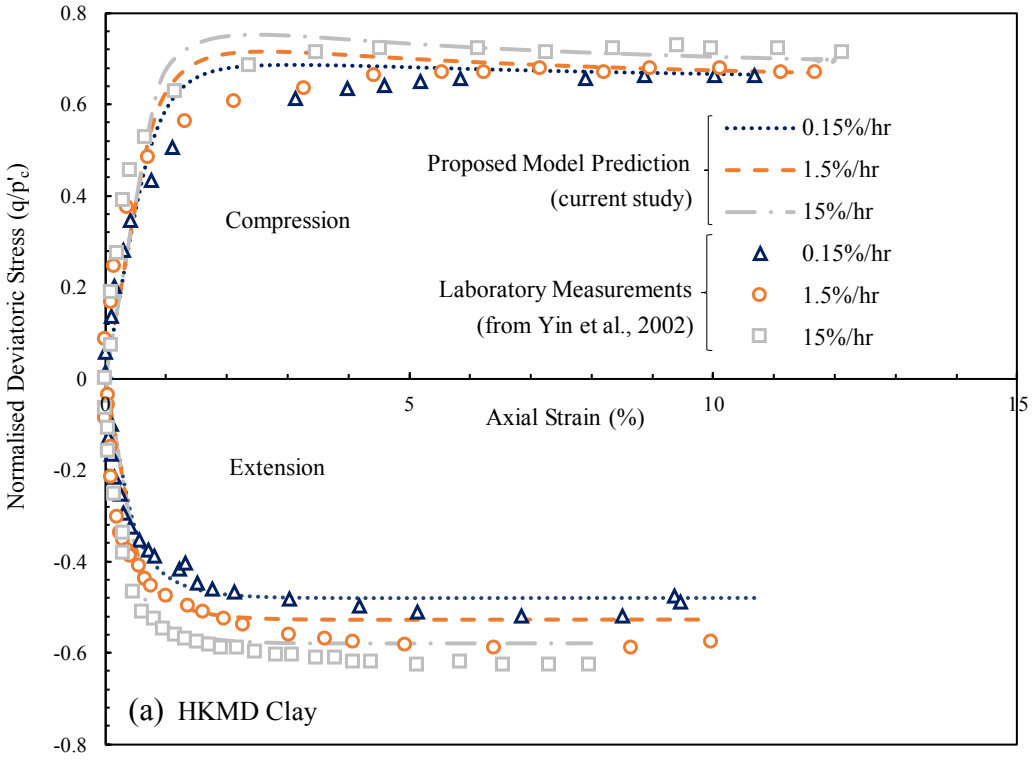

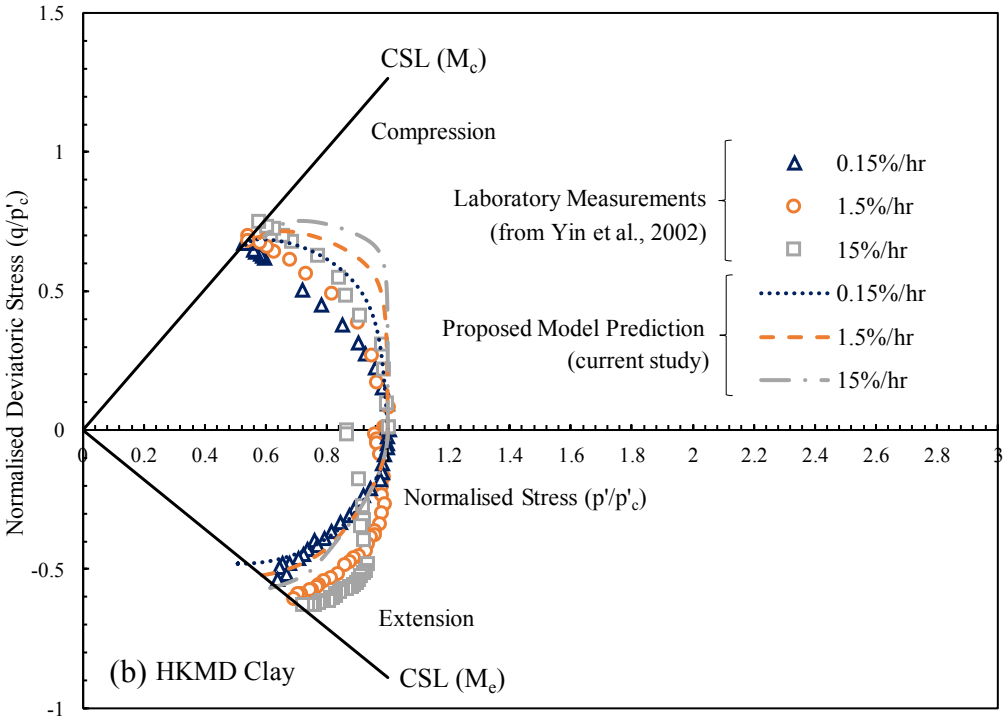

Figure 5.6: Comparison between the measured and predicted results for constant strain rate triaxial shearing tests on the HKMD under compression and extension tests: (a) normalised deviatoric stress (q/p_c) versus axial strain (ε_a); and (b) normalised effective stress paths

5.5 Application of the Proposed H-Creep Model to Undrained Triaxial Shearing Tests with Stress-Relaxation and Constant Rate of Strain

In this section, the required model parameters for investigating the capability of the proposed model in its application for predicting stress- and strain-dependent characteristics of HKMD clay are used from Table 5.1.

5.5.1 Undrained Triaxial Shearing Tests using Step-changed Strain Rates on HKMD Clay

Here, the application of the proposed model is further testified using a step-changed, constant strain rate, undrained triaxial shearing test combined with stress relaxation to demonstrate its capability in describing the stress relaxation behaviour. Yin et al. (2002) conducted an isotropically consolidated undrained triaxial compression tests using step-changed constant strain rates on normally consolidated HKMD clay. In these tests, the soil specimens were consolidated using an effective cell pressure of 300 kPa and a back pressure of 200 kPa to ensure the saturation of the specimens. The testing procedure and steps taken for predictions are recorded in Table 5.3.

Table 5.3: Test Procedure for Step-changed Triaxial Shearing Test with Constant Strain Rate and Stress Relaxation on HKMD Clay

Stage	1	2	3	4	5	6	7	8
Test Types	Shear	Unload	Reload	Relax	Shear	Relax	Shear	Relax
$\dot{\varepsilon}_a$ (%/hr)	6.00	-6.00	6.00	0	0.60	0	0.06	0
t (min)	29	7	20	2540	232	1320	830	705

5.5.1.1 Model Performance

The comparisons between the test results and the simulated predictions, using the proposed model are illustrated in Figure 5.7, in terms of the relationship between deviatoric stress (q) and the axial strain (ε_a) and the effective stress paths, respectively. It can be deduced that the numerical outcomes generated by the proposed model are in conformity with the laboratory data to an acceptable accuracy, demonstrating its applicability and pertinence in capturing the stress relaxation effects in addition to the strain rate response of HKMD clay.

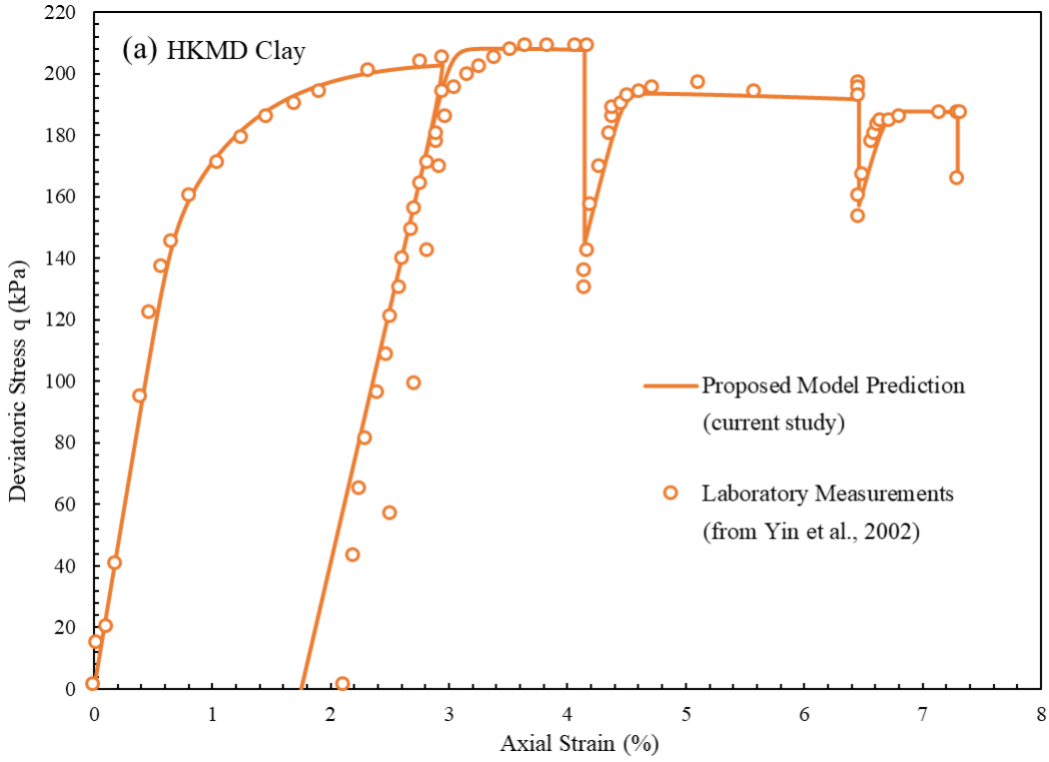
(a) HKMD Clay
Deviatoric Stress q (kPa)
Axial Strain (%)
Proposed Model Prediction
(current study)
Laboratory Measurements
(from Yin et al., 2002)

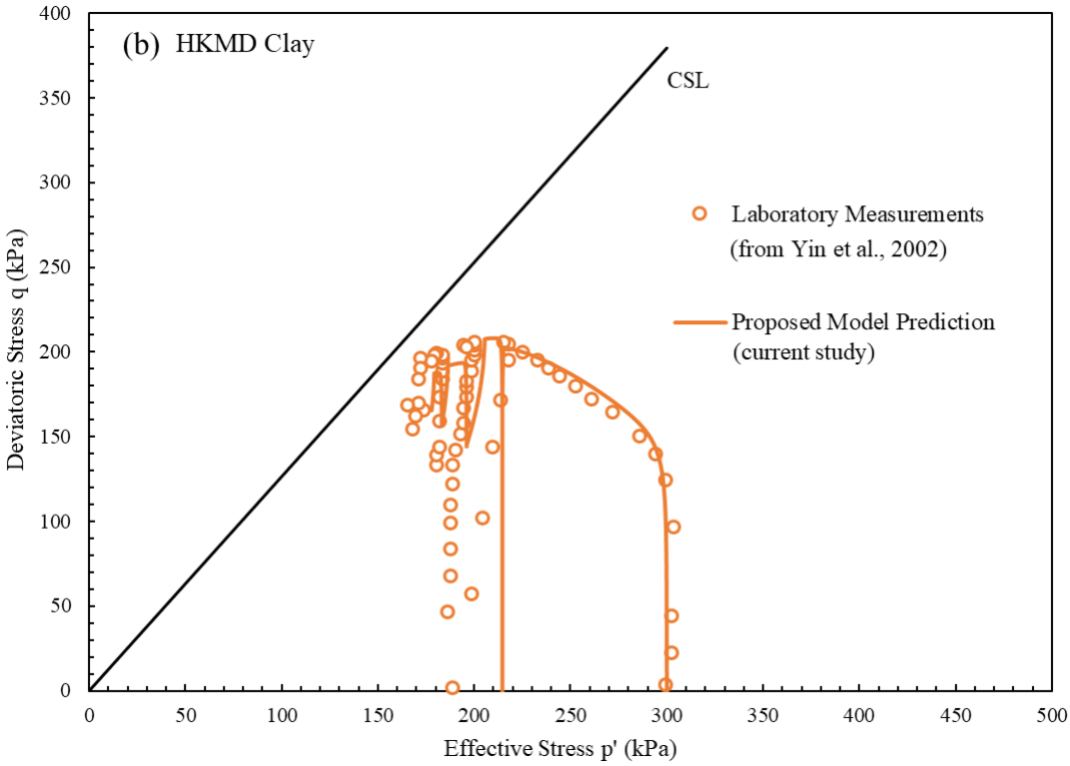
(b) HKMD Clay
CSL
Deviatoric Stress q (kPa)
Effective Stress p' (kPa)
Laboratory Measurements
(from Yin et al., 2002)
Proposed Model Prediction
(current study)

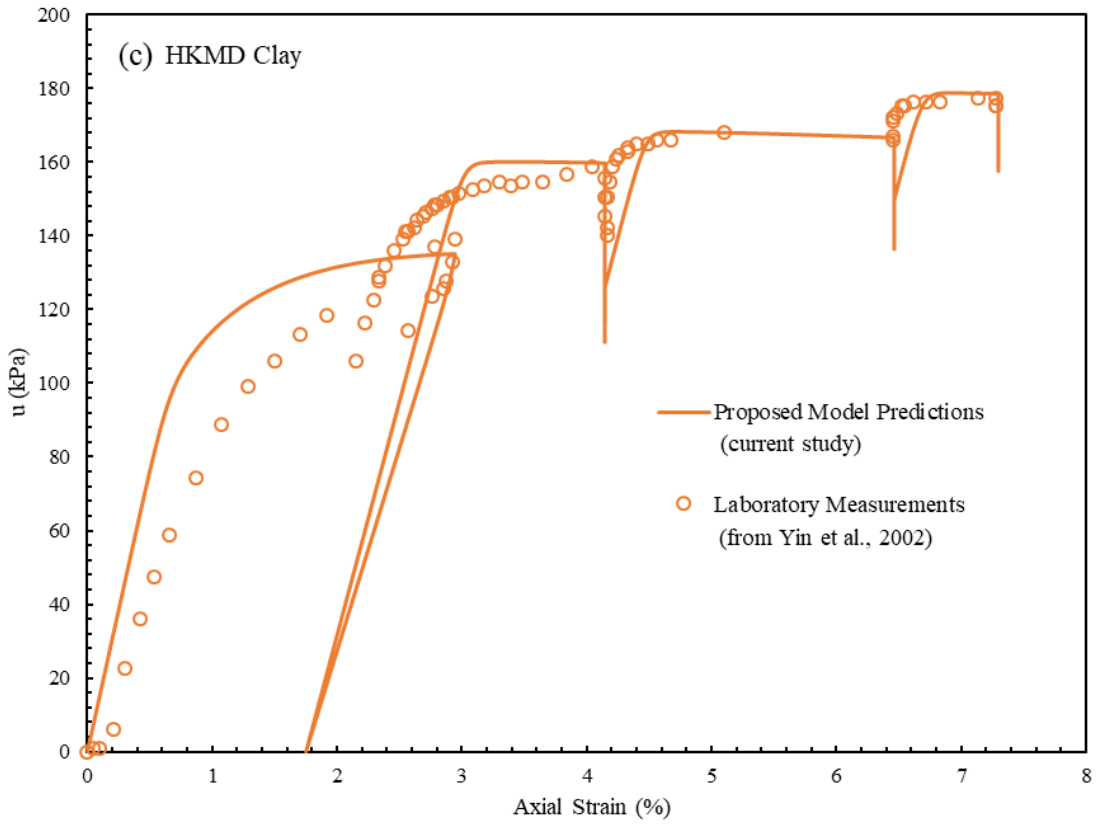

Figure 5.7: Comparison between the measured and predicted results for undrained triaxial tests for step-changed axial strain rate combined with stress relaxation on HKMD clay: (a) deviatoric stress (q) versus axial strain (ε_a); (b) effective stress paths; and (c) axial strain (ε_a) versus pore-water pressure (u)

Besides, Figure 5.7c illustrates the relationship of pore-water pressure variation corresponding to various axial strain values. It is apparent from Figure 5.7 that the undrained shear strength of the soil increases with the increasing strain rate, while reducing the excess pore water pressure dissipation. Considering the fact that the testing procedure was rather complicated, the predictions are in a good agreement with the measured results and by and large, can be considered as satisfactory.

5.6 Application of the Extended Model to Strain-controlled Undrained Triaxial Tests

In this section, the extended model described in Section 4.4 is applied to predict the undrained triaxial loading tests with constant rate of strain.

Table 5.4: Values of Model parameters for Soft Wenzhou Marine Clay and Shanghai Soft Clay

Model Properties	Soil Types	
	Soft Wenzhou Marine Clay	Shanghai Soft Clay
λ^*	0.384	0.212
κ^*	0.042	0.046
μ	0.005212	0.007218
K_0	0.4896	0.6
M_c(Compression)	1.23	1.277
M_e (Extension)	0.872	0.9
e_0	1.89	1.402
υ	0.25	0.2
α (Compression)	0.9 – 0.95	0.95
α (Extension)	1	-
γ (Compression)	0.7 – 0.75	0.55
γ (Extension)	1	-
m	1	1
β_0	0.581	0.41
D_β	0.039	0.0082
C_β	$10/\lambda^* - 15/\lambda^*$	$10/\lambda^* - 15/\lambda^*$

The summary of the model parameters employed in the extended model with the addition of fabric parameters were determined based on the procedure described in Section 5.2. The

required model parameters related to soft Wenzhou Marine clay and Shanghai soft clay for this section are summarised in Table 5.4.

5.6.1 Strain-controlled Undrained Triaxial Tests on Soft Wenzhou Marine Clay

In this section, the performance of the extended model is investigated by applying towards a series of consolidated undrained triaxial tests in compression and extension on K_0-consolidated soft Wenzhou Marine clay samples at constant axial strain rates, conducted by Yin et al. (2015). The effective cell pressure of 205 kPa was applied in increments, along with a back pressure of 200kPa, to ensure that all the test specimens were properly saturated. This was followed by consolidating the specimens under K_0-condition with final effective vertical pressures of 75.4 kPa, or 150 kPa, or 300 kPa whilst axially compressed without lateral deformation (or zero radial strain). Afterwards, the K_0-consolidated test specimens were sheared at constant axial strain rates of $\pm$0.2, $\pm$2 and $\pm$20%/hr under compression and extension conditions.

5.6.1.1 Model Performance

The predicted stress-strain behaviour of the K_0-consolidated test specimens being sheared at the aforementioned controlled axial strain rates are illustrated in Figures 5.8-5.12, in which the comparisons between the numerical results and the experimental measurements for the relationships between the deviatoric stress versus axial strain, along with the effective stress paths are exhibited. It is observable that the stress-strain curves reach their respective peak values after approximately 1-2% of axial strain level in the undrained compression tests on anisotropically consolidated test specimens. On the other hand, the predicted effective stress

paths converge towards the ultimate undrained strengths on the CSL, which is always a good indication.

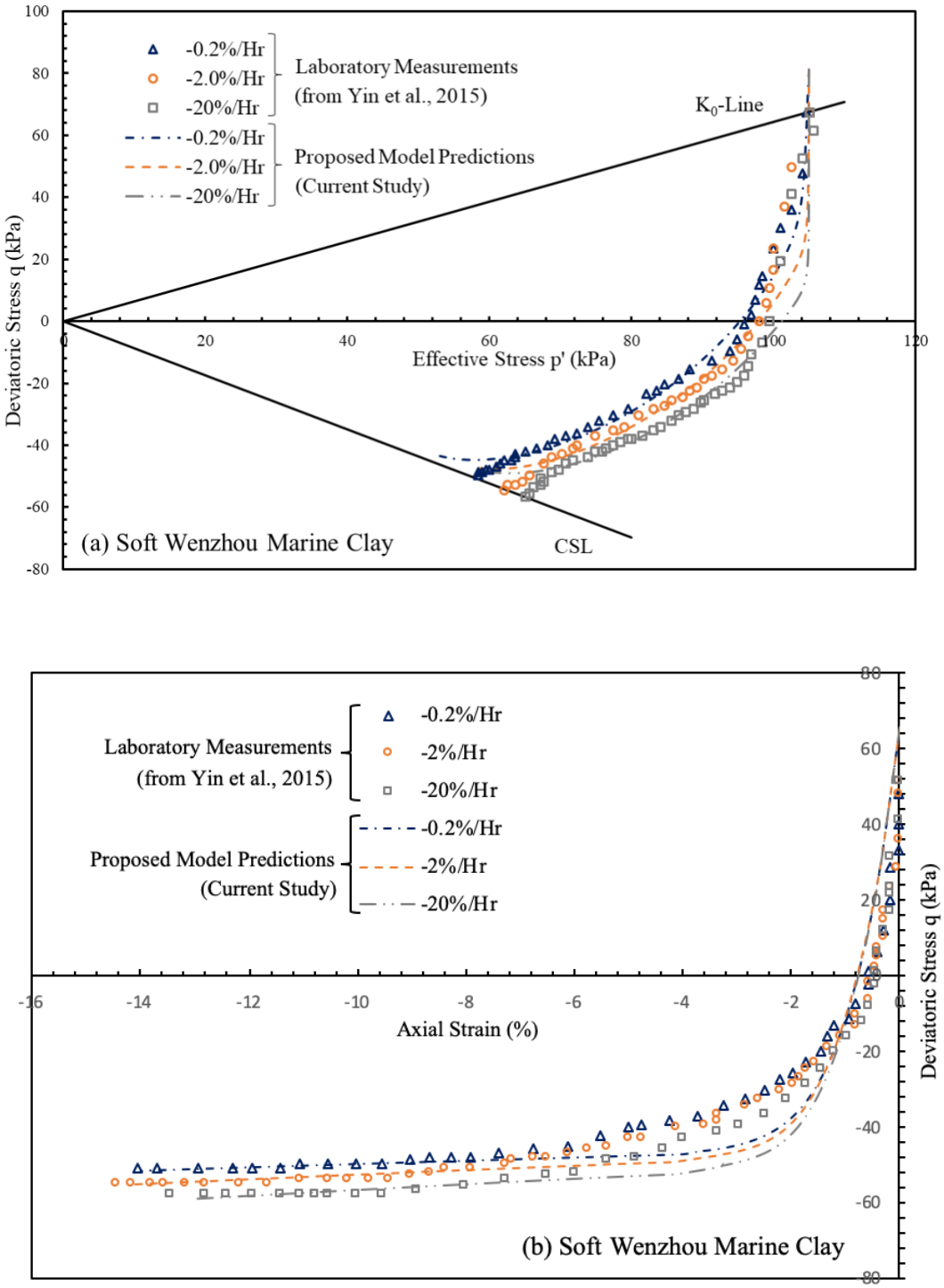

Figure 5.8: Comparison between the measured and predicted results for K0-consolidated undrained triaxial CRS tests at an effective pressure of 75.4 kPa on soft Wenzhou Marine clay in extension: (a) effective stress paths; and (b) deviatoric stress (q) versus axial strain (ε_a)

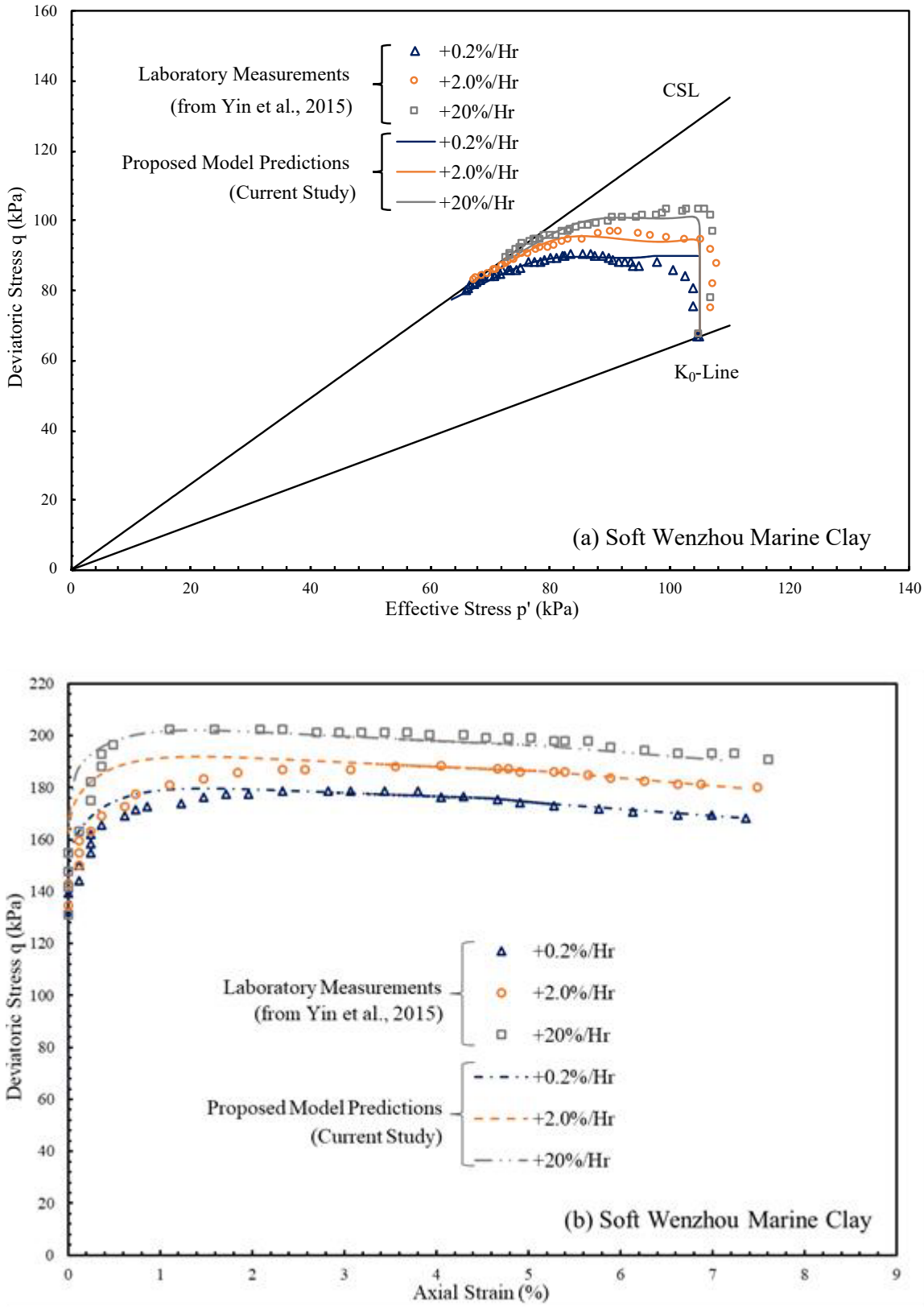

Figure 5.9: Comparison between the measured and predicted results for K0-consolidated undrained triaxial CRS tests at an effective pressure of 150 kPa on soft Wenzhou Marine clay in compression: (a) effective stress paths; and (b) deviatoric stress (q) versus axial strain (ε_a)

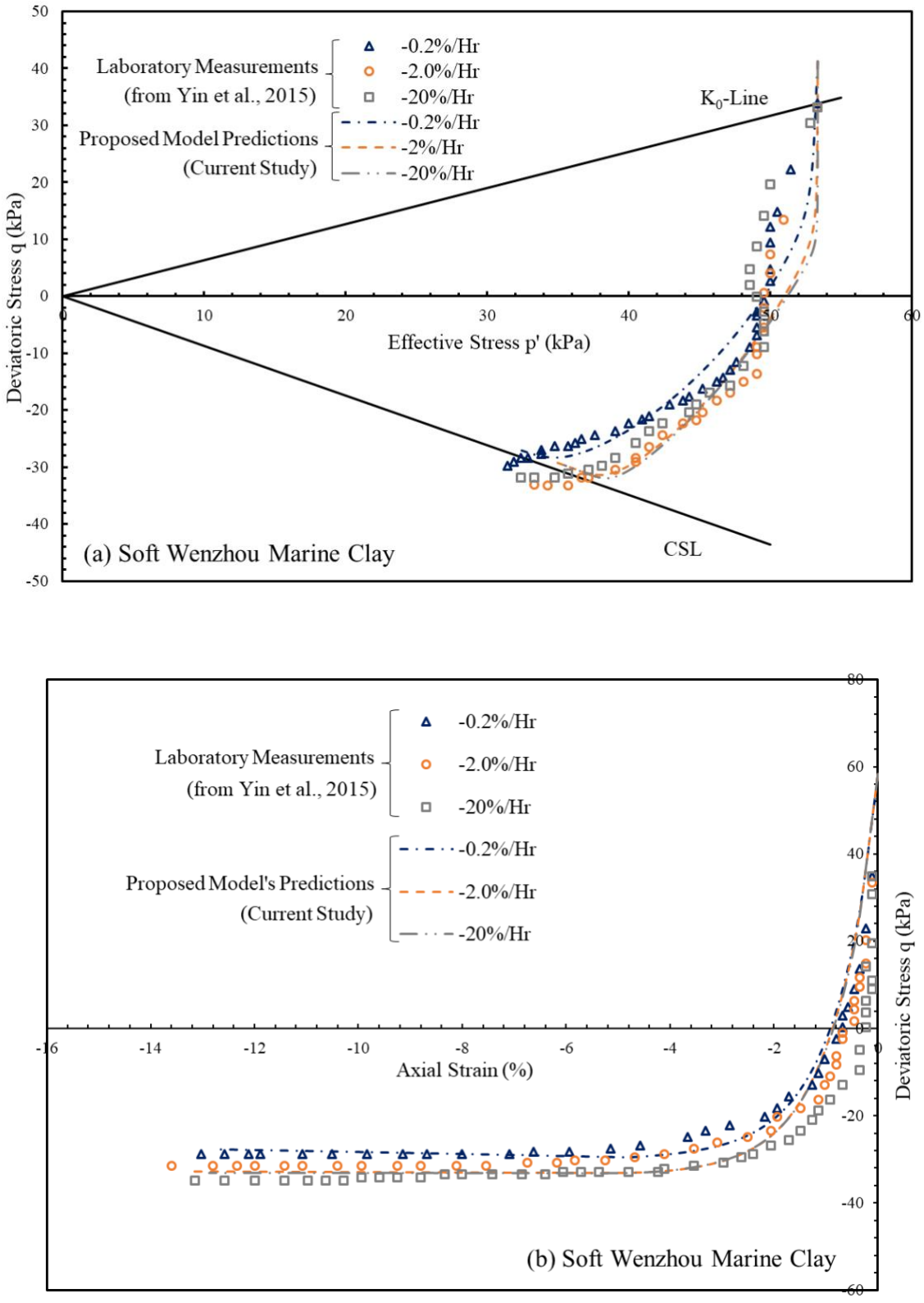

Figure 5.10: Comparison between the measured and predicted results for K0-consolidated undrained triaxial CRS tests at an effective pressure of 150 kPa on soft Wenzhou Marine clay in extension: (a) effective stress paths; and (b) deviatoric stress (q) versus axial strain (ε_a)

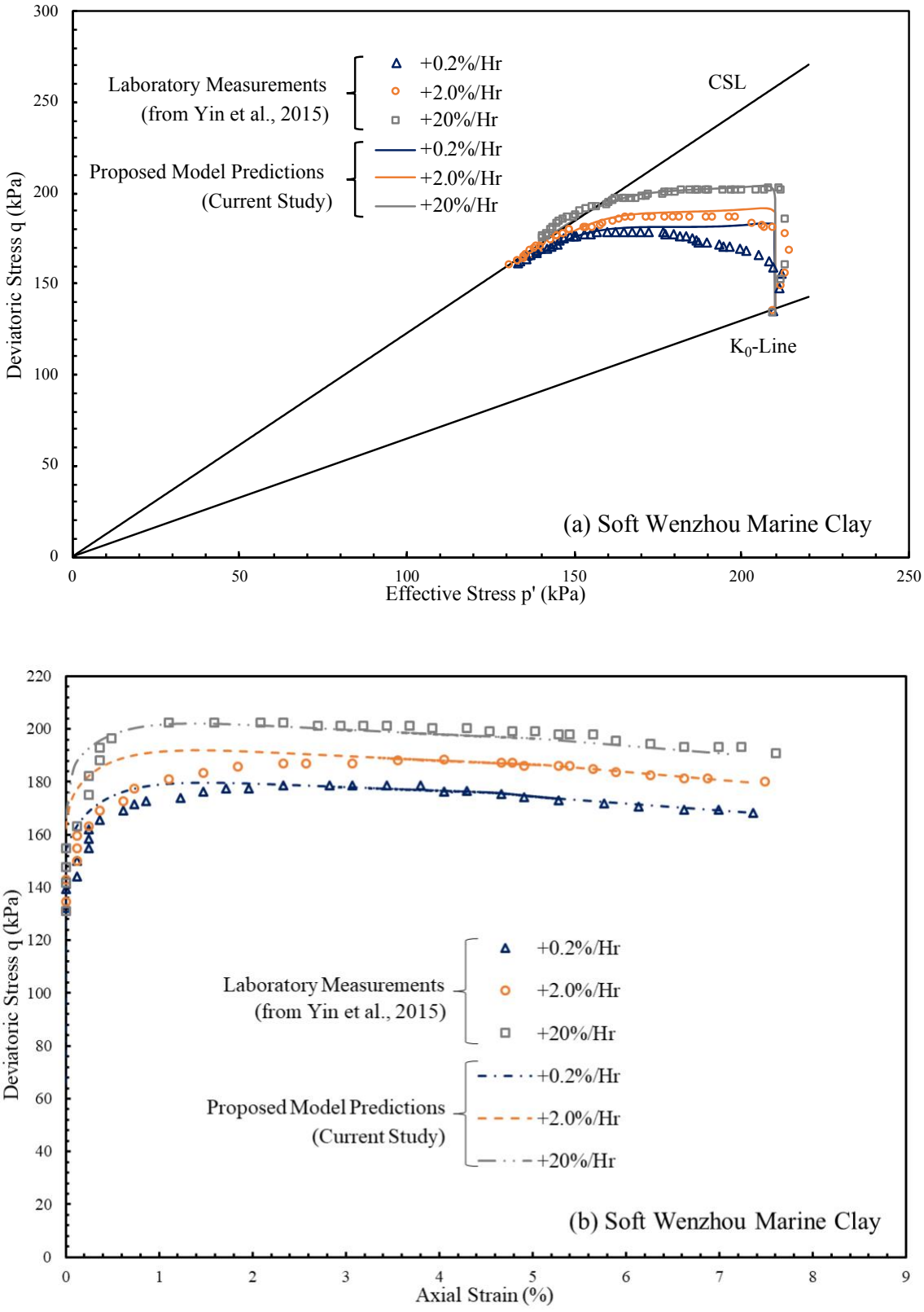

Figure 5.11: Comparison between the measured and predicted results for K0-consolidated undrained triaxial CRS tests at an effective pressure of 300 kPa on soft Wenzhou Marine clay in compression: (a) effective stress paths; and (b) deviatoric stress (q) versus axial strain (ε_a)

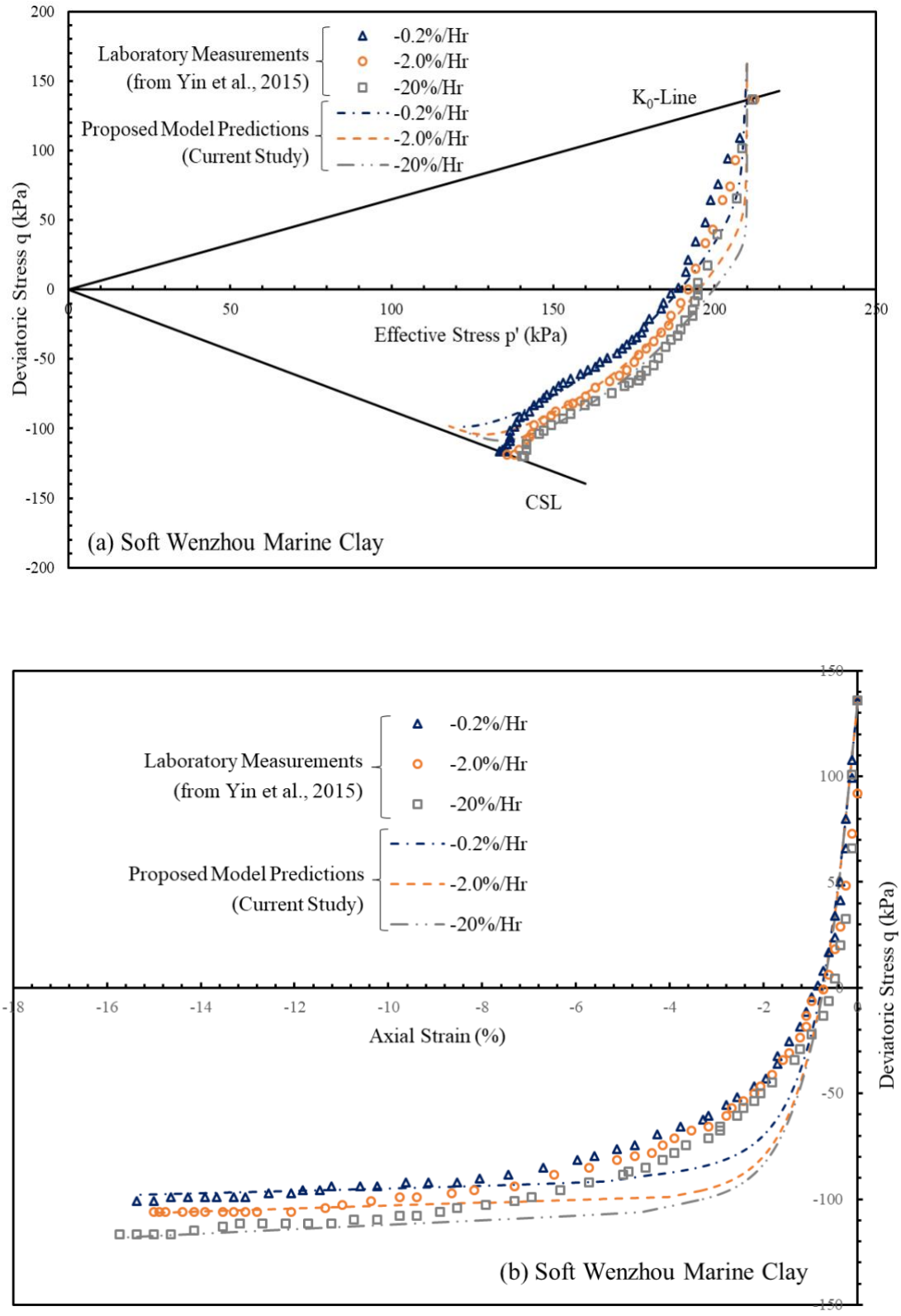

Figure 5.12: Comparison between the measured and predicted results for K0-consolidated undrained triaxial CRS tests at an effective pressure of 300 kPa on soft Wenzhou Marine clay in extension: (a) effective stress paths; and (b) deviatoric stress (q) versus axial strain (ε_a)

Although slight overpredictions can be observed for small strain levels owing to the fact that hysteretic effects are not being considered due to the requirement of additional parameters, the predictions begin to match closely with the measured results for axial strain levels greater than 2%, as shown in Figures 5.8b-5.12b. It can be observed from Figures 5.8b-5.12b that slight discrepancies occur in the predictions of the effective stress paths, particularly in the initial test durations but matches closely towards the experimental observations thereafter until the critical state line is reached. In the compression tests, the extended model is capable of capturing the changes in the deviatoric stresses against the axial strains for all three constant strain rates, apart from the slight deviations observed for 0.2% and 2%/hr tests between 1% and 2.5% of the axial strain levels. Similarly, the predictions related to the relationships between the deviatoric stress and axial strain have aligned with the laboratory data throughout the extension tests, with under-predictions to be observed between 2% and 6% of the axial strain levels. However, the extended model possesses the capability to effectively capture the rate-dependent effects on the changes in deviatoric stresses against the axial strain, highlighting the strain-softening and hardening effects, as overall, a good agreement with a reasonable accuracy is achieved between the laboratory data and the predicted outcomes for both compression and extension tests.

5.6.2 Strain-controlled Undrained Triaxial Loading Tests on Shanghai Soft Clay

This section enlightens further application of the extended calibrated model using the stress-strain behaviour of consolidated undrained triaxial loading tests at constant strain rate on Shanghai natural soft clay, performed by Huang et al. (2011). The natural undisturbed soil samples were extracted at depths of 10m, followed by the isotropic and anisotropic

consolidation under K_0-condition (i.e. $K_0 = 0.6$) using the initial horizontal and vertical reconsolidation stresses, provided in Table 5.5. Accordingly, the application of the extended model employing the corresponding model parameters outlined in Table 5.4 to reproduce the stress-strain behaviour of two undrained compression tests on K_0-consolidated test specimens with two different consolidation pressures of 50 and 100 kPa are elaborated.

Table 5.5: Experimental Conditions for Undrained Triaxial Loading Tests on Shanghai Soft Clay

Test Number	Horizontal Reconsolidation Stress (kPa)	Vertical Reconsolidation Stress (kPa)
CAU-1	41	68.60
CAU-2	81.80	136.4
CAU-3	245	408.3

5.6.2.1 Model Performance

As illustrated in Figures 5.13a and 5.13b, the relationships between the deviatoric stress versus the axial strain, and the behavioural trend for the effective stress paths are credibly captured by the extended model. It is also evident from Figure 5.13b that the extended model accurately captures not only the decrease in effective stress with an increase in axial strain once the effective stress reaches its peak value, i.e. the strain softening behaviour, but also the characteristics of high stiffness observed in natural soft clays. As shown in Figure 5.13a, the extended model successfully reproduces the effective stress paths, which gradually reach their peak strength, followed by approaching a narrow zone in the stress space; thus, demonstrating the application of critical state phenomenon employed in the extended model to conclusively predict the stress-strain behaviour of natural clays at large strains.

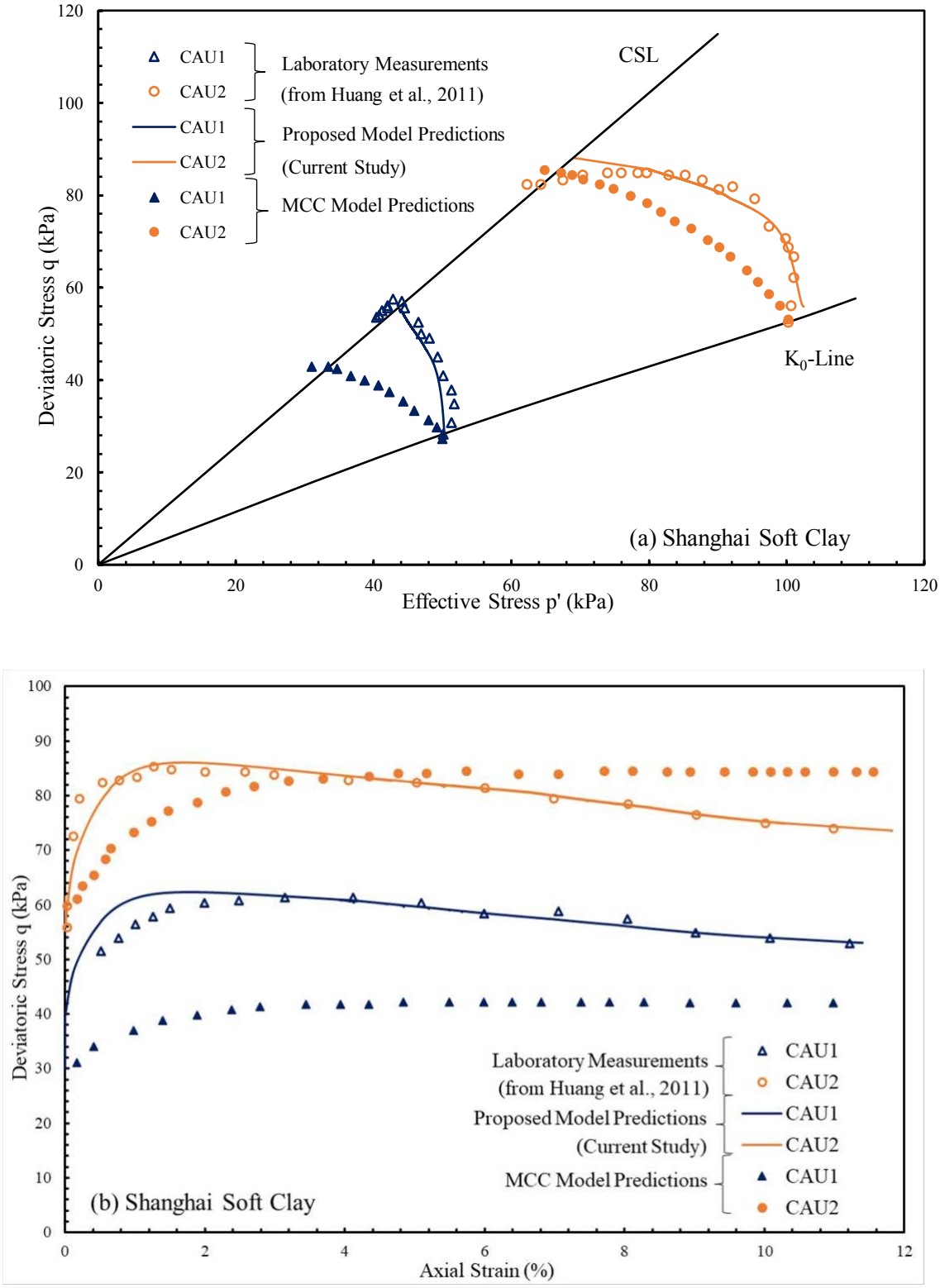

Figure 5.13: Comparison between the measured and predicted results for K0-consolidated undrained triaxial compression tests on Shanghai soft clay: (a) effective stress paths; and (b) deviatoric stress (q) versus axial strain (ε_a)

Moreover, Figure 5.13 displays comparisons between the simulations generated by the extended model and the MCC model for the undrained compression behaviour of Shanghai natural soft clay. In general, the MCC model predictions were less acceptable due to the negligence of the structural effects. Although slight over-predictions of non-linear responses at small strain levels are apparent, this could be rectified with the consideration of hysteretic response, as in Jiang et al. (2012), but rather at the expense of including additional model parameters, which was beyond the scope of the extended model. However, the predictions start to align with the laboratory results for axial strain levels higher than 2%; thus, highlighting the proposed model's capability in capturing the strain softening behaviour observed in natural soft soils.

5.7 Application of the Extended Model to Undrained Triaxial Shearing Tests Using Step-changed Strain Rates

In this section, the necessary model parameters related to K_0-consolidated HKMD clay, which were determined according to the descriptions provided in Section 5.2, are provided in the following table.

Table 5.6: Values of Model Parameters for K_0-consolidated HKMD Clay

Model Properties	Soil Types
	Hong Kong Marine Deposit (HKMD) Clay
λ^*	0.1988
κ^*	0.04712
μ	0.00637
K_0	0.4851
M_c(Compression)	1.2431
M_e (Extension)	0.879
e_0	1.506266
υ	0.3
α (Compression)	0.95 – 1
α (Extension)	1
γ (Compression)	0.65 – 0.7
γ (Extension)	0.95 – 1
m	1
β_0	0.6203
D_β	0.1348
C_β	$10/\lambda^* - 15/\lambda^*$

5.7.1 K_0-consolidated Undrained Triaxial Shearing Tests on HKMD Clay

The capability of the extended model is further validated against the laboratory measurements outlined by Zhou et al. (2005) on the K_0-consolidation and undrained triaxial shearing tests performed at various step-changed strain rates with unloading and reloading on HKMD clay. The soil specimens were saturated using a cell pressure up to 205 kPa and back-pressure up to 200 kPa by following the BS 1377 (BS 1990). Once the specimens were properly

saturated, the consolidation of each soil specimen was performed under an initial isotropic stress state with a small effective confining pressure of 10 kPa under K_0-consolidation, i.e. zero radial strain, until three final effective confining pressures of 50, 150, 400 kPa have been reached in the corresponding tests. After K_0-consolidation, the cell pressure was held constant, which was followed by shearing the test specimens at a step-changed strain rate, in a specified sequence from +2%/hr to +0.2%, +20%, -2% (unloading), and +2%/hr (reloading) for all the compression tests; and from -2%/hr to -0.2%, -20%, +2% (unloading), and -2%/hr (reloading) for all the extension tests. The initial inclination of the critical surface is estimated using the effective frictional angle ϕ', as outlined in the previous section.

5.7.1.1 Model Performance

The comparisons between the laboratory measurements and the predicted simulations for all the aforementioned step-changed strain rates for both triaxial compression and extension tests are demonstrated in the following Figures 5.14 - 5.19. The relationships for the deviatoric stress versus the axial strain and the excess pore water pressure versus the axial strain are illustrated and analysed. It is evident from Figures 5.14a-5.19a that the extended model successfully captures the strain rate effects in both compression and extension, particularly before +2%/hr (unloading), and -2%/hr (reloading) strain rates. Moreover, the obvious gradual decrease in deviatoric stress and pore-water pressure against high axial strain rate of 20%/hr, particularly in the extension tests, are credibly predicted. However, discrepancies are observed in simulating the unload-reload loop, since the hysteretic effects are not considered due to the requirement of additional parameters, as previously been pointed out.

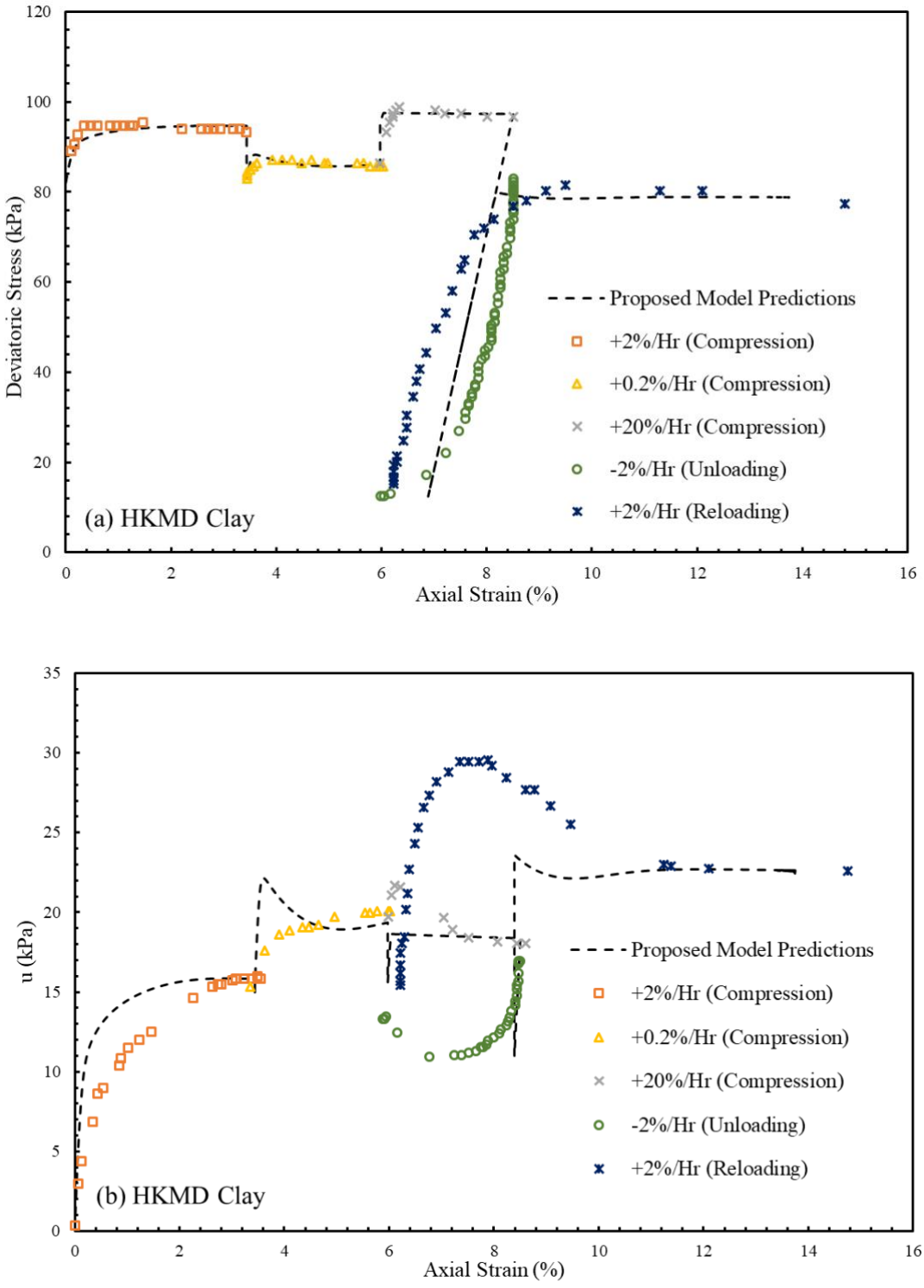

Figure 5.14: Comparison between the measured and predicted results for K0-consolidated step-changed axial strain compression test with unloading/reloading at effective pressure of 50kPa on HKMD clay: (a) deviatoric stress (q) versus axial strain (ε_a); (b) axial strain (ε_a) versus pore-water pressure (u)

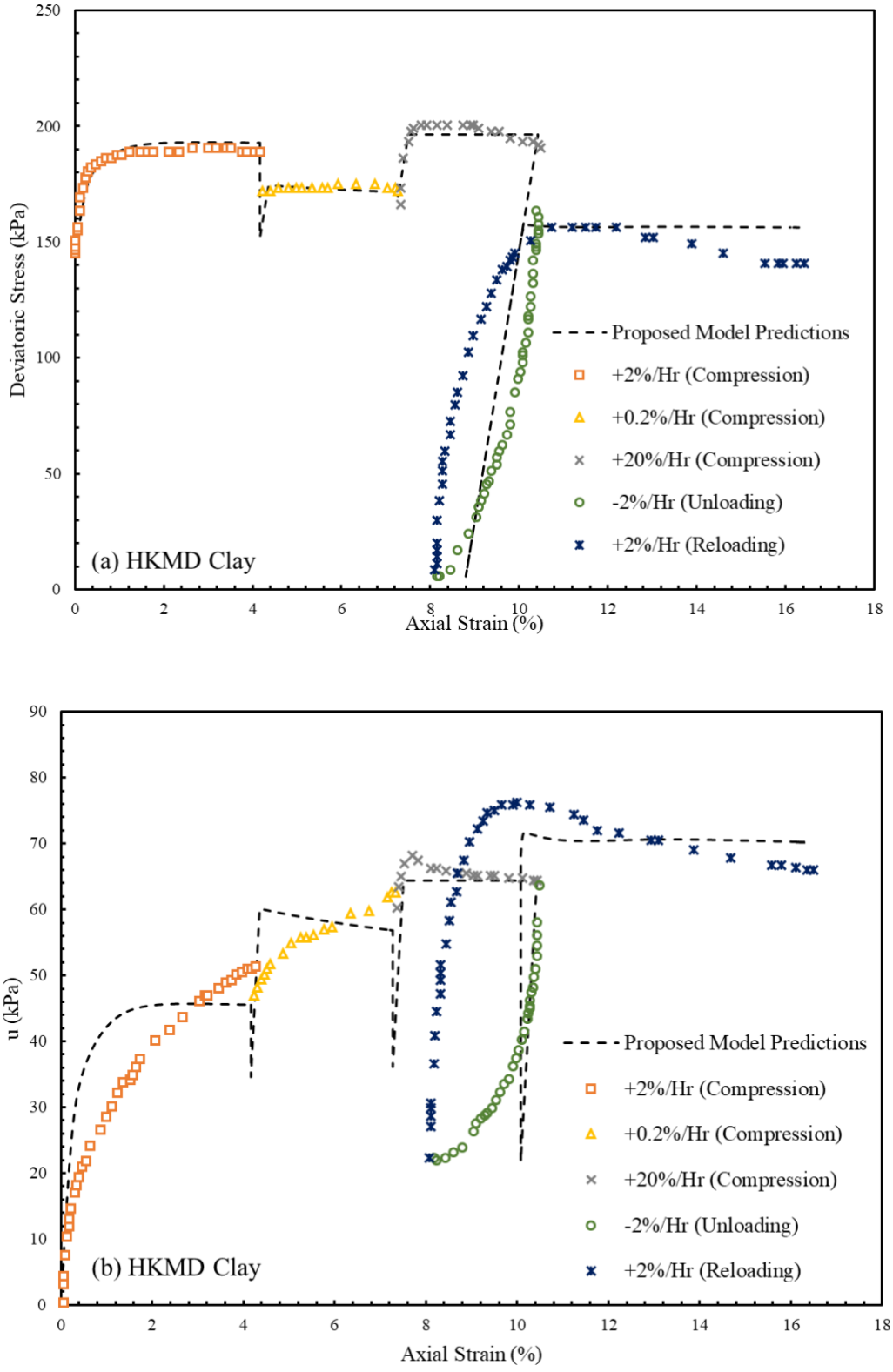

Figure 5.15: Comparison between the measured and predicted results for K0-consolidated step-changed axial strain compression test with unloading/reloading at effective pressure of 150kPa on HKMD clay: (a) deviatoric stress (q) versus axial strain (ε_a); (b) axial strain (ε_a) versus pore-water pressure (u)

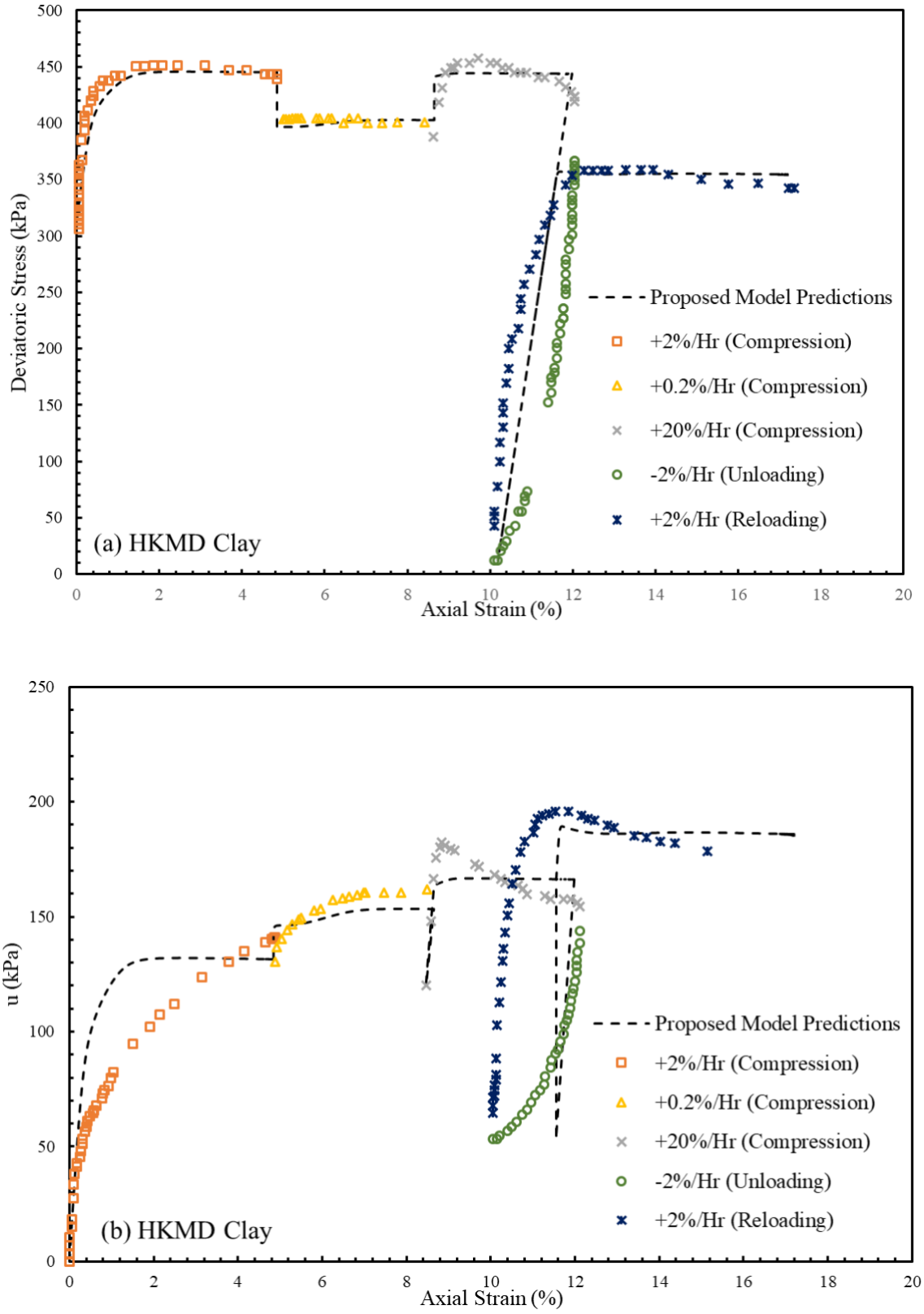

Figure 5.16: Comparison between the measured and predicted results for K0-consolidated step-changed axial strain compression test with unloading/reloading at effective pressure of 400kPa on HKMD clay: (a) deviatoric stress (q) versus axial strain (ε_a); (b) axial strain (ε_a) versus pore-water pressure (u)

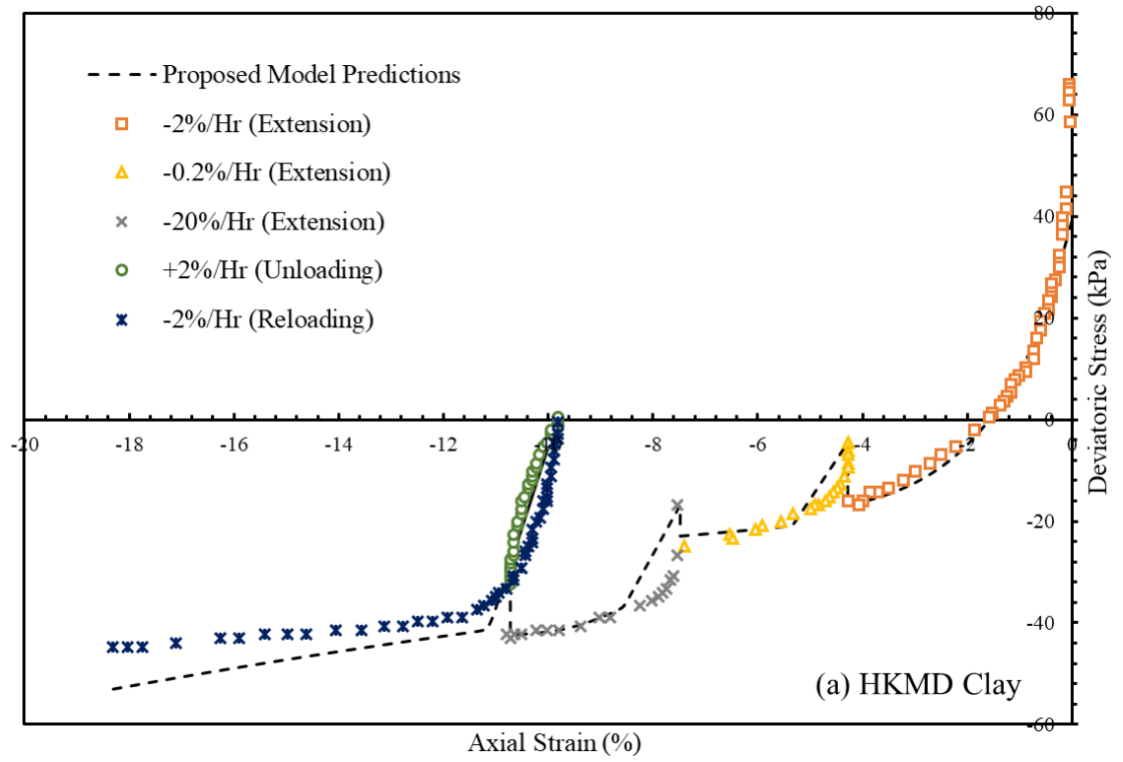

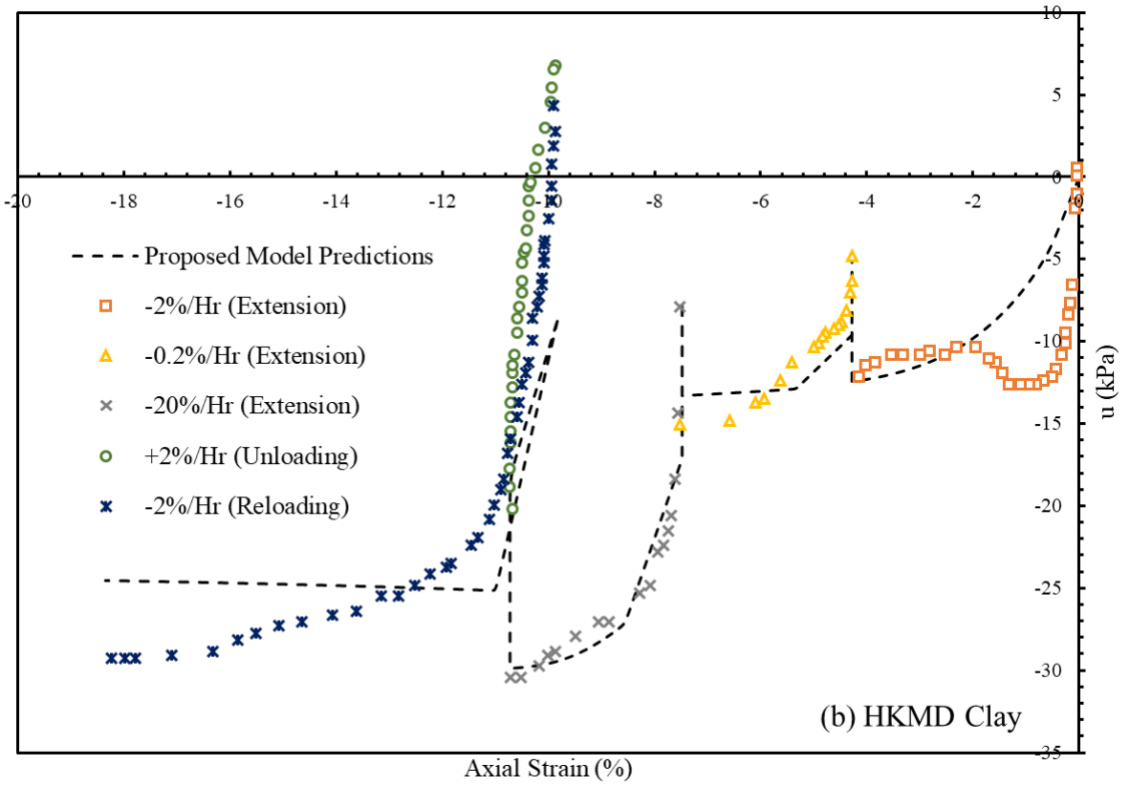

Figure 5.17: Comparison between the measured and predicted results for K0-consolidated step-changed axial strain extension test with unloading/reloading at effective pressure of 50kPa on HKMD clay: (a) deviatoric stress (q) versus axial strain (ε_a); (b) axial strain (ε_a) versus pore-water pressure (u)

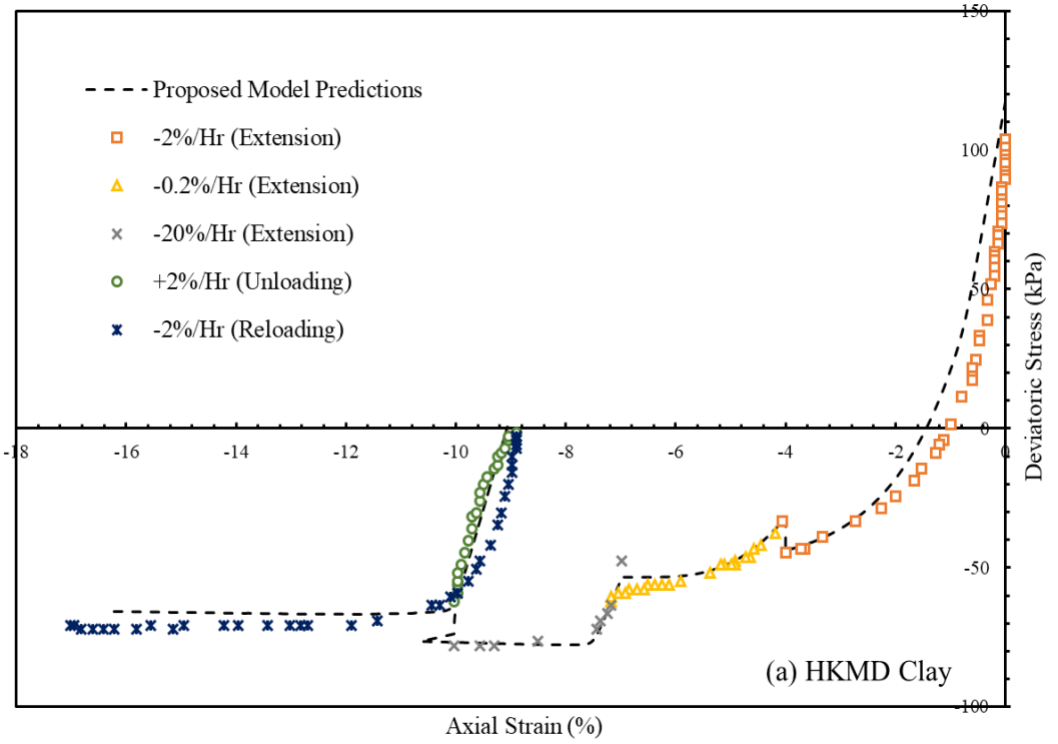

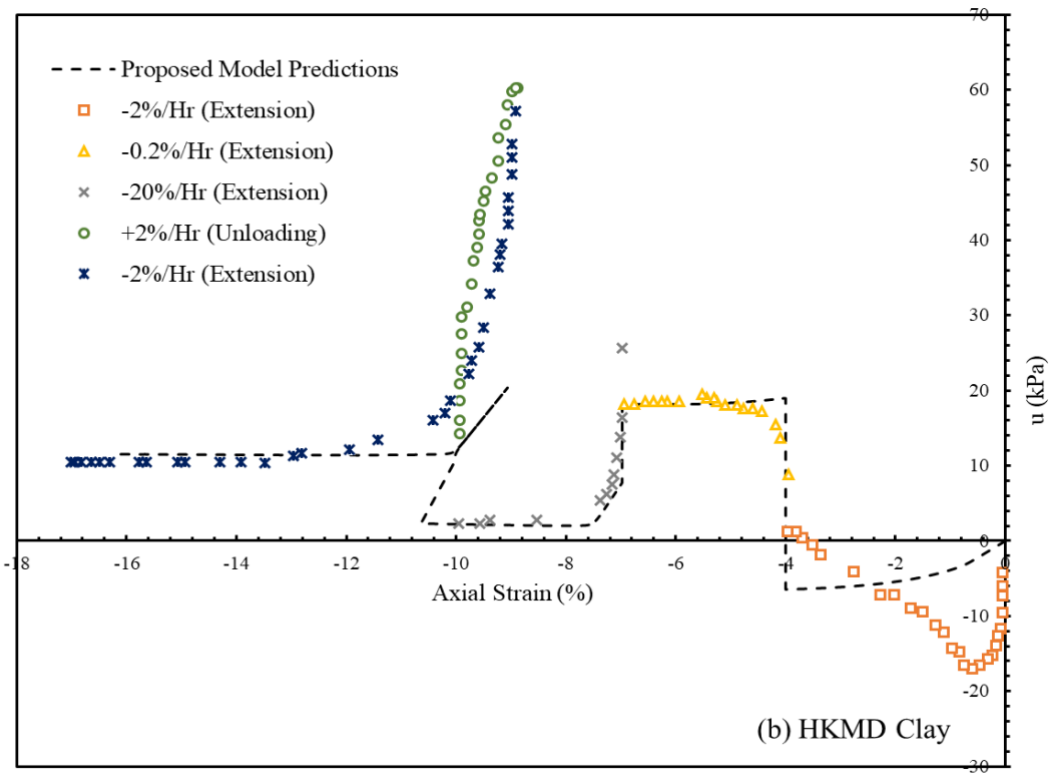

Figure 5.18: Comparison between the measured and predicted results for K0-consolidated step-changed axial strain extension test with unloading/reloading at effective pressure of 150kPa on HKMD clay: (a) deviatoric stress (q) versus axial strain (ε_a); (b) axial strain (ε_a) versus pore-water pressure (u)

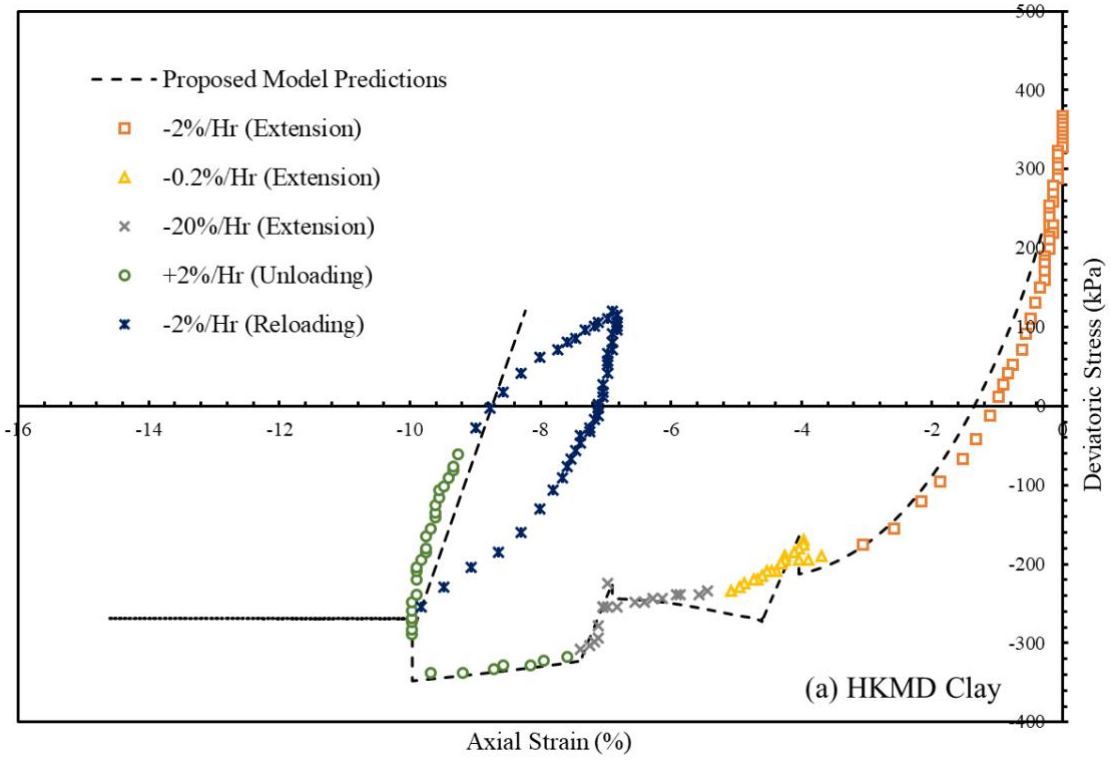

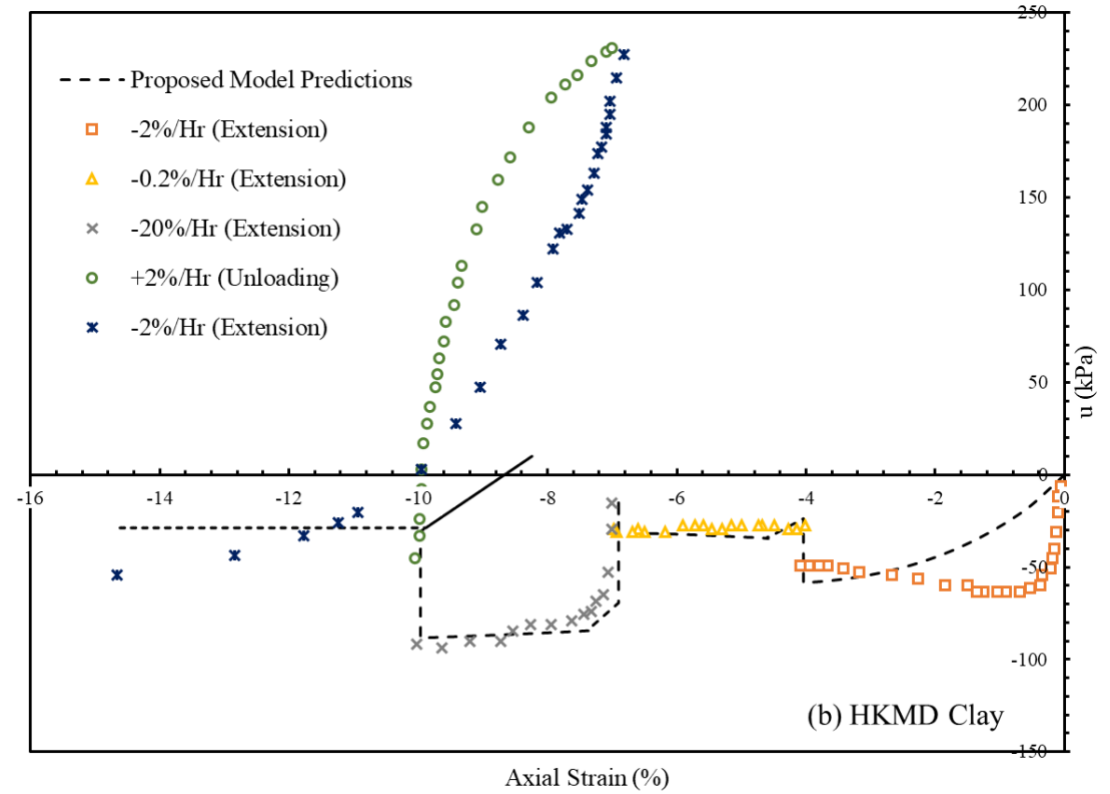

Figure 5.19: Comparison between the measured and predicted results for K0-consolidated step-changed axial strain extension test with unloading/reloading at effective pressure of 400kPa on HKMD clay: (a) deviatoric stress (q) versus axial strain (ε_a); (b) axial strain (ε_a) versus pore-water pressure (u)

As emphasised in Zhou et al. (2005), there were a few issues encountered during the tests, in which the employed triaxial system could not automatically run a following phase of test with a different loading condition after finishing the previous test phase, in the step-changed experiments. Since a manual reset was compulsory to run the next test phase in the employed controlling computer program and electronic hardware, certain unforeseen loading disturbances could likely affect the stress-strain behaviour and the pore-water pressure dissipation response of the testing specimens. Due to these negative influences on the laboratory observations, it is to be considered that there is, in general, a reasonably acceptable agreement between the proposed model predictions and the laboratory measurements for both compression and extension tests, provided that the testing procedure was also rather sophisticated.

5.8 Summary and Observations

In this chapter, the applications of the proposed H-Creep model and its extended counterpart are extensively elaborated to investigate the predictive performance and capabilities towards a variety of laboratory experiments. The model parameters required for the numerical implementations have been summarised, along with the details on their corresponding determination procedure. Taking into consideration of the illustrations and demonstrations, the following observations are concluded from this chapter:

(i) the proposed H-Creep model contains a total of 10 parameters, whereas the extended model consists of 11 parameters in total, with the addition of one parameter related to 'fabric' arrangements, for which the determination of all the model parameters is relatively straightforward;

(ii) the proposed model demonstrates its versatile capabilities in predicting time- and strain rate- dependent behaviour of soils under different loading and drainage conditions within a single framework with tight standardised theoretical structure;

(iii) the extended model is capable and competent to capture the loading-rate or strain-rate dependent stress-strain behaviour, highlighting the strain-softening/hardening effects, observed in natural soft soils and assessed against, but not limited to, undrained triaxial shearing tests using step-changed strain rates with stress-relaxation and consolidated strain-controlled undrained triaxial compression and extension tests using various strain rates, reported in the existing literature;

(iv) Although some discrepancies can be noticeable due to a few limitations, the extended model signified its multi-faceted capabilities and boundless potential in predicting time-dependency of undrained strength in natural soils subjected to various loading and drainage conditions within hyper-viscoplastic foundation with standardised theoretical structure.

On the other hand, the following limitations and recommendations are to be bestowed based on the observations deduced from this chapter:

(i) The proposed model might not be applicable for modelling scenarios, in which modelling stress-strain behaviour of soils under cyclic loading conditions, entailing hysteretic effects, and smooth transition from the elastic to the elasto-viscoplastic behaviour, is of paramount necessity.

(ii) If interpretation of more localised effects and dissipation of excess pore-water pressure through drainage boundaries during the testing would be of considerable importance, finite element approach could be implemented to simulate the laboratory observations by adopting the proposed model.

(iii) Not only the relative difficulty of EVP models could be resolved, but also the predictions of the proposed model might be enhanced if more meticulous numerical optimisation techniques (e.g. TRRLS algorithm in Le et al. (2016)) is adopted for the emphasis on the importance of employing non-linear creep formulation.

CHAPTER 6

CONCLUSIONS AND RECOMMENDATIONS

6.1 Summary

The fundamental intention of this study was not to propose a new constitutive soil model right from the very beginning, but rather to study the existing constitutive models and identify the associated drawbacks and requirements in order to remove those limitations by building upon a reliable foundation and consistent framework. Accordingly, the major objective of this study is to develop a series of mixed hardening rate-dependent constitutive soil models within a single framework with tight standardised theoretical structure based on the fundamental laws of thermodynamics to simulate time- and strain rate- dependent behaviour of soft soils under different loading and drainage conditions, together with the intention to capture the variation in the shapes of the yield loci by pursuing non-associated flow rules and accounting for isotropic and kinematic hardening effects. The most distinctive characteristic of the proposed model is their compliance with the physical phenomena, such as the conservation of mass and energy and the fundamental laws of thermodynamics, whilst circumventing the drawbacks of having to introduce a substantial number of assumptions. This is in stark contrast to most of the existing soil constitutive models, which often require a considerable number of 'ad hoc' assumptions without being related to the physical phenomena of real soils.

- Chapter 1 has outlined the introduction to the current study, with the emphasis on the importance of modelling time- and rate-dependent behaviour of geomaterials, particularly for the long-term settlement deformations. This has been followed by the problem statement, highlighting the fact that the constitutive soil models must comply with certain principles or axioms that govern the physical phenomena, such as the fundamental laws of thermodynamics and conservation of mass and energy. According to Houlsby and Puzrin (2006),

"The constitutive models that do not comply with the laws of thermodynamics may not be used with any confidence to predict the material behaviour."

Based on the strong theoretical foundation, the objectives and scope of the current study have been presented.

- Chapter 2 has provided a comprehensive literature review on the importance of modelling time- and rate- dependent stress-strain behaviour, including creep, stress relaxation and strain-rate dependency, of geomaterials, particularly soils. Moreover, the challenges associated with the development of constitutive soil models have been discussed, along with the study and investigation on the number of existing advanced constitutive soil modelling frameworks, with regards to the emphasis on the problem statement of the current study.
- In Chapter 3, the underlying principles of the Hyperplasticity theory, signifying its essential components and requisite foundation towards the development of a new Hyper-viscoplasticity theory have been elaborated. Moreover, the fundamental laws of thermodynamics have been discussed. This has been accompanied by the practical summary of rate-independent hyperplasticity approach, from which the rate-dependent hyperplasticity framework has been built upon using a constructive and consistent approach and thus, highlighting the rigidity, compactness and reliability acting as a strong foundation for the development of hyper-viscoplastic soil models in the current study.
- Chapter 4 has presented the development of a unique, yet simple mixed hardening hyper-viscoplasticity (H-Creep) model for the simulation of rate-dependent stress-strain behaviour of soils incorporating non-linear creep rate, while considering the variations in the shapes of the yield loci by pursuing non-associated flow behaviour, with the incorporation of important hardening effects. The important characteristics include, but not limited to, the encapsulation of the entire constitutive viscoplastic stress-strain response

within two thermodynamic potential functions, the derivation of critical surface and non-associated flow rule as necessary consequences of the viscoplastic dissipation potential function, whilst the latter is derived as a natural outcome if the postulated viscoplastic dissipation potential function is stress-dependent and the postulation of novel non-linear creep formulation acknowledging the experimental evidence of residual void ratio not being equal to zero as part of the creep strain limit. Moreover, the logical and rational extension towards the proposed H-Creep model has been presented by addressing a few of the observed limitations, particularly the need to consider for the arrangement of particles and the bonding between the particles during the time-dependent delayed deformation, which is considerably pronounced in natural soft soils. The extended model retains all the important characteristics of the H-Creep model, whilst augmenting with the enhanced capabilities in capturing the variations in the fundamental shapes of critical surface with a β-line defining the inclination of the non-symmetrical elliptical critical surface in the p'-q plane, whilst describing the additional rotational effects to the kinematic hardening behaviour and strain-softening/hardening effects of soft soils.

- In Chapter 5, the summary of all the model parameters required for the proposed and extended models has been provided, along with the description on the associated determination procedure. It has been documented that the proposed model is applicable to qualitatively and quantitatively capture the time- and rate- dependent stress-strain responses related to Osaka clay, Hong Kong marine deposit (HKMD) clay, Haney clay and Kaolin and Bentonite mixture. Furthermore, it has been demonstrated that the extended model is capable of predicting the stress-strain behaviour of K_0-consolidated soft Wenzhou Marine clay, Shanghai soft clay and Hong Kong marine deposit (HKMD) clay.

The proposed H-Creep model, along with its extended component, offer significant improvements on the predictive capabilities of the MCC model, and considerable

enhancements on the relatively recent EVP models developed by Yin and Zhu (1999) and Islam (2014).

6.2 Conclusions

During the past few decades, there have been a large number of constitutive soil models developed based on a variety of approaches and concepts and often, each constitutive model claims its advantages and superiority compared to the other existing models. However, the reality is that there is still no explicit model that has yet been acknowledged in possessing the capability to fully describe the behaviour of soil subjected to all possible conditions under general construction procedures. Moreover, it is important to emphasise on the previously highlighted point that all the constitutive models must obey certain principles or axioms that govern the physical phenomena of materials, such as the conservation of mass and energy and the fundamental laws of thermodynamics and so on. Based on the comprehensive literature review on the constitutive soil models, mainly related to the modelling of time- and rate-dependent behaviour of soils, many existing variants of plasticity approaches are yet flexible enough to violate the fundamental laws of thermodynamics, as they often have had to compensate with arbitrary assumptions without being related to physical aspects of the soil behaviour. In order to minimise the number of 'ad hoc' assumptions and with the need to comply with certain physical principles, the current study has been solely focused on the hyperplasticity approach, in which the extraction of plasticity theory is based on the fundamental laws of thermodynamics. The important feature of this approach is the encapsulation of the entire constitutive behaviour, entailing the yield condition and flow rule, along with the isotropic and kinematic hardening laws, as well as the elasticity law, within two thermodynamic potential functions, i.e. free-energy and dissipation potential functions.

Since this framework provides a rigorous, compact and consistent standardised procedure with the considerable use of potential functions and internal variables related to the physical phenomena of materials, a unique, yet simple and versatile constitutive soil model is developed based on rate-dependent hyperplasticity theory for the simulation of non-linear creep behaviour, along with the prediction of both isotropic and kinematic hardening behaviour of soils. Besides, the non-associated flow rule is derived as a necessary consequence of dissipation potential functions, explicitly dependent on the actual stress components. Moreover, there is no need to introduce an arbitrary plastic flow potential function, compared to the conventional plasticity models in which it is usual to express the plastic strain increments in terms of a plastic potential function to instigate the non-associated flow rule. Therefore, the derivation of non-associated flow rule as a natural outcome from the hyperplastic approach is demonstrated as more general, in which the transition between the yield surface and the flow rule is more seamless and coherent. Furthermore, the inclusion of viscoplastic strains in the inelastic free-energy function, by explicitly acknowledging the fact that not all the plastic work is dissipated, but some portion is stored, differentiates the proposed model from most of the existing traditional plasticity models, which generally assumes that the energy associated with inelastic strains to be irrecoverable. The additional viscoplastic free-energy function results in the 'shift' stress and the 'dissipative' stress, within the context of hyperplasticity, is used to describe the translational, kinematic hardening and the isotropic hardening or softening behaviour, respectively. It has also been demonstrated that the shift and dissipative stress components share an important role, in tandem, for the formulation of mixed hardening constitutive soil models of geomaterials. In addition, a novel non-linear creep formulation acknowledging the experimental observation of residual void ratio not being exactly equal to zero, with regards to the creep strain limit, is postulated and incorporated into the time-dependent viscosity scaling function employed within the dissipation potential function. On

the other hand, the required model parameters have been classified into three major categories, provided with the description on the determination procedure. Using the calibrated model parameters, it has been demonstrated that the presented model possesses the capability to predict the laboratory measurements from the consolidated and overconsolidated undrained strain-controlled and stress-controlled triaxial compression and extension tests, undrained triaxial shearing tests with stress-relaxation and constant rate of strain tests. Overall, the model's predictions are in satisfactory agreement, which is evident from the provided figures, capturing the stress- and strain- rate dependent behaviour of soils, including Osaka clay, HKMD clay, Haney clay and Kaolin and Bentonite mixture, while reinforcing the 'narrow region' phenomena by demonstrating that the critical state concepts are applicable to natural soft clays even at large strain levels. Moreover, comparisons are provided for the predictions of the proposed model in this current study and the predictions produced by the recent EVP model developed by Islam (2014) and the refined EVP model developed by Yin and Zhu (1999), exhibiting that the presented H-Creep model offers improved predictions, highlighting the reliability of the model in modelling time and strain-rate effects under different loading and drainage conditions.

Due to the advantages of having a strong theoretical foundation with rigorous, compact and consistent procedure, this allows for the resulting models to be developed within a single framework enabling efficient, yet convenient comparisons for further improvements. Since the composition of clayey soils, such as the irregularity of the clay platelets, one-dimensional consolidation and deposition procedures and so on, has a considerable influence on the associated stress-strain behaviour, it has become increasingly important to consider the effects of structure in soils, particularly for natural soft soils, due to the structural arrangement and the interparticle bonding among the particles. The consequence of neglecting such structural effects could result in rather inaccurate predictions of the stress-strain response of natural soft

clays, especially when they are subjected to different loading conditions, as have been pointed out in Zhou et al. (2005), Karstunen and Koskinen (2008) and Rezania et al. (2016). Consequently, there has been a substantial interest in attempting to merge 'fabric' effects and time-dependent delayed deformation in predicting the viscoplastic stress-strain response of soft clays, as an extension towards isotropic creep models (e.g. Zhou et al., 2005; Leoni et al.,2008), the MCC model with structured Cam-clay models (e.g. Horpibulsuk et al., 2010; Suebsuk et al., 2010), the traditional bounding surface plasticity models (e.g. Gajo and Muir, 2001; Dafalias et al., 2006; Yao et al., 2009) and the existing EVP models (e.g. Sivasithamparam et al., 2015; Jiang et al., 2017; Castro et al., 2018). Although the aforementioned approaches have paved the way to account for the modelling of structural effects for time-dependent deformation behaviour, most of the existing EVP models have not been constructed based on a strong thermodynamic foundation, but rather from an empirical or semi-empirical approach and thus, they are flexible enough to break the fundamental physical principles related to the real soil behaviour. Therefore, it is logical and rational for the presented H-Creep model to be extended based on the hyper-viscoplasticity concept by incorporating the 'fabric' effects, accounting for the arrangement of particles and the bonding between the particles, particularly observed in soft natural soils when subjected to different loading conditions.

The extended study highlights the emphasis on the strain-softening behaviour for certain natural soils and more prominently, the power and capability of working within the relatively modern hyperplasticity approach with a tight theoretical structure. As previously emphasised, the comprehensive incorporation of structural effects requires a sizeable number of additional model parameters, which makes it highly impractical, the extended model has been intended to minimise the number of required parameters, whilst having careful consideration on maintaining the acceptable level of accuracy in simulating the corresponding time- and rate-dependent behaviour of natural soft soils. Accordingly, the viscoplastic free-energy and

dissipation potential functions have been extended, in which not only the former incorporates the dependence on both volumetric and deviatoric viscoplastic strains, but also the fabric coupling parameter is introduced into both potential functions. The extended viscoplastic free-energy function results in the modified shift stress, supplementing the kinematic hardening behaviour with rotational effects by incorporating rotational kinematic evolution based on the discussions provided in Sivasithamparam and Castro (2016) and Zhang (2018), which is important in the retention of a unique asymptotic critical state surface for stress paths that also involve unloading. Hence, the extended model has been intended to capture the loading-rate or strain-rate dependent behaviour of soils, while still considering the variations in the fundamental shapes of critical surface with a β-line defining the inclination of the non-symmetrical elliptical critical surface in the p'-q plane, along with rotational, kinematic hardening effects and non-associated behaviour, derived as a natural consequence of this approach. The extended model consists of 11 parameters in total, with only one additional important parameter compared to its original counterpart, and thus, maintaining a relatively straightforward parameter determining procedure, considering the fact that the incorporation of fabric effects generally require a substantial number of additional model parameters, as highlighted above. Although some discrepancies could be observed from the comparisons between the model predictions and the experimental data on the time-dependent stress-strain behaviour of K_0-consolidated soft Wenzhou Marine clay, Shanghai soft clay and Hong Kong marine deposit (HKMD) clay, the extended model has exhibited its wide range of capabilities and boundless potential in predicting the rather complicated creep behaviour of natural soft soils under a variety of loading conditions and different drainage circumstances.

One of the prime features of the proposed model and its extended counterpart, which is of paramount importance, is the hierarchical nature, in which a viscoplastic version of the MCC model is recovered when the coupling factor β is set to zero and the value of parameters, α and

γ, are equal to one, whilst in combination with a sufficiently small creep parameter could eventually result in the universally acclaimed elastoplastic MCC model. As previously emphasised, the non-associated flow rule is naturally derived as a necessary consequence from the stress-inclusive dissipation potential function, which further promotes the versatility and usefulness of the current study in predicting the behaviour of a wider class of soils.

6.3 Recommendations for Future Studies

With the robustness of the theoretical foundation, the proposed model is an ideal dependable basis for further research in the following directions:

- The extensions towards the free-energy and dissipation potential functions, with the incorporation of 'breakage mechanics' into the proposed constitutive model, as recent studies have also suggested that the viscoplastic deformation of granular geomaterials may be influenced by numerous microscopic processes at low and/or high pressures (Tatsuoka et al., 2002; 2008) and thus, the deformation is controlled by the fragility of the grains resulting in the delayed breakage of individual particles in the rearrangement of the skeleton over time, as well as the rates of creep and stress relaxation (Karimpour & Lade, 2010). As a result, the understanding of such phenomena has led the way to study not only the detailed measurements of evolving particle size distribution during creep and relaxation tests (Leung et al., 1997; Lade et al., 2010) but also the micromechanical interpretations of environment-dependent creep based on the theory of crack growth kinetics (Oldecop and Alonso, 2001; 2007). Based on Hyperplasticity framework, the entire constitutive behaviour that undergoes plasticity and damage can be expressed through the definition of two thermodynamic potentials. This, again, ensures consistency with the fundamental laws of thermodynamics.

- The examination on the feasibility of a direct link between the evolving material fabric considered in the proposed study and the degree of anisotropy could also be conducted, particularly if it would be possible to use imaging techniques to identify and trace the movements of the grains and platelets throughout the loading procedure. This could offer improved relationships between the physical phenomena of geomaterials, especially soils, for instance, the liquid and plastic limits, and the numerical models of macroscopic behaviour of soils, which in turn serving as a point of departure on the development of continuum constitutive models based on micro-mechanical fabric interaction, rather than on an abstract representation of the behaviour of geomaterials.
- If the analyses of more localised effects and in-situ conditions, in which the evaluation of the model against boundary value problems is critical, the proposed models in this study can be adopted as a dependable basis for the implementation of final element approach.
- Numerical applications could also be implemented using the commercially available software packages, such as FLAC, ABAQUS and the developed constitutive codes in MATLAB, for simulating the field case studies to make comparisons with the corresponding undertaken measurements for further investigation of the performance and capabilities of the proposed model and its extended counterpart.
- The simulations would be enhanced if more rigorous numerical optimisation techniques, such as the trust-region reflective least square (TRRLS) algorithm applied in Le et al. (2016), are performed, which would not only augment the importance of the postulated non-linear creep formulation but also overcome the relative difficulty of elastic-vsicoplastic (EVP) models in determining the non-linear creep parameters.

REFERENCES

Aboshi, H., 1973. An experimental investigation on the similitude in the one-dimensional consolidation of a soft clay including the secondary creep settlement. *Proc. 8th ICSMFE*, Volume 4, pp. 88-93.

Abu Al-Rub, R. K. & Darabi, M. K., 2012. A thermodynamic framework for constitutive modeling of time- and rate-dependent materials. Part I: Theory. *International Journal of Plasticity,* Volume 34, pp. 61-92.

Adachi, T. & Oka, F., 1982. Constitutive equations for normally consolidated clay based on elasto-viscoplasticity. *Soils and Foundations,* 22(4), pp. 57-70.

Adachi, T. et al., 1995. Stress-strain behaviour and yielding characteristics of Eastern Osaka clay. *Soil and Foundation,* 35(3), pp. 1-13.

Adachi, T. & Okano, M., 1974. A constitutive equation for normally consolidated clay. *Soils and Foundations,* Volume 14, pp. 55-73.

Aldo, M., 2015. *A non-linear viscoplastic double yield surface constitutive model for geologic materials.* Trento: Università Degli Studi Di Trento.

Al-Shamrani, M. A. & Sture, S., 1998. A time-dependent bounding surface model for anisotropic cohesive soils. *Soils and Foundations,* 38(1), pp. 61-76.

Al-Tabbaa, A. & Wood, D. M., 1989. An experimentally based 'bubble' model for clay. *Numerical models in geomechanics,* Volume NUMOG III, pp. 91-99.

Atkinson, J. H., Richardson, D. & Stallebrass, S. E., 1990. Effect of recent stress history on stiffness of overconsolidated soil. *Geotechnique,* Volume 40, pp. 531-540.

Augustesen, A., Liingaard, M. & Lade, P. V., 2004. Evaluation of time-dependent behaviour of soils. *International Journal of Geomechanics,* 4(3), pp. 137-156.

Aung, Y., Khabbaz, H. & Fatahi, B., 2016. *Review on Thermo-mechanical Approach in the Modelling of Geo-materials Incorporating Non-Associated Flow Rules.* Portugal, Elsevier, pp. 331-338.

Azari, B., Fatahi, B. & Khabbaz, H., 2016. Assessment of the elastic-viscoplastic behaviour of soft soils improved with vertical drains capturing reduced shear strength of a disturbed zone. *International Journal of Geomechanics,* 16(1), p. B4014001.

Banerjee, P. K., Kumbhojkar, A. S. & Yousif, N. B., 1988. Finite element analysis of the stability of a vertical cut using an anisotropic soil model. *Canadian Geotechnical Journal,* Volume 25, pp. 119-127.

Barden, L., 1965. Consolidation of clay with non-linear viscosity. *Geotechnique,* 15(4), pp. 345-362.

Benaarbia, A., Rouse, J. P. & Sun, W., 2018. A thermodynamically-based viscoelastic-viscoplastic model for the high temperature cyclic behaviour of 9-12% Cr steels. *International Journal of Plasticity,* Volume 107, pp. 100-121.

Bjerrum, L., 1967. Engineering geology of Norwegian normally-consolidated marine clays as related to settlements of buildings. *Geotechnique,* 17(2), pp. 81-118.

Bodas Freitas, T. M., Potts, D. M. & Zdravkovic, L., 2011. A time-dependent constitutive model for soils with isotach viscosity. *Computer and Geotechnics,* 38(6), pp. 809-20.

Borja, R. I. & Kavazanjian, E., 1985. A constitutive model for the stress-strain-time behaviour of 'wet' clays. *Geotechnique,* 35(3), pp. 283-298.

Boumezerane, D., Grimstad, G. & Makdisi, A., 2015. *A framework for peat behaviour based on hyperplasticity principles.* Gothenburg, Sweden, Chalmers University of Technology, pp. 25-28.

Bousshine, L., Chaaba, A. & De Saxcè, G., 2001. Softening in stress-strain curve for Druker-Prager non-associated plasticity. *International Journal of Plasticity,* Volume 17, pp. 21-46.

Butterfield, R., 1979. A natural compression law for soils (an advance on e - log p'). *Geotechnique,* 29(4), pp. 469-480.

Callari, C., Auricchio, F. & Sacco, E., 1998. A finite-strain Cam-clay model in the framework of multiplicative elasto-plasticity. *International Journal of Plasticity,* 14(12), pp. 1155-1187.

Cao, Y. J., Shen, W. Q., Burlion, N. & Shao, J. F., 2018. Effects of inclusions and pores on plastic and viscoplastic deformation of rock-like materials. *International Journal of Plasticity,* Volume 108, pp. 107-124.

Casagrande, A. & Wilson, S. D., 1951. Effect of rate of loading on the strength of clays and shales at constant water content. *Geotechnique,* Volume 2, pp. 251-was 263.

Castro, J., Justo, J. & Sivasithamparam, N., 2018. *Elastic and plastic anisotropy in soft clays: A constitutive model.* Porto, Portugal, CRC Press, pp. 117-124.

Castro, J. & Sivasithamparam, N., 2017. A Constitutive Model for Soft Clays Incorporating Elastic and Plastic Cross-Anisotropy. *Journal of Materials Science,* Volume 10, pp. 584: 1-16.

Cheng, J., Qian, X. & Zhao, T., 2016. Rheological viscoplastic models of asphalt concrete and rate-dependent numerical implement. *International Journal of Plasticity,* Volume 81, pp. 209-230.

Collins, I. F., 1997. The use of Legendre transformations in developing the constitutive laws of geomechanics from thermodynamic principles. In: *In IUTAM Symposium on mechanics of granular and porous materials.* Netherlands: Kluwer Academic Publishers, pp. 151-159.

Collins, I. F., 2003. A systematic procedure for constructing critical state models in three dimensions. *International Journal of Solids and Structures,* Volume 40, pp. 4379-4397.

Collins, I. F., 2005. Elastic/plastic models for soils and sands. *International Journal of Mechanical Sciences,* 47(4), pp. 493-508.

Collins, I. F., 2005. The concept of stored plastic work or frozen elastic energy in soil mechanics. *Geotechnique,* 55(5), pp. 373-382.

Collins, I. F. & Hilder, T., 2002. A theoretical framework for constructing elastic/plastic constitutive models for triaxial tests. *International Journal of Numerical and Analytical Methods in Geomechanics,* vol. 26(no. 13), pp. pp. 1313-1347.

Collins, I. F. & Houlsby, G. T., 1997. Application of thermo-mechanical principles to the modelling of geotechnical materials. *Proc. R. Soc. London Ser,* Volume vol. 453, pp. pp. 1975-2001.

Collins, I. F. & Kelly, P. A., 2002. A thermo-mechanical analysis of a family of soil models. *Geotechnique,* vol. 52(no. 7), pp. pp. 507-518.

Coombs, W. M., 2017. Continuously unqiue anisotropic critical state hyperplasticity. *International Journal for Numerical and Analytical Methods in Geomechanics,* Volume 41, pp. 578-601.

Crouch, R. S. & Wolf, J. P., 1995. On a three-dimensional anisotorpic plasticity model for soil. *Geotechnique,* Volume 45, pp. 301-305.

Dafalias, Y. F., 1975. *On cyclic and anisotropic plasticity.* Berkeley: Department of Civil Engineering, University of California.

Dafalias, Y. F., 1982. Bounding surface elastoplasticity - viscoplasticity for particulate cohesive media. *Deformation and failure of granular materials, IUTAM symposium*, pp. 97-107.

Dafalias, Y. F., 1986. An anisotropic critical state clay plasticity model. *Mechanics Research Communications,* Volume 13, pp. 341-347.

Dafalias, Y. F. & Herrmann, L. R., 1986. Bounding Surface plasticity II: Application to isotropic cohesive soils. *Journal of Engineering Mechanics,* 112(12), pp. 1263-1291.

Dafalias, Y. F., Manzari, M. T. & Papadimitriou, A. G., 2006. SNAICLAY: simple anisotropic clay plasticity model. *International Journal for Numerical and Analytical Methods in Geomechanics,* Volume 30, pp. 1231-1257.

Dafalias, Y. F. & Taiebat, M., 2013. Anatomy of rotational hardening in clay plasticity. *Geotechnique,* Volume 63, pp. 1406-1418.

Dafalias, Y. F. & Taiebat, M., 2014. Rotational hardening with and without anisotropic fabric at critical state. *Geotechnique,* Volume 64, pp. 507-511.

Darabi, M. K., Abu Al-Rub, R. K., Masad, E. A. & Little, D. N., 2012. A thermodynamic framework for constitutive modeling of time- and rate-dependent materials. Part II: Numerical aspects and application to asphalt concrete. *International Journal of Plasticity,* Volume 35, pp. 67-99.

Darabi, M. K., Abu Al-Rub, R. K., Masad, E. A. & Little, D. N., 2012. Thermodynamic-based model for coupling temperature-dependent viscoelastic, viscoplastic, and viscodamage constitutive behaviour of asphalt mixtures. *International Journal for Numerical and Analytical Methods in Geomechanics,* Volume 36, pp. 817-854.

Darabi, M. K., Abu Al-Rub, R. K. & Omidi, O., 2018. A thermodynamically consistent framework to derive local/nonlocal generalized nonassociative plasticity/viscoplasticity theories. *International Journal of Plasticity,* Volume 110, pp. 19-37.

Davies, M. C. R. & Newson, T. A., 1993. A critical state constitutive model for anisotropic soils. In: G. T. Houlsby & A. N. Schofield, eds. *In Predictive soil mechanics.* London: Thomas Telford, pp. 219-229.

Desai, C. S. & Siriwardane, H. J., 1984. *Constitutive laws for engineering materials with emphasis on geologic materials.* NJ: Prentice-Hall, Inc..

Desai, C. S. & Zhang, D., 1987. Viscoplastic model for geologic materials with generalised flow rule. *International Journal for Numerical and Analytical Methods in Geomechanics,* Volume 11, pp. 603-620.

Drumright, E. E. & Nelson, J. D., 1985. *Three-dimensional stress relaxation behaviour of marine sediments.* Philadelphia, ASTM International, pp. 294-305.

Einav, I. & Collins, I. F., 2008. A Thermomechanical Framework of Plasticity based on Probabilistic Micromechanics. *Journal of Mechanics of Materials and Structures,* 3(5), pp. 867-892.

Einav, I. & Puzrin, A., 2004. Pressure-dependent elasticity and energy conservation in elastoplastic models for soils. *Journal of Geotechnical and Geoenvironmental Engineering,* 130(1), pp. 81-92.

Einav, I. & Puzrin, A. M., 2004. Continuous Hyperplastic Critical State (CHCS) Model Derivation. *International Journal of Solids and Structures,* Volume 41, pp. 199-226.

Fatahi, B., Le, T. M., Le, M. Q. & Khabbaz, H., 2013. Soil creep effects on ground lateral deformation and pore water pressure under embankments. *Geomechanics and Geoengineering,* Volume 8, pp. 107-124.

Feda, J., 1992. *Creep of Soils: and Related Phenomena.* Amsterdam, Netherlands: Elsevier Science.

Feng, T. -W., n.d. *Compressibility and permeability of natural soft clays and surcharging to reduce settlements.* s.l.:University of Illinois.

Feng, W. Q. et al., 2017. Time and strain-rate effects on viscous stress-strain behaviour of plasticine material. *International Journal of Geomechanics,* 17(5), pp. 04016115: 1-22.

Fodil, A., Aloulou, W. & Hicher, P. Y., 1997. Viscoplastic behaviour of soft clay. *Geotechnique,* 47(3), pp. 581-591.

Fuentes, W. M. et al., 2010. *Visco-hypoplastic model for structured soils.* s.l., American Society of Civil Engineers (ASCE), pp. 452-460.

Fu, P. & Dafalias, Y. F., 2010. Fabric evolution within shear bands of granular materials and its relation to critical state theory. *International Journal of Numerical and Analytical Methods in Geomechanics.*

Fu, P. & Dafalias, Y. F., 2011. Study of anisotropic shear strength of granular materials using DEM simulation. *International Journal of Numerical and Analytical Methods in Geomechanics,* Volume 35, pp. 1098-1126.

Gajo, A. & Muir, W. D., 2001. A new apporach to anisotropic, bounding surface plasticity: general formulation and simulations of natural and reconstitutied clay behaviour. *International Journal for Numerical and Analytical Methods in Geomechanics,* 25(3), pp. 207-241.

Garlanger, J. E., 1972. The consolidation soils exhibiting creep under constant effective stress. *Geotechnique,* 22(1), pp. 71-78.

Ghorbel, E., 2008. A viscoplastic constitutive model for polymeric materials. *International Journal of Plasticity,* 24(11), pp. 2032-2058.

Gibson, R. E. & Lo, K. Y., 1961. *A theory of consolidation exhibiting secondary compression.* s.l.:In: Norwegian Goetechnical Institute.

Gong, Y. P., Hyde, C. J., Sun, W. & Hyde, T. H., 2009. Determination of material properties in the Chaboche unified viscoplasticity model. *Journal of Materials: Design and Applications,* Volume 224, p. JMDA273.

Graham, J., Crooks, J. H. A. & Bell, A. L., 1983. Time effects on the stress-strain behaviour of natural soft clays. *Geotechnique,* 33(3), pp. 327-340.

Graham, J. & Houlsby, G. T., 1983. Anisotropic elasticity of a natural clay. *Geotechnique,* Volume 33, pp. 165-180.

Grimstad, G., Degado, S. A., Nordal, S. & Karstunen, M., 2010. Modelling creep and rate effects in structured anisotropic soft clays. *Acta Geotechnica,* Volume 5, pp. 69-81.

Gudehus, G., 2004. A visco-hypoplastic constitutive relation for soft soils. *Soils and Foundations,* 44(4), pp. 11-25.

Gudimetla, M. R. & Doghri, I., 2017. A finite strain thermodynamically-based constitutive framework coupling viscoelasticity and viscoplasticity with application to glassy polymers. *International Journal of Plasticity,* Volume 98, pp. 197-216.

Guo, Q., Zaïri, F. & Guo, X., 2018. A thermo-viscoelastic-damage constitutive model for cyclically loaded rubbers. Part I: Model Formulation and numerical examples. *International Journal of Plasticity,* Volume 101, pp. 106-124.

Gu, X., Hu, J. & Huang, M., 2017. Anisotropy of elasticity and fabric of granular soils. *Granular Matter,* pp. 33: 1-15.

Halphen, B. & Nguyen, Q. S., 1974. Plastic and visco-plastic materials with generalised potential. *Mechanics Research Communications,* 1(1), pp. 43-47.

Hashiguchi, K. & Chen, Z. P., 1998. Elastoplastic equation of soils with the subloading surface and the rotational hardening. *International Journal of Numerical and Analytical Methods in Geomechanics,* Volume 22, pp. 197-227.

Herrmann, L. R. et al., 1981. *A verification study for the bounding surface plasticity model for cohesive soils,* Port Hueneme, California: Naval Construction Battalion Center.

Hinchberger, S. D., Qu, G. F. & Lo, K. Y., 2010. Constitutive approach for rate-sensitive anisotropic structured clay. *International Journal for Numerical and Analytical Methods in Geomechanics,* Volume 34, pp. 1797-1830.

Hinchberger, S. D. & Rowe, R. K., 2005. Evaluation of the predictive ability of two elastic-viscoplastic constitutive models. *Canadian Geotechnical Journal,* 42(6), pp. 1675-1694.

Hohenemser, K. & Prager, W., 1932. Ueber die Ansaetze der Mechanik isotroper Kontinua. *Zeitschrift fuer Angewandte Mathematik and Mechanik,* Volume 12, pp. 216-226.

Horpibulsuk, S., Liu, M. D., Liyanapathirana, D. S. & Suebsuk, J., 2010. Behaviour of cemented clay simulated via the theretical framework of the Structured Cam-Clay model. *Computers and Geotechnics,* Volume 37, pp. 1-9.

Houlsby, G. T., 1981. *A study of plasticity theories and their application to soils,* UK: University of Cambridge.

Houlsby, G. T., 1985. The use of a variable shear modulus in elastic-plastic models for clays. *Computer and Geotechnics,* Volume 1, pp. 3-13.

Houlsby, G. T., 1999. *A model for the variable stiffness of undrained clay.* Torino, Proc. Int. Symp. on Pre-Failure Deformation of Soils, pp. 443-450.

Houlsby, G. T. & Puzrin, A. M., 2000. A thermo-mechanical framework for constitutive models for rate-independent dissipative materials. *International Journal of Plasticity,* vol. 16(no. 9), pp. pp. 1017-1047.

Houlsby, G. T. & Puzrin, A. M., 2002. Rate-dependent plasticity models derived from potential functions. *Journal of Rheology,* 46(1), pp. 113-126.

Houlsby, G. T. & Puzrin, A. M., 2006. *Principles of hyperplasticity: an approach to plasticity theory based on thermodynamics principles.* London: Springer-Verlag London Limited.

Hueckel, T. & Nova, R., 1979. Some hysteresis effects of the behaviour of geologic media. *International Journal of Solids and Structures,* Volume 15, pp. 625-642.

Islam, M. N., 2014. *Associated and non-associated flow rule based elastic-viscoplastic models for soft clays,* Canberra: The University of New South Wales.

Islam, M. N. & Gnanendran, C. T., 2017. Elastic-Viscoplastic Model for Clays: Development, Validation and Application. *Journal of Engineering Mechanics,* 143(10), pp. 04017121_1-16.

Iwan, W. D., 1967. On the class of models for the yielding behaviour of continuous and composite systems. *Journal of Applied Mechanics,* Volume 34, pp. 612-617.

Jamiolkowski, M., Ladd, C., Germaine, J. & Lancellotta, R., 1985. *New developments in field and laboratory testing of soils.* San Francisco, s.n., pp. 57-153.

Jardine, R. J., Potts, D. M., Fourie, A. B. & Burland, J. B., 1986. Studies of the influence of non-linear stress-strain characteristics in soil-structure interaction. *Geotechnique,* 36(3), pp. 377-396.

Jardine, R. J., Symes, M. J. & Burland, J. B., 1984. The measurement of soil stiffness in the triaxial apparatus. *Geotechnique,* 34(3), pp. 323-340.

Jiang, J., Ling, H. I. & Kaliakin, V. N., 2012. An associative and non-associative anisotropic bounding surface model for clay. *Journal of Applied Mechanics,* 79(3), pp. 031010(1-10).

Jia, R., Chai, J. -C., Hino, T. & Hong, Z. -S., 2010. Strain-rate effect on consolidation behaviour of Ariake clay. *Proceedings of the ICE-Geotechnical Engineering*, 163(5), pp. 267-277.

Kaliakin, V. N. & Dafalias, Y. F., 1990. Theoretical aspects of the elastoplastic-viscoplastic bounding surface model for cohesive soils. *Soils and Foundation Journal,* 30(3), pp. 11-24.

Karim, M. R. & Gnanendran, C., 2014. Review of constitutive models for describing the time-dependent behaviour of soft clays. *Geomechanics and Geoengineering,* 9(1), pp. 36-51.

Karstunen, M. & Koskinen, M., 2008. Plastic anisotropy of soft reconstituted clays. *Canadian Geotechnical Journal,* Volume 45, pp. 314-328.

Karstunen, M. et al., 2005. Effect of anisotropy and destructuration on the behvior of Murro Test Embankment. *International Journal of Geomechanics,* 5(2), pp. 87-97.

Karstunen, M. & Yin, Z. Y., 2010. Modelling time-dependent behaviour of Murro test embankment. *Geotechnique,* 60(10), pp. 735-749.

Kavazanjian, E. J. & Mitchell, J. K., 1977. *A general stress-strain-time formulation for soils.* s.l., s.n., pp. 113-119.

Kavvadas, M. & Kalos, A., 2019. A time-dependent plasticity model for structured soils (TMS) simulating drained tertiary creep. *Computers and Geotechnics,* Volume 109, pp. 130-143.

Kelln, C., Sharma, J., Hughes, D. & Graham, J., 2008. An improved elastic-viscoplastic soil model. *Canadian Geotechnical Journal,* Volume 45, pp. 1356-1376.

Kimoto, S. & Oka, F., 2005. An elasto-viscoplastic model for clay considering destructuralization and consolidation analysis of unstable behaviour. *Soils and Foundations,* 45(2), pp. 29-42.

Krabbenhoft, K., 2009. A variational principle of elastoplasticity and its application to the modelling of frictional materials. *International Journal of Soilds and Structures,* Volume 46, pp. 464-479.

Krenk, S., 1996. A characteristic state plasticity model for granular materials. In: *Mechanics of Granular Materials.* Dordrecht: Kluwer, pp. 83-94.

Kutter, B. L. & Sathialingam, N., 1992. Elastic-viscoplastic modelling of the rate-dependent behaviour of clays. *Geotechnique,* 42(3), pp. 427-441.

Lacerda, W. A. & Houston, W. N., 1973. *Stress relaxation in soils.* Moscow, Russia, s.n., pp. 221-227.

Ladd, C. C. et al., 1977. *Stress deformation and strength characteristics.* Tokyo, Japan, s.n., pp. 421-494.

Lade, P. V. & Inel, S., 1997. Rotational kinematic hardening model for sand. Part-1: Concept of rotating yield and plastic potential surfaces. *Computers and Geotechnics,* Volume 21, pp. 183-216.

Lade, P. V. & Liu, C. -T., 1998. Experimental study of drained creep behaviour of sand. *Journal of Engineering Mechanics,* 124(8), pp. 912-920.

Lai, Y., Liao, M. & Kai, H., 2016. A constitutive model of frozen saline sandy soil based on energy dissipation theory. *International Journal of Plasticity,* Volume 78, pp. 84-113.

Lai, Y., Wu, Z., Zhu, Y. & Zhu, L., 2000. Elastic visco-plastic analysis for earthquake response of tunnels in cold regions. *Cold Regions Science Technology,* Volume 31, pp. 175-188.

Lai, Y., Xu, X., Yu, W. & Qi, J., 2014. An experimental investigation of the mechanical behaviour and a hyperplastic constitutive model of frozen loess. *International Journal of Engineering Science,* Volume 84, pp. 29-53.

Laloui, L., Leroueil, S. & Vermeer, P. A., 2008. Modelling the combined effect of strain rate and temperature on one-dimensional compression of soils. *Canadian Geotechnical Journal,* Volume 45, pp. 1765-1777.

Leal, A. N., Kaliakin, V. N. & Mashayekhi, M., 2017. Improved rotational hardening rule for cohesive soils and definition of inherent anisotropy. *International Journal of Numerical and Analytical Methods in Geomechanics,* Volume 42, pp. 469-487.

Leoni, M., Karstunnen, M. & Vermeer, P. A., 2008. Anisotropic creep model for soft soils. *Geotechnique,* 58(3), pp. 215-226.

Leroueil, S., 2006. *The Isotache approach. Where are we 50 years after its development by Professor Šuklje? 2006 Prof. Šuklje's Memorial Lecture.* Ljubljana, Slovenia, s.n., pp. 29-31.

Leroueil, S., Kabbaj, M., Tavenas, F. & Bouchard, R., 1985. Stress-strain-strain rate relation for the compressibility of sensitive natural clays. *Geotechnique,* 35(2), pp. 159-180.

Leroueil, S. & Marques, M. E. S., 1996. Importance of strain rate and temperature effects in geotechnical engineering, Measuring and Modeling Time-Dependent Soil Behaviour. *ASCE GSP,* Volume 61, pp. 1-60.

Leroueil, S. & Vaughan, P. R., 1990. The general and congruent effects of structure in natural soils. *Geotechnique,* 40(3), pp. 467-488.

Le, T. M. & Fatahi, B., 2016. Trust-region reflective optimisation to obtain soil visco-plastic properties. *Engineering Computations: International Journal for Computer-Aided Engineering and Software,* 33(2), pp. 410-442.

Le, T. M., Fatahi, B. & Khabbaz, H., 2012. Viscous Behaviour of Soft Clay and Inducing Factors. *Journal of Geotechnical and Geologial Engineering,* Volume 30, pp. 1069-1083.

Le, T. M., Fatahi, B. & Khabbaz, H., 2015. Numerical optimisation to obtain elastic viscoplastic model parameters for soft clay. *International Journal of Plasticity,* Volume 65, pp. 1-21.

Le, T. M., Fatahi, B., Khabbaz, H. & Sun, W., 2017. Numerical optimisation applying trust-region reflective least squares algorithm with constraints to optimise the non-linear creep parameters of soft soil. *Applied Mathematical Modelling,* Volume 41, pp. 236-256.

Lewis, R. W. & Schrefler, B. A., 1999. The Finite Element Method in the Static and Dynamic Deformation and Consolidation of Porous Media. *Meccanica,* 34(3), pp. 231-232.

Liingaard, M., Augustesen, A. & Lade, P. V., 2004. Characterisation of models for time-dependent behaviour of soils. *International Journal of Geomechanics,* 4(3), pp. 157-177.

Likitlersuang, S., 2003. *A Hyperplasticity Model for Clay Behaviour: An Application to Bangkok Clay,* Oxford: University of Oxford.

Likitlersuang, S. & Houlsby, G. T., 2007. Predictions of a continuous hyperplasticity model for bangkok clay. *Geomechanics and Geoengineering,* 2(3), pp. 147-157.

Liu, E., Lai, Y., Wong, H. & Feng, J., 2018. An elastoplastic model for saturated freezing soils based on thermo-poromechanics. *International Journal of Plasticity,* Volume 107, pp. 246-285.

Lubliner, J., 1990. Plasticity Theory. Mineola, New York: Dover Publications, Inc.

Mašín, D., 2005. A hypoplastic constitutive model for clays. *International Journal for Numerical and Analytical Methods in Geomechanics,* 29(4), pp. 311-336.

Matsui, T. & Abe, N., 1985. Elasto/viscoplastic constitutive equation of normally consolidated clays based on flow surface theory. In: *Numerical methods in geomechanics, Nagoya.* Rotterdam, Netherlands: A.A. Balkema, pp. 407-413.

Matsui, T. & Abe, N., 1986. *Flow surface model of viscoplasticity for normally consolidated clay.* s.l., s.n., pp. 157-164.

Matsui, T. & Abe, N., 1988. Verification of elasto-viscoplastic model of normally consolidated clays in undrained creep. *Numerical Methods in Geomechanics,* Volume 6, pp. 453-459.

Matsui, T., Abe, N. & Hayashi, K., 1989. Viscoplastic modelling of time-dependent behaviour of clays. *Numerical models in geomechanics,* pp. 100-107.

Maugin, G. A., 1992. The Thermomechanics of Plasticity and Fracture. s.l.:Cambridge University Press.

Mesri, G. & Choi, Y. K., 1985. *The uniqueness of the end-of-primary (EOP) void ratio-effective stress relationship.* San Fransisco, California, s.n., pp. 587-590.

Mesri, G. & Feng, T., 1986. Discussion on "Stress-strain-strain rate relation for the compressibility of sensitive natural clays". *Geotechnique,* 36(2), pp. 283-287.

Mesri, G. & Godlewski, P. M., 1977. Time and stress-compressibility inter-relationship. *Journal of the Geotechnical Engineering Division,* 103(5), pp. 417-430.

Miao, L., Zhang, J., Wang, F. & Houston, S. L., 2008. Time-dependent Deformation Behaviour of Jiangsu Marine Clay. *Marine Georesources & Geotechnology,* 26(2), pp. 86-100.

Mitchell, J. K., 1956. *The fabric of natural clays and its relation to engineering properties.* Washington, D.C, Highway Research Board, pp. 693-713.

Mitchell, J. K., 1993. *Fundamentals of Soil Mechanics.* NY: John Wiley and Sons, inc.

Mroz , Z. & Norris, V. A., 1982. Elastoplastic and viscoplastic constitutive models for soils with application to cyclic loading. In: *Soil Mechanics, Cyclic and Transient Loads.* New York: John Wiley & Sons, pp. 173-218.

Mroz, Z., 1967. On the description of anisotropic work hardening. *Journal of Mechanics and Physics of Solids,* Volume 15, pp. 163-175.

Mroz, Z., 1998. Elastoplastic and viscoplastic constitutive models for granular materials. In: B. Cambou, ed. *In Behaviour of granular materials.* New York: Springer Wien, pp. 269-337.

Muhunthan, B., Chameau, J. L. & Masad, E., 1996. Fabric Effects on the Yield Behaviour of Soils. *Soils and Foundations,* 36(3), pp. 85-97.

Naghdi, P. M. & Murch, S. A., 1963. On the Mechanical Behaviour of Viscoelastic/Plastic Solids. *Journal of Applied Mechanics,* 30(3), pp. 321-328.

Nguyen, L. D., Fatahi, B. & Khabbaz, H., 2014. A constitutive model for cemented clays capturing cementation degradation. *International Journal of Plasticity,* Volume 56, pp. 1-18.

Nguyen, N. H. T., Bui, H. H., Nguyen, G. D. & Kodikara, J., 2017. A cohesive damage-plasticity model for DEM and its application for numerical investigation of soft rock fracture properties. *International Journal of Plasticity,* Volume 98, pp. 175-196.

Niemunis, A., 2003a. Anisotropic effects in hypoplasticity. *In Proceedings of International Symposium on Deformation Characteristics of Geomaterials*, Volume 1, pp. 1211-1217.

Niemunis, A., 2003b. *Extended hypoplastic models for soils.* s.l.:Inst. für Grundbau und Bodenmechanik.

Niemunis, A., Grandas-Tavera, C. E. & Prada-Sarmiento, L. F., 2009. Anisotropic visco-hypoplasticity. *Acta Geotechnica,* 4(4), pp. 293-314.

Niemunis, A. & Krieg, S., 1996. Viscous behaviour of soil under oedometric conditions. *Canadian Geotechnical Journal,* 33(1), pp. 159-168.

Nova, R., 1977. On the hardening of soils. *Archiwum Mechaniki Stosowanej,* Volume 29, pp. 445-458.

Nova, R., 1985. *Mathematical modelling of anisotropic clays.* Rotterdam, A.A. Balkema, pp. 607-611.

Nova, R. & Wood, D. M., 1979. A constitutive model for sand in triaxial compression. *International Journal of Numerical and Analytical Methods in Geomechanics,* Volume 3, pp. 255-278.

Oka, F., Adachi, T. & Mimura, M., 1988. Elasto-viscoplastic constitutive models for clays. *Proceedings of the international conference on rheology and soil mechanics*, pp. 12-28.

Oka, F., Adachi, T. & Okano, Y., 1986. Two-Dimensional Consolidation Analysis using an Elasto-Viscoplastic Constitutive Equation. *International Journal for Numerical and Analytical Methods in Geomechanics,* Volume 10, pp. 1-16.

Oka, F., Adachi, T. & Yashima, A., 1994. Instability of an elasto-viscoplastic constitutive mdoel for clay and strain localisation. *Mechanics of Materials,* Volume 18, pp. 119-129.

Olszak, W. & Perzyna, P., 1966. The constitutive equations of the flow theory for a non-stationary yield condition. In: *Applied Mechanics.* Berlin, Heidelberg: Springer Berlin Heidelberg, pp. 545-553.

Olszak, W. & Perzyna, P., 1970. *Stationary and non-stationary viscopalsticity.* New York: McGraw-Hill.

Palmer, A. C., 1967. Stress-strain relations for clays: an energy approach. *Geotechnique,* 17(4), pp. 348-358.

Perrone, V. J., 1998. *One dimensional computer analysis of simultaneous consolidation and creep of clay.* Blacksburg(Virginia): Virginia Polytechnic Institute and State University.

Perzyna, P., 1963. The constitutive equations for working hardening and rate sensitive plastic materials. *Proceedings of Vibration Problems,* 4(3), pp. 281-290.

Perzyna, P., 1966. Fundamental problems in viscoplasticity. *Advances in Applied Mechanics,* Volume 9, pp. 244-368.

Pestana, J. M. & Whittle , A. J., 1999. Formulationof a unified constitutive model for clays and sands. *International Journal for Numerical and Analytical Methods in Geomechanics,* Volume 22, pp. 1215-1243.

Prevost, J. -H., 1976. Undrained Stress-Strain-Time Behaviour of Clays. *American Society of Civil Engineers, Journal of the Geotechnical Engineering Division,* Volume 102, pp. 1245-1259.

Puzrin, A. M. & Houlsby, G. T., 2001a. A thermomechanical framework for rate-independent dissipative materials with internal functions. *International Journal of Plasticity,* Volume 38, pp. 1147-1165.

Puzrin, A. M. & Rabaiotti, C., 2009. A thermomechanical framework for non-linear hyperviscoelastic materials. *Journal of Rheology,* 54(3), pp. 619-642.

Qiao, Y., Ferrari, A., Laloui, L. & Ding, W., 2016. Non-stationary flow surface theory for modelling the viscoplastic behaviours of soils. *Computers and Geotechnics,* Volume 76, pp. 105-119.

Qiu, G. & Grabe, J., 2011. Explicit modelling of cone and strip footing penetration under drained and undrained conditions using a visco-hypoplastic model. *Geotechnik,* 34(3), pp. 205-217.

Rajot, J. P., 1992. *A theory for the time-dependent yielding and creep of clay.* Blacksburg(Virginia): Virginia Polytechnic Institute and State University.

Rezania, M., Taiebat, M. & Poletti, E., 2016. A viscoplastic SANICLAY model for natural soft soils. *Computers and Geotechnics,* Volume 73, pp. 128-141.

Roscoe, K. H. & Burland, J., 1968. On the generalised stress-strain behaviour of wet clay. *Engineering plasticity,* Cambridge: Cambridge University Press, pp. 535-609.

Roscoe, K. H., Schofield, A. N. & Thurairajah, A., 1963. Yielding of clays in states wetter than critical. *Geotechnique,* 13(3), pp. 211-240.

Salomoni, V. A. & Fincato, R., 2012. 3D subsidence analyses above gas reservoirs accounting for an unconventional plasticity model. *International Journal for Numerical and Analytical Methods in Geomechanics,* Volume 36, pp. 959-976.

Salomoni, V. A. & Schrefler, B. A., 2006. Stabilized-coupled modelling of creep phenomena for saturated porous media. *International Journal for Numerical Methods in Engineering,* Volume 66, pp. 1587-1617.

Samat, S., 2016. *Thermomechanical Modelling of Ground Response under Environmental Actions,* Barcelona: Universitat Politècnica de Catalunya.

Sansour, C., Karsaj, I. & Jurica, S., 2006. On free energy-based formulations for kinematic hardening and the decomposition F=f_p f_e. *International Journal of Solids and Structures,* Volume 43, pp. 7534-7552.

Schofield, A. N. & Wroth, P., 1968. *Critical State Soil Mechanics.* s.l.:McGraw-Hill.

Sekiguchi, H., 1984. Theory of undrained creep rupture of normally consolidated clay based on elasto-viscoplasticity. *Japanese Society of Soil Mechanics and Foundation Engineering,* 24(1), pp. 129-147.

Sekiguchi, H. & Ohta, H., 1977. *Induced anisotropy and time dependency in clays.* Tokyo, Constitutive equations of soils, pp. 229-238.

Shahrour, I. & Meimon, Y., 1995. Calculation of marine foundations subjected to repeated loads by means of the homogenization method. *Computers and Geotechnics,* 17(1), pp. 93-106.

Sheahan, T., Ladd, C. & Germaine, J., 1994. Time-dependent triaxial relaxation behaviour of a resedimented clay. *Geotechnical Testing Journal,* 17(4), pp. 444-452.

Silvestri, V., Soulie, M., Touchan, Z. & Fay, B., 1988. Triaxial relaxation tests on a soft clay. *Advanced triaxial testing of soil and rock - ASTM STP,* Volume 977, pp. 321-337.

Singh, A. & Mitchell, J. K., 1968. General stress-strain-time function for soils. *American Society of Civil Engineers Proceedings, Journal of the Soil Mechanics and Foundations Division*, Volume 94, pp. 21-46.

Sivasithamparam, N. & Castro, J., 2016. An anisotropic elastoplastic model for soft clays based on logarithmic contractancy. *International Journal for Numerical and Analytical Methods in Geomechanics,* Volume 40, pp. 596-621.

Sivasithamparam, N., Karstunen, M. & Bonnier, P., 2015. Modelling creep behaviour of anisotropic soft soils. *Computers and Geotechnics,* Volume 69, pp. 46-57.

Soga, K., Nakagawa, K. & Mitchell, J. K., 1995. *Measurement of stiffness degradation characteristics of clays using a torsional shear device.* Tokyo, First International Conference on Earthquake Geotechnical Engineering, pp. 107-112.

Suebsuk, J., Horpibulsuk, S. & Liu, M. D., 2010. Modified Structured Cam Clay: A generalised critical state model for destructured, naturally structured and artificially structured clays. *Computers and Geotechnics,* Volume 37, pp. 956-968.

Sukjie, L., 1957. *The analysis of the consolidation process by the isotache method.* London, England, Butterworths Scientific Publications, pp. 200-206.

Sun, Y., Gao, Y. & Zhu, Q., 2018. Fractional order plasticity modelling of state-dependent behaviour of granular soils without using plastic potential. *International Journal of Plasticity,* Volume 102, pp. 53-69.

Sun, Y. & Shen, Y., 2017. Constitutive Model of Granular Soils using Fractional-Order Plastic-Flow Rule. *International Journal of Geomechanics,* 17(8), pp. 04017025: 1-12.

Tatsuoka, F., 2000. *Impacts on geotechnical engineering of several recent findings from laboratory stress-strain tests on geomaterials.* s.l.:Columbia University.

Tavenas, F., Leroueil, S., LA Rochelle, P. & Roy, M., 1978. Creep behaviour of an undisturbed lightly overconsolidated clay. *Canadian Geotechnical Journal,* Volume 15, pp. 402-423.

Taylor, D. W., 1942. *Research on consolidation of clays.* Mass Institute of Technology -- Department of Civil and Sanitary Engineering: s.n.

Terzaghi, K., 1923. The computation of the permeability of soils from the hydrodynamic pressure gradients. *Sitzungsber. Math.-naturwiss. K1., Part IIa,* 132(3/4), pp. 125-138 (in German).

Terzaghi, K. & Karl, T., 1996. *Soil mechanics in engineering practice.* New York: New York: Wiley.

Thornton, C. & Liu, L., 2000. DEM simulations of axial compression and decompression. In: *Compaction of soils, granulates and powders.* Rotterdam: Balkema, pp. 251-261.

Ulm, F. J. & Coussy, O., 2003. *Mechanics and durability of solids.* Upper Saddle River, New Jersy: NJ: Prentice Hall.

Vaid, Y. & Campanella, R., 1977. Time-dependent behaviour of undisturbed clay. *Journal of the Geotechnical Engineering Division,* 103(7), pp. 693-709.

Valanis, K. C., 1966. Thermodynamics of large viscoelastic deformations. *Journal of Mathematical Physics,* Volume 45, pp. 197-212.

Van Den Ham, G., Rohn, J., Meier, T. & Czurda, K., 2009. Finite element simulation of a slow moving natural slope in the upper-austrian alps using a visco-hypoplastic constitutive model. *Geomorphology,* 103(1), pp. 136-142.

Vardoulakis, I. & Sulem, J., 1955. *Bifurcation analysis in geomechanics.* s.l.:Blackie Academic & Professional.

Vermeer, P. A. & Neher, H. P., 1999. *A soft soil model that accounts for creep.* Amsterdam, In: Proceedings of the Plaxis Symposium on Beyond 2000 in Computational Geotechnics, pp. 249-262.

Vermeer, P. A. & Neher, H. P., 2000. *A soft soil model that accounts for creep.* Rotterdam, In Proceedings of Beyond 2000 in Computational Geotechnics - 10 Years of PLAXIS International, pp. 249-261.

Vlahos, G., Cassidy, M. J. & Byrne, B. W., 2006. The behaviour of spudcan footings on clay subjected to combined cyclic loading. *Applied Ocean Research,* Volume 28, pp. 209-221.

Walker, L. K. & Raymond, G. P., 1968. The prediction of consolidation rates in a cemented clay. *Canadian Geotechnical Journal = Revue Canadienne de Geotechnique,* Volume 5, pp. 192-216.

Wang, S., 2016. *Numerical simulation of soil creep with hypoplasticity,* Vienna: s.n.

Wang, W., Liu, H. X., Zhu, Q. Z. & Shao, J. F., 2015. A micromechanics-based creep damage model for brittle rocks. *European Journal of Environmental and Civil Engineering,* 19(S1), pp. s1-s14.

Wheeler, S. J., Näätänen, A., Karstunen, M. & Lojander, M., 2003. An anisotropic elasto-plastic model for soft clays. *Canadian Geotechnical Journal,* 40(2), pp. 403-418.

Whittle, A. J. & Kavvadas, M. J., 1994. Formulation of MIT-E3 Constitutive Model for Overconsolidated Clays. *Journal of Geotechnical Engineering,* Volume ASCE 120, pp. 173-198.

Wood, D. M., 1990. Soil Behaviour and Critical State Soil Mechanics. Cambridge University Press.

Wroth, C. P. & Houlsby, G. T., 1980. A critical state model for predicting the behaviour of clays. *In Workship on Limit Equilibrium, Plasticity and Generalised Stress-Strain in Geotechnical Engineering*, pp. 592-627.

Wroth, C. P. & Houlsby, G. T., 1985. *Soil mechanics-property characterization and analysis procedures.* San Francisco, s.n., pp. 1-55.

Wroth, C. P., Randolph, M. F., Houlsby, G. T. & Fahey, M., 1979. *Correlations for the engineering properties of soils, with particular reference to the shear modulus,* UK: Cambridge University Engineering Department.

Wu, W., Bauer, E., Niemunis, A. & Herle, I., 1993. Visco-hypoplastic models for cohesive soils. *Modern Approaches to Plasticity,* pp. 365-383.

Wu, W. & Kolymbas, D., 1990. Numerical testing of the stability criterion for hypoplastic constitutive equations. *Mechanics of Materials,* 9(3), pp. 245-253.

YangPing, Y., WenJie, C. & NaiDong, W., 2013. Three-dimensional dissipative stress space considering yield behaviour in deviatoric plane. *Sci China Tech Sci,* vol. 56(no. 8), pp. pp. 1999-2009.

Yang, Y., Lai, Y., Dong, Y. & Li, S., 2010. The strength criterion and elastoplastic constitutive model of frozen soil under high confining pressures. *Cold Regions Science and Technology,* Volume 60, pp. 154-160.

Yao, Y. P., Hou, W. & Zhou, A. N., 2009. UH model: three-dimensional unified hardening model for over-consoldiated clays. *Geotechnique,* Volume 59, pp. 451-469.

Yin, J. H., 1999. Non-linear creep of soils in oedometer tests. *Geotechnique,* 49(5), pp. 699-707.

Yin, J. H., 2006. Elastic Visco-Plastic Models for the Time-Dependent Stress-Strain Behaviour of Geomaterials. In: *Modern Trends in Geomechanics.* Berlin: Springer, pp. 175-190.

Yin, J. H. & Cheng, C. M., 2006. Comparison of Strain-rate Dependent Stress-Strain Behaviour from K0-consolidated Compression and Extension Tests on Natural Hong Kong Marine Deposits. *Marine Georesources & Geotechnology,* 24(2), pp. 119-147.

Yin, J. H. & Feng, W. Q., 2016. A new simplified method and its verification for calculation of consolidation settlement of a clayey soil with creep. *Canadian Geotechnical Journal,* Volume 54, pp. 333-347.

Yin, J. H. & Graham, J., 1989. Viscous-elastic-plastic modelling of one-dimensional time-dependent behaviour of clays. *Canadian Geotechnical Journal,* Volume 26, pp. 199-209.

Yin, J. H. & Graham, J., 1999. Elastic viscoplastic modelling of time-dependent stress-strain behaviour of soils. *Canadian Geotechnical Journal,* Volume 36, pp. 736-745.

Yin, J. H. & Zhu, J. G., 1999. Measured and predicted time-dependent stress-strain behaviour of Hong Kong marine deposits. *Canadian Geotechnical Journal,* 36(4), pp. 760-766.

Yin, J. H., Zhu, J. G. & Graham, J., 1988. Viscous-elastic-plastic modelling of one-dimensional time-dependent behavoiur of clays. *Canadian Geotechnical Journal,* Volume 26, pp. 199-209.

Yin, J. H., Zhu, J. G. & Graham, J., 2002. A new elastic visco-plasticmodel for time-dependent behaviour of normally and overconsolidated clays: theory and verification. *Canadian Geotechnical Journal,* 39(1), pp. 157-173.

Yin, Z. Y. & Chang, C. S., 2009. Micro-structural modelling of stress-dependent behaviour of clay. *International Journal of Solids and Structures,* 46(6), pp. 1373-1388.

Yin, Z. Y., Chang, C. S., Karstunen, M. & Hicher, P. Y., 2010. An anisotropic elastic-viscoplastic model for soft clays. *International Journal of Solids and Structures,* Volume 47, pp. 665-677.

Yin, Z. Y. & Hicher, P. Y., 2008. Identifying parameters controlling soil delayed behaviour from laboratory and in situ pressuremeter testing. *International Journal for Numerical and Analytical Methods in Geomechanics,* 32(12), pp. 1515-1535.

Yin, Z. Y. & Karstunen, M., 2011. Modelling strain-rate-dependency of natural soft clays combined with anisotropy and destructuration. *Acta Mechanica Solida Sinica,* 24(3), pp. 216-230.

Yin, Z. Y. et al., 2011b. Modelling time-dependent behaviour of soft sensitive clay. *Journal of Geotechnical and Geoenvironmental Engineering,* 137(11), pp. 1103-1113.

Yin, Z. Y., Karstunen, M., Wang, J. H. & Yu, C., 2011c. Influence of features of natural soft clay on the behaviour of embankment. *Journal of Central South University of Technology,* 18(5), pp. 1667-1676.

Yin, Z. Y., Xu, Q. & Chuang, Y., 2015. Elastic-Viscoplastic Modelling for Natural Soft Clays Considering Non-linear Creep. *Journal of Geomechanics,* 15(5), pp. A6014001_1-10.

Yin, Z. Y., Yin, J. H. & Huang, H. W., 2015. Rate-dependent and Long-term Yield Stress and Strength of Soft Wenzhou Marine Clay: Experiments and Modeling. *Marine Georesources & Geotechnology,* Volume 33, pp. 79-91.

Yue, D., 2001. *An Anistropic and Time-dependent Bounding Surface Model for Clays and its Application to a Containment System Constructed over a Soft Foundation,* New York : Columbia University.

Zdravkovic, L., Potts, D. M. & Hight, D. W., 2002. The effect of strength anisotropy on the behaviour of embankments on soft ground. *Geotechnique,* Volume 52, pp. 447-457.

Zentar, R. et al., 2002b. *Comparison of two approaches for modelling anisotropy of soft clays.* Rotterdam, A.A. Balkema, pp. 115-121.

Zhang, H., 2018. An anisotropic plasticity clay model accounting for structural effects and overconsolidation. *Geomechanics and Geoengineering: An International Journal,* 13(1), pp. 1-10.

Zhang, Y. D. & Buscarnera, G., 2017. A rate-dependent breakage model based on the kinetics of crack growth at the grain scale. *Geotechnique,* 67(11), pp. 953-967.

Zhang, Z., 2017. A thermodynamics-based theory for the thermo-poro-mechanical modeling of saturated clay. *International Journal of Plasticity,* Volume 92, pp. 164-185.

Zhao, L. Y., Zhu, Q. Z. & Shao, J. F., 2018. A micro-mechanics based plastic damage model for quasi-brittle materials under a large range of compressive stress. *International Journal of Plasticity,* Volume 100, pp. 156-176.

Zhou, C., Leroueil, S., Fafard, M. & Ghorbel, S., 2017. Constitutive modeling of kinematic hardening behaviour of saturated anisotropic soils. *International Journal of Geomechanics,* 17(3), pp. 04016063:1-17.

Zhou, C., Leroueil, S., Fafard, M. & Yin, J. H., 2018. A Kinematic Hardening and Elastic Visco-plastic Model of Saturated Cohesive Anisotropic Soils. *KSCE Journal of Civil Engineering,* 22(2), pp. 532-543.

Zhou, C. & Ng, C. W., 2015. A thermomechanical model for saturated soil at small and large strains. *Canadian Geotechnical Journal,* Volume 52, pp. 1101-1110.

Zhou, C., Yin, J. H., Zhu, J. G. & Cheng, C. M., 2005. Elastic anisotropic viscoplastic modelling of the strain-rate-dependent stress-strain behaviour of K0-consolidated natural marine clays in triaxial shear tests. *ASCE International Journal of Geomechanics,* 5(3), pp. 218-232.

Zhou, H., Jia, Y. & Shao, J. F., 2008. A unified elastic-plastic and viscoplastic damage model for quasi-brittle rocks. *International Journal of Rock Mechanics and Mining Sciences,* Volume 45, pp. 1237-1251.

Zhou, Z. et al., 2016. Multiaxial creep of frozen loess. *Mechanics of Materials,* Volume 95, pp. 172-191.

Zhu, G. & Yin, J. H., 2000a. Elastic visco-plastic consolidation modelling of clay foundation at Berthierville test embankment. *International Journal for Numerical and Analytical Methods in Geomechanics,* Volume 24, pp. 491-508.

Zhu, J. G. & Yin, J. H., 2000b. Strain-rate-dependent stress-strain behaviour of overconsolidated Hong Kong marine clay. *Canadian Geotechnical Journal,* Volume 37, pp. 1272-1282.

Zhu, J. G. & Yin, J. H., 2001. Drained creep behaviour of soft Hong Kong marine deposits. *Geotechnique,* Volume 51, pp. 471-474.

Zhu, Q. Y., Yin, Z. Y., Hicher, P. Y. & Shen, S. L., 2016. Non-linearlity of one-dimensional creep characteristics of soft clays. *Acta Geotechnica,* Volume 11, pp. 887-900.

Zhu, Y. et al., 2016. Thermo-mechanically coupled cyclic elasto-viscoplastic constitutive model of metals: Theory and Application. *International Journal of Plasticity,* Volume 79, pp. 111-152.

Ziegler, H., 1977. *Principles of Structural Stability.* s.l.:Lehr- und Handbücher der Ingenieurwissenschaften.

Ziegler, H., 1981. Discussion of some objections to thermomechanical orthogonality. *Ingenieur Archiv,* Volume 50, pp. 149-164.

Ziegler, H., 1983. *An introduction to thermomechanics.* Amsterdam: North Holland.

Ziegler, H. & Wehrli, C., 1987. The Derivation of Constitutive Relations from the Free Energy and the Dissipation Function. *Advances in Applied Mechanics,* Volume 25, pp. 183-238.

Zienkiewicz, O. C. et al., 1998. *Computational Geomechanics.* Chichester: Wiley.

Zienkiewicz, O. C. & Cormeau, I. C., 1974. Viscoplasticity - plasticity and creep in elastic solids - a unified numerical solution approach. *International Journal for Numerical Methods in Engineering,* Volume 8, pp. 821-845.

APPENDICES

Appendix A: Relationship between Non-Associated Flow Rule and Stress-dependent Dissipation Potential Function

In the proposed model, the dissipation increment function takes the form $\delta\Phi\left(\varepsilon_{ij}^{p}, \dot{\varepsilon}_{ij}^{p}, \sigma_{ij}\right)$ instead of $\delta\Phi\left(\varepsilon_{ij}^{p}, \dot{\varepsilon}_{ij}^{p}\right)$ that depends explicitly on the effective stress components, as defined in Equation (4.14).

Considering the modelling of rate-dependent behaviour, the dissipation function in Equation (4.14) is separated into the force potential function and flow potential function, inspired by the discussions provided in Houlsby and Puzrin (2002). Thus, the force potential function $z\left(\varepsilon_{ij}^{p}, \dot{\varepsilon}_{ij}^{p}, \sigma_{ij}\right)$ is determined from the dissipation function in Equation (4.14), which is provided in Equation (4.17).

To take into account of rate-dependent behaviour, i.e., $\delta\Phi$ is homogeneous but not first order in $\dot{\varepsilon}_{ij}^{p}$, the following generalisation for the definition of the dissipative stress is adopted, which is given by:

$$\chi_{ij} = \frac{\partial z\left(\varepsilon_{ij}^{p}, \dot{\varepsilon}_{ij}^{p}, \sigma_{ij}\right)}{\partial\left(\dot{\varepsilon}_{ij}^{p}\right)} \tag{A-1}$$

A Legendre-Fenchel transformation is performed on the force potential function $z\left(\varepsilon_{ij}^{p}, \dot{\varepsilon}_{ij}^{p}, \sigma_{ij}\right)$ to introduce its dual function, $w\left(\varepsilon_{ij}^{p}, \chi_{ij}, \sigma_{ij}\right)$, which is provided in Equation (4.18) and is termed as 'flow potential function'.

The following property from Legendre-Fenchel transformation can be deduced, such that:

$$\dot{\varepsilon}_{ij}^{p} = \frac{\partial w\left(\varepsilon_{ij}^{p}, \chi_{ij}, \sigma_{ij}\right)}{\partial \chi_{ij}} \tag{A-2}$$

Since $w\left(\varepsilon_{ij}^{p}, \chi_{ij}, \sigma_{ij}\right)$ is denoted as plastic flow potential function, the expression determined in Equation (A-2) has a clear analogy with the associated flow rule in the conventional plasticity. Moreover, the dual relationships for the passive variables provided by Legendre-Fenchel transformation can also be deduced as follows:

$$\frac{\delta z\left(\varepsilon_{ij}^{p}, \dot{\varepsilon}_{ij}^{p}, \sigma_{ij}\right)}{\partial \varepsilon_{ij}^{p}} = -\frac{\partial w\left(\varepsilon_{ij}^{p}, \chi_{ij}, \sigma_{ij}\right)}{\partial \varepsilon_{ij}^{p}} \tag{A-3a}$$

$$\frac{\delta z\left(\varepsilon_{ij}^{p}, \dot{\varepsilon}_{ij}^{p}, \sigma_{ij}\right)}{\partial \sigma_{ij}} = -\frac{\partial w\left(\varepsilon_{ij}^{p}, \chi_{ij}, \sigma_{ij}\right)}{\partial \sigma_{ij}} \tag{A-3b}$$

However, the viscoplastic flow rules determined in Equation (A-2) are expressed in the dissipative stress space, not in the actual stress space. These expressions are required to be transformed to the actual stress space. In other words, it is required to replace χ_{ij} in $\mathrm{w}\left(\varepsilon_{ij}^{p}, \chi_{ij}, \sigma_{ij}\right)$ by σ_{ij} with the adoption of the Orthogonality principle. The adoption of the Orthogonality principle results in the fact that the effective stress $\left(\sigma_{ij}\right)$ is the sum of the shift stress $\left(\rho_{ij}\right)$ and the dissipative stress $\left(\chi_{ij}\right)$, as discussed in Aung et al. (2016). The shift stress component exists due to the additional plastic free-energy function, which is important to accommodate the effect of stress history of stiffness of soils. The resulting shift stress

component can determine the kinematic hardening behaviour of soils. The adoption of the Orthogonality principle yields:

$$\bar{\mathrm{w}}\left(\varepsilon_{ij}^{p}, \sigma_{ij}\right) = \mathrm{w}\left(\varepsilon_{ij}^{p}, \chi_{ij}, \sigma_{ij}\right) = \mathrm{w}\left(\varepsilon_{ij}^{p}, \sigma_{ij} - \rho_{ij}, \sigma_{ij}\right) = 0 \tag{A-4}$$

Differentiating (A-4) with respect to the stress components, (i.e. actual and dissipative stress components), yields:

$$\frac{\partial \bar{\mathrm{w}}}{\partial \sigma_{ij}} = \frac{\partial \mathrm{w}}{\partial \chi_{\mathrm{ij}}} + \frac{\partial \mathrm{w}}{\partial \sigma_{ij}} \tag{A-5}$$

Considering Equation (A-2), Equation (A-3b) and Equation (A-5), it can be deduced as follows:

$$\dot{\varepsilon}_{ij}^{p} = \frac{\partial \bar{\mathrm{w}}}{\partial \sigma_{ij}} + \frac{\delta \mathrm{z}}{\partial \sigma_{ij}} \tag{A-6}$$

Referring to Equation (A-6), the flow rule becomes non-associated in the actual stress space due to the presence of additional term on the right-hand side of the equation, as $\delta\Phi$ depends explicitly on effective stress component. If the dissipation increment function does not depend on the effective stress, the second term on the right-hand side of the equation (A-6) can then be ignored, thus retaining the associated flow rule in both dissipative and actual stress spaces. It can be deduced that the non-associated flow rule is derived naturally from the standardised procedure using Hyperplastic approach by postulating the stress-dependent $\delta\Phi$ function.

Appendix B: Derivation of Non-Associated Flow Rule for proposed H-Creep Model

When viscosity parameter (ψ') is equal to zero (i.e. without the consideration of time-dependent and coupling effects, $\Lambda = 0$), the homogeneous first order dissipation function in Equation (4.14) can be written as follows:

$$\delta\Phi = \sqrt{A^2\left(\dot{\varepsilon}_v^{vp}\right)^2 + B^2\left(\dot{\varepsilon}_q^{vp}\right)^2} \tag{B-1}$$

As discussed in Nguyen et al. (2014), the internal plastic energy per unit volume (dW_{in}) available for the energy dissipation of a soil sample in the triaxial test under the applied mean effective stress (p') and the deviatoric stress (q) can be expressed as follows:

$$dW_{in} = p' \cdot \dot{\varepsilon}_v^{vp} + q \cdot \dot{\varepsilon}_q^{vp} \tag{B-2}$$

Combining Equations (B-1) and (B-2), the resulting energy equation proposed in this study can be expressed as follows:

$$p' \cdot \dot{\varepsilon}_v^{vp} + q \cdot \dot{\varepsilon}_q^{vp} = \sqrt{A^2\left(\dot{\varepsilon}_v^{vp}\right)^2 + B^2\left(\dot{\varepsilon}_q^{vp}\right)^2} \tag{B-3}$$

Substituting the stress-like quantities (i.e. functions A and B), which are defined in Equation (4.14), into Equation (B-3), along with the expansion and simplification, yields:

$$2p'q \cdot \dot{\varepsilon}_v^{vp}\dot{\varepsilon}_q^{vp} + q^2 \cdot \left(\dot{\varepsilon}_q^{vp}\right)^2 = (Mp'[1 - \alpha + \alpha\gamma])^2 \cdot \left(\dot{\varepsilon}_q^{vp}\right)^2 \tag{B-4}$$

Dividing both sides by $\dot{\varepsilon}_q^{vp}$ leads to:

$$2p'q \cdot \dot{\varepsilon}_v^{vp} + q^2 \cdot \dot{\varepsilon}_q^{vp} = (Mp'[1 - \alpha + \alpha\gamma])^2 \cdot \dot{\varepsilon}_q^{vp} \tag{B-5}$$

By re-arranging Equation (B-5), the flow rule can be obtained as follows:

$$\frac{\dot{\varepsilon}_v^{vp}}{\dot{\varepsilon}_q^{vp}} = \frac{(Mp'[1-\alpha+\alpha\gamma])^2 - q^2}{2p'q} \quad \text{(B-6)}$$

Substituting the stress ratio (i.e. $\eta = q/p$) into Equation (B-6) results in the flow rule taking the following form:

$$\frac{\dot{\varepsilon}_v^{vp}}{\dot{\varepsilon}_q^{vp}} = \frac{(M[1-\alpha+\alpha\gamma])^2 - \eta^2}{2\eta} \quad \text{(B-7)}$$

When $\alpha = 1$ and $\gamma = 1$, the following relationship can be deduced from Equation (B-7):

$$\frac{\dot{\varepsilon}_v^{vp}}{\dot{\varepsilon}_q^{vp}} = \frac{M^2 - \eta^2}{2\eta} \quad \text{(B-8)}$$

As determined in Equation (B-8), the associated flow rule obtained in the Modified Cam-clay model can be recovered only when $\alpha = 1$ and $\gamma = 1$. If α and γ values are other than one, i.e. the functions A and B consisting of effective stress components, it can be stated that the dissipation function in Equation (B-1) depends explicitly on effective stress component. As discussed earlier, the non-associated flow rule is derived naturally by postulating the stress-dependent dissipation ($\delta\Phi$) function.

Appendix C: Derivation of Non-Associated Flow Rule for extended Model

Without considering time- or rate-dependent effects, i.e. time-dependent viscosity scaling function $\Lambda = 0$, the dissipation increment function in Equation (4.38) is expressed as follows:

$$\delta\Phi = \sqrt{A^2\left(\dot{\varepsilon}_v^{vp} + \beta\dot{\varepsilon}_q^{vp}\right)^2 + B^2\left(\dot{\varepsilon}_q^{vp}\right)^2} \tag{C-1}$$

When a soil sample is subjected to the applied mean effective stress (p') and the deviatoric stress (q) in a triaxial test, the internal plastic energy per unit volume (dW_{in}) available for the energy dissipation (Lai et al., 2016) is conveyed as follows:

$$dW_{in} = p' \cdot \dot{\varepsilon}_v^{vp} + q \cdot \dot{\varepsilon}_q^{vp} \tag{C-2}$$

Combining Equations (C-1) and (C-2), the resulting energy equation in the extended model is expressed as follows:

$$p' \cdot \dot{\varepsilon}_v^{vp} + q \cdot \dot{\varepsilon}_q^{vp} = \sqrt{A^2\left(\dot{\varepsilon}_v^{vp} + \beta\dot{\varepsilon}_q^{vp}\right)^2 + B^2\left(\dot{\varepsilon}_q^{vp}\right)^2} \tag{C-3}$$

Substituting functions A and B, defined in Equation (4.38), into Equation (C-3), along with the expansion and simplification, results as follows:

$$\begin{aligned} &2p'q \cdot \dot{\varepsilon}_v^{vp}\dot{\varepsilon}_q^{vp} + q^2 \cdot \left(\dot{\varepsilon}_q^{vp}\right)^2 \\ &= 2\beta(p')^2 \cdot \dot{\varepsilon}_v^{vp}\dot{\varepsilon}_q^{vp} + \beta^2(p')^2 \cdot \left(\dot{\varepsilon}_q^{vp}\right)^2 + (Mp'[1-\alpha+\alpha\gamma])^2 \cdot \left(\dot{\varepsilon}_q^{vp}\right)^2 \end{aligned} \tag{C-4}$$

Dividing both sides by $\dot{\varepsilon}_q^{vp}$ leads to:

$$\begin{aligned} &2p'q \cdot \dot{\varepsilon}_v^{vp} + q^2 \cdot \dot{\varepsilon}_q^{vp} \\ &= 2\beta(p')^2 \cdot \dot{\varepsilon}_v^{vp} + \beta^2(p')^2 \cdot \dot{\varepsilon}_q^{vp} + (Mp'[1-\alpha+\alpha\gamma])^2 \cdot \dot{\varepsilon}_q^{vp} \end{aligned} \tag{C-5}$$

Re-arranging Equation (C-5) results in the viscoplastic flow rule being derived as follows:

$$\frac{\dot{\varepsilon}_v^{vp}}{\dot{\varepsilon}_q^{vp}} = \frac{\beta^2(p')^2 + (Mp'[1-\alpha+\alpha\gamma])^2 - q^2}{2p'q - 2\beta(p')^2} \quad \text{(C-6)}$$

Substituting the stress ratio (i.e. $\eta = q/p$) into Equation (C-6) results in the flow rule taking the following form:

$$\frac{\dot{\varepsilon}_v^{vp}}{\dot{\varepsilon}_q^{vp}} = \frac{\beta^2 + (M[1-\alpha+\alpha\gamma])^2 - \eta^2}{2(\eta - \beta)} \quad \text{(C-7)}$$

When α and γ values are equal to 1 and $\beta = 0$ in Equation (C-7), the following familiar expression can be obtained:

$$\frac{\dot{\varepsilon}_v^{vp}}{\dot{\varepsilon}_q^{vp}} = \frac{M^2 - \eta^2}{2\eta} \quad \text{(C-8)}$$

Therefore, the associated flow rule obtained in the MCC model can be retraced only when $\alpha = 1$, $\gamma = 1$ and $\beta = 0$. Therefore, dissipation function in Equation (C-1) being dependent explicitly upon the inclusion of effective stress components, as part of functions A and B, i.e. when α and γ values are other than one, results in the natural derivation of non-associated flow behaviour.

Appendix D: Non-Associated Flow Rule using Parametric Representation

When $\psi = 0$, (i.e. without the consideration of time-dependent and coupling effects), the homogeneous first order dissipation function in Equation (4.38) results in:

$$\delta\Phi = \sqrt{A^2\left(\dot{\varepsilon}_v^{vp} + \beta\dot{\varepsilon}_q^{vp}\right)^2 + B^2\left(\dot{\varepsilon}_q^{vp}\right)^2} \tag{D-1}$$

The volumetric and deviatoric components of the dissipative stresses, (i.e. p_D and q_D), can then be derived from the force potential function determined in Equation (D-1) as follows:

$$p_D = \frac{\partial(\delta\Phi)}{\partial(\dot{\varepsilon}_v^{vp})} = \frac{A^2\left(\dot{\varepsilon}_v^{vp} + \beta\dot{\varepsilon}_q^{vp}\right)}{\delta\Phi} \tag{D-2}$$

$$q_D = \frac{\partial(\delta\Phi)}{\partial(\dot{\varepsilon}_q^{vp})} = \frac{A^2 \cdot \beta\left(\dot{\varepsilon}_v^{vp} + \beta\dot{\varepsilon}_q^{vp}\right) + B^2\dot{\varepsilon}_q^{vp}}{\delta\Phi} \tag{D-3}$$

From Equations (D-2) and (D-3), it follows that:

$$q_D - p_D \cdot \beta = \frac{B^2\dot{\varepsilon}_q^{vp}}{\delta\Phi} \tag{D-4}$$

Re-arranging Equation (D-2) provides:

$$\dot{\varepsilon}_v^{vp} = \frac{p_D \cdot \delta\Phi}{A^2} - \beta\dot{\varepsilon}_q^{vp} \tag{D-5}$$

Re-arranging Equation (D-4) provides:

$$\dot{\varepsilon}_q^{vp} = \frac{(q_D - p_D \cdot \beta)\delta\Phi}{B^2} \tag{D-6}$$

Substituting Equation (D-6) into Equation (D-5), it follows that:

$$\dot{\varepsilon}_v^{vp} = \delta\Phi\left\{\frac{p_D}{A^2} - \beta\frac{(q_D - p_D \cdot \beta)}{B^2}\right\} \tag{D-7}$$

Substituting Equations (D-6) and (D-7) into Equation (D-1) and eliminating the plastic strain increments provides:

$$\frac{p_D^2}{A^2} + \frac{(q_D - p_D \cdot \beta)^2}{B^2} - 1 = 0 \tag{D-8}$$

It can be noted that the above expression in Equation (D-8) is identical to the critical surface equation obtained in Equation (4.44).

Using the expressions for viscoplastic strain increment vectors, $\dot{\varepsilon}_v^{vp}$ and $\dot{\varepsilon}_q^{vp}$ from Equations (D-7) and (D-6), respectively, the flow rule can be obtained as follows:

$$-\frac{\dot{\varepsilon}_v^{vp}}{\dot{\varepsilon}_q^{vp}} = \frac{\delta\Phi\left\{\frac{p_D}{A^2} - \beta\frac{(q_D - p_D \cdot \beta)}{B^2}\right\}}{\frac{(q_D - p_D \cdot \beta)\delta\Phi}{B^2}} = -\frac{{p_D}/{A^2}}{{(q_D - p_D \cdot \beta)}/{B^2}} + \beta \tag{D-9}$$

The resulting expression in Equation (D-9) is inconvenient for calculations and it is preferable to take advantage of the elliptical shape of the critical surface in dissipative stress space (Collins & Hilder, 2002).

From Figure 4.7, the parametric angle ω is chosen so that it is zero on the positive q_D axis. It follows that:

$$p_D = A\,cos\omega \tag{D-10a}$$

$$q_D = A\,cos\omega \cdot \beta + B\,sin\omega \tag{D-10b}$$

Simplifying Equation (D-9), the following relationship between the dilation and parametric angles can be obtained:

$$\tan\psi \equiv -\frac{\dot{\varepsilon}_v^{vp}}{\dot{\varepsilon}_q^{vp}} = \beta - \left({B}/{A}\right)\cot\omega \tag{D-11}$$

Appendix E: Sample MATLAB Codes for the Application of Proposed Hyper-viscoplastic Constitutive Models

E.1 MATLAB Code for Strain-controlled Undrained Compression Tests on Osaka Clay

```
function UndrainedShearing_StrainControlled_OsakaClay

%% For Strain-controlled Undrained Compression Tests on Osaka Clay
close all;
clear;
clc;

%% Undrained Compression Test - Strain-Controlled

%     Lambda = input('Enter the Lambda value (eg., 0.355) = ');
%     Kappa = input('Enter the Kappa value (eg., 0.047) = ');
%     Mu = input('Enter the Mu value (eg., 0.006) = ');
%     M_c = input('Enter the value for M in compression (eg., 1.278) = ');
%     M_e = input('Enter the value for M in extension (eg., 0.95) = ');
%     e0 = input('Enter the initial void ratio (eg., 2.41) = ');
%     nu = input('Enter the value for Poisson Ratio (eg.,0.3) = ');
%     p0 = input('Enter the value for initial Applied pressure (kPa) = ');
%     Pc0 = input('Enter the value for initial Pre-consolidation pressure
(kPa = ');
%     q0 = input('Enter the value for initial Deviatoric Pressure (kPa) =
');
%
%     Alpha = input('Enter the Alpha value (0<=Alpha<=1) = ');
%     Gamma = input('Enter the Gamma value (0<=Gamma<=1) = ');
%     theta = input('Enter the initial inclination angle value for Coupling
= ');
%
%     StrainQ_Rate = input('Enter the value for Controlled Deviatoric
Strain Rate = ');
%     t = input('Enter the value for reference time parameter = ');

%% Model Parameters
    Lambda = 0.355;
    Kappa = 0.047;
    M_c = 1.278;
    e0 = 2.41;
    nu = 0.3;
    Mu = 0.0142; % Determined from C-Alpha Value

    Alpha = 1;
    Gamma = 0.95;
    theta = 0;
```

```
%% Test Number - 1
    p0 = 176.4;         % OCR=1
    Pc0 = 176.4;

%% Test Number - 2
%     p0 = 235.2;       % OCR=1
%     Pc0 = 235.2;

    q0 = 0;

    StrainQ_Rate = 0.144; % 14.40%/Day
    t = 1; % Day

    V0 = e0+1;
    eR = 0;
    m = 1;

    Omega = (Lambda-Kappa)/Mu;

    % Undrained Shearing - No Volume Change
    dV = 0;
    V = V0;
    e = e0;

    % Coupling
    theta_radian=theta*(pi/180);
    Beta = tan(theta_radian);

    %% Determine Initial Values
    Stress_R0 = q0/p0;

    K0 = (V/Kappa)*p0;
    G0 = (3*(1-2*nu)*K0)/(2*(1+nu));

    syms Peq0

    A0 = (1-Gamma)*p0 + 0.5*Gamma*Peq0;
    B0 = (1-Alpha)*M_c*p0 + 0.5*Alpha*Gamma*M_c*Peq0;
    C_Surface = sqrt((((p0-0.5*Gamma*Peq0)^2)/A0^2) + (((q0-
Beta*p0)^2)/B0^2)) - 1;
    eqn = C_Surface == 0;
    Peq0 = vpasolve(eqn,Peq0);
    Peq0 = double(Peq0);

    % Applied Shear Strain Rate - 30%/Day
    StrainQ = 0; % Initial Shear Strain

    t0 = 0.0001;

    dStrainQ0 = StrainQ_Rate*t0;

    dStrain_vpQ_Rate0 = 0;
    dStrain_vpQ0 = dStrain_vpQ_Rate0*t0;
    dStrain_eQ0 = dStrainQ0 - dStrain_vpQ0;
    dq0 = dStrain_eQ0*3*G0;
```

```
    dStrain_vpV_Rate0 = (Mu./V).*(((e-eR)./e0).^m).*(1./t).*((M_c^2-
Stress_R0^2)./(M_c^2-Beta^2)).*(Peq0./Pc0).^Omega;

    dStrain_vpV0 = dStrain_vpV_Rate0*t0;
    dStrain_eV0 = -dStrain_vpV0;
    dp0 = dStrain_eV0.*K0;

    dPc0 = ((Pc0*V)./(Lambda-Kappa)).*(dStrain_vpV0 + Beta.*dStrain_vpQ0);

    % Initial Values at t0
    dp = dp0;
    p = p0+dp;
    dq = dq0;
    q = dq;
    dPc = dPc0;
    Pc = Pc0+dPc;
    StrainQ = StrainQ+dStrainQ0;
    Stress_R = q/p;

    K = (V/Kappa)*p;
    G = (3*(1-2*nu)*K)/(2*(1+nu));

    syms Peq

    A = (1-Gamma)*p + 0.5*Gamma*Peq;
    B = (1-Alpha)*M_c*p + 0.5*Alpha*Gamma*M_c*Peq;
    C_Surface = sqrt((((p-0.5*Gamma*Peq)^2)/A^2) + (((q-Beta*p)^2)/B^2)) -
1;
    eqn = C_Surface == 0;
    Peq = vpasolve(eqn,Peq);
    Peq = double(Peq);

    % Write Initial Values into Excel File
    y01 = sprintf('%6.4f', t0);
    y02 = sprintf('%18.15f',dStrainQ0);
    y03 = sprintf('%18.15f',StrainQ);
    y04 = sprintf('%18.15f',dStrain_vpQ_Rate0);
    y05 = sprintf('%18.15f',dStrain_vpQ0);
    y06 = sprintf('%18.15f',dStrain_eQ0);
    y07 = sprintf('%18.15f',dq0);
    y08 = sprintf('%18.15f',q);
    y09 = sprintf('%18.15f',dStrain_vpV_Rate0);
    y010 = sprintf('%18.15f',dStrain_vpV0);
    y011 = sprintf('%18.15f',dStrain_eV0);
    y012 = sprintf('%18.15f',dp0);
    y013 = sprintf('%18.15f',p);
    y014 = sprintf('%18.15f',dPc0);
    y015 = sprintf('%18.15f',Pc);
    y016 = sprintf('%18.15f',Stress_R);
    y017 = sprintf('%18.15f',Peq);
    filename='Test Simulations for Osaka Clay_Test Number_1.xls';

Y0={y01,y02,y03,y04,y05,y06,y07,y08,y09,y010,y011,y012,y013,y014,y015,y016,
y017};
    sheet=1;
    z0=sprintf('E%d',9);
    xlswrite(filename,Y0,sheet,z0)

    %% Commence Integration Procedure
    tol = 1e-9;
```

```
    i_size = 0.0001;

    % Viscoplastic Strain Rates at t=0.002
     dStrain_vpQ_Rate = (Mu./V).*(((e-eR)./e0).^m).*(1./t).*((M_c^2-
Stress_R^2)./(M_c^2-Beta^2)).*((2*(Stress_R-Beta))./(Beta^2+(M_c^2*(1-
Alpha+Alpha*Gamma).^2)-Stress_R^2)).*(Peq./Pc).^Omega;
     dStrain_vpV_Rate = (Mu./V).*(((e-eR)./e0).^m).*(1./t).*((M_c^2-
Stress_R^2)./(M_c^2-Beta^2)).*(Peq./Pc).^Omega;

    dt = 0.0001;
    a = 1;

    StrainQ = dStrainQ0;

    tf = 1;
    iter = tf/dt;
    iter = round(iter);

    coder.varsize('Y1');
    Y1 = zeros(iter,17);

    while dt < tf
        i_size = min(i_size, tf-dt);

        dStrainQ = i_size*StrainQ_Rate;
        StrainQ = StrainQ+dStrainQ;

        Qk1 = i_size*Q_f(dt,dStrain_vpQ_Rate);
        Qk2 = i_size*Q_f(dt+i_size/4, dStrain_vpQ_Rate+Qk1/4);
        Qk3 = i_size*Q_f(dt+3*i_size/8,
dStrain_vpQ_Rate+3*Qk1/32+9*Qk2/32);
        Qk4 = i_size*Q_f(dt+12*i_size/13, dStrain_vpQ_Rate+1932*Qk1/2197-
7200*Qk2/2197+7296*Qk3/2197);
        Qk5 = i_size*Q_f(dt+i_size, dStrain_vpQ_Rate+439*Qk1/216-
8*Qk2+3680*Qk3/513-845*Qk4/4104);
        Qk6 = i_size*Q_f(dt+i_size/2, dStrain_vpQ_Rate-8*Qk1/27+2*Qk2-
3544*Qk3/2565+1859*Qk4/4104-11*Qk5/40);
        Q_w1 = dStrain_vpQ_Rate + 25*Qk1/216+1408*Qk3/2565+2197*Qk4/4104-
Qk5/5;
        Q_w2 = dStrain_vpQ_Rate +
16*Qk1/135+6656*Qk3/12825+28561*Qk4/56430-9*Qk5/50+2*Qk6/55;
        Q_R = abs(Q_w1-Q_w2)/i_size;
        Q_delta = 0.84*(tol./Q_R).^(1/4);

        Vk1 = i_size*V_f(dt,dStrain_vpV_Rate);
        Vk2 = i_size*V_f(dt+i_size/4, dStrain_vpV_Rate+Vk1/4);
        Vk3 = i_size*V_f(dt+3*i_size/8,
dStrain_vpV_Rate+3*Vk1/32+9*Vk2/32);
        Vk4 = i_size*V_f(dt+12*i_size/13, dStrain_vpV_Rate+1932*Vk1/2197-
7200*Vk2/2197+7296*Vk3/2197);
        Vk5 = i_size*V_f(dt+i_size, dStrain_vpV_Rate+439*Vk1/216-
8*Vk2+3680*Vk3/513-845*Vk4/4104);
        Vk6 = i_size*V_f(dt+i_size/2, dStrain_vpV_Rate-8*Vk1/27+2*Vk2-
3544*Vk3/2565+1859*Vk4/4104-11*Vk5/40);
        V_w1 = dStrain_vpV_Rate + 25*Vk1/216+1408*Vk3/2565+2197*Vk4/4104-
Vk5/5;
        V_w2 = dStrain_vpV_Rate +
16*Vk1/135+6656*Vk3/12825+28561*Vk4/56430-9*Vk5/50+2*Vk6/55;
        V_R = abs(V_w1-V_w2)/i_size;
```

```
        V_delta = 0.84*(tol./V_R).^(1/4);

        if (rms(Q_delta) >= 2) && (rms(V_delta) >= 2)
            dStrain_vpQ_Rate = Q_w1;
            dStrain_vpV_Rate = V_w1;

        elseif (rms(Q_delta) >=1) && (rms(Q_delta) >=1)
            dStrain_vpQ_Rate = Q_w1;
            dStrain_vpV_Rate = V_w1;
        end

        dStrain_vpQ = dStrain_vpQ_Rate*i_size;
        dStrain_eQ = dStrainQ - dStrain_vpQ;
        dq = dStrain_eQ*3*G;
        q = q + dq;

        dStrain_vpV = dStrain_vpV_Rate*i_size;
        dStrain_eV = -dStrain_vpV;
        dp = dStrain_eV.*K;
        p = p + dp;

        K = (V/Kappa)*p;
        G = (3*(1-2*nu)*K)/(2*(1+nu));

        Stress_R = q/p;

        dPc = ((Pc*V)./(Lambda-Kappa)).*(dStrain_vpV + Beta.*dStrain_vpQ);
        Pc = Pc + dPc;

        syms Peq

        A = (1-Gamma).*p + 0.5*Gamma.*Peq;
        B = (1-Alpha).*M_c.*p + 0.5*Alpha.*Gamma.*M_c.*Peq;
        C_Surface = sqrt((((p-0.5*Gamma*Peq).^2)./A.^2) + (((q-
Beta*p).^2)./B.^2)) - 1;
        eqn = C_Surface == 0;
        Peq = vpasolve(eqn,Peq);
        Peq = double(Peq);

          %% Plot Data
%         figure(1);
%         hold on
%         plot(StrainQ,q,'o');
%         xlabel('\epsilon_q');
%         ylabel('q (kPa)');
%         ax = gca;
%         ax.XAxisLocation = 'origin';
%         ax.YAxisLocation = 'origin';

          %% Write Data into Excel File
%         y1 = sprintf('%6.4f', dt+0.001);
%         y2= sprintf('%18.15f',dStrainQ);
%         y3= sprintf('%18.15f',StrainQ);
%         y4 = sprintf('%18.15f',dStrain_vpQ_Rate);
%         y5 = sprintf('%18.15f',dStrain_vpQ);
%         y6 = sprintf('%18.15f',dStrain_eQ);
%         y7 = sprintf('%18.15f',dq);
%         y8 = sprintf('%18.15f',q);
%         y9 = sprintf('%18.15f',dStrain_vpV_Rate);
```

```
%          y10 = sprintf('%18.15f',dStrain_vpV);
%          y11 = sprintf('%18.15f',dStrain_eV);
%          y12 = sprintf('%18.15f',dp);
%          y13 = sprintf('%18.15f',p);
%          y14 = sprintf('%18.15f',dPc);
%          y15 = sprintf('%18.15f',Pc);
%          y16= sprintf('%18.15f',Stress_R);
%          y17= sprintf('%18.15f',Peq);
%          Y1={y1,y2,y3,y4,y5,y6,y7,y8,y9,y10,y11,y12,y13,y14,y15,y16,y17};
%          sheet=1;
%          z1=sprintf('E%d',a+10);
%          xlswrite(filename,Y1,sheet,z1)

        Y1(a,:)= [dt+0.0001 dStrainQ StrainQ dStrain_vpQ_Rate dStrain_vpQ
dStrain_eQ dq q dStrain_vpV_Rate dStrain_vpV dStrain_eV dp p dPc Pc
Stress_R Peq];

        dStrain_vpQ_Rate = (Mu./V).*(((e-eR)./e0).^m).*(1./t).*((M_c^2-
Stress_R^2)./(M_c^2-Beta^2)).*((2*(Stress_R-Beta))./(Beta^2+(M_c^2*(1-
Alpha+Alpha*Gamma).^2)-Stress_R^2)).*(Peq./Pc).^Omega;
        dStrain_vpV_Rate = (Mu./V).*(((e-eR)./e0).^m).*(1./t).*((M_c^2-
Stress_R^2)./(M_c^2-Beta^2)).*(Peq./Pc).^Omega;

        if (rms(Q_delta) >= 2) && (rms(V_delta) >= 2)
            i_size = 2*i_size;
            dt = dt+i_size;
            a = a+1;

        elseif (rms(Q_delta) >=1) && (rms(Q_delta) >=1)
            dt = dt+i_size;
            a = a+1;

        elseif rms(Q_delta) < 1
            i_size = 0.5*i_size;
            dt = dt + i_size;
            a = a+1;
        end

    end

    %% Write Data into Excel File
    xlswrite(filename,Y1,sheet,'E10');

    function dStrain_vpQ = Q_f(dt,dStrain_vpQ_Rate)
        dStrain_vpQ = dStrain_vpQ_Rate*dt;
    end

    function dStrain_vpV = V_f(dt,dStrain_vpV_Rate)
        dStrain_vpV = dStrain_vpV_Rate*dt;
    end

end
```

E.2 MATLAB Code for Stress-controlled Undrained Compression Tests on HKMD Clay

```
function UndrainedShearing_StressControlled_HKMD

%% For Stress-controlled Undrained Compression Tests on HKMD Clay
close all;
clear;
clc;

%% Undrained Compression Test - Stress-Controlled

%     Lambda = input('Enter the Lambda value (eg., 0.1987) = ');
%     Kappa = input('Enter the Kappa value (eg., 0.0451) = ');
%     Mu = input('Enter the Mu value (eg., 0.00627) = ');
%     M_c = input('Enter the value for M in compression (eg., 1.265 = ');
%     M_e = input('Enter the value for M in extension (eg., 0.95) = ');
%     V0 = input('Enter the initial Specific Volume (eg., 2.506266) = ');
%     nu = input('Enter the value for Poisson Ratio (eg.,0.3) = ');
%     p0 = input('Enter the value for initial Applied pressure (kPa) = ');
%     Pc0 = input('Enter the value for initial Pre-consolidation pressure
(kPa = ');
%     q0 = input('Enter the value for initial Deviatoric Pressure (kPa) =
');
%
%     Alpha = input('Enter the Alpha value (0<=Alpha<=1) = ');
%     Gamma = input('Enter the Gamma value (0<=Gamma<=1) = ');
%     theta = input('Enter the initial inclination angle value for Coupling
= ');
%
%     StressQ_Rate = input('Enter the value for Controlled Deviatoric
Stress Rate = ');
%     t = input('Enter the value for reference time parameter = ');

    %% Model Parameters
    Lambda = 0.1987;
    Kappa = 0.0451;
    M_c = 1.265;
    V0 = 2.506266;
    nu = 0.3;
    Mu = 0.00627;

    Alpha = 1;
    Gamma = 0.925;
    theta = 0;

    %% Applied Pressures
    p0 = 400;
    Pc0 = 400;
    q0 = 0;

    StressQ_Rate = 0.125; % Deviatoric stress rate of 30kPa/Hour
    t = 24; % Hour

    e0 = V0-1;
```

```
    eR = 0;
    m = 1.0881;

    Omega = (Lambda-Kappa)/Mu;

    % Undrained Shearing - No Volume Change
    dV = 0;
    V = V0;
    e = e0;

    % Coupling
    theta_radian=theta*(pi/180);
    Beta = tan(theta_radian);

    %% Determine Initial Values
    Stress_R0 = q0/p0;

    K0 = (V/Kappa)*p0;
    G0 = (3*(1-2*nu)*K0)/(2*(1+nu));

    syms Peq0

    A0 = (1-Gamma)*p0 + 0.5*Gamma*Peq0;
    B0 = (1-Alpha)*M_c*p0 + 0.5*Alpha*Gamma*M_c*Peq0;
    C_Surface = sqrt((((p0-0.5*Gamma*Peq0)^2)/A0^2) + (((q0-
Beta*p0)^2)/B0^2)) - 1;
    eqn = C_Surface == 0;
    Peq0 = vpasolve(eqn,Peq0);
    Peq0 = double(Peq0);

    % Applied Shear Strain Rate - 30%/Day
    Strain_Qi = 0; % Initial Shear Strain
    Stress_Qi = 0; % Initial Shear Stress
    Strain_Vi = 0; % Intial Volumetric Strain

    t0 = 0.02;
    dq0 = StressQ_Rate*t0; %     dStrainQ0 = StrainQ_Rate*t0;

    dStrain_vpV_Rate0 = (Mu./V).*(((e-eR)./e0).^m).*(1./t).*((M_c^2-
Stress_R0^2)./(M_c^2-Beta^2)).*(Peq0./Pc0).^Omega;
    dStrain_vpV0 = dStrain_vpV_Rate0*t0;
    dStrain_eV0 = -dStrain_vpV0;
    dp0 = dStrain_eV0.*K0;

    dStrain_eQ0 = dq0/(3*G0); % dStrain_eQ0 = dStrainQ0 - dStrain_vpQ0;
    dStrain_vpQ_Rate0 = 0;
    dStrain_vpQ0 = dStrain_vpQ_Rate0*t0;
    dStrain_Q0 = dStrain_eQ0 + dStrain_vpQ0;
    Strain_Q0 = Strain_Qi + dStrain_Q0;

    dPc0 = ((Pc0*V)./(Lambda-Kappa)).*(dStrain_vpV0 + Beta.*dStrain_vpQ0);

    % Initial Values at t0
    dp = dp0;
    p = p0+dp;
    dq = dq0;
    q = Stress_Qi+dq;
    dPc = dPc0;
    Pc = Pc0+dPc;
```

```
    Stress_R = q/p;
    Strain_Q = Strain_Q0;

    K = (V/Kappa)*p;
    G = (3*(1-2*nu)*K)/(2*(1+nu));

    syms Peq

    A = (1-Gamma)*p + 0.5*Gamma*Peq;
    B = (1-Alpha)*M_c*p + 0.5*Alpha*Gamma*M_c*Peq;
    C_Surface = sqrt((((p-0.5*Gamma*Peq)^2)/A^2) + (((q-Beta*p)^2)/B^2)) -
1;
    eqn = C_Surface == 0;
    Peq = vpasolve(eqn,Peq);
    Peq = double(Peq);

    % Write Initial Values into Excel File
    y01 = sprintf('%18.15f',t0);
    y02 = sprintf('%18.15f',dq0);
    y03 = sprintf('%18.15f',q);
    y04 = sprintf('%18.15f',dStrain_vpV_Rate0);
    y05 = sprintf('%18.15f',dStrain_vpV0);
    y06 = sprintf('%18.15f',dStrain_eV0);
    y07 = sprintf('%18.15f',dp0);
    y08 = sprintf('%18.15f',p);
    y09 = sprintf('%18.15f',dStrain_eQ0);
    y010 = sprintf('%18.15f',dStrain_vpQ_Rate0);
    y011 = sprintf('%18.15f',dStrain_vpQ0);
    y012 = sprintf('%18.15f',dStrain_Q0);
    y013 = sprintf('%18.15f',Strain_Q0);
    y014 = sprintf('%18.15f',Peq);
    y015 = sprintf('%18.15f',dPc0);
    y016 = sprintf('%18.15f',Pc);
    y017 = sprintf('%18.15f',Stress_R);
    y018 = sprintf('%18.15f',V);

    filename='Test Simulations_Stress-controlled for HKMD Clay.xls';

Y0={y01,y02,y03,y04,y05,y06,y07,y08,y09,y010,y011,y012,y013,y014,y015,y016,
y017,y018};
    sheet=2;
    z0=sprintf('E%d',9);
    xlswrite(filename,Y0,sheet,z0)

    %% Commence Integration Procedure
    tol = 1e-9;
    i_size = 0.02;

    % Viscoplastic Strain Rates at t=0.002
     dStrain_vpQ_Rate = (Mu./V).*(((e-eR)./e0).^m).*(1./t).*((M_c^2-
Stress_R^2)./(M_c^2-Beta^2)).*((2*(Stress_R-Beta))./(Beta^2+(M_c^2*(1-
Alpha+Alpha*Gamma).^2)-Stress_R^2)).*(Peq./Pc).^Omega;
     dStrain_vpV_Rate = (Mu./V).*(((e-eR)./e0).^m).*(1./t).*((M_c^2-
Stress_R^2)./(M_c^2-Beta^2)).*(Peq./Pc).^Omega;

    dt = 0.02;
    a = 1;

    tf = 400;
```

```
    iter = tf/dt;

    coder.varsize('Y1');
    Y1 = zeros(iter,18);

    while dt < tf
        i_size = min(i_size, tf-dt);

        dq = i_size*StressQ_Rate;
        q = q+dq;

        Qk1 = i_size*Q_f(dt,dStrain_vpQ_Rate);
        Qk2 = i_size*Q_f(dt+i_size/4, dStrain_vpQ_Rate+Qk1/4);
        Qk3 = i_size*Q_f(dt+3*i_size/8,
dStrain_vpQ_Rate+3*Qk1/32+9*Qk2/32);
        Qk4 = i_size*Q_f(dt+12*i_size/13, dStrain_vpQ_Rate+1932*Qk1/2197-
7200*Qk2/2197+7296*Qk3/2197);
        Qk5 = i_size*Q_f(dt+i_size, dStrain_vpQ_Rate+439*Qk1/216-
8*Qk2+3680*Qk3/513-845*Qk4/4104);
        Qk6 = i_size*Q_f(dt+i_size/2, dStrain_vpQ_Rate-8*Qk1/27+2*Qk2-
3544*Qk3/2565+1859*Qk4/4104-11*Qk5/40);
        Q_w1 = dStrain_vpQ_Rate + 25*Qk1/216+1408*Qk3/2565+2197*Qk4/4104-
Qk5/5;
        Q_w2 = dStrain_vpQ_Rate +
16*Qk1/135+6656*Qk3/12825+28561*Qk4/56430-9*Qk5/50+2*Qk6/55;
        Q_R = abs(Q_w1-Q_w2)/i_size;
        Q_delta = 0.84*(tol./Q_R).^(1/4);

        Vk1 = i_size*V_f(dt,dStrain_vpV_Rate);
        Vk2 = i_size*V_f(dt+i_size/4, dStrain_vpV_Rate+Vk1/4);
        Vk3 = i_size*V_f(dt+3*i_size/8,
dStrain_vpV_Rate+3*Vk1/32+9*Vk2/32);
        Vk4 = i_size*V_f(dt+12*i_size/13, dStrain_vpV_Rate+1932*Vk1/2197-
7200*Vk2/2197+7296*Vk3/2197);
        Vk5 = i_size*V_f(dt+i_size, dStrain_vpV_Rate+439*Vk1/216-
8*Vk2+3680*Vk3/513-845*Vk4/4104);
        Vk6 = i_size*V_f(dt+i_size/2, dStrain_vpV_Rate-8*Vk1/27+2*Vk2-
3544*Vk3/2565+1859*Vk4/4104-11*Vk5/40);
        V_w1 = dStrain_vpV_Rate + 25*Vk1/216+1408*Vk3/2565+2197*Vk4/4104-
Vk5/5;
        V_w2 = dStrain_vpV_Rate +
16*Vk1/135+6656*Vk3/12825+28561*Vk4/56430-9*Vk5/50+2*Vk6/55;
        V_R = abs(V_w1-V_w2)/i_size;
        V_delta = 0.84*(tol./V_R).^(1/4);

        if (rms(Q_delta) >= 2) && (rms(V_delta) >= 2)
            dStrain_vpQ_Rate = Q_w1;
            dStrain_vpV_Rate = V_w1;

        elseif (rms(Q_delta) >=1) && (rms(Q_delta) >=1)
            dStrain_vpQ_Rate = Q_w1;
            dStrain_vpV_Rate = V_w1;
        end

        dStrain_vpV = dStrain_vpV_Rate*i_size;
        dStrain_eV = -dStrain_vpV;
        dp = dStrain_eV.*K;
        p = p + dp;
```

```
        dStrain_vpQ = dStrain_vpQ_Rate*i_size;
        dStrain_eQ = dq/(3*G);
        dStrain_Q = dStrain_eQ + dStrain_vpQ;
        Strain_Q = Strain_Q + dStrain_Q;

        K = (V/Kappa)*p;
        G = (3*(1-2*nu)*K)/(2*(1+nu));

        Stress_R = q/p;

        dPc = ((Pc*V)./(Lambda-Kappa)).*(dStrain_vpV + Beta.*dStrain_vpQ);
        Pc = Pc + dPc;

        syms Peq

        A = (1-Gamma).*p + 0.5*Gamma.*Peq;
        B = (1-Alpha).*M_c.*p + 0.5*Alpha.*Gamma.*M_c.*Peq;
        C_Surface = sqrt((((p-0.5*Gamma*Peq).^2)./A.^2) + (((q-
Beta*p).^2)./B.^2)) - 1;
        eqn = C_Surface == 0;
        Peq = vpasolve(eqn,Peq);
        Peq = double(Peq);

          %% Plot Data
%         figure(1);
%         hold on
%         plot(StrainQ,q,'o');
%         xlabel('\epsilon_q');
%         ylabel('q (kPa)');
%         ax = gca;
%         ax.XAxisLocation = 'origin';
%         ax.YAxisLocation = 'origin';
%
          %% Write Data into Excel File
%         y1 = sprintf('%6.4f', dt+0.001);
%         y2= sprintf('%18.15f',dStrainQ);
%         y3= sprintf('%18.15f',StrainQ);
%         y4 = sprintf('%18.15f',dStrain_vpQ_Rate);
%         y5 = sprintf('%18.15f',dStrain_vpQ);
%         y6 = sprintf('%18.15f',dStrain_eQ);
%         y7 = sprintf('%18.15f',dq);
%         y8 = sprintf('%18.15f',q);
%         y9 = sprintf('%18.15f',dStrain_vpV_Rate);
%         y10 = sprintf('%18.15f',dStrain_vpV);
%         y11 = sprintf('%18.15f',dStrain_eV);
%         y12 = sprintf('%18.15f',dp);
%         y13 = sprintf('%18.15f',p);
%         y14 = sprintf('%18.15f',dPc);
%         y15 = sprintf('%18.15f',Pc);
%         y16= sprintf('%18.15f',Stress_R);
%         y17= sprintf('%18.15f',Peq);
%         Y1={y1,y2,y3,y4,y5,y6,y7,y8,y9,y10,y11,y12,y13,y14,y15,y16,y17};
%         sheet=1;
%         z1=sprintf('E%d',a+10);
%         xlswrite(filename,Y1,sheet,z1)

        Y1(a,:)= [dt+0.02 dq q dStrain_vpV_Rate dStrain_vpV dStrain_eV dp p
dStrain_eQ dStrain_vpQ_Rate dStrain_vpQ dStrain_Q Strain_Q Peq dPc Pc
Stress_R V];
```

```
        dStrain_vpQ_Rate = (Mu./V).*(((e-eR)./e0).^m).*(1./t).*((M_c^2-
Stress_R^2)./(M_c^2-Beta^2)).*((2*(Stress_R-Beta))./(Beta^2+(M_c^2*(1-
Alpha+Alpha*Gamma).^2)-Stress_R^2)).*(Peq./Pc).^Omega;
        dStrain_vpV_Rate = (Mu./V).*(((e-eR)./e0).^m).*(1./t).*((M_c^2-
Stress_R^2)./(M_c^2-Beta^2)).*(Peq./Pc).^Omega;

        dt = dt+i_size;
        a = a+1;

       if (rms(Q_delta) >= 2) && (rms(V_delta) >= 2)
            i_size = 2*i_size;
            dt = dt+i_size;
            a = a+1;

       elseif (rms(Q_delta) >=1) && (rms(Q_delta) >=1)
            dt = dt+i_size;
            a = a+1;

       elseif rms(Q_delta) < 1
            i_size = 0.5*i_size;
            dt = dt + i_size;
            a = a+1;
       end

    end

    %% Write Data into Excel File
    xlswrite(filename,Y1,sheet,'E10');

end
```

E.3 MATLAB Code for Strain-controlled Drained Compression Tests on HKMD Clay

```
function DrainedShearing_StrainControlled_HKMDClay

%% For Strain-controlled Drained Compression Tests on HKMD Clay
close all;
clear;
clc;

%% Drained Compression Test - Strain-Controlled

%     Lambda = input('Enter the Lambda value (eg., 0.1987) = ');
%     Kappa = input('Enter the Kappa value (eg., 0.0451) = ');
%     Mu = input('Enter the Mu value (eg., 0.00627) = ');
%     M_c = input('Enter the value for M in compression (eg., 1.265 = ');
%     M_e = input('Enter the value for M in extension (eg., 0.95) = ');
%     V0 = input('Enter the initial Specific Volume (eg., 2.506266) = ');
%     nu = input('Enter the value for Poisson Ratio (eg.,0.3) = ');
%     p0 = input('Enter the value for initial Applied pressure (kPa) = ');
%     Pc0 = input('Enter the value for initial Pre-consolidation pressure
(kPa = ');
%     q0 = input('Enter the value for initial Deviatoric Pressure (kPa) =
');
%
%     Alpha = input('Enter the Alpha value (0<=Alpha<=1) = ');
%     Gamma = input('Enter the Gamma value (0<=Gamma<=1) = ');
%     theta = input('Enter the initial inclination angle value for Coupling
= ');
%
%     StrainQ_Rate = input('Enter the value for Controlled Deviatoric
Strain Rate = ');
%     t = input('Enter the value for reference time parameter = ');

    %% Model Parameters
    Lambda = 0.1987;
    Kappa = 0.0451;
    M_c = 1.265;
    V0 = 2.506266;
    nu = 0.3;
    Mu = 0.00627;

    Alpha = 1;
    Gamma = 0.9;
    theta = 0;

    %% Applied Pressures
    p0 = 200;
    Pc0 = 200;
    q0 = 0;

    StrainQ_Rate = 0.0936; % 9.36%/Day
    t = 1; % Day

    e0 = V0-1;
```

```
    eR = 0;
    m = 1.0881;

    Omega = (Lambda-Kappa)/Mu;

    % Undrained Shearing - No Volume Change
    dV = 0;
    V = V0;
    e = e0;

    % Coupling
    theta_radian=theta*(pi/180);
    Beta = tan(theta_radian);

    %% Determine Initial Values
    Stress_R0 = q0/p0;

    K0 = (V/Kappa)*p0;
    G0 = (3*(1-2*nu)*K0)/(2*(1+nu));

    syms Peq0

    A0 = (1-Gamma)*p0 + 0.5*Gamma*Peq0;
    B0 = (1-Alpha)*M_c*p0 + 0.5*Alpha*Gamma*M_c*Peq0;
    C_Surface = sqrt((((p0-0.5*Gamma*Peq0)^2)/A0^2) + (((q0-
Beta*p0)^2)/B0^2)) - 1;
    eqn = C_Surface == 0;
    Peq0 = vpasolve(eqn,Peq0);
    Peq0 = double(Peq0);

    % Applied Shear Strain Rate - 30%/Day
    StrainQ = 0; % Initial Shear Strain
    Strain_Vi = 0.2041; % Initial Volumetric Strain

    t0 = 0.0005;

    dStrainQ0 = StrainQ_Rate*t0;

    dStrain_vpQ_Rate0 = 0;
    dStrain_vpQ0 = dStrain_vpQ_Rate0*t0;
    dStrain_eQ0 = dStrainQ0 - dStrain_vpQ0;
    dq0 = dStrain_eQ0*3*G0;

    dStrain_vpV_Rate0 = (Mu./V).*(((e-eR)./e0).^m).*(1./t).*((M_c^2-
Stress_R0^2)./(M_c^2-Beta^2)).*(Peq0./Pc0).^Omega;

    dStrain_vpV0 = dStrain_vpV_Rate0*t0;
    dp0 = dq0*(1/3);
    dStrain_eV0 = (Kappa/V)*(dp0/p0);
    dStrain_V0 = Strain_Vi + dStrain_eV0 + dStrain_vpV0;
    dV = -V*dStrain_V0;
    dPc0 = ((Pc0*V)./(Lambda-Kappa)).*(dStrain_vpV0 + Beta.*dStrain_vpQ0);

    % Initial Values at t0
    dp = dp0;
    p = p0+dp;
    dq = dq0;
    q = dq;
    V = V+dV;
```

```
    dPc = dPc0;
    Pc = Pc0+dPc;
    StrainQ = StrainQ+dStrainQ0;
    Stress_R = q/p;

    e = V-1;
    K = (V/Kappa)*p;
    G = (3*(1-2*nu)*K)/(2*(1+nu));

    syms Peq

    A = (1-Gamma)*p + 0.5*Gamma*Peq;
    B = (1-Alpha)*M_c*p + 0.5*Alpha*Gamma*M_c*Peq;
    C_Surface = sqrt((((p-0.5*Gamma*Peq)^2)/A^2) + (((q-Beta*p)^2)/B^2)) -
1;
    eqn = C_Surface == 0;
    Peq = vpasolve(eqn,Peq);
    Peq = double(Peq);

    % Write Initial Values into Excel File
    y01 = sprintf('%18.15f', t0);
    y02 = sprintf('%18.15f',dStrainQ0);
    y03 = sprintf('%18.15f',StrainQ);
    y04 = sprintf('%18.15f',dStrain_vpQ_Rate0);
    y05 = sprintf('%18.15f',dStrain_vpQ0);
    y06 = sprintf('%18.15f',dStrain_eQ0);
    y07 = sprintf('%18.15f',dq0);
    y08 = sprintf('%18.15f',q);
    y09 = sprintf('%18.15f',dStrain_vpV_Rate0);
    y010 = sprintf('%18.15f',dStrain_vpV0);
    y011 = sprintf('%18.15f',dStrain_eV0);
    y012 = sprintf('%18.15f',dp0);
    y013 = sprintf('%18.15f',p);
    y014 = sprintf('%18.15f',dPc0);
    y015 = sprintf('%18.15f',Pc);
    y016 = sprintf('%18.15f',Stress_R);
    y017 = sprintf('%18.15f',Peq);
    y018 = sprintf('%18.15f',dV);
    y019 = sprintf('%18.15f',V);
    y020 = sprintf('%18.15f',e);
    filename='Test Simulations_Strain-controlled for HKMD Clay.xls';

Y0={y01,y02,y03,y04,y05,y06,y07,y08,y09,y010,y011,y012,y013,y014,y015,y016,
y017,y018,y019,y020};
    sheet=1;
    z0=sprintf('E%d',9);
    xlswrite(filename,Y0,sheet,z0)

    %% Commence Integration Procedure
    tol = 1e-9;
    i_size = 0.0005;

    % Viscoplastic Strain Rates at t=0.002
     dStrain_vpQ_Rate = (Mu./V).*(((e-eR)./e0).^m).*(1./t).*((M_c^2-
Stress_R^2)./(M_c^2-Beta^2)).*((2*(Stress_R-Beta))./(Beta^2+(M_c^2*(1-
Alpha+Alpha*Gamma).^2)-Stress_R^2)).*(Peq./Pc).^Omega;
     dStrain_vpV_Rate = (Mu./V).*(((e-eR)./e0).^m).*(1./t).*((M_c^2-
Stress_R^2)./(M_c^2-Beta^2)).*(Peq./Pc).^Omega;

    dt = 0.0005;
```

```
    a = 1;
    StrainQ = dStrainQ0;

    tf = 2.2;
    iter = tf/dt;
    iter = round(iter);

    coder.varsize('Y1');
    Y1 = zeros(iter,20);

    while dt < tf
        i_size = min(i_size, tf-dt);

        dStrainQ = i_size*StrainQ_Rate;
        StrainQ = StrainQ+dStrainQ;

        Qk1 = i_size*Q_f(dt,dStrain_vpQ_Rate);
        Qk2 = i_size*Q_f(dt+i_size/4, dStrain_vpQ_Rate+Qk1/4);
        Qk3 = i_size*Q_f(dt+3*i_size/8,
dStrain_vpQ_Rate+3*Qk1/32+9*Qk2/32);
        Qk4 = i_size*Q_f(dt+12*i_size/13, dStrain_vpQ_Rate+1932*Qk1/2197-
7200*Qk2/2197+7296*Qk3/2197);
        Qk5 = i_size*Q_f(dt+i_size, dStrain_vpQ_Rate+439*Qk1/216-
8*Qk2+3680*Qk3/513-845*Qk4/4104);
        Qk6 = i_size*Q_f(dt+i_size/2, dStrain_vpQ_Rate-8*Qk1/27+2*Qk2-
3544*Qk3/2565+1859*Qk4/4104-11*Qk5/40);
        Q_w1 = dStrain_vpQ_Rate + 25*Qk1/216+1408*Qk3/2565+2197*Qk4/4104-
Qk5/5;
        Q_w2 = dStrain_vpQ_Rate +
16*Qk1/135+6656*Qk3/12825+28561*Qk4/56430-9*Qk5/50+2*Qk6/55;
        Q_R = abs(Q_w1-Q_w2)/i_size;
        Q_delta = 0.84*(tol./Q_R).^(1/4);

        Vk1 = i_size*V_f(dt,dStrain_vpV_Rate);
        Vk2 = i_size*V_f(dt+i_size/4, dStrain_vpV_Rate+Vk1/4);
        Vk3 = i_size*V_f(dt+3*i_size/8,
dStrain_vpV_Rate+3*Vk1/32+9*Vk2/32);
        Vk4 = i_size*V_f(dt+12*i_size/13, dStrain_vpV_Rate+1932*Vk1/2197-
7200*Vk2/2197+7296*Vk3/2197);
        Vk5 = i_size*V_f(dt+i_size, dStrain_vpV_Rate+439*Vk1/216-
8*Vk2+3680*Vk3/513-845*Vk4/4104);
        Vk6 = i_size*V_f(dt+i_size/2, dStrain_vpV_Rate-8*Vk1/27+2*Vk2-
3544*Vk3/2565+1859*Vk4/4104-11*Vk5/40);
        V_w1 = dStrain_vpV_Rate + 25*Vk1/216+1408*Vk3/2565+2197*Vk4/4104-
Vk5/5;
        V_w2 = dStrain_vpV_Rate +
16*Vk1/135+6656*Vk3/12825+28561*Vk4/56430-9*Vk5/50+2*Vk6/55;
        V_R = abs(V_w1-V_w2)/i_size;
        V_delta = 0.84*(tol./V_R).^(1/4);

        if (rms(Q_delta) >= 2) && (rms(V_delta) >= 2)
            dStrain_vpQ_Rate = Q_w1;
            dStrain_vpV_Rate = V_w1;

        elseif (rms(Q_delta) >=1) && (rms(Q_delta) >=1)
            dStrain_vpQ_Rate = Q_w1;
            dStrain_vpV_Rate = V_w1;
        end
```

```
        dStrain_vpQ = dStrain_vpQ_Rate*i_size;
        dStrain_eQ = dStrainQ - dStrain_vpQ;
        dq = dStrain_eQ*3*G;
        q = q + dq;

        dStrain_vpV = dStrain_vpV_Rate*i_size;
        dp = dq*(1/3);
        dStrain_eV = (Kappa/V)*(dp/p);
        p = p + dp;
        dStrain_V = dStrain_eV + dStrain_vpV;
        dV = -V*dStrain_V;

        K = (V/Kappa)*p;
        G = (3*(1-2*nu)*K)/(2*(1+nu));

        Stress_R = q/p;

        dPc = ((Pc*V)./(Lambda-Kappa)).*(dStrain_vpV + Beta.*dStrain_vpQ);
        Pc = Pc + dPc;

        V = V+dV;
        e = V-1;

        syms Peq

        A = (1-Gamma).*p + 0.5*Gamma.*Peq;
        B = (1-Alpha).*M_c.*p + 0.5*Alpha.*Gamma.*M_c.*Peq;
        C_Surface = sqrt((((p-0.5*Gamma*Peq).^2)./A.^2) + (((q-
Beta*p).^2)./B.^2)) - 1;
        eqn = C_Surface == 0;
        Peq = vpasolve(eqn,Peq);
        Peq = double(Peq);

          %% Plot Data
%         figure(1);
%         hold on
%         plot(StrainQ,q,'o');
%         xlabel('\epsilon_q');
%         ylabel('q (kPa)');
%         ax = gca;
%         ax.XAxisLocation = 'origin';
%         ax.YAxisLocation = 'origin';

          %% Write Data into Excel File
%         y1 = sprintf('%6.4f', dt+0.001);
%         y2= sprintf('%18.15f',dStrainQ);
%         y3= sprintf('%18.15f',StrainQ);
%         y4 = sprintf('%18.15f',dStrain_vpQ_Rate);
%         y5 = sprintf('%18.15f',dStrain_vpQ);
%         y6 = sprintf('%18.15f',dStrain_eQ);
%         y7 = sprintf('%18.15f',dq);
%         y8 = sprintf('%18.15f',q);
%         y9 = sprintf('%18.15f',dStrain_vpV_Rate);
%         y10 = sprintf('%18.15f',dStrain_vpV);
%         y11 = sprintf('%18.15f',dStrain_eV);
%         y12 = sprintf('%18.15f',dp);
%         y13 = sprintf('%18.15f',p);
%         y14 = sprintf('%18.15f',dPc);
```

```
%          y15 = sprintf('%18.15f',Pc);
%          y16= sprintf('%18.15f',Stress_R);
%          y17= sprintf('%18.15f',Peq);
%          Y1={y1,y2,y3,y4,y5,y6,y7,y8,y9,y10,y11,y12,y13,y14,y15,y16,y17};
%          sheet=1;
%          z1=sprintf('E%d',a+10);
%          xlswrite(filename,Y1,sheet,z1)

        Y1(a,:)= [dt+0.0005 dStrainQ StrainQ dStrain_vpQ_Rate dStrain_vpQ
dStrain_eQ dq q dStrain_vpV_Rate dStrain_vpV dStrain_eV dp p dPc Pc
Stress_R Peq dV V e];

        dStrain_vpQ_Rate = (Mu./V).*(((e-eR)./e0).^m).*(1./t).*((M_c^2-
Stress_R^2)./(M_c^2-Beta^2)).*((2*(Stress_R-Beta))./(Beta^2+(M_c^2*(1-
Alpha+Alpha*Gamma).^2)-Stress_R^2)).*(Peq./Pc).^Omega;
        dStrain_vpV_Rate = (Mu./V).*(((e-eR)./e0).^m).*(1./t).*((M_c^2-
Stress_R^2)./(M_c^2-Beta^2)).*(Peq./Pc).^Omega;

        if (rms(Q_delta) >= 2) && (rms(V_delta) >= 2)
            i_size = 2*i_size;
            dt = dt+i_size;
            a = a+1;

        elseif (rms(Q_delta) >=1) && (rms(Q_delta) >=1)
            dt = dt+i_size;
            a = a+1;

        elseif rms(Q_delta) < 1
            i_size = 0.5*i_size;
            dt = dt + i_size;
            a = a+1;
        end

    end

    %% Write Data into Excel File
    xlswrite(filename,Y1,sheet,'E10');

    function dStrain_vpQ = Q_f(dt,dStrain_vpQ_Rate)
        dStrain_vpQ = dStrain_vpQ_Rate*dt;
    end

    function dStrain_vpV = V_f(dt,dStrain_vpV_Rate)
        dStrain_vpV = dStrain_vpV_Rate*dt;
    end

end
```

E.4 MATLAB Code for Undrained Triaxial Shearing Tests using Various Constant Strain Rates on Haney Clay

```
function UndrainedShearing_StrainControlled_HaneyClay

%% For Undrained Triaxial Shearing Tests using Various Constant Strain
Rates on Haney Clay
close all;
clear;
clc;

%% Undrained Triaxial Shearing Test - Strain-Controlled

%     Lambda = input('Enter the Lambda value (eg., 0.1055) = ');
%     Kappa = input('Enter the Kappa value (eg., 0.01635) = ');
%     Mu = input('Enter the Mu value (eg., 0.004) = ');
%     M_c = input('Enter the value for M in compression (eg., 1.2872) = ');
%     M_e = input('Enter the value for M in extension (eg., 0.95) = ');
%     e0 = input('Enter the initial void ratio (eg., 0.0896) = ');
%     nu = input('Enter the value for Poisson Ratio (eg.,0.15) = ');
%     p0 = input('Enter the value for initial Applied pressure (kPa) = ');
%     Pc0 = input('Enter the value for initial Pre-consolidation pressure
(kPa = ');
%     q0 = input('Enter the value for initial Deviatoric Pressure (kPa) =
');
%
%     Alpha = input('Enter the Alpha value (0<=Alpha<=1) = ');
%     Gamma = input('Enter the Gamma value (0<=Gamma<=1) = ');
%     theta = input('Enter the initial inclination angle value for Coupling
= ');
%
%     StrainQ_Rate = input('Enter the value for Controlled Deviatoric
Strain Rate = ');
%     t = input('Enter the value for reference time parameter = ');
;

    %% Model Parameters
    Lambda = 0.1055;
    Kappa = 0.01635;
    e0 = 0.896;
    nu = 0.15;
    M_c = 1.2872;
    Mu = 0.004;
%     Mu = 0.00001;

    Alpha = 1;
    Gamma = 0.75;
    theta = 0;

    p0 = 525;
    Pc0 = 525;
    q0 = 0;

%% Various Constant Strain Rates

%% Various Constant Strain Rate - 1
```

```
% %     StrainQ_Rate = 9.4e-06; % 0.00094%/Min
% %     StrainQ_Rate = 5.64e-04; % 0.0564%/Hr
    StrainQ_Rate = 0.013536; % 1.3536%/Day

%% Various Constant Strain Rate - 2
%     StrainQ_Rate = 0.0015; % 0.15%/Min
%     StrainQ_Rate = 0.09; % 9%/Hr
%     StrainQ_Rate = 2.16; % 216%/Day

%% Various Constant Strain Rate - 3
%         StrainQ_Rate = 0.011; % 1.10%/Min
%     StrainQ_Rate = 0.66; % 66%/Hr
%     StrainQ_Rate = 15.84; % 1584%/Day

    t = 1;

    V0 = e0+1;
    eR = 0;
    m = 1;

    Omega = (Lambda-Kappa)/Mu;

    % Undrained Shearing - No Volume Change
    dV = 0;
    V = V0;
    e = e0;

    % Coupling
    theta_radian=theta*(pi/180);
    Beta = tan(theta_radian);

    %% Determine Initial Values

    Stress_R0 = q0/p0;

    K0 = (V/Kappa)*p0;
    G0 = (3*(1-2*nu)*K0)/(2*(1+nu));

    syms Peq0

    A0 = (1-Gamma).*p0 + 0.5*Gamma.*Peq0;
    B0 = (1-Alpha).*M_c.*p0 + 0.5*Alpha.*Gamma.*M_c.*Peq0;
    C_Surface = sqrt((((p0-0.5*Gamma.*Peq0)^2)./A0^2) + (((q0-
Beta.*p0)^2)./B0^2)) - 1;
    eqn = C_Surface == 0;
    Peq0 = vpasolve(eqn,Peq0);
    Peq0 = double(Peq0);

    % Applied Shear Strain Rate - 30%/Day
    StrainQ = 0; % Initial Shear Strain

    t0 = 0.0001;
    dStrainQ0 = StrainQ_Rate*t0;

    dStrain_vpQ_Rate0 = 0;
    dStrain_vpQ0 = dStrain_vpQ_Rate0*t0;
    dStrain_eQ0 = dStrainQ0 - dStrain_vpQ0;
    dq0 = dStrain_eQ0*3*G0;
```

```
    dStrain_vpV_Rate0 = (Mu./V).*(((e-eR)./e0).^m).*(1./t).*((M_c^2-
Stress_R0^2)./(M_c^2-Beta^2)).*(Peq0./Pc0).^Omega;

    dStrain_vpV0 = dStrain_vpV_Rate0*t0;
    dStrain_eV0 = -dStrain_vpV0;
    dp0 = dStrain_eV0.*K0;

    dPc0 = ((Pc0*V)./(Lambda-Kappa)).*(dStrain_vpV0 + Beta.*dStrain_vpQ0);

    % Initial Values at t0
    dp = dp0;
    p = p0+dp;
    dq = dq0;
    q = dq;
    dPc = dPc0;
    Pc = Pc0+dPc;
    StrainQ = StrainQ+dStrainQ0;
    Stress_R = q/p;

    K = (V/Kappa)*p;
    G = (3*(1-2*nu)*K)/(2*(1+nu));

    syms Peq

    A = (1-Gamma).*p + 0.5*Gamma.*Peq;
    B = (1-Alpha).*M_c.*p + 0.5*Alpha.*Gamma.*M_c.*Peq;
    C_Surface = sqrt((((p-0.5*Gamma.*Peq)^2)./A^2) + (((q-Beta*p)^2)./B^2))
- 1;
    eqn = C_Surface == 0;
    Peq = vpasolve(eqn,Peq);
    Peq = double(Peq);

    % Write Initial Values into Excel File
    y01 = sprintf('%18.15f', t0);
    y02 = sprintf('%18.15f',dStrainQ0);
    y03 = sprintf('%18.15f',StrainQ);
    y04 = sprintf('%18.15f',dStrain_vpQ_Rate0);
    y05 = sprintf('%18.15f',dStrain_vpQ0);
    y06 = sprintf('%18.15f',dStrain_eQ0);
    y07 = sprintf('%18.15f',dq0);
    y08 = sprintf('%18.15f',q);
    y09 = sprintf('%18.15f',dStrain_vpV_Rate0);
    y010 = sprintf('%18.15f',dStrain_vpV0);
    y011 = sprintf('%18.15f',dStrain_eV0);
    y012 = sprintf('%18.15f',dp0);
    y013 = sprintf('%18.15f',p);
    y014 = sprintf('%18.15f',dPc0);
    y015 = sprintf('%18.15f',Pc);
    y016 = sprintf('%18.15f',Stress_R);
    y017 = sprintf('%18.15f',Peq);
    filename='Test Simulations for Haney Clay_Constant Strain Rate_1.xls';

Y0={y01,y02,y03,y04,y05,y06,y07,y08,y09,y010,y011,y012,y013,y014,y015,y016,
y017};
    sheet=11;
    z0=sprintf('E%d',9);
    xlswrite(filename,Y0,sheet,z0)

    %% Commence Integration Procedure
    tol = 1e-5;
```

```
    i_size = 0.0001;

    % Viscoplastic Strain Rates at t=0.002
     dStrain_vpQ_Rate = (Mu./V).*(((e-eR)./e0).^m).*(1./t).*((M_c^2-
Stress_R^2)./(M_c^2-Beta^2)).*((2*(Stress_R-Beta))./(Beta^2+(M_c^2.*(1-
Alpha+Alpha.*Gamma).^2)-Stress_R^2)).*(Peq./Pc).^Omega;
     dStrain_vpV_Rate = (Mu./V).*(((e-eR)./e0).^m).*(1./t).*((M_c^2-
Stress_R^2)./(M_c^2-Beta^2)).*(Peq./Pc).^Omega;

    dt = 0.0001;
    a = 1;
    StrainQ = dStrainQ0;

    tf = 2;
    iter = tf/dt;
    iter = round(iter);

    coder.varsize('Y1');
    Y1 = zeros(iter,17);

    while dt < tf
        i_size = min(i_size, tf-dt);

        dStrainQ = i_size*StrainQ_Rate;
        StrainQ = StrainQ+dStrainQ;

        Qk1 = i_size*Q_f(dt,dStrain_vpQ_Rate);
        Qk2 = i_size*Q_f(dt+i_size/4, dStrain_vpQ_Rate+Qk1/4);
        Qk3 = i_size*Q_f(dt+3*i_size/8,
dStrain_vpQ_Rate+3*Qk1/32+9*Qk2/32);
        Qk4 = i_size*Q_f(dt+12*i_size/13, dStrain_vpQ_Rate+1932*Qk1/2197-
7200*Qk2/2197+7296*Qk3/2197);
        Qk5 = i_size*Q_f(dt+i_size, dStrain_vpQ_Rate+439*Qk1/216-
8*Qk2+3680*Qk3/513-845*Qk4/4104);
        Qk6 = i_size*Q_f(dt+i_size/2, dStrain_vpQ_Rate-8*Qk1/27+2*Qk2-
3544*Qk3/2565+1859*Qk4/4104-11*Qk5/40);
        Q_w1 = dStrain_vpQ_Rate + 25*Qk1/216+1408*Qk3/2565+2197*Qk4/4104-
Qk5/5;
        Q_w2 = dStrain_vpQ_Rate +
16*Qk1/135+6656*Qk3/12825+28561*Qk4/56430-9*Qk5/50+2*Qk6/55;
        Q_R = abs(Q_w1-Q_w2)/i_size;
        Q_delta = 0.84*(tol./Q_R).^(1/4);

        Vk1 = i_size*V_f(dt,dStrain_vpV_Rate);
        Vk2 = i_size*V_f(dt+i_size/4, dStrain_vpV_Rate+Vk1/4);
        Vk3 = i_size*V_f(dt+3*i_size/8,
dStrain_vpV_Rate+3*Vk1/32+9*Vk2/32);
        Vk4 = i_size*V_f(dt+12*i_size/13, dStrain_vpV_Rate+1932*Vk1/2197-
7200*Vk2/2197+7296*Vk3/2197);
        Vk5 = i_size*V_f(dt+i_size, dStrain_vpV_Rate+439*Vk1/216-
8*Vk2+3680*Vk3/513-845*Vk4/4104);
        Vk6 = i_size*V_f(dt+i_size/2, dStrain_vpV_Rate-8*Vk1/27+2*Vk2-
3544*Vk3/2565+1859*Vk4/4104-11*Vk5/40);
        V_w1 = dStrain_vpV_Rate + 25*Vk1/216+1408*Vk3/2565+2197*Vk4/4104-
Vk5/5;
        V_w2 = dStrain_vpV_Rate +
16*Vk1/135+6656*Vk3/12825+28561*Vk4/56430-9*Vk5/50+2*Vk6/55;
        V_R = abs(V_w1-V_w2)/i_size;
        V_delta = 0.84*(tol./V_R).^(1/4);
```

```
        if (rms(Q_delta) >= 2) && (rms(V_delta) >= 2)
            dStrain_vpQ_Rate = Q_w1;
            dStrain_vpV_Rate = V_w1;

        elseif (rms(Q_delta) >=1) && (rms(Q_delta) >=1)
            dStrain_vpQ_Rate = Q_w1;
            dStrain_vpV_Rate = V_w1;
        end

        dStrain_vpQ = dStrain_vpQ_Rate*i_size;
        dStrain_eQ = dStrainQ - dStrain_vpQ;
        dq = dStrain_eQ*3*G;
        q = q + dq;

        dStrain_vpV = dStrain_vpV_Rate*i_size;
        dStrain_eV = -dStrain_vpV;
        dp = dStrain_eV.*K;
        p = p + dp;

        K = (V/Kappa)*p;
        G = (3*(1-2*nu)*K)/(2*(1+nu));

        Stress_R = q/p;

        dPc = ((Pc*V)./(Lambda-Kappa)).*(dStrain_vpV + Beta.*dStrain_vpQ);
        Pc = Pc + dPc;

        syms Peq

        A = (1-Gamma).*p + 0.5*Gamma.*Peq;
        B = (1-Alpha).*M_c.*p + 0.5*Alpha.*Gamma.*M_c.*Peq;
        C_Surface = sqrt((((p-0.5*Gamma*Peq).^2)./A.^2) + (((q-
Beta*p).^2)./B.^2)) - 1;
        eqn = C_Surface == 0;
        Peq = vpasolve(eqn,Peq);
        Peq = double(Peq);

          %% Plot Data
%         figure(1);
%         hold on
%         plot(StrainQ,q,'o');
%         xlabel('\epsilon_q');
%         ylabel('q (kPa)');
%         ax = gca;
%         ax.XAxisLocation = 'origin';
%         ax.YAxisLocation = 'origin';

          %% Write Data into Excel File
%         y1 = sprintf('%6.4f', dt+0.001);
%         y2= sprintf('%18.15f',dStrainQ);
%         y3= sprintf('%18.15f',StrainQ);
%         y4 = sprintf('%18.15f',dStrain_vpQ_Rate);
%         y5 = sprintf('%18.15f',dStrain_vpQ);
%         y6 = sprintf('%18.15f',dStrain_eQ);
%         y7 = sprintf('%18.15f',dq);
%         y8 = sprintf('%18.15f',q);
%         y9 = sprintf('%18.15f',dStrain_vpV_Rate);
%         y10 = sprintf('%18.15f',dStrain_vpV);
```

```
%          y11 = sprintf('%18.15f',dStrain_eV);
%          y12 = sprintf('%18.15f',dp);
%          y13 = sprintf('%18.15f',p);
%          y14 = sprintf('%18.15f',dPc);
%          y15 = sprintf('%18.15f',Pc);
%          y16= sprintf('%18.15f',Stress_R);
%          y17= sprintf('%18.15f',Peq);
%          Y1={y1,y2,y3,y4,y5,y6,y7,y8,y9,y10,y11,y12,y13,y14,y15,y16,y17};
%          sheet=1;
%          z1=sprintf('E%d',a+10);
%          xlswrite(filename,Y1,sheet,z1)

        Y1(a,:)= [dt+0.0001 dStrainQ StrainQ dStrain_vpQ_Rate dStrain_vpQ
dStrain_eQ dq q dStrain_vpV_Rate dStrain_vpV dStrain_eV dp p dPc Pc
Stress_R Peq];

        dStrain_vpQ_Rate = (Mu./V).*(((e-eR)./e0).^m).*(1./t).*((M_c^2-
Stress_R^2)./(M_c^2-Beta^2)).*((2*(Stress_R-Beta))./(Beta^2+(M_c^2*(1-
Alpha+Alpha*Gamma).^2)-Stress_R^2)).*(Peq./Pc).^Omega;
        dStrain_vpV_Rate = (Mu./V).*(((e-eR)./e0).^m).*(1./t).*((M_c^2-
Stress_R^2)./(M_c^2-Beta^2)).*(Peq./Pc).^Omega;

        if (rms(Q_delta) >= 2) && (rms(V_delta) >= 2)
            i_size = 2*i_size;
            dt = dt+i_size;
            a = a+1;

        elseif (rms(Q_delta) >=1) && (rms(Q_delta) >=1)
            dt = dt+i_size;
            a = a+1;

        elseif rms(Q_delta) < 1
            i_size = 0.5*i_size;
            dt = dt + i_size;
            a = a+1;
        end

    end

    %% Write Data into Excel File
    xlswrite(filename,Y1,sheet,'E10');

    function dStrain_vpQ = Q_f(dt,dStrain_vpQ_Rate)
        dStrain_vpQ = dStrain_vpQ_Rate*dt;
    end

    function dStrain_vpV = V_f(dt,dStrain_vpV_Rate)
        dStrain_vpV = dStrain_vpV_Rate*dt;
    end

end
```

E.5 MATLAB Code for Strain-controlled Undrained Compression Tests using Various OCRs on Kaolin and Bentonite Mixture

```
function UndrainedShearing_StrainControlled_KB Mixture

%% For Strain-controlled Undrained Compression Tests on KB Mixture
close all;
clear;
clc;

%% Undrained Compression Test - Strain-Controlled

%     Lambda = input('Enter the Lambda value (eg., 0.093) = ');
%     Kappa = input('Enter the Kappa value (eg., 0.012) = ');
%     Mu = input('Enter the Mu value (eg., 0.0037) = ');
%     M_c = input('Enter the value for M in compression (eg., 1.2479) = ');
%     M_e = input('Enter the value for M in extension (eg., 0.95) = ');
%     e0 = input('Enter the initial void ratio (eg., 0.6207) = ');
%     nu = input('Enter the value for Poisson Ratio (eg.,0.3) = ');
%     p0 = input('Enter the value for initial Applied pressure (kPa) = ');
%     Pc0 = input('Enter the value for initial Pre-consolidation pressure
(kPa = ');
%     q0 = input('Enter the value for initial Deviatoric Pressure (kPa) =
');
%
%     Alpha = input('Enter the Alpha value (0<=Alpha<=1) = ');
%     Gamma = input('Enter the Gamma value (0<=Gamma<=1) = ');
%     theta = input('Enter the initial inclination angle value for Coupling
= ');
%
%     StrainQ_Rate = input('Enter the value for Controlled Deviatoric
Strain Rate = ');
%     t = input('Enter the value for reference time parameter = ');

    %% Model Parameters
    Lambda_V = 0.093;
    Kappa_V = 0.012;
    M_c = 1.2479;
    e0 = 0.6207;   % Determined from Strain Limit
    nu = 0.3;
    Mu_V = 0.0037;

    Alpha = 1;
    Gamma = 0.85;
    theta = 0;

%% Various OCRs
%     p0 = 392;    % OCR=1
%     p0 = 301.5;    % OCR=1.3
    p0 = 196;    % OCR=2
%     p0 = 65.33;    % OCR=6

    Pc0 = 392;
    q0 = 0;

    StrainQ_Rate = 0.006; % 0.6%/Hr
```

```
    t = 24; % Hour
    V0 = e0+1;
    eR = 0;
    m = 1;

    Omega = (Lambda_V-Kappa_V)/Mu_V;

    % Undrained Shearing - No Volume Change
    dV = 0;
    V = V0;
    e = e0;

    % Coupling
    theta_radian=theta*(pi/180);
    Beta = tan(theta_radian);

    %% Determine Initial Values
    Stress_R0 = q0/p0;

    K0 = (1/Kappa_V)*p0;
    G0 = (3*(1-2*nu)*K0)/(2*(1+nu));

    syms Peq0

    A0 = (1-Gamma)*p0 + 0.5*Gamma*Peq0;
    B0 = (1-Alpha)*M_c*p0 + 0.5*Alpha*Gamma*M_c*Peq0;
    C_Surface = sqrt((((p0-0.5*Gamma*Peq0)^2)/A0^2) + (((q0-
Beta*p0)^2)/B0^2)) - 1;
    eqn = C_Surface == 0;
    Peq0 = vpasolve(eqn,Peq0);
    Peq0 = double(Peq0);

    % Applied Shear Strain Rate - 30%/Day
    StrainQ = 0; % Initial Shear Strain

    t0 = 0.005;

    dStrainQ0 = StrainQ_Rate*t0;

    dStrain_vpQ_Rate0 = 0;
    dStrain_vpQ0 = dStrain_vpQ_Rate0*t0;
    dStrain_eQ0 = dStrainQ0 - dStrain_vpQ0;
    dq0 = dStrain_eQ0*3*G0;

    dStrain_vpV_Rate0 = (Mu_V).*(((e-eR)./e0).^m).*(1./t).*((M_c^2-
Stress_R0^2)./(M_c^2-Beta^2)).*(Peq0./Pc0).^Omega;

    dStrain_vpV0 = dStrain_vpV_Rate0*t0;
    dStrain_eV0 = -dStrain_vpV0;
    dp0 = dStrain_eV0.*K0;

    dPc0 = (Pc0./(Lambda_V-Kappa_V)).*(dStrain_vpV0 + Beta.*dStrain_vpQ0);

    % Initial Values at t0
    dp = dp0;
    p = p0+dp;
    dq = dq0;
    q = dq;
```

```
    dPc = dPc0;
    Pc = Pc0+dPc;
    StrainQ = StrainQ+dStrainQ0;
    Stress_R = q/p;

    K = (1/Kappa_V)*p;
    G = (3*(1-2*nu)*K)/(2*(1+nu));

    syms Peq

    A = (1-Gamma)*p + 0.5*Gamma*Peq;
    B = (1-Alpha)*M_c*p + 0.5*Alpha*Gamma*M_c*Peq;
    C_Surface = sqrt((((p-0.5*Gamma*Peq)^2)/A^2) + (((q-Beta*p)^2)/B^2)) -
1;
    eqn = C_Surface == 0;
    Peq = vpasolve(eqn,Peq);
    Peq = double(Peq);

    % Write Initial Values into Excel File
    y01 = sprintf('%18.15f',t0);
    y02= sprintf('%18.15f',dStrainQ0);
    y03= sprintf('%18.15f',StrainQ);
    y04 = sprintf('%18.15f',dStrain_vpQ_Rate0);
    y05 = sprintf('%18.15f',dStrain_vpQ0);
    y06 = sprintf('%18.15f',dStrain_eQ0);
    y07 = sprintf('%18.15f',dq0);
    y08 = sprintf('%18.15f',q);
    y09 = sprintf('%18.15f',dStrain_vpV_Rate0);
    y010 = sprintf('%18.15f',dStrain_vpV0);
    y011 = sprintf('%18.15f',dStrain_eV0);
    y012 = sprintf('%18.15f',dp0);
    y013 = sprintf('%18.15f',p);
    y014 = sprintf('%18.15f',dPc0);
    y015 = sprintf('%18.15f',Pc);
    y016= sprintf('%18.15f',Stress_R);
    y017= sprintf('%18.15f',Peq);
    filename='Draft_Test Simulations for KB Mixture_JH Yin_Fig9_VS2.xls';

Y0={y01,y02,y03,y04,y05,y06,y07,y08,y09,y010,y011,y012,y013,y014,y015,y016,
y017};
    sheet=6;
    z0=sprintf('E%d',9);
    xlswrite(filename,Y0,sheet,z0)

    %% Commence Integration Procedure
    tol = 1e-9;

    i_size = 0.005;

    % Viscoplastic Strain Rates at t=0.002
     dStrain_vpQ_Rate = (Mu_V).*(((e-eR)./e0).^m).*(1./t).*((M_c^2-
Stress_R^2)./(M_c^2-Beta^2)).*((2*(Stress_R-Beta))./(Beta^2+(M_c^2*(1-
Alpha+Alpha*Gamma).^2)-Stress_R^2)).*(Peq./Pc).^Omega;
     dStrain_vpV_Rate = (Mu_V).*(((e-eR)./e0).^m).*(1./t).*((M_c^2-
Stress_R^2)./(M_c^2-Beta^2)).*(Peq./Pc).^Omega;

    dt = 0.005;

    a = 1;
```

```
    StrainQ = dStrainQ0;

    tf = 25;
    iter = tf/dt;
    iter = round(iter);

    coder.varsize('Y1');
    Y1 = zeros(iter,17);

    while dt < tf
        i_size = min(i_size, tf-dt);

        dStrainQ = i_size*StrainQ_Rate;
        StrainQ = StrainQ+dStrainQ;

        Qk1 = i_size*Q_f(dt,dStrain_vpQ_Rate);
        Qk2 = i_size*Q_f(dt+i_size/4, dStrain_vpQ_Rate+Qk1/4);
        Qk3 = i_size*Q_f(dt+3*i_size/8,
dStrain_vpQ_Rate+3*Qk1/32+9*Qk2/32);
        Qk4 = i_size*Q_f(dt+12*i_size/13, dStrain_vpQ_Rate+1932*Qk1/2197-
7200*Qk2/2197+7296*Qk3/2197);
        Qk5 = i_size*Q_f(dt+i_size, dStrain_vpQ_Rate+439*Qk1/216-
8*Qk2+3680*Qk3/513-845*Qk4/4104);
        Qk6 = i_size*Q_f(dt+i_size/2, dStrain_vpQ_Rate-8*Qk1/27+2*Qk2-
3544*Qk3/2565+1859*Qk4/4104-11*Qk5/40);
        Q_w1 = dStrain_vpQ_Rate + 25*Qk1/216+1408*Qk3/2565+2197*Qk4/4104-
Qk5/5;
        Q_w2 = dStrain_vpQ_Rate +
16*Qk1/135+6656*Qk3/12825+28561*Qk4/56430-9*Qk5/50+2*Qk6/55;
        Q_R = abs(Q_w1-Q_w2)/i_size;
        Q_delta = 0.84*(tol./Q_R).^(1/4);

        Vk1 = i_size*V_f(dt,dStrain_vpV_Rate);
        Vk2 = i_size*V_f(dt+i_size/4, dStrain_vpV_Rate+Vk1/4);
        Vk3 = i_size*V_f(dt+3*i_size/8,
dStrain_vpV_Rate+3*Vk1/32+9*Vk2/32);
        Vk4 = i_size*V_f(dt+12*i_size/13, dStrain_vpV_Rate+1932*Vk1/2197-
7200*Vk2/2197+7296*Vk3/2197);
        Vk5 = i_size*V_f(dt+i_size, dStrain_vpV_Rate+439*Vk1/216-
8*Vk2+3680*Vk3/513-845*Vk4/4104);
        Vk6 = i_size*V_f(dt+i_size/2, dStrain_vpV_Rate-8*Vk1/27+2*Vk2-
3544*Vk3/2565+1859*Vk4/4104-11*Vk5/40);
        V_w1 = dStrain_vpV_Rate + 25*Vk1/216+1408*Vk3/2565+2197*Vk4/4104-
Vk5/5;
        V_w2 = dStrain_vpV_Rate +
16*Vk1/135+6656*Vk3/12825+28561*Vk4/56430-9*Vk5/50+2*Vk6/55;
        V_R = abs(V_w1-V_w2)/i_size;
        V_delta = 0.84*(tol./V_R).^(1/4);

        if (rms(Q_delta) >= 2) && (rms(V_delta) >= 2)
            dStrain_vpQ_Rate = Q_w1;
            dStrain_vpV_Rate = V_w1;

        elseif (rms(Q_delta) >=1) && (rms(Q_delta) >=1)
            dStrain_vpQ_Rate = Q_w1;
            dStrain_vpV_Rate = V_w1;
        end
```

```
        dStrain_vpQ = dStrain_vpQ_Rate*i_size;
        dStrain_eQ = dStrainQ - dStrain_vpQ;
        dq = dStrain_eQ*3*G;
        q = q + dq;

        dStrain_vpV = dStrain_vpV_Rate*i_size;
        dStrain_eV = -dStrain_vpV;
        dp = dStrain_eV.*K;
        p = p + dp;

        K = (1/Kappa_V)*p;
        G = (3*(1-2*nu)*K)/(2*(1+nu));

        Stress_R = q/p;

        dPc = (Pc./(Lambda_V-Kappa_V)).*(dStrain_vpV + Beta.*dStrain_vpQ);
        Pc = Pc + dPc;

        syms Peq

        A = (1-Gamma).*p + 0.5*Gamma.*Peq;
        B = (1-Alpha).*M_c.*p + 0.5*Alpha.*Gamma.*M_c.*Peq;
        C_Surface = sqrt((((p-0.5*Gamma*Peq).^2)./A.^2) + (((q-
Beta*p).^2)./B.^2)) - 1;
        eqn = C_Surface == 0;
        Peq = vpasolve(eqn,Peq);
        Peq = double(Peq);

          %% Plot Data
%         figure(1);
%         hold on
%         plot(StrainQ,q,'o');
%         xlabel('\epsilon_q');
%         ylabel('q (kPa)');
%         ax = gca;
%         ax.XAxisLocation = 'origin';
%         ax.YAxisLocation = 'origin';

          %% Write Data into Excel File
%         y1 = sprintf('%18.15f', dt+0.00001);
%         y2= sprintf('%18.15f',dStrainQ);
%         y3= sprintf('%18.15f',StrainQ);
%         y4 = sprintf('%18.15f',dStrain_vpQ_Rate);
%         y5 = sprintf('%18.15f',dStrain_vpQ);
%         y6 = sprintf('%18.15f',dStrain_eQ);
%         y7 = sprintf('%18.15f',dq);
%         y8 = sprintf('%18.15f',q);
%         y9 = sprintf('%18.15f',dStrain_vpV_Rate);
%         y10 = sprintf('%18.15f',dStrain_vpV);
%         y11 = sprintf('%18.15f',dStrain_eV);
%         y12 = sprintf('%18.15f',dp);
%         y13 = sprintf('%18.15f',p);
%         y14 = sprintf('%18.15f',dPc);
%         y15 = sprintf('%18.15f',Pc);
%         y16= sprintf('%18.15f',Stress_R);
%         y17= sprintf('%18.15f',Peq);
```

```
        Y1(a,:)= [dt+0.005 dStrainQ StrainQ dStrain_vpQ_Rate dStrain_vpQ
dStrain_eQ dq q dStrain_vpV_Rate dStrain_vpV dStrain_eV dp p dPc Pc
Stress_R Peq];

        dStrain_vpQ_Rate = (Mu_V).*(((e-eR)./e0).^m).*(1./t).*((M_c^2-
Stress_R^2)./(M_c^2-Beta^2)).*((2*(Stress_R-Beta))./(Beta^2+(M_c^2*(1-
Alpha+Alpha*Gamma).^2)-Stress_R^2)).*(Peq./Pc).^Omega;
        dStrain_vpV_Rate = (Mu_V).*(((e-eR)./e0).^m).*(1./t).*((M_c^2-
Stress_R^2)./(M_c^2-Beta^2)).*(Peq./Pc).^Omega;


        if (rms(Q_delta) >= 2) && (rms(V_delta) >= 2)
            i_size = 2*i_size;
            dt = dt+i_size;
            a = a+1;

        elseif (rms(Q_delta) >=1) && (rms(Q_delta) >=1)
            dt = dt+i_size;
            a = a+1;

        elseif rms(Q_delta) < 1
            i_size = 0.5*i_size;
            dt = dt + i_size;
            a = a+1;
        end

    end

    %% Write Data into Excel File
    xlswrite(filename,Y1,sheet,'E10');

    function dStrain_vpQ = Q_f(dt,dStrain_vpQ_Rate)
        dStrain_vpQ = dStrain_vpQ_Rate*dt;
    end

    function dStrain_vpV = V_f(dt,dStrain_vpV_Rate)
        dStrain_vpV = dStrain_vpV_Rate*dt;
    end

end
```

E.6 MATLAB Code for Strain-controlled Undrained Triaxial Loading Tests on Shanghai Soft Clay

```
function UndrainedS_StrainC _Shanghai_SC_CAU1

%% For Strain-controlled Undrained Triaxial Loading Tests on Shanghai Soft
Clay
% 2%/Hr (Compression)
% Test Number: CAU-1
close all;
clear;
clc;

%% Undrained Triaxial Shearing Test - Strain-Controlled

%     Lambda = input('Enter the Lambda value (eg., 0.212) = ');
%     Kappa = input('Enter the Kappa value (eg., 0.046) = ');
%     Mu = input('Enter the Mu value (eg., 0.007218) = ');
%     M_c = input('Enter the value for M in compression (eg., 1.277) = ');
%     M_e = input('Enter the value for M in extension (eg., 0.95) = ');
%     e0 = input('Enter the initial Void Ratio (eg., 1.402) = ');
%     nu = input('Enter the value for Poisson Ratio (eg.,0.2) = ');
%     p0 = input('Enter the value for initial Applied pressure (kPa) = ');
%     Pc0 = input('Enter the value for initial Pre-consolidation pressure
(kPa = ');
%     q0 = input('Enter the value for initial Deviatoric Pressure (kPa) =
');
%
%     Alpha = input('Enter the Alpha value (0<=Alpha<=1) = ');
%     Gamma = input('Enter the Gamma value (0<=Gamma<=1) = ');
%     theta = input('Enter the initial inclination angle value for Coupling
= ');
%     phi = input('Enter the value for Friction Angle (degree) = ');
%
%     Strain_Rate = input('Enter the value for Controlled Deviatoric Strain
Rate = ');
%     t = input('Enter the value for reference time parameter = ');


%% Model Parameters for Shanghai Soft Clay
    Lambda = 0.212;
    Kappa = 0.046;
    M_c = 1.277;
%     M_c = 0.9; % Extension
    phi = 31.77; % Determined from M_c Value
    e0 = 1.402;
    nu = 0.2;

    Mu = 0.007218; % Determined from C-Alpha Value

    Alpha = 0.95;
    Gamma = 0.55;

    p0 = 72.50;         % OCR=1
    Pc0 = 72.50;
```

```
    %% Part i
%     StrainQ_Rate = 3.333e-03; % 0.3333%/Min
% %     StrainQ_Rate = 0.2; % 20%/Hr
% %     StrainQ_Rate = 4.8; % 480%/Day

%     t = 1440; % Mins
% %     t = 24; % Hour
% %     t = 1; % Day

    %% Part ii
    StrainQ_Rate = 3.333e-04; % 0.03333%/Min
%     StrainQ_Rate = 0.02; % 2%/Hr
%     StrainQ_Rate = 0.48; % 48%/Day

    t = 1440; % Mins
%     t = 24; % Hour
%     t = 1; % Day

    %% Part iii
%     StrainQ_Rate = 3.333e-05; % 0.003333%/Min
% %     StrainQ_Rate = 0.002; % 0.2%/Hr
% %     StrainQ_Rate = 0.048; % 4.8%/Day

%     t = 1440; % Mins
% %     t = 24; % Hour
% %     t = 1; % Day

    V0 = e0+1;
    eR = 0;
    m = 1;

    Omega = (Lambda-Kappa)/Mu;

    % Undrained Shearing - No Volume Change
    dV = 0;
    V = V0;
    e = e0;

    %% Determine Initial Values
    phi_radian = phi*(pi/180);
    K0 = 1 - sin(phi_radian);

    Stress_R_K0 = (3*(1-K0))/(1+2*K0);
    q0 = Stress_R_K0*p0;

    K_0 = (V/Kappa)*p0;
    G_0 = (3*(1-2*nu)*K_0)/(2*(1+nu));

%% Determine Initial Fabric Paramater
%% Associated Flow Rule
%     beta0 = Stress_R_K0 - ((M_c^2 - Stress_R_K0^2)/3);
%     D_beta = (3*(4*M_c^2 - 4*Stress_R_K0^2 -
3*Stress_R_K0))/(8*(Stress_R_K0^2 - M_c^2 + 2*Stress_R_K0));
% %     C_beta = (1/Lambda)*log((10*M_c^2 - 2*beta0*D_beta)/(M_c^2 -
2*beta0*D_beta));
%     C_beta = 56.60;   % 12/Lambda
```

```
%% Non-associated Flow Rule
    syms beta_S
    eqn_beta1 = beta_S^2 + 3*beta_S;
    eqn_beta2 = Stress_R_K0^2 - M_c^2.*(1-Alpha+Alpha*Gamma).^2 +
3*Stress_R_K0;
    beta_S = vpasolve(eqn_beta1 == eqn_beta2,beta_S);
    beta_S = double(beta_S);

    beta0 = beta_S(2);

    D_beta = (3*(3*Stress_R_K0 - 4*beta0)*(beta0^2 + (M_c^2.*(1-
Alpha+Alpha*Gamma).^2) - Stress_R_K0^2))/(8*(Stress_R_K0-
(3*beta0)).*(Stress_R_K0 - beta0));
    C_beta = 56.60;     % 12/Lambda

    syms Peq0

    A0 = (1-Gamma)*p0 + 0.5*Gamma*Peq0;
    B0 = (1-Alpha)*M_c*p0 + 0.5*Alpha*Gamma*M_c*Peq0;
    C_Surface0 = sqrt((((p0-0.5*Gamma*Peq0).^2)./A0.^2) + (((q0-
beta0*p0).^2)./B0.^2)) - 1;
    eqn = C_Surface0 == 0;
    Peq0 = vpasolve(eqn,Peq0);
    Peq0 = double(Peq0);

    % Applied Shear Strain Rate - 30%/Day
    StrainQ = 0; % Initial Shear Strain

    t0 = 0.007;

    dStrainQ0 = StrainQ_Rate*t0;

    %     dStrain_vpQ_Rate0 = 0;
    dStrain_vpQ_Rate0 = (Mu./V).*(((e-eR)./e0).^m).*(1./t).*((M_c^2-
Stress_R_K0^2)./(M_c^2-beta0^2)).*((2*(Stress_R_K0-
beta0))./(beta0^2+(M_c^2*(1-Alpha+Alpha*Gamma).^2)-
Stress_R_K0^2)).*(Peq0./Pc0).^Omega;

    dStrain_vpQ0 = dStrain_vpQ_Rate0*t0;
    dStrain_eQ0 = dStrainQ0 - dStrain_vpQ0;
    dq0 = dStrain_eQ0*3*G_0;

    dStrain_vpV_Rate0 = (Mu./V).*(((e-eR)./e0).^m).*(1./t).*((M_c^2-
Stress_R_K0^2)./(M_c^2-beta0^2)).*(Peq0./Pc0).^Omega;

    dStrain_vpV0 = dStrain_vpV_Rate0*t0;
    dStrain_eV0 = -dStrain_vpV0;
    dp0 = dStrain_eV0.*K_0;

    dPc0 = ((Pc0*V)./(Lambda-Kappa)).*(dStrain_vpV0 + beta0.*dStrain_vpQ0);

    % Initial Values at t0
    dp = dp0;
    p = p0+dp;
    dq = dq0;
    q = q0+dq;
    dPc = dPc0;
    Pc = Pc0+dPc;
    StrainQ = StrainQ+dStrainQ0;
```

```
    Stress_R = q/p;

    % Macaulay bracket for volumetric viscoplastic strain rate
    if dStrain_vpV0 < 0
        dStrain_vpV0_MB0 = 0;
    else
        dStrain_vpV0_MB0 = dStrain_vpV0;
    end

    beta_Rate0 = C_beta.*(((((3/4).*Stress_R) - beta0).*dStrain_vpV0_MB0) +
(D_beta.*(((1/3).*Stress_R) - beta0).*abs(dStrain_vpQ0)));

    Beta = beta0 + beta_Rate0;

    K = (V/Kappa)*p;
    G = (3*(1-2*nu)*K)/(2*(1+nu));

    syms Peq

    A = (1-Gamma)*p + 0.5*Gamma*Peq;
    B = (1-Alpha)*M_c*p + 0.5*Alpha*Gamma*M_c*Peq;
    C_Surface = sqrt((((p-0.5*Gamma*Peq).^2)./A^2) + (((q-
Beta*p).^2)./B^2)) - 1;
    eqn = C_Surface == 0;
    Peq = vpasolve(eqn,Peq);
    Peq = double(Peq);

    % Write Initial Values into Excel File
    y01 = sprintf('%18.15f',t0);

    y02 = sprintf('%18.15f',dStrainQ0);
    y03 = sprintf('%18.15f',StrainQ);
    y04 = sprintf('%18.15f',dStrain_vpQ_Rate0);
    y05 = sprintf('%18.15f',dStrain_vpQ0);
    y06 = sprintf('%18.15f',dStrain_eQ0);
    y07 = sprintf('%18.15f',dq0);
    y08 = sprintf('%18.15f',q);
    y09 = sprintf('%18.15f',dStrain_vpV_Rate0);
    y010 = sprintf('%18.15f',dStrain_vpV0);
    y011 = sprintf('%18.15f',dStrain_eV0);
    y012 = sprintf('%18.15f',dp0);
    y013 = sprintf('%18.15f',p);
    y014 = sprintf('%18.15f',dPc0);
    y015 = sprintf('%18.15f',Pc);
    y016 = sprintf('%18.15f',Stress_R);
    y017 = sprintf('%18.15f',Peq);
    y018 = sprintf('%18.15f',beta0);
    y019 = sprintf('%18.15f',beta_Rate0);
    filename='Simulations_Shanghai_SC_CAU1.xls';

Y0={y01,y02,y03,y04,y05,y06,y07,y08,y09,y010,y011,y012,y013,y014,y015,y016,
y017,y018,y019};
    sheet=1;
    z0=sprintf('E%d',9);
    xlswrite(filename,Y0,sheet,z0)

    %% Commence Integration Procedure
    tol = 1e-9;
    i_size = 0.007;
```

```
    % Viscoplastic Strain Rates at t=0.002
     dStrain_vpQ_Rate = (Mu./V).*(((e-eR)./e0).^m).*(1./t).*((M_c^2-
Stress_R^2)./(M_c^2-Beta^2)).*((2*(Stress_R-Beta))./(Beta^2+(M_c^2*(1-
Alpha+Alpha*Gamma).^2)-Stress_R^2)).*(Peq./Pc).^Omega;
     dStrain_vpV_Rate = (Mu./V).*(((e-eR)./e0).^m).*(1./t).*((M_c^2-
Stress_R^2)./(M_c^2-Beta^2)).*(Peq./Pc).^Omega;

    dt = 0.007;
    a = 1;

    tf = 105;

    iter = tf/dt;
    iter = round(iter);

    coder.varsize('Y1');
    Y1 = zeros(iter,19);

    while dt < tf
        i_size = min(i_size, tf-dt);

        dStrainQ = i_size*StrainQ_Rate;
        StrainQ = StrainQ+dStrainQ;

        Qk1 = i_size*Q_f(dt,dStrain_vpQ_Rate);
        Qk2 = i_size*Q_f(dt+i_size/4, dStrain_vpQ_Rate+Qk1/4);
        Qk3 = i_size*Q_f(dt+3*i_size/8,
dStrain_vpQ_Rate+3*Qk1/32+9*Qk2/32);
        Qk4 = i_size*Q_f(dt+12*i_size/13, dStrain_vpQ_Rate+1932*Qk1/2197-
7200*Qk2/2197+7296*Qk3/2197);
        Qk5 = i_size*Q_f(dt+i_size, dStrain_vpQ_Rate+439*Qk1/216-
8*Qk2+3680*Qk3/513-845*Qk4/4104);
        Qk6 = i_size*Q_f(dt+i_size/2, dStrain_vpQ_Rate-8*Qk1/27+2*Qk2-
3544*Qk3/2565+1859*Qk4/4104-11*Qk5/40);
        Q_w1 = dStrain_vpQ_Rate + 25*Qk1/216+1408*Qk3/2565+2197*Qk4/4104-
Qk5/5;
        Q_w2 = dStrain_vpQ_Rate +
16*Qk1/135+6656*Qk3/12825+28561*Qk4/56430-9*Qk5/50+2*Qk6/55;
        Q_R = abs(Q_w1-Q_w2)/i_size;
        Q_delta = 0.84*(tol./Q_R).^(1/4);

        Vk1 = i_size*V_f(dt,dStrain_vpV_Rate);
        Vk2 = i_size*V_f(dt+i_size/4, dStrain_vpV_Rate+Vk1/4);
        Vk3 = i_size*V_f(dt+3*i_size/8,
dStrain_vpV_Rate+3*Vk1/32+9*Vk2/32);
        Vk4 = i_size*V_f(dt+12*i_size/13, dStrain_vpV_Rate+1932*Vk1/2197-
7200*Vk2/2197+7296*Vk3/2197);
        Vk5 = i_size*V_f(dt+i_size, dStrain_vpV_Rate+439*Vk1/216-
8*Vk2+3680*Vk3/513-845*Vk4/4104);
        Vk6 = i_size*V_f(dt+i_size/2, dStrain_vpV_Rate-8*Vk1/27+2*Vk2-
3544*Vk3/2565+1859*Vk4/4104-11*Vk5/40);
        V_w1 = dStrain_vpV_Rate + 25*Vk1/216+1408*Vk3/2565+2197*Vk4/4104-
Vk5/5;
        V_w2 = dStrain_vpV_Rate +
16*Vk1/135+6656*Vk3/12825+28561*Vk4/56430-9*Vk5/50+2*Vk6/55;
        V_R = abs(V_w1-V_w2)/i_size;
        V_delta = 0.84*(tol./V_R).^(1/4);
```

```
        if (rms(Q_delta) >= 2) && (rms(V_delta) >= 2)
            dStrain_vpQ_Rate = Q_w1;
            dStrain_vpV_Rate = V_w1;

        elseif (rms(Q_delta) >=1) && (rms(Q_delta) >=1)
            dStrain_vpQ_Rate = Q_w1;
            dStrain_vpV_Rate = V_w1;
        end

        dStrain_vpQ = dStrain_vpQ_Rate*i_size;
        dStrain_eQ = dStrainQ - dStrain_vpQ;
        dq = dStrain_eQ*3*G;
        q = q + dq;

        dStrain_vpV = dStrain_vpV_Rate*i_size;
        dStrain_eV = -dStrain_vpV;
        dp = dStrain_eV.*K;
        p = p + dp;

        K = (V/Kappa)*p;
        G = (3*(1-2*nu)*K)/(2*(1+nu));

        Stress_R = q/p;

        % Macaulay bracket for volumetric viscoplastic strain rate
        if dStrain_vpV < 0
            dStrain_vpV_MB = 0;
        else
            dStrain_vpV_MB = dStrain_vpV;
        end

        beta_Rate = C_beta.*(((((3/4).*Stress_R) - Beta).*dStrain_vpV_MB) +
(D_beta.*(((1/3)*Stress_R) - Beta).*abs(dStrain_vpQ)));

        Beta = Beta + beta_Rate;

        dPc = ((Pc*V)./(Lambda-Kappa)).*(dStrain_vpV + Beta.*dStrain_vpQ);
        Pc = Pc + dPc;

        syms Peq

        A = (1-Gamma).*p + 0.5*Gamma.*Peq;
        B = (1-Alpha).*M_c.*p + 0.5*Alpha.*Gamma.*M_c.*Peq;
        C_Surface = sqrt((((p-0.5*Gamma*Peq).^2)./A.^2) + (((q-
Beta*p).^2)./B.^2)) - 1;
        eqn = C_Surface == 0;
        Peq = vpasolve(eqn,Peq);
        Peq = double(Peq);

          %% Plot Data
%         figure(1);
%         hold on
%         plot(StrainQ,q,'o');
%         xlabel('\epsilon_q');
%         ylabel('q (kPa)');
%         ax = gca;
%         ax.XAxisLocation = 'origin';
%         ax.YAxisLocation = 'origin';
```

```
          %% Write Data into Excel File
%         y1 = sprintf('%6.4f', dt+0.001);
%         y2= sprintf('%18.15f',dStrainQ);
%         y3= sprintf('%18.15f',StrainQ);
%         y4 = sprintf('%18.15f',dStrain_vpQ_Rate);
%         y5 = sprintf('%18.15f',dStrain_vpQ);
%         y6 = sprintf('%18.15f',dStrain_eQ);
%         y7 = sprintf('%18.15f',dq);
%         y8 = sprintf('%18.15f',q);
%         y9 = sprintf('%18.15f',dStrain_vpV_Rate);
%         y10 = sprintf('%18.15f',dStrain_vpV);
%         y11 = sprintf('%18.15f',dStrain_eV);
%         y12 = sprintf('%18.15f',dp);
%         y13 = sprintf('%18.15f',p);
%         y14 = sprintf('%18.15f',dPc);
%         y15 = sprintf('%18.15f',Pc);
%         y16= sprintf('%18.15f',Stress_R);
%         y17= sprintf('%18.15f',Peq);
%         Y1={y1,y2,y3,y4,y5,y6,y7,y8,y9,y10,y11,y12,y13,y14,y15,y16,y17};
%         sheet=1;
%         z1=sprintf('E%d',a+10);
%         xlswrite(filename,Y1,sheet,z1)

        Y1(a,:)= [dt+0.007 dStrainQ StrainQ dStrain_vpQ_Rate dStrain_vpQ
dStrain_eQ dq q dStrain_vpV_Rate dStrain_vpV dStrain_eV dp p dPc Pc
Stress_R Peq Beta beta_Rate];

        dStrain_vpQ_Rate = (Mu./V).*(((e-eR)./e0).^m).*(1./t).*((M_c^2-
Stress_R^2)./(M_c^2-Beta^2)).*((2*(Stress_R-Beta))./(Beta^2+(M_c^2*(1-
Alpha+Alpha*Gamma).^2)-Stress_R^2)).*(Peq./Pc).^Omega;
        dStrain_vpV_Rate = (Mu./V).*(((e-eR)./e0).^m).*(1./t).*((M_c^2-
Stress_R^2)./(M_c^2-Beta^2)).*(Peq./Pc).^Omega;

        if (rms(Q_delta) >= 2) && (rms(V_delta) >= 2)
            i_size = 2*i_size;
            dt = dt+i_size;
            a = a+1;

        elseif (rms(Q_delta) >=1) && (rms(Q_delta) >=1)
            dt = dt+i_size;
            a = a+1;

        elseif rms(Q_delta) < 1
            i_size = 0.5*i_size;
            dt = dt + i_size;
            a = a+1;
        end

    end

    %% Write Data into Excel File
    xlswrite(filename,Y1,sheet,'E10');

    function dStrain_vpQ = Q_f(dt,dStrain_vpQ_Rate)
        dStrain_vpQ = dStrain_vpQ_Rate*dt;
    end

    function dStrain_vpV = V_f(dt,dStrain_vpV_Rate)
        dStrain_vpV = dStrain_vpV_Rate*dt;
```

```
    end
end
```